Identification and Preliminary Validation of Potential Endogenous Targets for Maltanedienol

Submitted in partial fulfilment

of the requirements of the

Degree of Master of Pharmacy

Ella Coppini

Department of Pharmacy

2021

L-Università ta' Malta

University of Malta Library – Electronic Thesis & Dissertations (ETD) Repository

The copyright of this thesis/dissertation belongs to the author. The author's rights in respect of this work are as defined by the Copyright Act (Chapter 415) of the Laws of Malta or as modified by any successive legislation.

Users may access this full-text thesis/dissertation and can make use of the information contained in accordance with the Copyright Act provided that the author must be properly acknowledged. Further distribution or reproduction in any format is prohibited without the prior permission of the copyright holder.

Dedicated to all those who impacted my journey in one way or another.

Abstract

Maltanedienol is the active principle of the alga, *Padina pavonica. In vivo* studies have shown that this species has the potential to produce and release a substance that has a positive effect on calcium fixation through its fronds. Maltanedienol has the utility in managing bone conditions such as osteoporosis. This study has two main aims: to identify the optimal biological targets for Maltanedienol, related to calcium deposition or bone remodelling and secondly, to study Maltanedienol's interaction with these targets from an atomic perspective.

A previous study utilising a ligand-based approach to identify endogenous targets for Maltanedienol discovered a potential of 59 candidates. The targets were filtered, based on their relationship to bone remodelling or calcium fixation, narrowing these to 36, of which only 26 were crystallographically described on the protein data bank. These 26 targets represented the study cohort. For each target, the small cognate molecule was extracted from its ligand binding pocket (LBP) and mutual affinity calculated in each case. Maltanedienol was subsequently docked into each target *apo* LBP and conformational analysis carried out. The conformer with the greatest peak height difference, between ligand binding affinity (pKd) and ligand binding energy (kcal/mol), was the optimal conformer and identified as the most likely bioactive scaffold based on high affinity and greatest stability.

Seven of the 26 identified targets bound to Maltanedienol with higher affinity than their co-crystallised ligand. These targets were used for *de novo* design and formulated hypotheses regarding the biological activity of Maltanedienol.

A 2D topology map was used to illustrate Maltanedienol's optimal conformers interactions with its respective receptor active site. Additionally, this was used to exhibit the pharmacophoric moieties which were inhibiting the receptor's active site. Different seeds were produced from each optimal conformer and allowed growth in each of their respective *apo* receptors.

These seed structures were then filtered according to affinity and activity at their respective target LBP. Based on evidence from literature, a hypothesis of which of the selected receptors should be further studied as potential *in vivo* targets for Maltanedienol and mediators of calcium deposition in association with this molecule was made.

Acknowledgements

I would like to express my sincere gratitude to my supervisor, Doctor Claire Shoemake, of the Pharmacy Department, Faculty of Medicine and Surgery at the University of Malta, for her support, patience and guidance throughout the process of writing this dissertation.

A special thanks also goes to Professor Lilian Azzopardi, Professor Anthony Serracino Inglott and all the staff of the Pharmacy Department, Faculty of Medicine and Surgery at the University of Malta.

I would also like to convey my heartfelt appreciation towards the pharmacists and all the staff at Balzan Pharmacy, my family and friends who supported me and helped throughout the five years.

Table of Contents:

List of Tables ..... **viii**

List of Figures ..... **xiii**

Glossary ..... **xxii**

List of Abbreviations ..... **xxv**

Chapter 1 Introduction **1**

1.1 Discovery 2

1.2 *Padina pavonica* 3

1.3 Structure of Maltanedienol 4

1.4 Previous studies carried out 6

1.4.1 Previously investigated endogenously expressed targets for Maltanedienol 6

1.4.2 *In vivo* results 7

1.5 Additional Uses for Maltanedienol 9

1.6 Potential Endogenous Targets for Maltanedienol 10

1.6.1 Prostaglandin E Synthase (PGES) 13

1.6.2 Oestrogen Receptor (ER) 14

1.6.3 Glucocorticoid Receptor (GR) 15

1.6.4 Sex Hormone-Binding Globulin 17

1.6.5 Cholinesterase 18

1.6.6 Progesterone Receptor (PR) 19

1.6.7 Insulin-Like Growth Factor 1 Receptor (IGF-1) 20

1.6.8 Mineralocorticoid Receptor (MR) 21

1.6.9 Cytochrome P450 3A4 22

1.6.10 Androgen Receptor (AR) 23

1.6.11 Vitamin D3 Receptor 24

1.6.12 Aromatase 25

1.6.13 Proto-Oncogene Tyrosine-Protein Kinase Src 26

1.6.14 Oestradiol 17-Beta-Dehydrogenase 1 27

1.6.15 Aldo-Keto Reductase Family 1 Member B1 28

1.6.16 Tyrosine-Protein Phosphatase Non-Receptor Type 2 (PTPN2) 29

1.6.17 Tyrosine-Protein Phosphatase Non-Receptor Type 1 (PTP-1B) 29

1.6.18 3-Oxo-5-Alpha-Steroid 4-Dehydrogenase 1 30
1.6.19 Acetylcholinesterase (AChE) 30
1.6.20 Low Molecular Weight Phosphotyrosine Protein Phosphatase 31
1.6.21 Corticosteroid 11-Beta-Dehydrogenase Isozyme 1 32
1.6.22 M-Phase Inducer Phosphatase 2 33
1.6.23 Tyrosine-Protein Kinase Receptor UFO 34
1.6.24 3-Oxo-5-Alpha Steroid 4-Dehydrogenase 2 35
1.6.25 Nitric Oxide Synthase, Inducible 36
1.6.26 Vascular Endothelial Growth Factor Receptor 2 (VEGFR2) 36
1.6.27 Testosterone 17-Beta-Dehydrogenase 3 38
1.6.28 Oestradiol 17-Beta-Dehydrogenase 2 38
1.6.29 Corticosteroid 11-Beta-Dehydrogenase Isozyme 2 38
1.6.30 Focal Adhesion Kinase 1 38
1.6.31 Peptidyl-Prolyl Cis-Trans Isomerase NIMA-Interacting 1 (PIN1) 39
1.6.32 Voltage-Dependent L-Type Calcium Channel Subunit Alpha-1C 40
1.6.33 Hypoxia-Inducible Factor 1-Alpha 41
1.6.34 G-Protein Coupled Bile Acid Receptor 1 41
1.6.35 Oestrogen Receptor Beta 41
1.6.36 Cysteine Protease ATG4B 42
1.7 Computational Design 43

1.7.1 BIOVIA Draw® 43
1.7.2 BIOVIA Discovery Studio Visualizer® 43
1.7.3 Sybyl®-X 43
1.7.4 X-Score 44
1.7.5 LigBuilder® 44
1.8 Aim and Objectives 46

Chapter 2 Methodology 47
2.1 Introduction and study overview 48

2.2 Selection of targets related to *in vivo* calcium deposition or bone remodelling ... 50

2.3 Selection of target receptors on the PDB 54

2.4 Extraction of Ligands 57

2.5 Conformational Analysis 58

2.5.1 Calculating the Ligand Binding Energy (LBE) (kcal/mol) 58
2.5.2 Calculating the Ligand Binding Affinity (LBA) (pKd) 58
2.5.3 Choosing the Optimal Conformer 59
2.6 Recruiting Receptor Targets 60
2.7 2D Topology Maps 61

2.7.1 Docking Optimal Conformer of Maltanedienol to the *apo* receptor 61
2.7.2 Creating 2D Ligand Protein Contact Maps 61
2.8 *De novo* Drug Design 63

2.8.1 Creating 3D maps of the LBP 63
2.8.2 Creating Seed Structures 63
Chapter 3 Results 68
3.1 Estimating the LBA and LBE of Maltanedienol conformers 69

3.2 Comparison of LBA 83

3.3 *De novo* Growth 88

3.3.1 2D Ligand Protein Contact Maps 88
3.3.2 Seed Structures 95
3.3.3 Ligands Generated by Structure-Based Drug Design 101
Chapter 4 Discussion 141
References 154
List of Publications and Abstracts 171
Appendices 172

List of Tables

Table Number	Table Title	Page
1.1	Potential targets (n=59) for Maltanedienol as identified through a bioinformatics-based approach.	10
2.1	Group A - Potential *in vivo* targets (n=36) for Maltanedienol as identified by the data mining software of D'Emanuele (2019) whose function is related to calcium fixation or bone remodelling.	50
2.2	Group B - Potential *in vivo* targets (n=23) for Maltanedienol as identified by the data mining software of D'Emanuele (2019) whose function is not related to calcium fixation or bone remodelling.	52
2.3	Potential *in vivo* targets (n=26) for Maltanedienol as identified by the data mining software of D'Emanuele (2019) which are crystallographically resolved on the PDB and whose function is related to calcium fixation or bone remodelling, which were consequently recruited for this study.	54
2.4	Parameters used in the GROW algorithm in LigBuilder® v1.2 to generate *de novo* molecules.	65
2.5	Parameters used for the PROCESS algorithm in LigBuilder® v1.2.	66
2.6	Parameters set to filter the results from the molecules produced by LigBuilder® v1.2 in Microsoft Excel, according to Lipinski's Rule of 5.	67
3.1	LBA (pKd) of the optimal conformers of Maltanedienol for its potential *in vivo* targets (n=26) as identified by the datamining software of D'Emanuele (2019) whose function is related to calcium	83

fixation or bone remodelling and which are crystallographically resolved on the PDB.

3.2 LBA (pKd) of the optimal conformers of Maltanedienol for its potential *in vivo* targets (n=7), as identified by the data mining software of D'Emanuele (2019). which are crystallographically resolved on the PDB and which had a LBA (pKd) of Maltanedienol for its specific target which is greater or equal to that of the bound small molecule for its specific target. 85

3.3 Potential *in vivo* targets (n=19) for Maltanedienol, as identified by the datamining software of D'Emanuele (2019) which are crystallographically resolved the PDB and which have a LBA (pKd) of Maltanedienol for its specific target which is smaller than that of the bound small molecule for its specific target. 86

3.4 Seed molecules of Maltanedienol for the Acetylcholinesterase Receptor (PDB 1VOT) with selected H.spc atoms represented by a light blue stick, capable of sustaining molecular growth. Seeds were generated in Sybyl®-X v1.1. 95

3.5 Seed molecules of Maltanedienol for the Corticosteroid 11-Beta-Dehydrogenase Isozyme 1 (PDB 2RBE) with selected H.spc atoms represented by a light blue stick, capable of sustaining molecular growth. Seeds were generated in Sybyl®-X v1.1. 96

3.6 Seed molecules of Maltanedienol for the Low Molecular Weight Phosphotyrosine Protein Phosphatase (PDB 5JNT) with selected H.spc atoms represented by a light blue stick, capable of sustaining molecular growth. Seeds were generated in Sybyl®-X v1.1. 97

3.7	Seed molecules of Maltanedienol for the Peptidyl-Prolyl Cis-Trans Isomerase NIMA-Interacting 1 (PDB 6DUN) with selected H.spc atoms represented by a light blue stick, capable of sustaining molecular growth. Seeds were generated in Sybyl®-X v1.1.	98
3.8	Seed molecules of Maltanedienol for the Progesterone Receptor (PDB 3ZR7) with selected H.spc atoms represented by a light blue stick, capable of sustaining molecular growth. Seeds were generated in Sybyl®-X v1.1.	99
3.9	Seed molecules of Maltanedienol for the Sex Hormone-Binding Globulin (PDB 1LHU) with selected H.spc atoms represented by a light blue stick, capable of sustaining molecular growth. Seeds were generated in Sybyl®-X v1.1.	100
3.10	The highest affinity molecule generated from each family for the Acetylcholinesterase Receptor (PDB 1VOT) 1votseed10.	101
3.11	The highest affinity molecule generated from each family for the Corticosteroid 11-Beta-Dehydrogenase Isozyme 1 (PDB 2RBE) 2rbeseed2.	106
3.12	The highest affinity molecule generated from each family for the Corticosteroid 11-Beta-Dehydrogenase Isozyme 1 (PDB 2RBE) 2rbeseed7.	110
3.13	The highest affinity molecule generated from each family for the Low Molecular Weight Phosphotyrosine Protein Phosphatase (PDB 5JNT) 5jntseed5.	112

3.14	The highest affinity molecule generated from each family for the Low Molecular Weight Phosphotyrosine Protein Phosphatase (PDB 5JNT) 5jntseed6.	116
3.15	The highest affinity molecule generated from each family for the Peptidyl-Prolyl Cis-Trans Isomerase NIMA-Interacting 1 (PDB 6DUN) 6dunseed7.	118
3.16	The highest affinity molecule generated from each family for the Peptidyl-Prolyl Cis-Trans Isomerase NIMA-Interacting 1 (PDB 6DUN) 6dunseed8.	121
3.17	The highest affinity molecule generated from each family for the Progesterone Receptor (PDB 3ZR7) 3zr7seed7.	124
3.18	The highest affinity molecule generated from each family for the Progesterone Receptor (PDB 3ZR7) 3zr7seed8.	126
3.19	The highest affinity molecule generated from each family for the Sex Hormone-Binding Globulin (PDB 1LHU) 1lhuseed7.	131
3.20	The highest affinity molecule generated from each family for the Sex Hormone-Binding Globulin (PDB 1LHU) 1lhuseed8.	138
4.1	Shows the critical bonding interactions between the optimal conformer of Maltanedienol for the PR, the highest affinity *de novo* design molecule and the endogenous molecule of the PDB ID 3ZR7 as small ligands, and the amino acids lining the LBP perimeter. Amino acid interactions common to all three can be see above the dark line.	149

4.2	Table showing the unfavourable bumps forged between the optimal conformer of Maltanedienol and the highest affinity *de novo* design molecule with the amino acids lining the LBP perimeter.	150
4.3	Comparing the affinities (pKd) of the optimal conformer of Maltanedienol, the highest affinity *de novo* design molecule and the endogenous molecule.	150

List of Figures

Figure Number	Figure Title	Page
1.1	2D representation of Maltanedienol.	4
1.2	3D representation of Maltanedienol, the active principle of the marine alga *Padina pavonica.*	5
1.3	2D representation of 17-beta-oestradiol.	7
1.4	The structure of Prostaglandin E Synthase bound to an inhibitor.	14
1.5	The structure of the Oestrogen Receptor in complex with 4-Hydroxytamoxifen.	15
1.6	The structure of the Glucocorticoid Receptor bound to an antagonist.	16
1.7	The structure of Sex Hormone-Binding Globulin in complex with Oestradiol.	17
1.8	The structure of Acetylcholinesterase in complex with Dihydrotanshinone I.	18
1.9	The structure of the Progesterone Receptor bound to progesterone receptor modulators.	19
1.10	The structure of the Insulin-Like Growth Factor 1 Receptor in complex with a pyrimidine inhibitor.	20
1.11	The structure of the Mineralocorticoid Receptor bound to Aldosterone.	21
1.12	The structure of Cytochrome P450 3A4 bound to glycerol.	22
1.13	The structure of the Androgen Receptor bound to a small molecule.	23

1.14	The structure of the Vitamin D3 Receptor bound to (4S)-4-hydroxy-5-[2-methyl-4-(3-{3-methyl-4-[4,4,4-trifluoro-3-hydroxy-3-(trifluoromethyl)but-1-yn-1-yl]phenyl}pentan-3-yl)phenoxy]pentanoic acid.	24
1.15	The structure of Aromatase in complex with Androstenedione.	25
1.16	The structure of Proto-Oncogene Tyrosine-Protein Kinase Src bound to Kinase Inhibitor Bosutinib.	26
1.17	The structure of Oestradiol 17-Beta-Dehydrogenase 1 complexed with 3-{[(9beta,14beta,16alpha,17alpha)-3,17-dihydroxyestra-1,3,5(10)-trien-16-yl]methyl}benzamide.	27
1.18	The structure of Aldo-Keto Reductase Family 1 Member B1complexed with Schl12134 (3-[5-(3-nitrophenyl)-2-thienyl]propanoic acid).	28
1.19	The structure of Tyrosine-Protein Phosphatase Non-Receptor Type 1 complexed with 5-Iodo-2-(Oxalyl-Amino)-Benzoic Acid.	29
1.20	The structure of Acetylcholinesterase complexed with Huperzine A.	31
1.21	The structure of Low Molecular Weight Phosphotyrosine Protein Phosphatase complexed with 2-(N-Morpholino)-Ethanesulfonic Acid.	32
1.22	The structure of Corticosteroid 11-Beta-Dehydrogenase Isozyme 1 complexed with 2-anilinothiazolones.	33
1.23	The structure of the M-Phase Inducer Phosphatase 2 with a bound inhibitor.	34
1.24	The structure of Tyrosine-Protein Kinase Receptor UFO in complex with a macrocyclic inhibitor.	35

1.25	The structure of Inducible Nitric Oxide Synthase with inhibitor AR-C95791.	36
1.26	The structure of Vascular Endothelial Growth Factor Receptor 2 in complex with a novel 4-amino-furo[2,3-d]pyrimidine.	37
1.27	The structure of Focal Adhesion Kinase 1 in complex with N-{3-[(5-Cyano-2-Phenyl-1h-Pyrrolo[2,3-B]Pyridin-4-Ylamino)-Methyl]-Pyridin-2-Yl}-N-Methyl-Methanesulfonamide.	39
1.28	The structure of Peptidyl-Prolyl Cis-Trans Isomerase NIMA-Interacting 1 in complex with Trihydroxyarsenite (III).	40
1.29	The structure of Oestrogen Receptor Beta in Complex with (R,R)-5,11-cis-diethyl-5,6,11,12-tetrahydrochrysene-2,8-diol.	42
3.1	Graph of LBA (pKd) on the primary y-axis and LBA (kcal/mol) on the secondary y-axis vs Conformer Number on the x-axis for Maltanedienol docked into the LBP of Prostaglandin E Synthase as described in PDB ID: 5T37.	70
3.2	Graph of LBA (pKd) on the primary y-axis and LBA (kcal/mol) on the secondary y-axis vs Conformer Number on the x-axis for Maltanedienol docked into the LBP of the Oestrogen Receptor as described in PDB ID: 3ERT.	70
3.3	Graph of LBA (pKd) on the primary y-axis and LBA (kcal/mol) on the secondary y-axis vs Conformer Number on the x-axis for Maltanedienol docked into the LBP of the Glucocorticoid Receptor as described in PDB ID: 1NHZ.	71
3.4	Graph of LBA (pKd) on the primary y-axis and LBA (kcal/mol) on the secondary y-axis vs Conformer Number on the x-axis for	71

	Maltanedienol docked into the LBP of the Sex Hormone-Binding Globulin as described in PDB ID: 1LHU.	
3.5	Graph of LBA (pKd) on the primary y-axis and LBA (kcal/mol) on the secondary y-axis vs Conformer Number on the x-axis for Maltanedienol docked into the LBP of Cholinesterase as described in PDB ID: 4M0E.	72
3.6	Graph of LBA (pKd) on the primary y-axis and LBA (kcal/mol) on the secondary y-axis vs Conformer Number on the x-axis for Maltanedienol docked into the LBP of the Progesterone Receptor as described in PDB ID: 3ZR7.	72
3.7	Graph of LBA (pKd) on the primary y-axis and LBA (kcal/mol) on the secondary y-axis vs Conformer Number on the x-axis for Maltanedienol docked into the LBP of the Insulin-Like Growth Factor 1 Receptor as described in PDB ID: 5FXS.	73
3.8	Graph of LBA (pKd) on the primary y-axis and LBA (kcal/mol) on the secondary y-axis vs Conformer Number on the x-axis for Maltanedienol docked into the LBP of the Mineralocorticoid Receptor as described in PDB ID: 2AA2.	73
3.9	Graph of LBA (pKd) on the primary y-axis and LBA (kcal/mol) on the secondary y-axis vs Conformer Number on the x-axis for Maltanedienol docked into the LBP of the Cytochrome P450 3A4 as described in PDB ID: 5VCC.	74
3.10	Graph of LBA (pKd) on the primary y-axis and LBA (kcal/mol) on the secondary y-axis vs Conformer Number on the x-axis for	74

	Maltanedienol docked into the LBP of the Androgen Receptor as described in PDB ID: 2PIV.	
3.11	Graph of LBA (pKd) on the primary y-axis and LBA (kcal/mol) on the secondary y-axis vs Conformer Number on the x-axis for Maltanedienol docked into the LBP of the Vitamin D3 Receptor as described in PDB ID: 3W0A.	75
3.12	Graph of LBA (pKd) on the primary y-axis and LBA (kcal/mol) on the secondary y-axis vs Conformer Number on the x-axis for Maltanedienol docked into the LBP of Aromatase as described in PDB ID: 3EQM.	75
3.13	Graph of LBA (pKd) on the primary y-axis and LBA (kcal/mol) on the secondary y-axis vs Conformer Number on the x-axis for Maltanedienol docked into the LBP of the Proto-Oncogene Tyrosine-Protein Kinase Src as described in PDB ID: 4MXO.	76
3.14	Graph of LBA (pKd) on the primary y-axis and LBA (kcal/mol) on the secondary y-axis vs Conformer Number on the x-axis for Maltanedienol docked into the LBP of Oestradiol 17-Beta-Dehydrogenase 1 as described in PDB ID: 3HB4.	76
3.15	Graph of LBA (pKd) on the primary y-axis and LBA (kcal/mol) on the secondary y-axis vs Conformer Number on the x-axis for Maltanedienol docked into the LBP of the Aldo-Keto Reductase Family 1 Member B1 as described in PDB ID: 4YU1.	77
3.16	Graph of LBA (pKd) on the primary y-axis and LBA (kcal/mol) on the secondary y-axis vs Conformer Number on the x-axis for	77

	Maltanedienol docked into the LBP of the Tyrosine-Protein Phosphatase Non-Receptor Type 1 as described in PDB ID: 1ECV.	
3.17	Graph of LBA (pKd) on the primary y-axis and LBA (kcal/mol) on the secondary y-axis vs Conformer Number on the x-axis for Maltanedienol docked into the LBP of Acetylcholinesterase as described in PDB ID: 1VOT.	78
3.18	Graph of LBA (pKd) on the primary y-axis and LBA (kcal/mol) on the secondary y-axis vs Conformer Number on the x-axis for Maltanedienol docked into the LBP of the Low Molecular Weight Phosphotyrosine Protein Phosphatase as described in PDB ID: 5JNT.	78
3.19	Graph of LBA (pKd) on the primary y-axis and LBA (kcal/mol) on the secondary y-axis vs Conformer Number on the x-axis for Maltanedienol docked into the LBP of the Corticosteroid 11-Beta-Dehydrogenase Isozyme 1 as described in PDB ID: 2RBE.	79
3.20	Graph of LBA (pKd) on the primary y-axis and LBA (kcal/mol) on the secondary y-axis vs Conformer Number on the x-axis for Maltanedienol docked into the LBP of the M-Phase Inducer Phosphatase 2 as described in PDB ID: 4WH9.	79
3.21	Graph of LBA (pKd) on the primary y-axis and LBA (kcal/mol) on the secondary y-axis vs Conformer Number on the x-axis for Maltanedienol docked into the LBP of the Tyrosine-Protein Kinase Receptor UFO as described in PDB ID: 5U6B.	80
3.22	Graph of LBA (pKd) on the primary y-axis and LBA (kcal/mol) on the secondary y-axis vs Conformer Number on the x-axis for	80

	Maltanedienol docked into the LBP of Nitric Oxide Synthase Inducible as described in PDB ID: 3EG7.	
3.23	Graph of LBA (pKd) on the primary y-axis and LBA (kcal/mol) on the secondary y-axis vs Conformer Number on the x-axis for Maltanedienol docked into the LBP of the Vascular Endothelial Growth Factor Receptor 2 as described in PDB ID: 1YWN.	81
3.24	Graph of LBA (pKd) on the primary y-axis and LBA (kcal/mol) on the secondary y-axis vs Conformer Number on the x-axis for Maltanedienol docked into the LBP of the Focal Adhesion Kinase 1 as described in PDB ID: 4GU6.	81
3.25	Graph of LBA (pKd) on the primary y-axis and LBA (kcal/mol) on the secondary y-axis vs Conformer Number on the x-axis for Maltanedienol docked into the LBP of Peptidyl-Prolyl Cis-Trans Isomerase NIMA-Interacting 1 as described in PDB ID: 6DUN.	82
3.26	Graph of LBA (pKd) on the primary y-axis and LBA (kcal/mol) on the secondary y-axis vs Conformer Number on the x-axis for Maltanedienol docked into the LBP of the Oestrogen Receptor Beta as described in PDB ID: 1L2J.	82
3.27	2D topology map describing the critical ligand binding interactions forged between Maltanedienol and the amino acids lining the LPB ID: 1LHU.	88
3.28	2D topology map describing the critical ligand binding interactions forged between Maltanedienol and the amino acids lining the LPB as described in PDB ID: 3ZR7.	89

3.29	2D topology map describing the critical ligand binding interactions forged between Maltanedienol and the amino acids lining the LPB as described in PDB ID: 5VCC.	90
3.30	2D topology map describing the critical ligand binding interactions forged between Maltanedienol and the amino acids lining the LPB as described in PDB ID: 1VOT.	91
3.31	2D topology map describing the critical ligand binding interactions forged between Maltanedienol and the amino acids lining the LPB as described in PDB ID: 5JNT.	92
3.32	2D topology map describing the critical ligand binding interactions forged between Maltanedienol and the amino acids lining the LPB as described in PDB ID: 2RBE.	93
3.33	2D topology map describing the critical ligand binding interactions forged between Maltanedienol and the amino acids lining the LPB as described in PDB ID: 6DUN.	94
4.1	2D topology map describing the critical ligand binding interactions forged between the optimal conformer of Maltanedienol for the PR and the amino acids lining the LPB as described in PDB ID: 3ZR7 generated in BIOVIA Discovery Studio Visualizer® v20.1.	146
4.2	2D topology map describing the critical ligand binding interactions forged between the highest affinity *de novo* design molecule and the amino acids lining the LPB as described in PDB ID: 3ZR7 generated in BIOVIA Discovery Studio Visualizer® v20.1.	147
4.3	2D topology map describing the critical ligand binding interactions forged between the co-crystallised molecule of the PR and the	148

amino acids lining the LPB as described in PDB ID: 3ZR7 generated in BIOVIA Discovery Studio Visualizer® v20.1.

Glossary

1ECV	the PDB identification code for the Tyrosine-Protein Phosphatase Non-Receptor Type 1
1L2J	the PDB identification code for the Oestrogen Receptor Beta
1LHU	the PDB identification code for the Sex Hormone-Binding Globulin
1NHZ	the PDB identification code for the Glucocorticoid Receptor
1VOT	the PDB identification code for Acetylcholinesterase
1YWN	the PDB identification code for the Vascular Endothelial Growth Factor Receptor 2
2AA2	the PDB identification code for the Mineralocorticoid Receptor
2PIV	the PDB identification code for the Androgen Receptor
2RBE	the PDB identification code for the Corticosteroid 11-Beta-Dehydrogenase Isozyme 1
3E7G	the PDB identification code for the Nitric Oxide Synthase, Inducible
3EQM	the PDB identification code for Aromatase
3ERT	the PDB identification code for the Oestrogen Receptor
3HB4	the PDB identification code for the Oestradiol 17-Beta-Dehydrogenase 1
3W0A	the PDB identification code for the Vitamin D3 Receptor
3ZR7	the PDB identification code for the Progesterone Receptor
4GU6	the PDB identification code for the Focal Adhesion Kinase 1
4M0E	the PDB identification code for the Cholinesterase

4MXO	the PDB identification code for the Proto-Oncogene Tyrosine-Protein Kinase Src
4WH9	the PDB identification code for the M-Phase Inducer Phosphatase 2
4YU1	the PDB identification code for the Aldo-Keto Reductase Family 1 Member B1
5FXS	the PDB identification code for the Insulin-Like Growth Factor 1 Receptor
5JNT	the PDB identification code for the Low Molecular Weight Phosphotyrosine Protein Phosphatase
5T37	the PDB identification code for the Prostaglandin E Synthase
5U6B	the PDB identification code for the Tyrosine-Protein Kinase Receptor UFO
5VCC	the PDB identification code for the Cytochrome P450 3A4
6DUN	the PDB identification code for the Peptidyl-Prolyl Cis-Trans Isomerase NIMA-Interacting 1
apo	an unbound receptor
Conformational Analysis	the special arrangement of molecules and atoms which may adopt different conformations by means of rotation about single bonds
De novo drug design	the generation of novel molecules by implementing molecular modelling studies of a targeted active site
In silico	an action performed computationally in reference to chemistry.
In vitro	an experimental process in a controlled environment outside their normal biological context
In vivo	an experimental procedure performed on a living organism

Lead	a compound that proves to be therapeutically useful due to its chemical and physical properties
Ligand	a chemical structure that binds to a target protein/s
Ligand Binding Affinity	quantified and measured in pKd, it is the ability of a molecule to bind to a receptor's active site
Ligand Binding Energy	quantified and measured in kcal/mol, it is the predicted energy of a ligand – receptor complex
Ligand Binding Pocket	the portion on the surface or interior part of the protein which is able to bind or form an interaction with a ligand
Moieties	the functional group/s in a molecule
Scaffold	the molecular framework of a bioactive compound

List of Abbreviations

2D – Two-dimensional

3D – Three-dimensional

AChE – Acetylcholinesterase

AR - Androgen Receptor

CS – Chemical Score

CDK1 - Cyclin-Dependent Kinase 1

CSF1R - Colony-Stimulating Factor 1 Receptor

DNA - Deoxyribonucleic acid

E1 - Estrone

E2 - Oestradiol

EPP - Extract of *Padina pavonica* (L.)

ER - Oestrogen receptor

FPPS - Farnesyl Pyrophosphate Synthase

GC - Glucocorticoid

GR - Glucocorticoid Receptor

HAC - Hydrogen Acceptor Count

HDC - Hydrogen Donor Count

IGF-1 - Insulin-Like Growth Factor 1 Receptor

IL-1 - Interleukin-1

LBA - Ligand Binding Affinity

LBE - Ligand Binding Energy

LBP - Ligand Binding Pocket

MF – Molecular Formula

MR - Mineralocorticoid Receptor

MW - Molecular Weight

PDB - Protein Data Bank

PGES - Prostaglandin E synthase

PIN1 - Peptidyl-Prolyl Cis-Trans Isomerase NIMA-Interacting 1

PTP-1B - Tyrosine-Protein Phosphatase Non-Receptor Type 1

PTPN2 - Tyrosine-Protein Phosphatase Non-Receptor Type 2

SERM - Selective Oestrogen Receptor Modulators

VEGFR2 - Vascular Endothelial Growth Factor Receptor 2

YAP - Yes-Associated Protein

Chapter 1

Introduction

1.1 Discovery

Many different species of marine algae are currently being researched and studied as they produce substances which could make potential useful lead molecules. These molecules are known as biogenic compounds (Kolanjinathan et al., 2014) and due to their exceptional biological effects, they may bind to endogenous targets, to produce a desirable effect (Smit, 2004; El Gamel, 2010; Al-Enazi et al., 2018). Throughout the years, numerous compounds have been isolated from various types of marine alga and have been used to produce antimicrobial, antiviral, cytotoxic, anti-parasitic and anti-inflammatory drugs, amongst others (Blunden, 2001). Maltanedienol represents such an example. Maltanedienol was discovered and isolated by Gutierrez and Saliba as the active principle of the Mediterranean alga *Padina pavonica*. The active components of this seaweed were investigated following the observation that this alga was capable of calcium deposition, through its fronds. [1,2,3]

[1] The Malta Independent. A molecule made in Malta [Internet]. Malta: The Malta Independent; 2004 [cited 2021 Jul 14]. Available from: http://www.independent.com.mt/articles/2004-04-23/news/a-molecule-made-in-malta-65552/.

[2] The Malta Independent. Research on agriculture products used to cope with physical stress [Internet]. Malta; The Malta Independent; 2004 [cited 2021 Jul 14]. Available from: http://www.independent.com.mt/articles/2004-12-22/news/research-on-agriculture-products-used-to-cope-with-physical-stress-70212/.

[3] The Times of Malta. Seaweed extract being turned into a food supplement [Internet]. Malta; The Times of Malta; 2004 [cited 2021 Jul 14]. Available from: https://www.timesofmalta.com/articles/view/20041218/local/seaweed-extract-being-turned-into-a-food-supplement.104206.

1.2 *Padina pavonica*

Maltanedienol originates from *Padina pavonica* (L.), an alga indigenous to the Atlantic Ocean and Mediterranean Sea (Pace Debono, 1998). However, it can also be found in the Indian Ocean, Pacific Ocean and limits of the British Isles, which are namely tropical and temperate seas (Silberfeld et al., 2013). Also known as Peacock's tail (Ismail et al., 2016), this species belongs to a class of brown algae called Phaephycea and in the order Dictyotales (Khaled et al., 2012; Herbert et al., 2016). Distinct, in its own way, *Padina* is the only calcareous genus of the Phaeophyceae class (Okazaki et al., 1986). All brown algae, together with the red and the green algae may also be grouped together and are collectively known as macroalgae. These macroalge are used as bio-indicators in the marine environment. The bio-indicative property of these species is carried out by measuring the amount of unusual white appearance on its fan-shaped thallus surface (El Gamal, 2010; Gil-Díaz et al., 2014). It was shown that the unusual white appearance on the surface of the thallus, was due to a non-spontaneous deposition of calcium carbonate in the aragonite form. This finding led to the hypothesis that *Padina pavonica* (L.) was capable of synthesising and emitting a substance that had a positive effect on calcium fixation through its fronds (Galea, 2009). These aragonite needles deposited in concentric zones on the species' thallus were only produced under strict environmental conditions of pressure and temperature (Okazaki et al., 1986; Johnson et al., 2012; Cassar et al., 2013; Falzon, 2017).

1.3 Structure of Maltanedienol

The main extract of *Padina pavonica* (L.) (EPP) has been resolved, concluded and registered as Maltanedienol, as can be seen in Figures 1.1 and 1.2 below. It was officially named in mid-February 2004, after the island of Malta. This is due to the abundance of the algae growth seen on the southern side of the Mediterranean.[1]

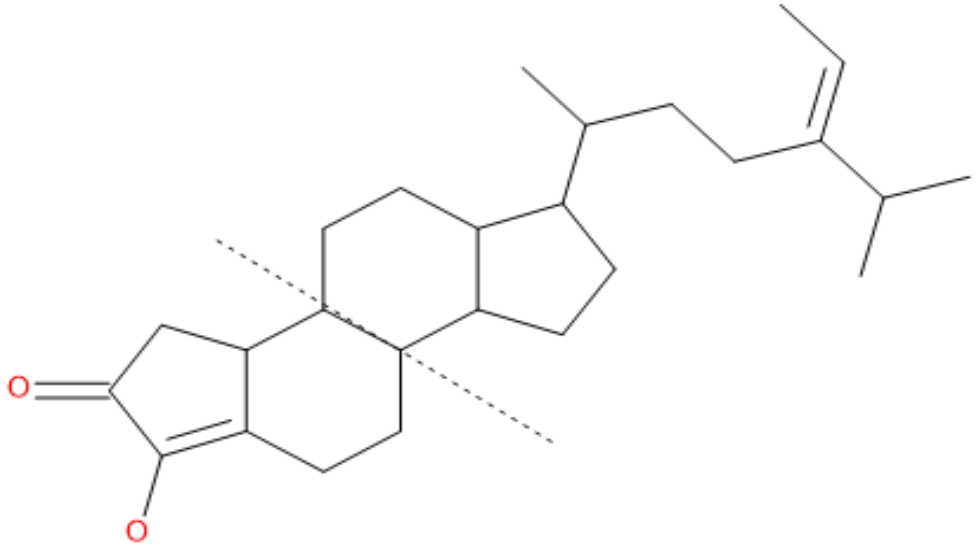

Figure 1.1 2D representation of Maltanedienol rendered in BIOVIA Draw® v17.1.[4] The dotted line indicates the symmetry of the molecule.

[1] The Malta Independent. A molecule made in Malta [Internet]. Malta: The Malta Independent; 2004 [cited 2021 Jul 14]. Available from: http://www.independent.com.mt/articles/2004-04-23/news/a-molecule-made-in-malta-65552/.
[4] Dassault Systèmes. BIOVIA Draw. Version 17.1 [software]. Dassault Systèmes. 2017 [cited 2021 Jul 14; downloaded 2021 May 25]. Available from: https://hts.c2b2.columbia.edu/draw/.

This symmetrical molecule has an empirical formula of $C_{28}H_{44}O_2$. Its structure is made up of two cyclohexane rings attached to each other creating a plane of attachment and at each end bonded to a 5-cyclic carbon structure. This overall 3D structural formation resembles a primitive steroidal molecule. This central symmetry is characteristically seen in numerous primitive compounds such as the tetraterpenes and the carotenoids (Cassar et al., 2013).

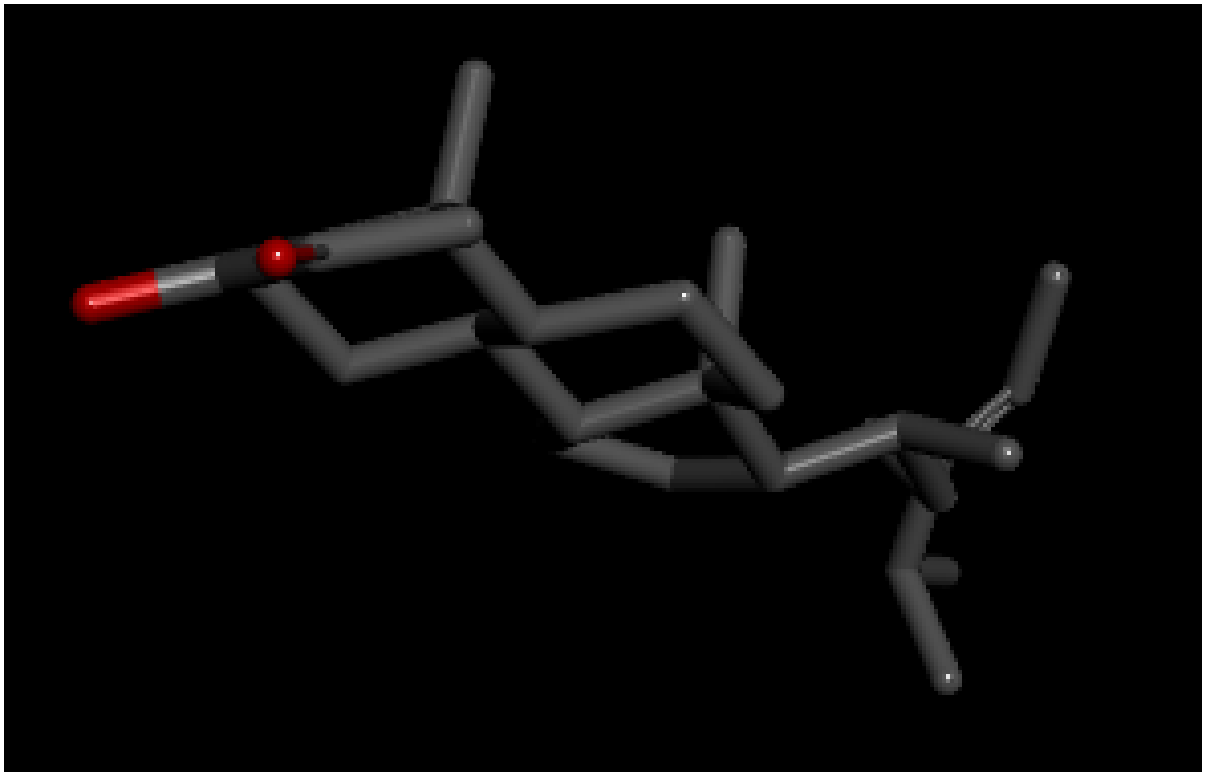

Figure 1.2 3D representation of Maltanedienol, the active principle of the marine alga *Padina pavonica* as modelled in Sybyl®-X (Ash et al., 2010).

1.4 Previous studies carried out

1.4.1 Previously investigated endogenously expressed targets for Maltanedienol

This study is a continuation of 2 previous studies carried out at the University of Malta by Cassar et al., (2013) and Falzon (2017), in which Maltanedienol was challenged with two endogenous receptors; these were the Oestrogen Receptor (ER) and Farnesyl Pyrophosphate Synthase (FPPS) receptor, respectively. Both of these targets are involved in bone deposition which explains the evident calcium fixation properties of this molecule.

The ER receptor was investigated based on the similarity between Maltanedienol and 17-beta-oestradiol as seen in Figure 1.3, the latter molecule being the endogenous ligand for the ER. The ER was even more attractive from an investigational perspective since it has been implicated in the bone mineralisation process with selective oestrogen receptor modulators (SERMs) such as raloxifene being used successfully in the management of osteoporosis (Cassar et al., 2013).

On the other hand, the FPPS receptor, is the established target for the bisphosphonate class of drugs of which alendronic and ibandronic acids are examples. The bisphosphonates are FPPS agonists. The result of bisphosphonate mediated FPPS is associated with increased osteoclastic calcium deposition resulting in increased bone turnover rate in post-menopausal women (Cremers & Papapoulos, 2011). Both studies seemed to indicate that Maltanedienol did not mediate its calcium depositing effect at either of these targets, consequently implying that the search for its endogenous target

must continue, in the interest of potentially identifying a novel pathway for bone remineralisation that could be exploited from a drug design perspective (Falzon, 2017).

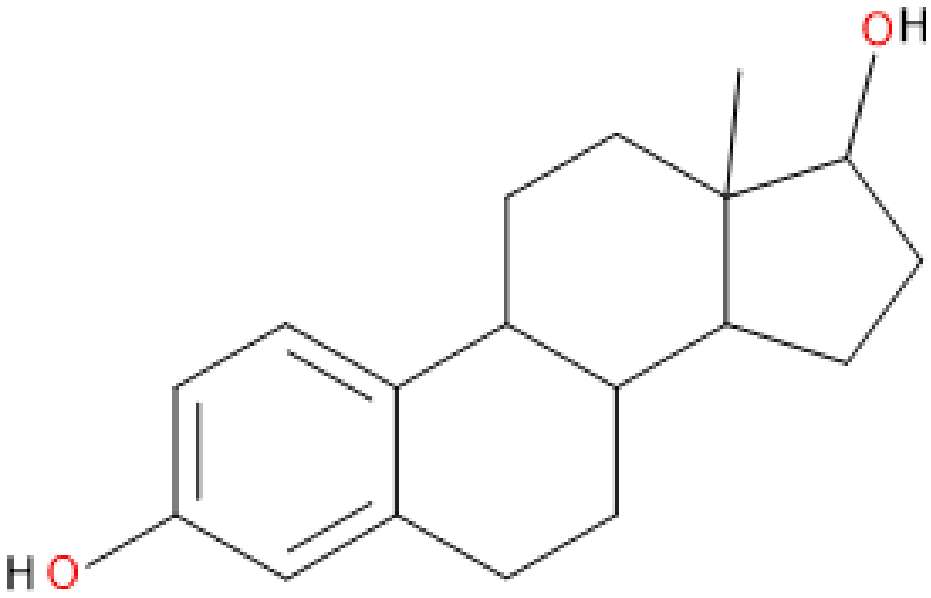

Figure 1.3 2D representation of 17-beta-oestradiol BIOVIA Draw® v17.1. [4]

1.4.2 *In vivo* results

The results of the *in vivo* studies proved that Maltanedienol is capable of calcium fixation and that it may consequently be utilized in managing bone conditions such as osteoporosis (Galea, 2009). Osteoporosis is a highly prevalent condition amongst post-menopausal women, causing significant morbidity among this cohort. In the *in vivo* studies, Maltanedienol showed an increase in calcium fixation through osteoblast activity. The

[4] Dassault Systèmes. BIOVIA Draw. Version 17.1 [software]. Dassault Systèmes. 2017 [cited 2021 Jul 14; downloaded 2021 May 25]. Available from: https://hts.c2b2.columbia.edu/draw/.

osteoblasts are cells which are responsible for laying bone matrix and thus increasing their activity through Maltanedienol and thus causing an increase in bone mass which is highly beneficial in osteoporosis (Krassas & Papadopoulou, 2001; Khalid & Krum, 2016). The increase in calcium fixation by Maltanedienol took place even when it was in the presence of a calcium channel inhibitor or Interleukin-1 (IL-1), proving that calcium fixation does not occur through either alpha and beta subtypes of the ER, found in bone cells (Galea, 2009; Cassar et al., 2013; Khalid & Krum, 2016). However, it is only the beta receptor is involved in bone remodelling. Therefore, it has been suggested by Falzon (2017) that the beta receptor that should be revised, by using *in vitro* assays such that the viability of this target may be exhaustively excluded. As a result, this target will be revisited in this study.

1.5 Additional Uses for Maltanedienol

Maltanedienol also has an additional use as a contemporary food additive in poultry, prawn, rabbit and fish farming. [2,3] In poultry farming, its positive effect on calcium deposition enables battery chickens to stand for longer periods and enables the harvest of more robust eggshells capable of better withstanding transport. In prawn farms, Maltanedienol has supported the rearing of prawns with harder exoskeletons also capable of better withstanding transport conditions (Galea, 2009). Whilst in rabbit farming, it is fed to rabbits as it has proved to have showed an increase in meat growth and decrease in mortality when used for less than 56 days (Guriec et al., 2014).

[2] The Malta Independent. Research on agriculture products used to cope with physical stress [Internet]. Malta; The Malta Independent; 2004 [cited 2021 Jul 14]. Available from: http://www.independent.com.mt/articles/2004-12-22/news/research-on-agriculture-products-used-to-cope-with-physical-stress-70212/.

[3] The Times of Malta. Seaweed extract being turned into a food supplement [Internet]. Malta; The Times of Malta; 2004 [cited 2021 Jul 14]. Available from: https://www.timesofmalta.com/articles/view/20041218/local/seaweed-extract-being-turned-into-a-food-supplement.104206.

1.6 Potential Endogenous Targets for Maltanedienol

This study depends on the results obtained from inhouse data mining software using a bioinformatics perspective, developed by D'Emanuele (2019). The study involved systematically probing the ChEMBL® database (Bento et al., 2014), searching for molecules which were structurally, morphologically and electronically similar to that of Maltanedienol. The targets for this molecule, expressed according to UniProt ID, (The UniProt Consortium, 2017) were subsequently identified, a process which identified 59 potential targets, as seen in the table below. This preliminary data by D'Emanuele (2019) indicates that these are receptors which Maltanedienol can dock into and therefore will be further investigated in this study.

Table 1.1 Potential targets (n=59) for Maltanedienol as identified through a bioinformatics-based approach. Adopted from: D'Emanuele J. Discovery of Medicinal Molecules Based on Similarity Networks [dissertation]. Msida (Malta): University of Malta; 2019.

Number	**UniProt ID**	**Identified Target Name**
1	O00748	Cocaine Esterase
2	O14684	Prostaglandin E Synthase
3	O15245	Solute Carrier Family 22 Member 1
4	O60218	Aldo-Keto Reductase Family 1 Member B10
5	O75469	Nuclear Receptor Subfamily 1 Group I Member 2
6	P03372	Oestrogen Receptor
7	P04150	Glucocorticoid Receptor

8	P04278	Sex Hormone-Binding Globulin
9	P06276	Cholinesterase
10	P06401	Progesterone Receptor
11	P07339	Cathepsin D
12	P08069	Insulin-Like Growth Factor 1 Receptor
13	P08235	Mineralocorticoid Receptor
14	P08684	Cytochrome P450 3A4
15	P10253	Lysosomal Alpha-Glucosidase
16	P10275	Androgen Receptor
17	P10586	Receptor-Type Tyrosine-Protein Phosphatase F
18	P11388	DNA Topoisomerase 2-Alpha
19	P11413	Glucose-6-Phosphate 1-Dehydrogenase
20	P11473	Vitamin D3 Receptor
21	P11511	Aromatase
22	P12931	Proto-Oncogene Tyrosine-Protein Kinase Src
23	P14061	Oestradiol 17-Beta-Dehydrogenase 1
24	P15121	Aldo-Keto Reductase Family 1 Member B1
25	P17706	Tyrosine-Protein Phosphatase Non-Receptor Type 2
26	P18031	Tyrosine-Protein Phosphatase Non-Receptor Type 1
27	P18405	3-Oxo-5-Alpha-Steroid 4-Dehydrogenase 1
28	P22303	Acetylcholinesterase
29	P23415	Glycine Receptor Subunit Alpha-1
30	P24666	Low Molecular Weight Phosphotyrosine Protein Phosphatase
31	P25024	C-X-C Chemokine Receptor Type 1

32	P28845	Corticosteroid 11-Beta-Dehydrogenase Isozyme 1
33	P29350	Tyrosine-Protein Phosphatase Non-Receptor Type 6
34	P30305	M-Phase Inducer Phosphatase 2
35	P30530	Tyrosine-Protein Kinase Receptor UFO
36	P31213	3-Oxo-5-Alpha Steroid 4-Dehydrogenase 2
37	P35228	Nitric Oxide Synthase, Inducible
38	P35968	Vascular Endothelial Growth Factor Receptor 2
39	P37058	Testosterone 17-Beta-Dehydrogenase 3
40	P37059	Oestradiol 17-Beta-Dehydrogenase 2
41	P49354	Protein Farnesyltransferase/Geranylgeranyltransferase Type-1 Subunit Alpha
42	P49356	Protein Farnesyltransferase Subunit Beta
43	P51449	Nuclear Receptor ROR-Gamma
44	P55055	Oxysterols Receptor LXR- Beta
45	P56817	Beta-Secretase 1
46	P80365	Corticosteroid 11-Beta-Dehydrogenase Isozyme 2
47	Q02880	DNA Topoisomerase 2-Beta
48	Q05397	Focal Adhesion Kinase 1
49	Q13133	Oxysterols Receptor LXR-Alpha
50	Q13526	Peptidyl-Prolyl Cis-Trans Isomerase NIMA-Interacting 1
51	Q13936	Voltage-Dependent L-Type Calcium Channel Subunit Alpha-1C
52	Q16665	Hypoxia-Inducible Factor 1-Alpha
53	Q8TDU6	G-Protein Coupled Bile Acid Receptor 1
54	Q92731	Oestrogen Receptor Beta

55	Q9UHC9	NPC1-Like Intracellular Cholesterol Transporter 1
56	Q9UM73	ALK Tyrosine Kinase Receptor
57	Q9Y4P1	Cysteine Protease ATG4B
58	Q9UBE0	SUMO-Activating Enzyme Subunit 1
59	Q9UBT2	SUMO-Activating Enzyme Subunit 2

It is important to note that the ER receptor (Cassar et al., 2013) is listed above as a possible target whilst the FPPS is not (Falzon, 2017). The FPPS receptor which was investigated *in silico*, based on being the target for the bisphosphonates was neither identified by the software of D'Emanuele (2019) nor by *in silico* work as being a potential target for Maltanedienol.

Each of the 59 endogenous receptors from the study conducted by D'Emanuele (2019) were evaluated and recruited into the study exclusively if literature showed that their endogenous function was in some way related to *in vivo* calcium fixation or bone remodelling. This process filtered the recruited targets down to 36. Below is a summary of each of the 36 receptors' function and their link to calcium fixation or bone remodelling.

1.6.1 Prostaglandin E Synthase (PGES)

The PGES enzyme stimulates bone resorption whilst principally converting prostaglandin H2, a cyclooxygenase-derived prostaglandin, to prostaglandin E2 (Murakami et al., 2002; Inada et al., 2006).

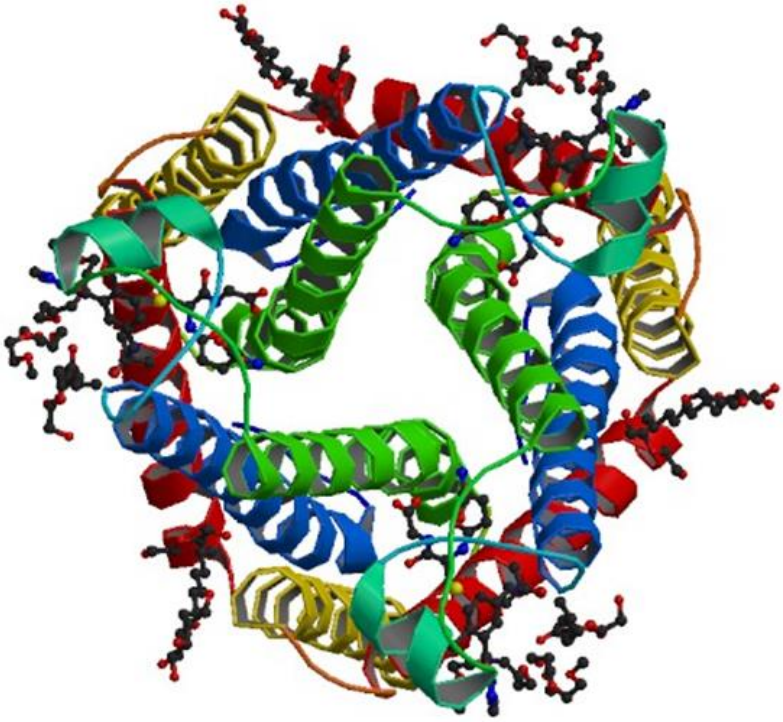

Figure 1.4 The structure of Prostaglandin E Synthase bound to an inhibitor. Adopted from: Partridge KM, Antonysamy S, Bhattachar SN, Chandrasekhar S, Fisher MJ, Fretland A, et al. Discovery and Characterization of [(cyclopentyl)ethyl] benzoic Acid Inhibitors of Microsomal Prostaglandin E Synthase-1. Bioorganic and Medicinal Chemistry Letters. 2017; 27(6):1478-83.

1.6.2 Oestrogen Receptor (ER)

This nuclear hormone receptor binds oestrogen, a sex steroid which is vital in the development of the reproductive organs and bone remodelling, amongst other processes. During menopause there is a decrease of oestrogen binding to this receptor, resulting in a loss of bone mass in various women. There are two ERs subtypes; ER alpha and ER beta, both of which are highly expressed in osteoblasts and osteoclasts, however in this case,

the ER refers to the alpha sub-unit, whilst the beta subunit can be seen in Section 1.6.35 (Manolagas et al., 2013; Bado et al, 2017).

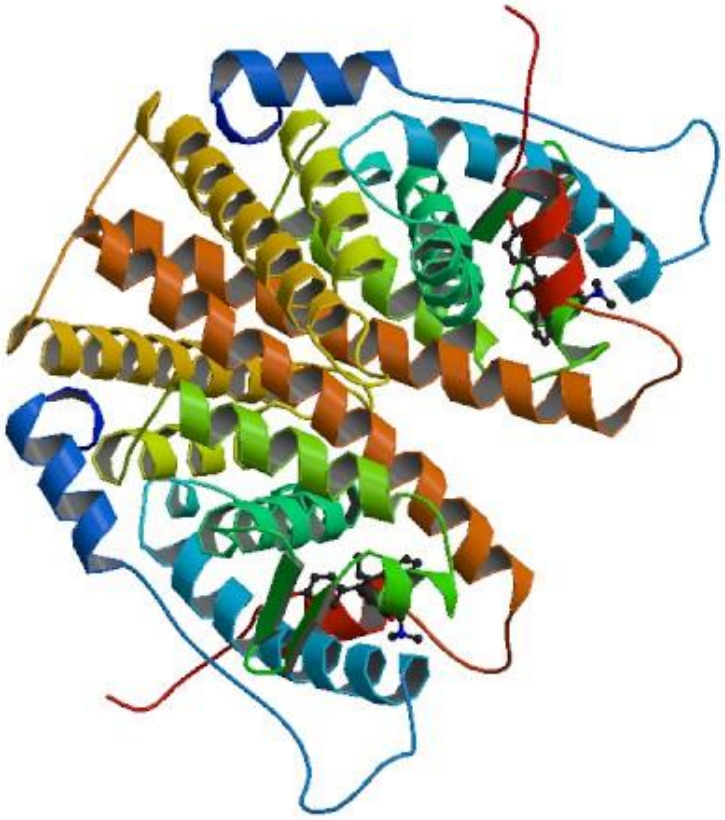

Figure 1.5 The structure of the Oestrogen Receptor in complex with 4-Hydroxytamoxifen. Adopted from: Shiau AK, Barstad D, Loria PM, Cheng L, Kushner PJ, Agard DA, et al. The Structural Basis of Oestrogen Receptor/Coactivator Recognition and the Antagonism of This Interaction by Tamoxifen. Cell. 1998; 95(7):927-37.

1.6.3 Glucocorticoid Receptor (GR)

The GR is a nuclear hormone receptor, expressed in all bone cells. When glucocorticoids (GCs) bind to the GR, they control the functions of this receptor by inhibiting osteoblast proliferation, regulating the development of osteoclasts and induce apoptotic pathway for osteoblasts and osteocytes. GCs are also involved in regulating several signalling

molecules such as growth factors and cytokines which are linked to the bone metabolism process (Moutsatsou et al., 2012).

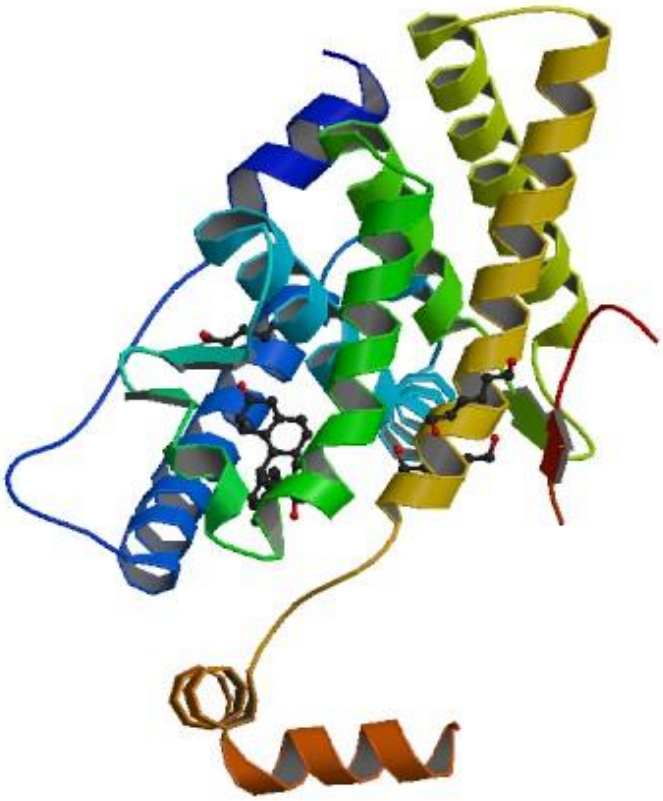

Figure 1.6 The structure of the Glucocorticoid Receptor bound to an antagonist. Adopted from: Kauppi B, Jakob C, Färnegårdh M, Yang J, Ahola H, Alarcon M, et al. The three-dimensional structures of antagonistic and agonistic forms of the glucocorticoid receptor ligand-binding domain: RU-486 induces a transconformation that leads to active antagonism. The Journal of Biological Chemistry [Internet]. 2003; 278(25):22748-54 [cited 2021 Jul 14]. Available from: http://www.jbc.org/cgi/pmidlookup?view=long&pmid=12686538.

1.6.4 Sex Hormone-Binding Globulin

This plasma glycoprotein binds gonadocorticoid molecules and studies have shown that Sex Hormone-Binding Globulin plays a part in bone remodelling. An increase this glycoprotein results in a decrease in bioavailable sex steroids (which are beneficial for bone formation) and thus causes a significant amount of bone loss (Legrand et al., 2001; Hoppé et al., 2010).

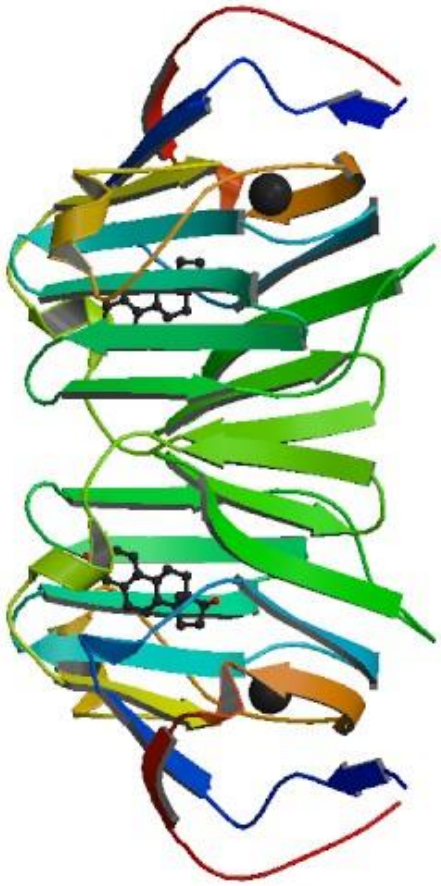

Figure 1.7 The structure of Sex Hormone-Binding Globulin in complex with Oestradiol. Adopted from: Grishkovskaya I, Avvakumov GV, Hammond GL, Catalano MG, Muller YA. Steroid Ligands Bind Human Sex Hormone-Binding Globulin in Specific Orientations and Produce Distinct Changes in Protein Conformation. The Journal of Biological Chemistry [Internet]. 2002; 277(35):32086-93 [cited 2021 Jul 14]. Available from: http://www.jbc.org/cgi/pmidlookup?view=long&pmid=12065592.

1.6.5 Cholinesterase

Also known as butyrylcholinesterase, this enzyme (to a lesser extent) hydrolyses acetylcholine together with acetylcholinesterase (AChE). However, it was discovered that this enzyme may be found in other non-neuronal cells such as bony tissue, where it may carry out the mentioned hydrolysis reaction during bone development. This protein's concentration in bone depends on blood supply. An experiment carried out by Spieker et al., (2017) showed a substantial increase in bone differentiation in the absence of cholinesterase and concluded that this enzyme may be associated with osteoclastic function (Haupt et al., 2015; Spieker et al., 2016; Spieker et al., 2017).

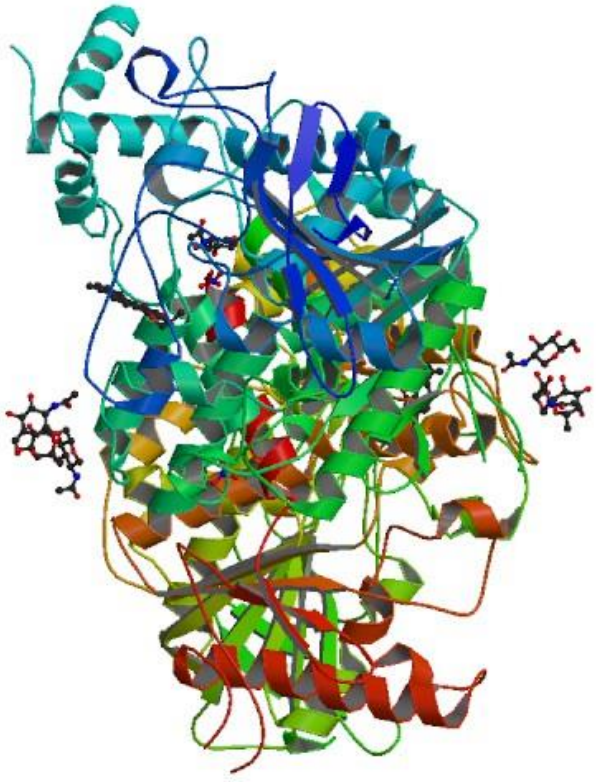

Figure 1.8 The structure of Acetylcholinesterase in complex with Dihydrotanshinone I. Adopted from: Cheung J, Gary EN, Shiomi K, Rosenberry TL. Structures of Human Acetylcholinesterase Bound to Dihydrotanshinone I and Territrem B Show Peripheral

Site Flexibility. American Chemical Society Medicinal Chemistry Letters [Internet]. 2013; 4(11):1091-6 [cited 2021 Jul 14]. Available from: https://pubs.acs.org/doi/10.1021/ml400304w

1.6.6 Progesterone Receptor (PR)

This receptor has a vital role in the reproductive system; however, the PR receptor is highly expressed in bone tissue (in osteoblasts and osteoclasts) and plays an important part in this organ's homeostasis. It has been proved that during rapid growth periods, the PR inhibits bone acquisition and formation. On the other hand, when this receptor was inhibited, there was augmentation of bone mass and bone formation (Yao et al., 2010).

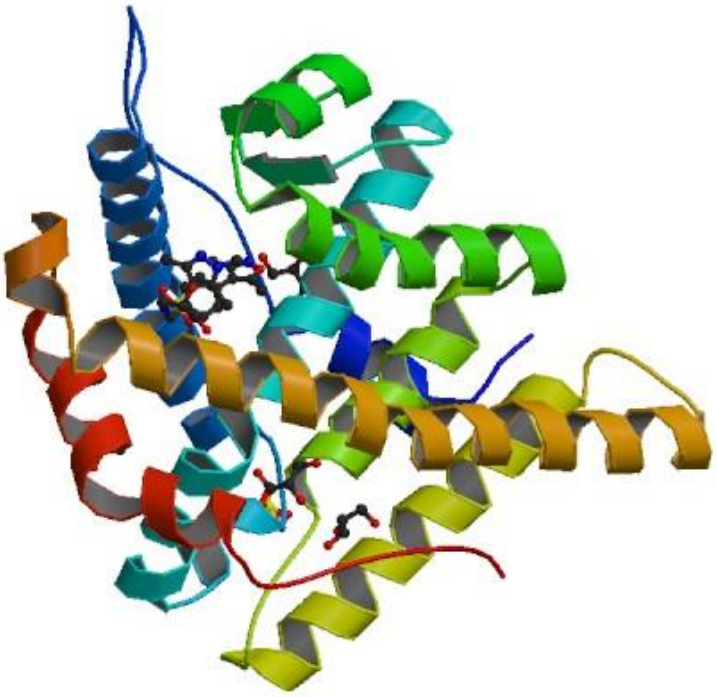

Figure 1.9 The structure of the Progesterone Receptor bound to progesterone receptor modulators. Adopted from: Lusher SJ, Raaijmakers HC, Vu-Pham D, Dechering K, Lam TW, Brown AR, et al. Structural Basis for Agonism and Antagonism for a Set of Chemically Related Progesterone Receptor Modulators. The Journal of Biological

Chemistry [Internet]. 2011; 286(40):35079-86 [cited 2021 Jul 14]. Available from: http://www.jbc.org/cgi/pmidlookup?view=long&pmid=21849509.

1.6.7 Insulin-Like Growth Factor 1 Receptor (IGF-1)

IGF-1 is crucial in several processes in the human body whilst also being an essential component of bone formation. IGF-1 shows a significant anabolic effect through enhanced osteoblastic function and osteocyte survival, this is done by increasing bone formation and positively affecting the bone remodelling process (Locatelli & Bianchi, 2014; Bikle et al., 2015).

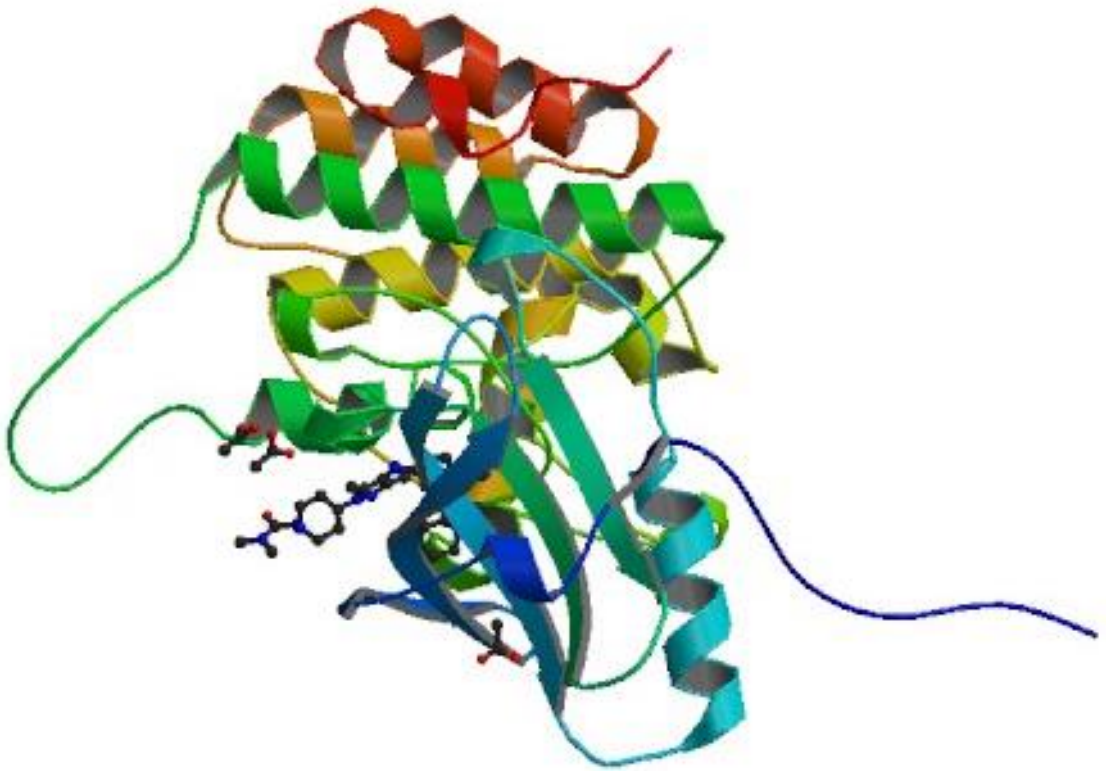

Figure 1.10 The structure of the Insulin-Like Growth Factor 1 Receptor in complex with a pyrimidine inhibitor. Adopted from: Degorce SL, Boyd S, Curwen JO, Ducray R, Halsall CT, Jones CD, et al. Discovery of a Potent, Selective, Orally Bioavailable and Efficacious Novel 2-(Pyrazol-4-ylamino)-pyrimidine Inhibitor of the Insulin-like Growth Factor-1 Receptor (IGF-1R). Journal of Medicinal Chemistry. 2016; 59(10):4859-66.

1.6.8 Mineralocorticoid Receptor (MR)

This receptor protein differs from other steroid receptors as it is responsive to two endogenous hormones, namely aldosterone and cortisol. The MR is found in osteoclasts, osteoblasts and osteocytes (Beavan et al., 2001; Fumoto et al., 2014), amongst other areas in the body. In a study produced by Fumoto et al., (2014) when steroidal anti-mineralocorticoid drug eplerenone was administered to mice, MR inhibition function occurred causing an increase in bone mass, together with an increased stimulus for osteogenesis and a decrease in bone resorption.

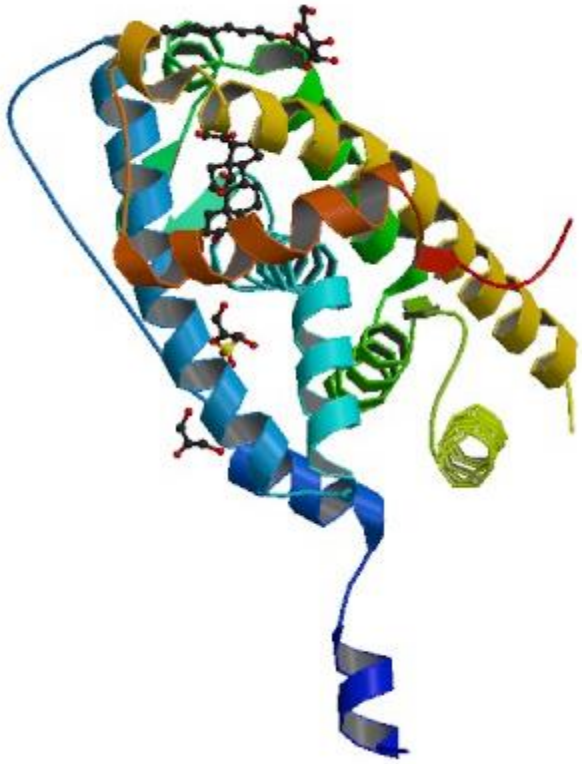

Figure 1.11 The structure of the Mineralocorticoid Receptor bound to Aldosterone. Adopted from: Bledsoe RK, Madauss KP, Holt JA, Apolito CJ, Lambert MH, Pearce KH, et al. A ligand-mediated hydrogen bond network required for the activation of the mineralocorticoid receptor. The Journal of Biological Chemistry [Internet]. 2005;

280(35):31283-93 [cited on 2021 Jul 14]. Available from: https://www.jbc.org/content/280/35/31283.long.

1.6.9 Cytochrome P450 3A4

Located mostly in the liver and intestine, this enzyme subtype is crucial for the metabolism of endogenous and exogenous chemicals and toxins. The cytochrome P450 3A4 18 variant was proved to rapidly oxidize sex steroids (such as oestrogen and T) which are implicated in bone homeostasis, resulting in low bone mineral density (Kang et al., 2009). It has also been discovered that this microsomal subtype is capable of hydroxylation of vitamin D2 and D3 and thus can also be involved in regular bone health, as may be seen in Section 1.6.11 (Jones et al., 2014).

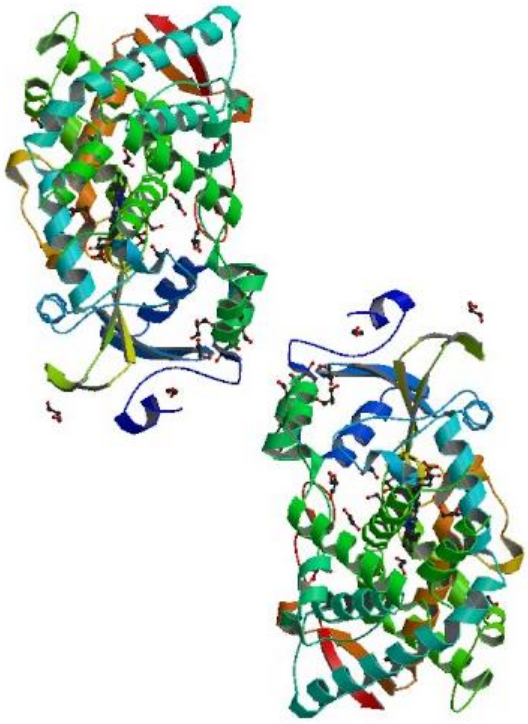

Figure 1.12 The structure of Cytochrome P450 3A4 bound to glycerol. Adopted from: Sevrioukova IF. High-Level Production and Properties of the Cysteine-Depleted Cytochrome P450 3A4. Biochemistry. 2017; 56(24):3058-67.

1.6.10 Androgen Receptor (AR)

The presence and binding of androgens to the AR is essential since this is necessary for bone development and maintenance. In studies performed it was concluded that male mice which did not express the AR had a lower bone mass, decreased periosteal osteogenesis and high bone turnover when compared to the male mice that expressed the receptor (Manolagas et al., 2013; Wu et al., 2019).

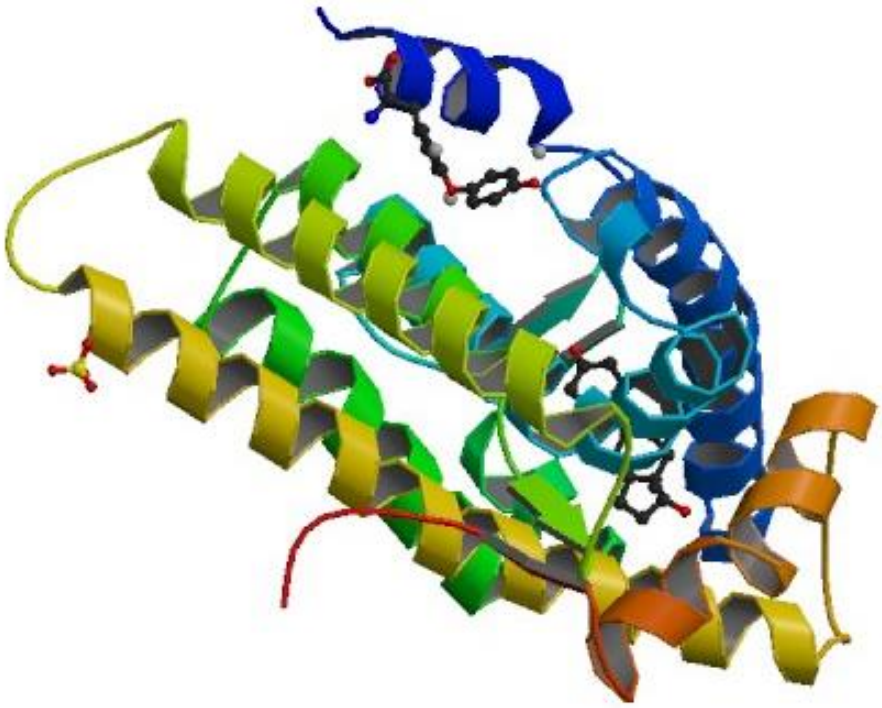

Figure 1.13 The structure of the Androgen Receptor bound to a small molecule. Adopted from: Estébanez-Perpiñá E, Arnold LA, Nguyen P, Rodrigues ED, Mar E, Bateman R, et al. A Surface on the Androgen Receptor That Allosterically Regulates Coactivator Binding. Proceedings of the National Academy of Sciences of the United States of America. 2007; 104(41):16074-9.

1.6.11 Vitamin D3 Receptor

This nuclear hormone receptor is found at high levels in immature osteoblasts, whilst it is found in significantly lower concentrations in mature osteoblastic cells and osteocytes. It is thought that the former bone cell type is responsible for vitamin D hormone signalling, permitting calcium release and thus bone formation. In a study produced by Yamamoto et al., (2013) it was shown that when the vitamin D3 Receptor in is found in osteoblastic cells, the receptor negatively regulates bone mass homeostasis (Yamamoto et al., 2013; Wang et al., 2014).

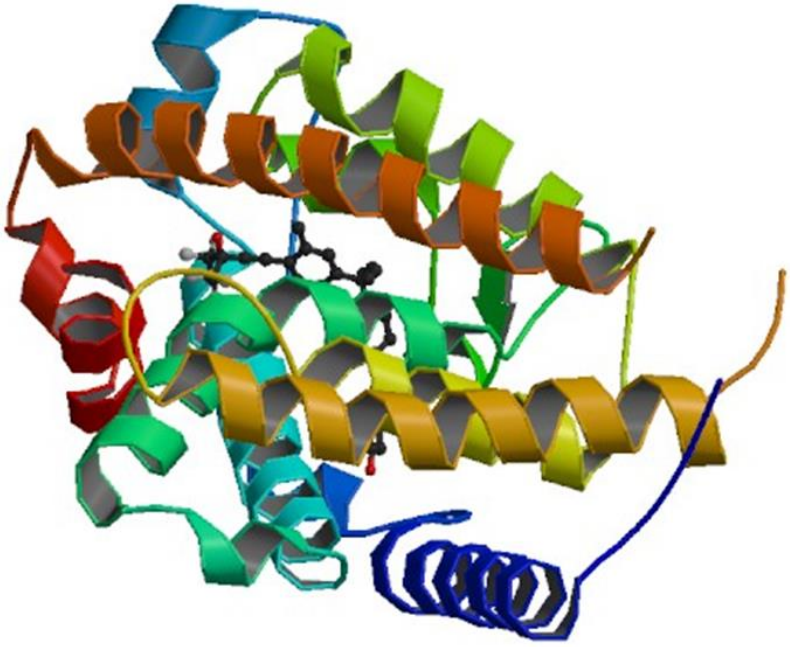

Figure 1.14 The structure of the Vitamin D3 Receptor bound to (4S)-4-hydroxy-5-[2-methyl-4-(3-{3-methyl-4-[4,4,4-trifluoro-3-hydroxy-3-(trifluoromethyl)but-1-yn-1-yl]phenyl}pentan -3-yl)phenoxy] pentanoic acid. [5]

[5] RCSB Protein Data Bank (PDB). 3W0A - Crystal Structure Analysis of Vitamin D receptor [Internet]. United States of America: RCSB PDB; 2013 [cited 2021 Jul 14]. Available from: https://www.rcsb.org/structure/3w0a.

1.6.12 Aromatase

This Cytochrome P450 Family 19 Subfamily A Member 1 enzyme catalyses the conversion of testosterone (T) to oestradiol (E2) and androstenedione to estrone (E1). It is found expressed in osteoblasts, osteocytes and osteoblast-like cells, amongst other places and it is vital in maintaining bone mass (Sasano et al., 1997; Merlotti et al., 2011).

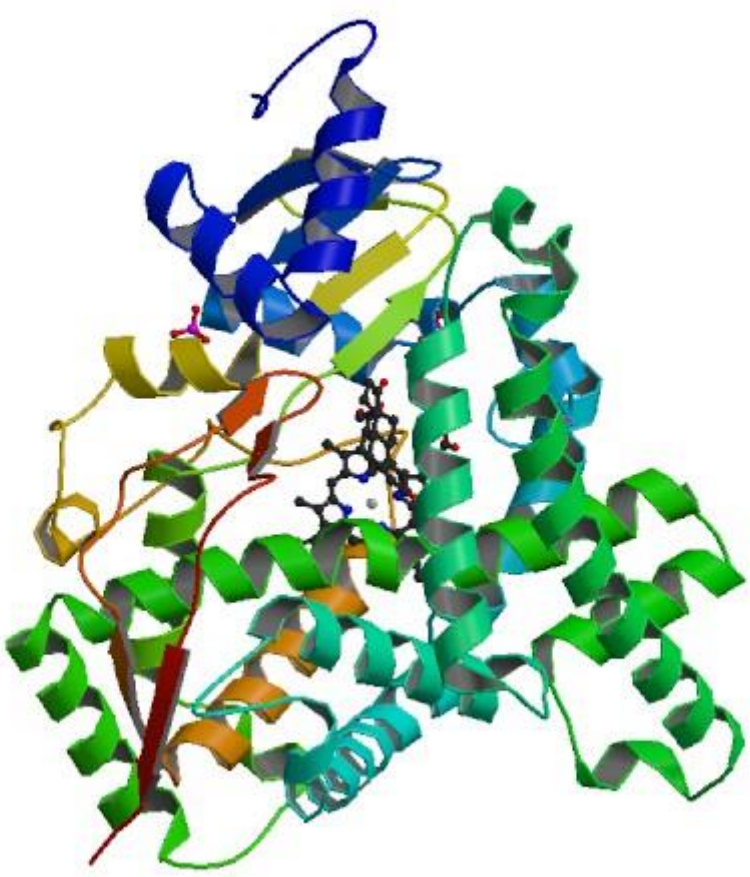

Figure 1.15 The structure of Aromatase in complex with Androstenedione. Adopted from: Ghosh D, Griswold J, Erman M, Pangborn W. Structural Basis for Androgen Specificity and Oestrogen Synthesis in Human Aromatase. Nature. 2009; 457(7226):219-23.

1.6.13 Proto-Oncogene Tyrosine-Protein Kinase Src

Apart from this non-receptor tyrosine kinase protein having various cellular roles, it is involved in regulating osteoblastic and osteoclastic activity during bone homeostasis. This protein is widely found in osteoclasts and stimulates bone resorption. On the other hand, when it is expressed in osteoblasts, it activates signalling pathways and inhibits osteoblastic differentiation and bone formation through Yes-associated protein (YAP), to repress Runx2 activity (Marzia et al., 2000; Zaidi et al., 2004; Kim et al., 2018).

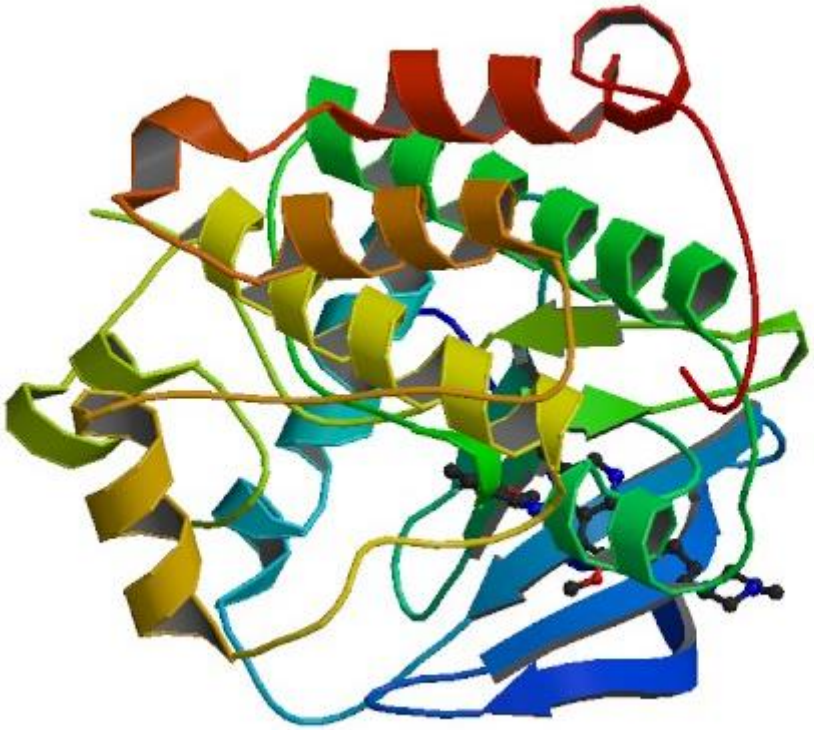

Figure 1.16 The structure of Proto-Oncogene Tyrosine-Protein Kinase Src bound to Kinase Inhibitor Bosutinib. Adopted from: Levinson NM, Boxer SG. A Conserved Water-Mediated Hydrogen Bond Network Defines Bosutinib's Kinase Selectivity. Nature Chemical Biology. 2014; 10(2):127-32.

1.6.14 Oestradiol 17-Beta-Dehydrogenase 1

The predominant activity of this enzyme is reductive, as it converts E1 to E2. It also catalyses dehydroepiandrosterone to androstendiol and dihydrotestosterone to 3-alpha-androstanediol and 3-beta-androstanediol. Since these are gonadocorticoids, this enzyme affects the bone remodelling process (Hilborn et al., 2017)

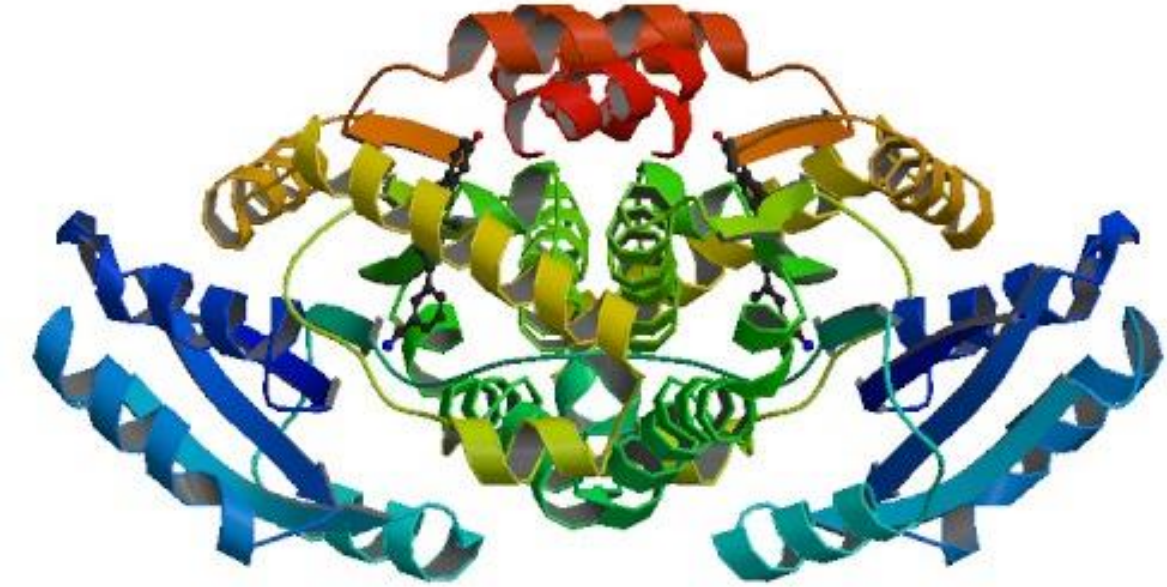

Figure 1.17 The structure of Oestradiol 17-Beta-Dehydrogenase 1 complexed with 3-{[(9beta,14beta,16alpha,17alpha)-3,17-dihydroxyestra-1,3,5(10)-trien-16-yl]methyl}benzamide. Adopted from: Mazumdar M, Fournier D, Zhu DW, Cadot C, Poirier D, Lin SX. Binary and Ternary Crystal Structure Analyses of a Novel Inhibitor With 17beta-HSD Type 1: A Lead Compound for Breast Cancer Therapy. The Biochemical Journal. 2009; 424(3):357-66.

1.6.15 Aldo-Keto Reductase Family 1 Member B1

This enzyme is also known as aldose reductase. In a study carried out by Inaba et al., (1999) it was proved that epalrestat, an aldose reductase inhibitor partially protected osteoblastic function whilst also suggesting that the sorbitol-aldose reductase pathway may be involved in the development of abnormal bone metabolism in galactose-fed rats (Inaba et al., 1999).

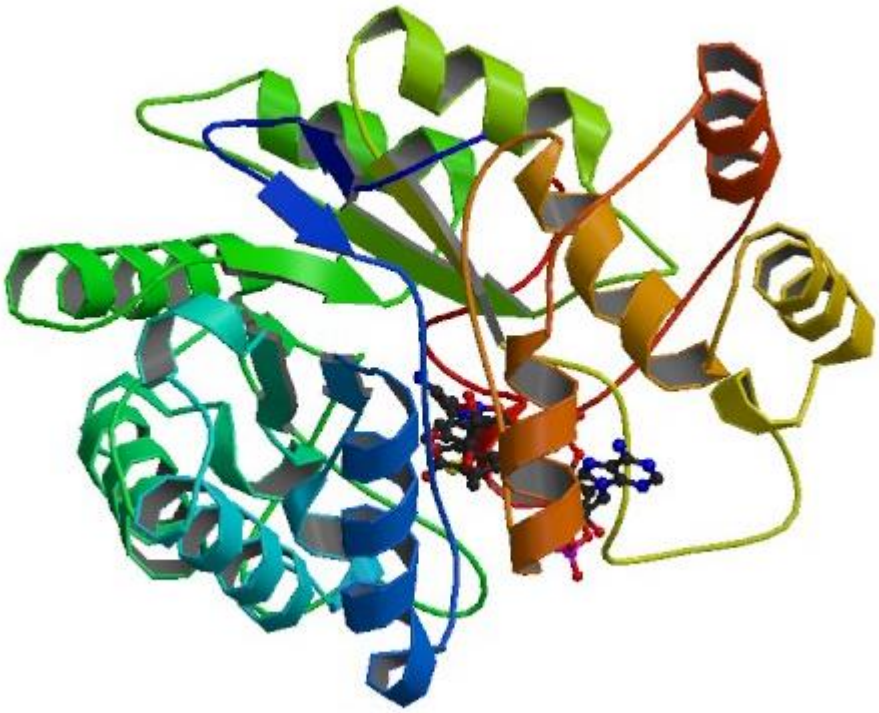

Figure 1.18 The structure of Aldo-Keto Reductase Family 1 Member B1 complexed with Schl12134 (3-[5-(3-nitrophenyl)-2-thienyl]propanoic acid). [6]

[6] RCSB Protein Data Bank (PDB). 4YU1- Human Aldose Reductase complexed with Schl12134 (3-[5-(3-nitrophenyl)-2-thienyl]propanoic acid) at 1.02 A [Internet]. United States of America: RCSB PDB; 2013 [cited 2021 Jul 14]. Available from: https://www.rcsb.org/structure/4YU1.

1.6.16 Tyrosine-Protein Phosphatase Non-Receptor Type 2 (PTPN2)

Doody et al., (2012) have proved that this tyrosine receptor is needed for regular bone development. It was observed that in PTPN2 knockout mice, osteoclast density and bone resorption increased, resulting in smaller skeletons. Another study carried out by Zhang et al., (2019) discovered a substrate for PTPN2 called colony-stimulating factor 1 receptor (CSF1R) which is directly dephosphorylated by PTPN2 at the Y807 site and it is responsible for bone resorption by controlling osteoclastic development and function (Doody et al., 2012; Zhang et al., 2019).

1.6.17 Tyrosine-Protein Phosphatase Non-Receptor Type 1 (PTP-1B)

The PTP-1B has a variety of roles including its involvement in metabolic homeostasis, inflammation and immunity. PTP-1B is stimulated by numerous molecules, most notably the insulin receptor which is expressed in osteoblasts and may be involved in bone development (Wheeler et al., 2002; Ferron et al., 2010; Zee et al., 2012).

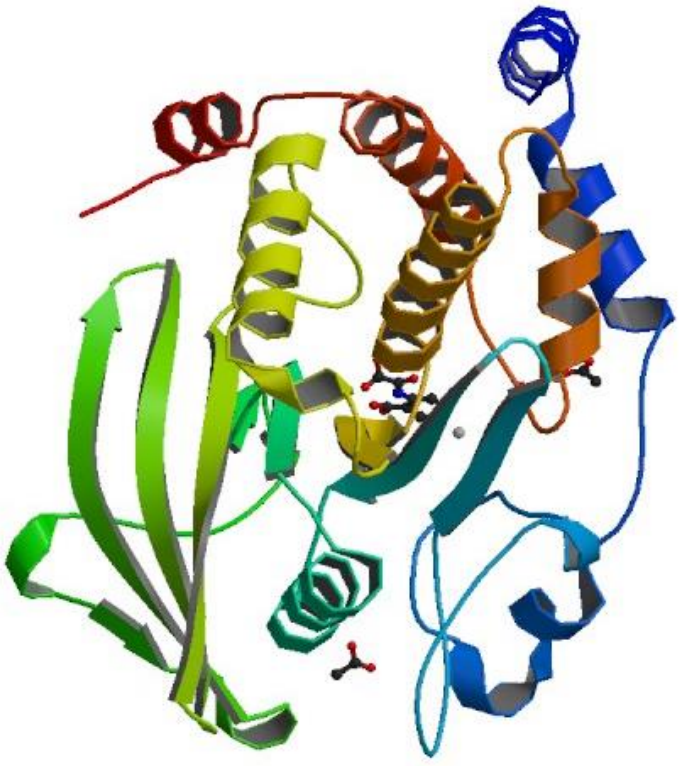

Figure 1.19 The structure of Tyrosine-Protein Phosphatase Non-Receptor Type 1 complexed with 5-Iodo-2-(Oxalyl-Amino)-Benzoic Acid. Adopted from: Andersen HS, Iversen LF, Jeppesen CB, Branner S, Norris K, Rasmussen HB, et al. 2-(oxalylamino)-benzoic Acid Is a General, Competitive Inhibitor of Protein-Tyrosine Phosphatases. The Journal of Biological Chemistry [Internet]. 2000; 275(10):7101–8 [cited 2021 Jul 14]. Available from: https://www.jbc.org/content/275/10/7101.long.

1.6.18 3-Oxo-5-Alpha-Steroid 4-Dehydrogenase 1

This isoenzyme is found predominantly in the liver but it has also been detected in bone. Also known as 5-alpha-reductase type 1, this enzyme catalyses the conversion of T to 5-alpha-dihydrotestosterone, which is involved in bone metabolism. From studies conducted on male mice it was noted that these this study sample had a lower bone mass and a decrease in forelimb strength, due to the absence of this enzyme in their bone and muscle cells, when compared to the wildtype mice (Issa et al., 2002; Windahl et al., 2011).

1.6.19 Acetylcholinesterase (AChE)

The main role of this enzyme is to hydrolyse acetylcholine to choline and acetate. However, it was discovered that AChE has a function in bone, as it can be found as a proline-rich membrane anchor (PRiMA)-linked globular form in osteoblasts, in which it is suggested to undertake a noncholinergic role in osteoblastic differentiation. A direct correlation exists between AChE expression and osteoblastic differentiation, since AChE expression increases with osteoblastic differentiation (Grisaru et al., 1999; Inkson et al., 2004; Vogel-Hopker et al., 2012; Spieker et al., 2016; Tamini et al., 2017; Xu et al., 2017).

Figure 1.20 The structure of Acetylcholinesterase complexed with Huperzine A. Adopted from: Raves ML, Harel M, Pang YP, Silman I, Kozikowski AP, Sussman JL. Structure of Acetylcholinesterase Complexed with the Nootropic Alkaloid, (-)-Huperzine A. Nature Structural Biology. 1997; 4(1):57–63.

1.6.20 Low Molecular Weight Phosphotyrosine Protein Phosphatase

This enzyme modulates Src kinase activity during osteoblastic differentiation (Zambuzzi et al., 2008).

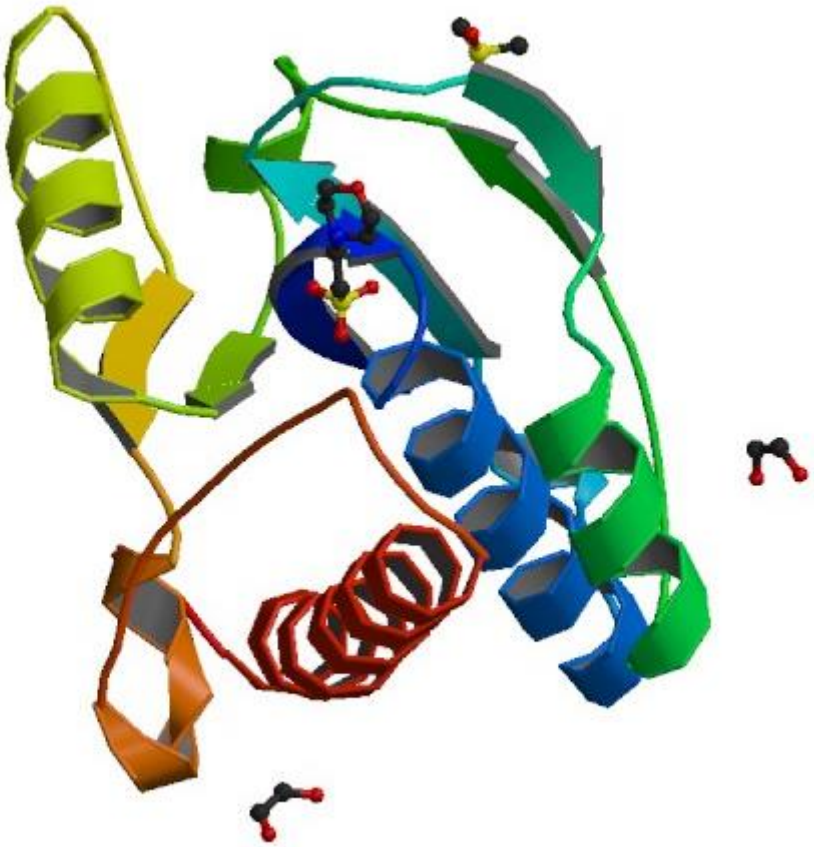

Figure 1.21 The structure of Low Molecular Weight Phosphotyrosine Protein Phosphatase complexed with 2-(N-Morpholino)-Ethanesulfonic Acid. Adopted from: Stanford SM, Aleshin AE, Zhang V, Ardecky RJ, Hedrick MP, Zou J, et al. Diabetes Reversal by Inhibition of the Low-Molecular-Weight Tyrosine Phosphatase. Nature Chemical Biology. 2017; 13(6):624–32.

1.6.21 Corticosteroid 11-Beta-Dehydrogenase Isozyme 1

Through its reducing property, this enzyme converts cortisone to cortisol which is important in regular bone function and it is expressed in osteoclasts and osteoblast cells (Bland et al., 1999; Cooper et al., 2000; Cooper et al., 2001; Stewart, 2003).

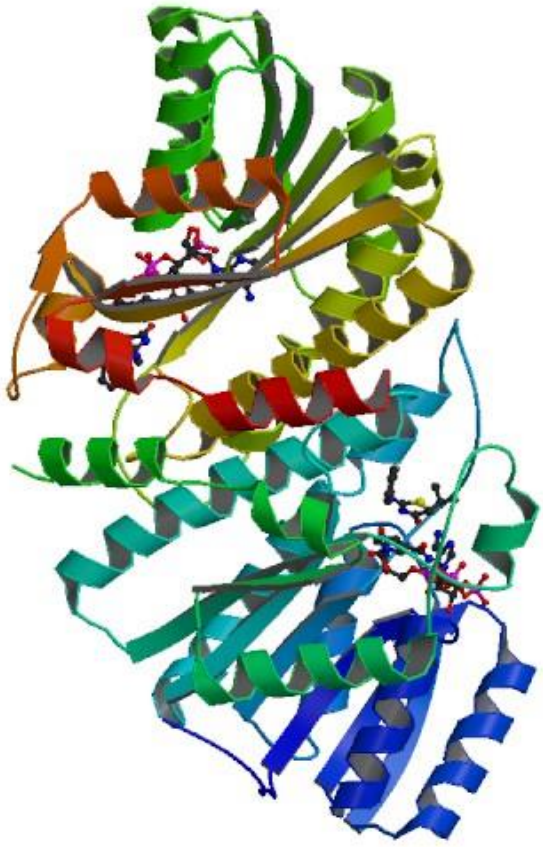

Figure 1.22 The structure of Corticosteroid 11-Beta-Dehydrogenase Isozyme 1 complexed with 2-anilinothiazolones. Adopted from: Yuan C, St Jean DJ Jr, Liu Q, Cai L, Li A, Han N et al. The Discovery of 2-anilinothiazolones as 11beta-HSD1 Inhibitors. Bioorganic and Medicinal Chemistry Letters. 2007; 17(22):6056–61.

1.6.22 M-Phase Inducer Phosphatase 2

This enzyme has various roles including its ability to dephosphorylate cyclin-dependent kinase 1 (CDK1) and thus propagate its kinase activity. This protein kinase activity is vital in osteoblastic cell function (Takahashi et al., 2018).

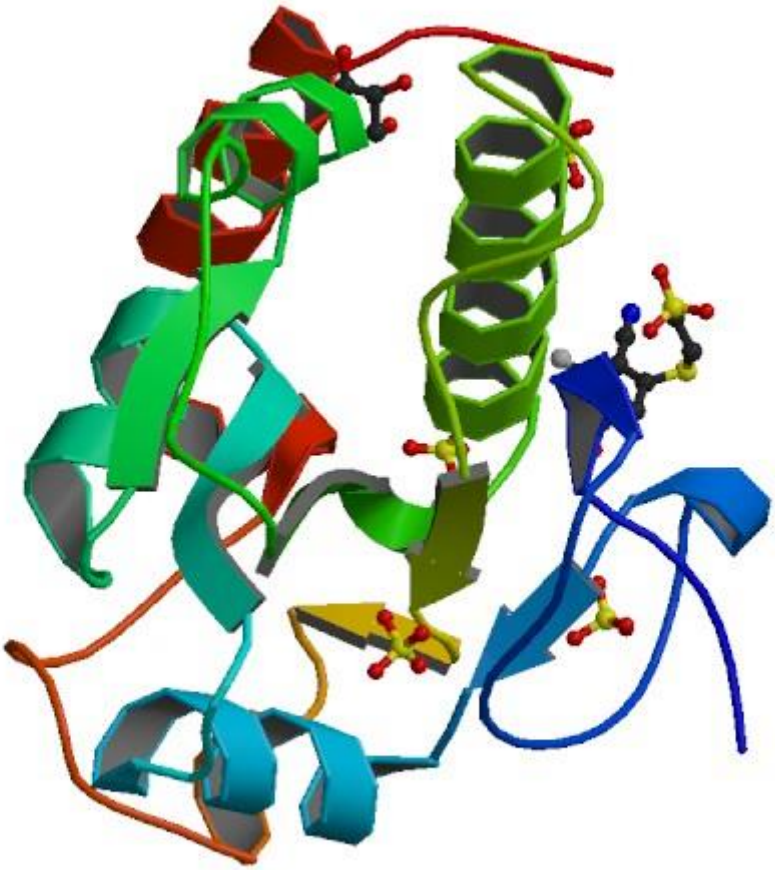

Figure 1.23 The structure of the M-Phase Inducer Phosphatase 2 with a bound inhibitor. Adopted from: Lund G, Dudkin S, Borkin D, Ni W, Grembecka J and Cierpicki T. Inhibition of CDC25B Phosphatase Through Disruption of Protein-Protein Interaction. American Chemical Society Chemical Biology. 2015; 10(2):390–4.

1.6.23 Tyrosine-Protein Kinase Receptor UFO

Also known as receptor tyrosine kinase AXL, this protein is found in a diverse number of tissues, including bone marrow stroma (Gay et al., 2017).

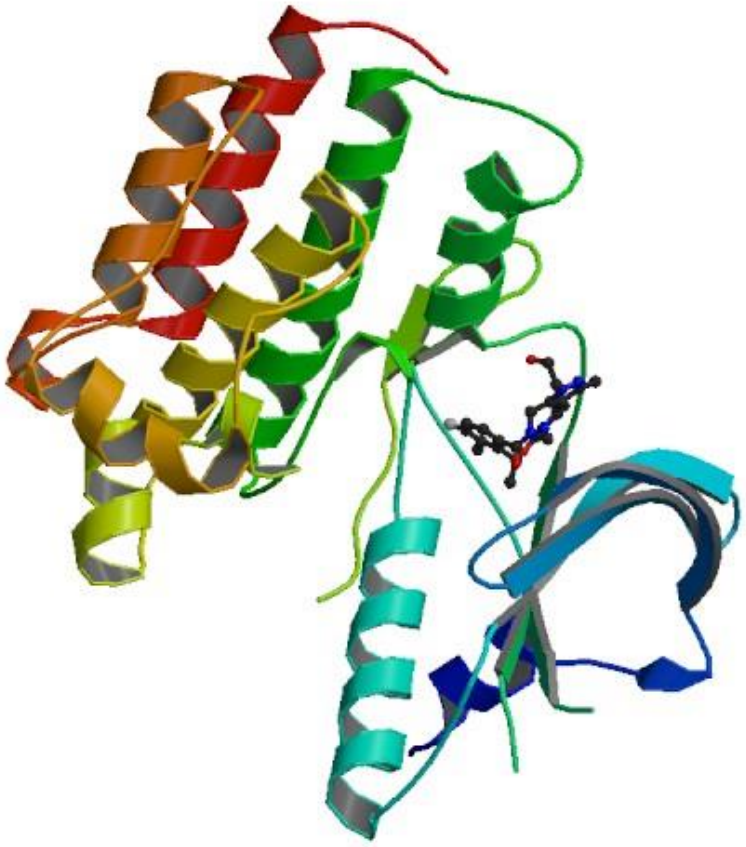

Figure 1.24 The structure of Tyrosine-Protein Kinase Receptor UFO in complex with a macrocyclic inhibitor. Adopted from: Gajiwala KS, Grodsky N, Bolaños B, Feng J, Ferre R, Timofeevski S, et al. The Axl Kinase Domain in Complex with a Macrocyclic Inhibitor Offers First Structural Insights Into an Active TAM Receptor Kinase. The Journal of Biological Chemistry [Internet]. 2017; 292(38):15705–16 [cited 2021 Jul 14]. Available from: https://www.jbc.org/content/292/38/15705.long.

1.6.24 3-Oxo-5-Alpha Steroid 4-Dehydrogenase 2

This isoenzyme is predominantly expressed in male reproductive tissues. Also known as 5alpha-reductase type 2, this enzyme is converts T to dihydrotestosterone, which is involved in maintaining and developing bone mineral density (Issa et al., 2002; Sobel et al., 2006; Windahl et al., 2011).

1.6.25 Nitric Oxide Synthase, Inducible

The inducible nitric oxide synthase are located in bone marrow stromal cells, osteoblasts, osteocytes, and osteoclasts. Nitric oxide synthase is composed of three isoforms, however the inducible type is the leading isoform which stimulates synthesis of nitric oxide by osteoblasts (Wimalawansa, 2010; Lee et al., 2018).

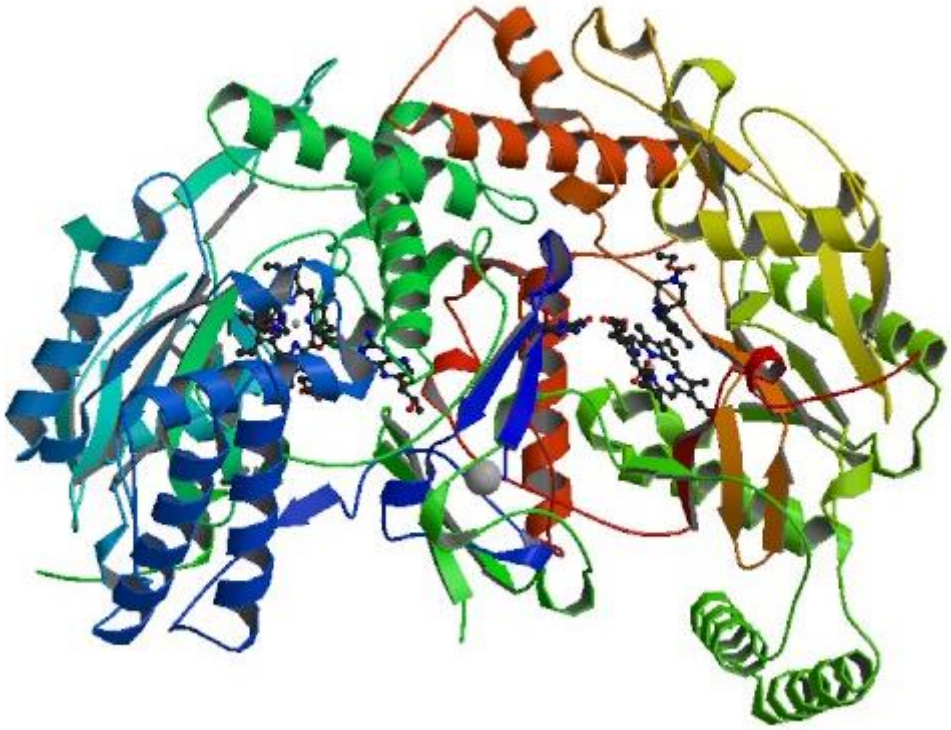

Figure 1.25 The structure of Inducible Nitric Oxide Synthase with inhibitor AR-C95791. Adopted from: Garcin ED, Arvai AS, Rosenfeld RJ, Kroeger MD, Crane BR, Andersson G, et al. Anchored Plasticity Opens Doors for Selective Inhibitor Design in Nitric Oxide Synthase. Nature Chemical Biology. 2008; 4(11):700–7.

1.6.26 Vascular Endothelial Growth Factor Receptor 2 (VEGFR2)

Primarily, the VEGFR2 is involved in angiogenesis, vasculogenesis and an increase in vessel permeability in response to its ligand, vascular endothelial growth factor. This

tyrosine-kinase receptor is also expressed in osteoclasts and as a result of ligand binding, it promotes osteoclastic survival through the stimulation of PI3K/Akt signalling. VEGFR2 can also be found in osteoblastic cells however, there is conflicting theories on whether this receptor acts as a positive or negative regulator of bone formation and development (Hu & Olsen, 2016; Hu & Olsen, 2017).

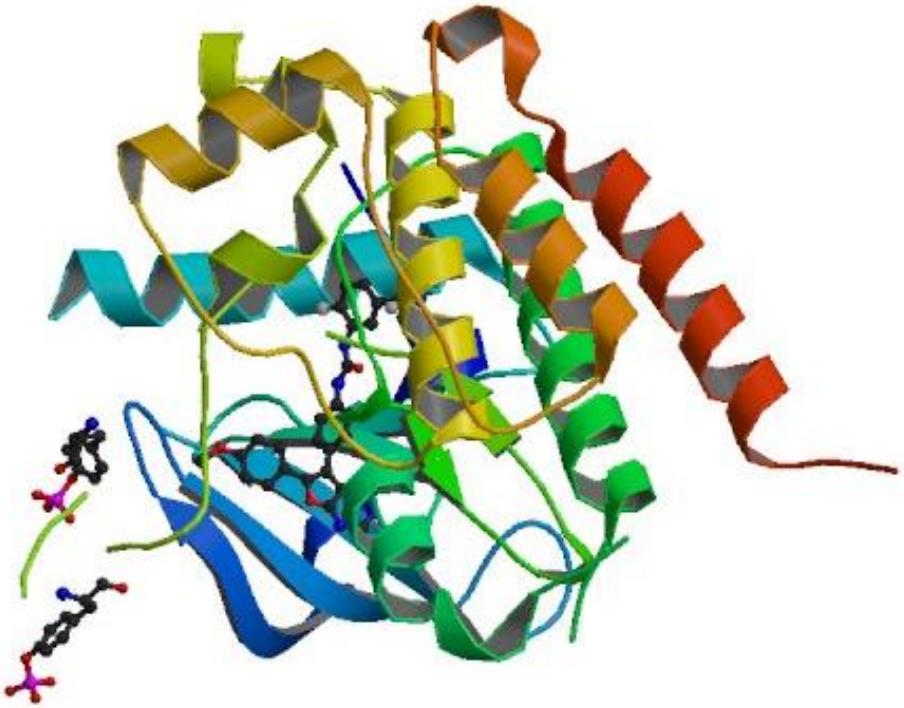

Figure 1.26 The structure of Vascular Endothelial Growth Factor Receptor 2 in complex with a novel 4-amino-furo[2,3-d]pyrimidine. Adopted from: Miyazaki Y, Matsunaga S, Tang J, Maeda Y, Nakano M, Philippe RJ, et al. Novel 4-amino-furo[2,3-d]pyrimidines as Tie-2 and VEGFR2 Dual Inhibitors. Bioorganic and Medicinal Chemistry Letters. 2005; 15(9):2203–7.

1.6.27 Testosterone 17-Beta-Dehydrogenase 3

This oxidoreductase enzyme is found predominantly in the testicles and is responsible for the production of T from 4-androstenedione. Studies have also concluded that this isoenzyme is expressed in bone, amongst other locations (George et al., 2010).

1.6.28 Oestradiol 17-Beta-Dehydrogenase 2

This isoenzyme predominantly oxidizes E2 to E1, T to androstenedione and androstendiol to dehydroepiandrosterone apart from being expressed in osteoblastic cells (Dong et al., 1998; Hilborn et al., 2017).

1.6.29 Corticosteroid 11-Beta-Dehydrogenase Isozyme 2

This enzyme is responsible for the conversion of cortisol to cortisone. Additionally, it plays a crucial part in bone homeostasis and is present in osteoblasts at low levels (Bland et al., 1999; Cooper et al., 2000; Cooper et al., 2001; Stewart, 2003).

1.6.30 Focal Adhesion Kinase 1

When this cytoplasmic non-receptor protein tyrosine kinase is phosphorylated, it activates numerous signalling molecules and kinase reactions which are essential to stimulate osteoblastic function, bone development and remodelling (Tamura et al.,2001; Castillo et al., 2012).

Figure 1.27 The structure of Focal Adhesion Kinase 1 in complex with N-{3-[(5-Cyano-2-Phenyl-1h-Pyrrolo[2,3-B]Pyridin-4-Ylamino)-Methyl]-Pyridin-2-Yl}-N-Methyl-Methanesulfonamide. Adopted from: Heinrich T, Seenisamy J, Emmanuvel L, Kulkarni SS, Bomke J, Rohdich F, et al. Fragment-based Discovery of New Highly Substituted 1H-pyrrolo[2,3-b]- and 3H-imidazolo[4,5-b]-pyridines as Focal Adhesion Kinase Inhibitors. Journal of Medicinal Chemistry. 2013; 56(3):1160–70.

1.6.31 Peptidyl-Prolyl Cis-Trans Isomerase NIMA-Interacting 1 (PIN1)

PIN1 regulates phosphorylation reactions, signalling molecules and cytokines which are involved in many different processes. This enzyme has been proved to be present in bone cells and may regulate osteoblastic activity and osteoclastic function (Shen et al. 2013; Cho et al., 2015).

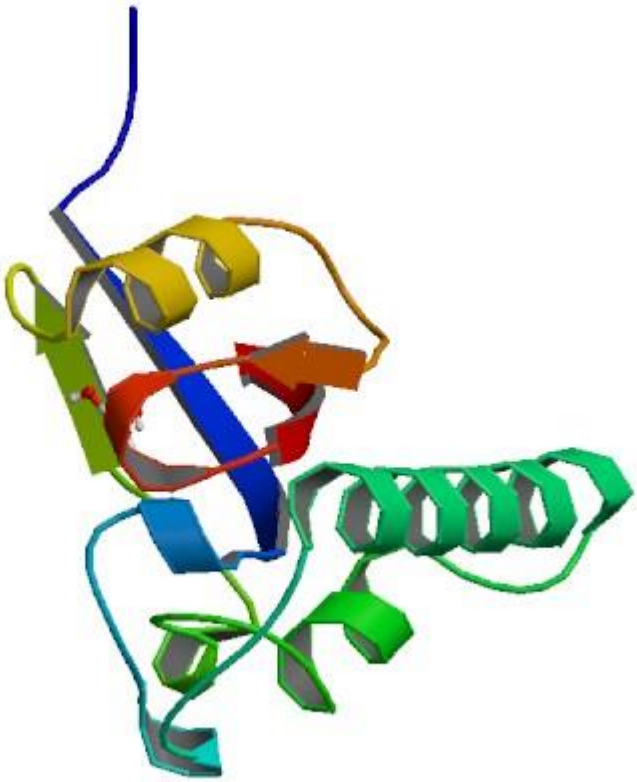

Figure 1.28 The structure of Peptidyl-Prolyl Cis-Trans Isomerase NIMA-Interacting 1 in complex with Trihydroxyarsenite (III) . Adopted from: Kozono S, Lin YM, Seo HS, Pinch B, Lian X, Qiu C, et al. Arsenic Targets Pin1 And Cooperates with Retinoic Acid to Inhibit Cancer-Driving Pathways and Tumor-Initiating Cells. Nature Communications [Internet]. 2018; 9(1):1-17 [cited 2021 Jul 14]. Available from: https://www.nature.com/articles/s41467-018-05402-2.

1.6.32 Voltage-Dependent L-Type Calcium Channel Subunit Alpha-1C

This channel allows for calcium influx into a cell and its function is crucial to permit calcium-mediated cellular signalling. This subunit is found abundantly in rodent

osteoblasts, allowing calcium influx into these bone cells and thus playing an essential part in osteoblastic activity and function (Li et al., 2011; Zhang et al., 2015).

1.6.33 Hypoxia-Inducible Factor 1-Alpha

This protein does not regulate osteoclastogensis, instead it functions by increasing bone resorption activity of mature osteoclasts via the von Hippel–Lindau tumour suppressor protein and prolyl-4-hydroxylase enzymes at normal oxygen levels. In developing bone, this subunit is found in osteoblasts and it plays a vital part in stimulating angiogenesis and osteoblastic specification. On the other hand, in mature bone, a decrease in this subunit in osteoblasts leads to bone formation (Frey et al., 2014; Hulley et al., 2017; Kang et al., 2017).

1.6.34 G-Protein Coupled Bile Acid Receptor 1

G-protein coupled bile acid receptor 1 is crucial in carbohydrate metabolism, bile acid and energy homeostasis. During receptor activation through its ligand, GPBARA, the receptor promotes osteoblastic differentiation and mineralization through the 5' adenosine monophosphate-activated protein kinase signalling pathway (Wang et al., 2018).

1.6.35 Oestrogen Receptor Beta

This oestrogen receptor subtype has numerous roles and may be found in various locations in the body including osteoblasts, osteocytes and osteoclasts. It is still not fully understood how this receptor functions however, through *in vitro* studies it is thought to oppose the effects of ER alpha. On the other hand, *in vivo* studies show that the ER alpha

and beta stimulate bone formation in response to mechanical loading (Lee et al., 2004; Castillo et al., 2014; Khalid & Krum, 2016).

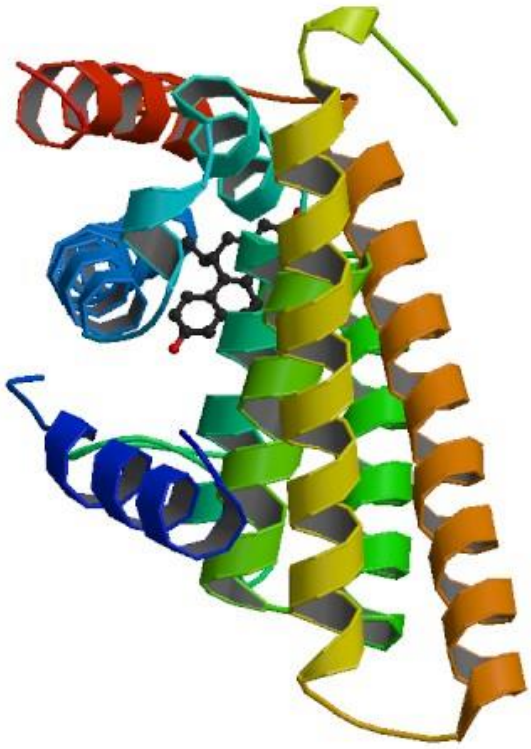

Figure 1.29 The structure of Oestrogen Receptor Beta in Complex with (R,R)-5,11-cis-diethyl-5,6,11,12-tetrahydrochrysene-2,8-diol. Adopted from: Shiau AK, Barstad D, Radek JT, Meyers MJ, Nettles KW, Katzenellenbogen BS, et al. Structural Characterization of a Subtype-Selective Ligand Reveals A Novel Mode of Oestrogen Receptor Antagonism. Nature Structural Biology. 2002; 9(5):359-64.

1.6.36 Cysteine Protease ATG4B

This enzyme is necessary in autophagy but is also involved in bone homeostasis, as it permits bone resorption by creating the osteoclast ruffled border and stimulating the secretory function of osteoclasts (DeSelm et al., 2011).

1.7 Computational Design

1.7.1 BIOVIA Draw®

Also a Dassault Systèmes Biovia software computational program, BIOVIA Draw® v17.1 permits viewing, drawing, building and modifying chemical structures computationally and thus is very useful in the chemical and pharmaceutical sector. [4]

1.7.2 BIOVIA Discovery Studio Visualizer®

Dassault Systèmes Biovia produced and licenses BIOVIA Discovery Studio Visualizer® v20.1, a freeware program. Users can run simulations, view and edit chemical structures, execute ligand design, structure-based design, macromolecule design, pharmacophore modelling and validation and macromolecule engineering. [7]

1.7.3 Sybyl®-X

Sybyl®-X v1.1 is another computational software program used for both macromolecules and small molecules. This program is purposed for molecular modelling and may be used for high throughput screening and late lead optimization (Ash et al., 2010).

[4] Dassault Systèmes. BIOVIA Draw. Version 17.1 [software]. Dassault Systèmes. 2017 [cited 2021 Jul 14; downloaded 2021 May 25]. Available from: https://hts.c2b2.columbia.edu/draw/.

[7] Dassault Systèmes. BIOVIA Discovery Studio Visualizer. Version 20.1 [software]. Dassault Systèmes. 2020 [cited 2021 Jul 14; downloaded 2021 May 25]. Available from: https://www.3dsbiovia.com/products/collaborative-science/biovia-discovery-studio/visualization-download.php.

1.7.4 X-Score

X-Score v1.3 is the third computational program used, developed by the University of Michigan whose basic function is to calculate the binding score (ligand binding affinity and/or ligand binding energy) of a given ligand molecule-protein receptor structure (Zhang et al., 2009). The receptor is required to be in a PDB file format, whilst the ligand molecule must be stored in a *.mol2* file format. This version of the program uses three empirical scoring functions (HPSCORE, HMSCORE and HSSCORE) by using several properties such as Van der Waals interactions, hydrophobicity and hydrogen bonding.

1.7.5 LigBuilder®

LigBuilder® v1.2 (Wang et al., 2000) enables the building and synthetic analysis of ligands within the constraints of the LBP provided, using a library of organic fragments.

This program contains four main modules; POCKET, GROW, LINK and PROCESS. The POCKET algorithm analyses and creates a map of the LBP and prepares the necessary data for the LINK and GROW functions and allows the input of seeds. The GROW or LINK modules are used to virtually grow the seed structures via genetic algorithm. Both the LINK and GROW algorithms utilise ‘growing sites' on the seed structure that are supplied by the user. The GROW module allows for the removal of specific groups at specific termini, as well as the recognition of growth zones and, if possible, the addition of fragments to a particular area. The LINK module, on the other hand, joins two parts of a chopped molecule, to maximize interactions with the target receptor (Wang et al., 2000).

Following the utilisation of the GROW or LINK function, the PROCESS module acts as the organiser portion of the programme. It groups up all the molecules that have been

create and sorts them into families. All the *.index* files in LigBuilder® v1.2 (Wang et al., 2000) are instruction files for the programme. These files instruct the programme which the input files are and from where to read them and where to place the output files. The *link.index* and *grow.index* also contain the parameters that approach Lipinski's Rule (Lipinski et al., 2001).

1.8 Aim and Objectives

The aim of this study is to identify the specific endogenous target receptor of Maltanedienol. This study relies on the results obtained by D'Emanuele (2019), which identified 59 potential targets (refer to Table 1.1 above). Furthermore, the biological role of each of the 59 targets was identified from literature. Those targets with *in vivo* calcium deposition or bone remodelling associated functions will be considered and the contacts Maltanedienol forges with these ligands will be elucidated and molecular modelling performed.

The implication of the results is that the answer to the calcium fixing abilities of this molecule may be modulated through one of these 59 targets. The broader implication is that Maltanedienol scaffold may be used in order to mediate hitherto unexplored, biological and clinically useful responses. This study is consequently exploratory and seeks to provide preliminary answers to these questions.

Therefore, the aim of this study is, using a bioinformatics approach, is to identify the target to which Maltanedienol could potentially bind as per data mining results from a previous study by D'Emanuele (2019). Subsequently, the results will be utilized in the design of analogues with similar biological activity as Maltanedienol, in the context of a multi-target drug design strategy.

Chapter 2

Methodology

2.1 Introduction and study overview

This study is designed to identify the endogenous target for Maltanedienol. This molecule is the active ingredient isolated from the marine seaweed *Padina pavonica*. Maltanedienol has been proven to be involved in a calcium fixation process, not only through the seaweed itself and but also through *in vivo* studies carried out (Okazaki et al., 1986; Galea, 2009).

The methodology carried out, allowing the aim of this study to be achieved is as follows; 59 endogenous targets from a study performed by D'Emanuele (2019) were recruited. Following that, two groups were created depending on whether the target's function was or was not related to bone remodelling or calcium fixation; Group A – targets whose function is related to *in vivo* calcium deposition or bone remodelling and Group B – targets whose function appeared to be unrelated to *in vivo* calcium deposition or bone remodelling.

The endogenous targets found in group A were utilised for next step of this study, whilst those targets in Group B will be further investigated and used in upcoming studies. Those receptors found as small molecule:protein complexes on the protein data bank (PDB) (Bernstein et al., 1977) only were recruited as candidates for this study. Each PDB crystallographic deposition was analysed from a content perspective. For each PDB crystallographic deposition, the resident small molecule was computationally extracted and ligand binding affinity (LBA) (pKd) for its cognate receptor was calculated *in silico*.

Maltanedienol was then docked into each *apo* receptor ligand binding pocket (LBP) and conformational analysis was performed. The affinity of the optimal Maltanedienol

conformer for each proposed receptor was calculated and was compared to that of the cognate ligand, to reach the final scope of this study. *De novo* design was carried out using Ligbuilder® v1.2 (Wang et al., 2000).

2.2 Selection of targets related to *in vivo* calcium deposition or bone remodelling

Each of the 59 endogenous receptors from the study conducted by D'Emanuele (2019) were evaluated and recruited into the study exclusively if literature showed that their endogenous function (as seen in Section 1.6) was in some way related to *in vivo* calcium fixation or bone remodelling. This process filtered the recruited targets down to 36. The table below (Table 2.1) summarises the list of targets and this group of targets was titled Group A. Group A consists of the targets whose function is related to *in vivo* calcium deposition or bone remodelling and thus were used in the next stage of this study.

Table 2.1 Group A - Potential *in vivo* targets (n=36) for Maltanedienol as identified by the data mining software of D'Emanuele (2019) whose function is related to calcium fixation or bone remodelling.

Number	**UniProt ID**	**Identified Target Name**
1	O14684	Prostaglandin E Synthase
2	P03372	Oestrogen Receptor
3	P04150	Glucocorticoid Receptor
4	P04278	Sex Hormone-Binding Globulin
5	P06276	Cholinesterase
6	P06401	Progesterone Receptor
7	P08069	Insulin-Like Growth Factor 1 Receptor
8	P08235	Mineralocorticoid Receptor
9	P08684	Cytochrome P450 3A4
10	P10275	Androgen Receptor

11	P11473	Vitamin D3 Receptor
12	P11511	Aromatase
13	P12931	Proto-Oncogene Tyrosine-Protein Kinase Src
14	P14061	Oestradiol 17-Beta-Dehydrogenase 1
15	P15121	Aldo-Keto Reductase Family 1 Member B1
16	P17706	Tyrosine-Protein Phosphatase Non-Receptor Type 2
17	P18031	Tyrosine-Protein Phosphatase Non-Receptor Type 1
18	P18405	3-Oxo-5-Alpha-Steroid 4-Dehydrogenase 1
19	P22303	Acetylcholinesterase
20	P24666	Low Molecular Weight Phosphotyrosine Protein Phosphatase
21	P28845	Corticosteroid 11-Beta-Dehydrogenase Isozyme 1
22	P30305	M-Phase Inducer Phosphatase 2
23	P30530	Tyrosine-Protein Kinase Receptor UFO
24	P31213	3-Oxo-5-Alpha Steroid 4-Dehydrogenase 2
25	P35228	Nitric Oxide Synthase, Inducible
26	P35968	Vascular Endothelial Growth Factor Receptor 2
27	P37058	Testosterone 17-Beta-Dehydrogenase 3
28	P37059	Oestradiol 17-Beta-Dehydrogenase 2
29	P80365	Corticosteroid 11-Beta-Dehydrogenase Isozyme 2
30	Q05397	Focal Adhesion Kinase 1
31	Q13526	Peptidyl-Prolyl Cis-Trans Isomerase NIMA-Interacting 1
32	Q13936	Voltage-Dependent L-Type Calcium Channel Subunit Alpha-1C

33	Q16665	Hypoxia-Inducible Factor 1-Alpha
34	Q8TDU6	G-Protein Coupled Bile Acid Receptor 1
35	Q92731	Oestrogen Receptor Beta
36	Q9Y4P1	Cysteine Protease ATG4B

On the other hand, those targets whose function is not related to *in vivo* calcium fixation or bone remodelling, can be seen summarised in the table below (Table 2.2). This group of targets was titled Group B and was not used for this study, however, should be used for future studies of Maltanedienol.

Table 2.2 Group B - Potential *in vivo* targets (n=23) for Maltanedienol as identified by the data mining software of D'Emanuele (2019) whose function is not related to calcium fixation or bone remodelling.

Number	**UniProt ID**	**Identified Target Name**
1	O00748	Cocaine Esterase
2	O15245	Solute Carrier Family 22 Member 1
3	O60218	Aldo-Keto Reductase Family 1 Member B10
4	O75469	Nuclear Receptor Subfamily 1 Group I Member 2
5	P07339	Cathepsin D
6	P10253	Lysosomal Alpha-Glucosidase
7	P10586	Receptor-Type Tyrosine-Protein Phosphatase F
8	P11388	DNA Topoisomerase 2-Alpha

9	P11413	Glucose-6-Phosphate 1-Dehydrogenase
10	P23415	Glycine Receptor Subunit Alpha-1
11	P25024	C-X-C Chemokine Receptor Type 1
12	P29350	Tyrosine-Protein Phosphatase Non-Receptor Type 6
13	P49354	Protein Farnesyltransferase/Geranylgeranyltransferase Type-1 Subunit Alpha
14	P49356	Protein Farnesyltransferase Subunit Beta
15	P51449	Nuclear Receptor ROR-Gamma
16	P55055	Oxysterols Receptor LXR- Beta
17	P56817	Beta-Secretase 1
18	Q02880	DNA Topoisomerase 2-Beta
19	Q13133	Oxysterols Receptor LXR-Alpha
20	Q9UHC9	NPC1-Like Intracellular Cholesterol Transporter 1
21	Q9UM73	ALK Tyrosine Kinase Receptor
22	Q9UBE0	SUMO-Activating Enzyme Subunit 1
23	Q9UBT2	SUMO-Activating Enzyme Subunit 2

2.3 Selection of target receptors on the PDB

Following the segregation of the endogenous target receptors based on calcium fixation or bone remodelling properties, the 36 targets forming part of this group were searched on the PDB (Bernstein et al., 1977).

The PDB (Berman et al., 2000) was founded in 1971 by a group of scientists at the Brookhaven National Library. This archive is composed of different macromolecular biomolecules, which started with just 7 protein archives, however over the years has grown and is currently composed of over a hundred thousand entries (Goodsell et al., 2015).

Only 26 targets of the 36 endogenous recruited targets were crystallographically described on the PDB (Bernstein et al., 1977). These 26 targets, consequently, represented the target cohort considered in this study. This can be seen in the following table (Table 2.3).

Table 2.3 Potential *in vivo* targets (n=26) for Maltanedienol as identified by the data mining software of D'Emanuele (2019) which are crystallographically resolved on the PDB (Bernstein et al., 1977) and whose function is related to calcium fixation or bone remodelling, which were consequently recruited for this study.

Number	**UniProt ID**	**Identified Target Name**	**PDB ID**
1	O14684	Prostaglandin E Synthase	5T37
2	P03372	Oestrogen Receptor	3ERT

3	P04150	Glucocorticoid Receptor	1NHZ
4	P04278	Sex Hormone-Binding Globulin	1LHU
5	P06276	Cholinesterase	4M0E
6	P06401	Progesterone Receptor	3ZR7
7	P08069	Insulin-Like Growth Factor 1 Receptor	5FXS
8	P08235	Mineralocorticoid Receptor	2AA2
9	P08684	Cytochrome P450 3A4	5VCC
10	P10275	Androgen Receptor	2PIV
11	P11473	Vitamin D3 Receptor	3W0A
12	P11511	Aromatase	3EQM
13	P12931	Proto-Oncogene Tyrosine-Protein Kinase Src	4MXO
14	P14061	Oestradiol 17-Beta-Dehydrogenase 1	3HB4
15	P15121	Aldo-Keto Reductase Family 1 Member B1	4YU1
16	P18031	Tyrosine-Protein Phosphatase Non-Receptor Type 1	1ECV
17	P22303	Acetylcholinesterase	1VOT
18	P24666	Low Molecular Weight Phosphotyrosine Protein Phosphatase	5JNT
19	P28845	Corticosteroid 11-Beta-Dehydrogenase Isozyme 1	2RBE
20	P30305	M-Phase Inducer Phosphatase 2	4WH9
21	P30530	Tyrosine-Protein Kinase Receptor UFO	5U6B
22	P35228	Nitric Oxide Synthase, Inducible	3E7G
23	P35968	Vascular Endothelial Growth Factor Receptor 2	1YWN
24	Q05397	Focal Adhesion Kinase 1	4GU6

25	Q13526	Peptidyl-Prolyl Cis-Trans Isomerase NIMA-Interacting 1	6DUN
26	Q92731	Oestrogen Receptor Beta	1L2J

2.4 Extraction of Ligands

Sybyl®-X v1.1 (Ash et al., 2010) was used for PDB (Bernstein et al., 1977) visualisation and molecular modelling. For each PDB crystallographic deposition (Bernstein et al., 1977), the resident small molecule was computationally extracted and removed from its receptor to obtain the *apo* structure of the endogenous receptor.

The resident small molecule was exported onto a separate *.mol2* file format and the *apo* receptor was saved as a PDB file format. This was done for each of the 26 targets (and their respective resident small molecules) recruited for this study.

2.5 Conformational Analysis

Since no information regarding the possible bioactive conformation of Maltanedienol within the 26 *apo* targets was available, conformational analysis was performed in order to identify the optimal conformer of Maltanedienol within the LBP. An assumption was made that the bound conformer with the highest affinity and lowest potential energy would be the most likely to exist in nature. These conformers were identified as optimal. Conformer generation was carried out using Sybyl®-X v1.1 (Ash et al., 2010), by utilising the 'Similarity Suite' function. This probed the conformational space within each *apo* LBP and identified the 20 highest affinity conformers of Maltanedienol in each case. Each conformer was extracted in *.mol2* file format and numbered and named to facilitate identification.

2.5.1 Calculating the Ligand Binding Energy (LBE) (kcal/mol)

The LBE of all the 20 conformers of each receptor were calculated using X-Score v1.3 (Wang et al., 2002). Each conformer was imported one by one and all their respective energies were calculated in kcal/mol. Stability between the ligand and the molecule is extremely important. Henceforth, a conformer with a low LBE is preferred over a higher LBE.

2.5.2 Calculating the Ligand Binding Affinity (LBA) (pKd)

pKd is a measure of affinity. X-Score v1.3 (Wang et al., 2002) calculates the HPSCORE, HMSCORE and HSSCORE by using several properties such as Van der Waals interactions, hydrophobicity and hydrogen bonding and these values are used to measure the average affinity LBA, expressed in pKd. Therefore, X-Score v1.3 (Wang et al., 2002),

is a computational programme specifically designed to calculate the binding score of a given molecule:protein complex. This method was used to calculate the different binding affinities between the different conformers of Maltanedienol. The *apo* form of each receptor (26 receptor targets) as a PDB file format and their respective conformers of Maltanedienol (each receptor had 20 conformers) as a *.mol2* file format were entered and X-Score v1.3 was run.

The LBA (pKd) of each small molecule for its respective cognate receptor (n=26) was quantified in X-Score v1.3 (Wang et al., 2002) and established as a comparative baseline. A higher pKd value is preferred to a lower one, since a higher pKd represents a ligand which will be tightly bound to its receptor, which is the desirable scenario.

2.5.3 Choosing the Optimal Conformer

The LBA (pKd) and LBE (kcal/mol) values for each receptor and its conformers, obtained from X-Score (Wang et al., 2002) were used to produce line graphs. Graphs (n=26) of LBA (pKd) and LBE (kcal/mol) on the y-axis against Maltanedienol Conformer Number, on the x-axis, were plotted and can be seen in Section 3.1. The conformer with the greatest peak height difference, between LBA (pKd) and LBE (kcal/mol), was the optimal conformer and identified as the most likely bioactive scaffold based on high affinity and greatest stability.

2.6 Recruiting Receptor Targets

After conformational analysis and the LBA (pKd) of the optimal conformer of Maltanedienol docked into each target LBP was quantified *in silico,* it was compared to that of the co-crystallised small molecule, set as a baseline affinity for comparison (Table 3.1). This created a scenario in which it could be established whether the optimal conformer of Maltanedienol bound to each of the targets with an affinity that exceeded that of the endogenous small molecule. For those cases where the affinity of the optimal conformer of Maltanedienol was greater than that of the endogenous small molecule, a predicted case could be made for the optimal conformer of Maltanedienol binding to the target preferentially in a competitive scenario.

This process yielded 7 target proteins for which the optimal conformer of Maltanedienol had an LBA (pKd) value greater or equal to that of the co-crystallized small molecules. This means that 26.9% of the targets recruited into this study identified by the software of D'Emanuele (2019) produced complexes with Maltanedienol that had an affinity greater or equal to those complexes formed by the same target complexed with the high affinity small molecules described on the PDB (Bernstein et al., 1977).

2.7 2D Topology Maps

2D topology maps showcase the ligand binding contacts between each optimal conformer of Maltanedienol and its respective receptor. These maps act as guides and aid the formation of seeds. Ligand binding maps were produced for each of the seven receptors which were recruited for this study.

2.7.1 Docking Optimal Conformer of Maltanedienol to the *apo* receptor

Sybyl®-X v1.1 (Ash et al., 2010) was used to dock the optimal conformer of Maltanedienol to its respective *apo* receptor. The *apo* receptor (M1) in PDB file format and its respective optimal Maltanedienol conformer (M2) in *.mol2* file format were imported into Sybyl®-X v1.1 (Ash et al., 2010) and merged by using the command line as follows - merge M2 M1. Then the complexed molecule was extracted as a PDB file. This was repeated for the seven receptors recruited for this study.

2.7.2 Creating 2D Ligand Protein Contact Maps

Ligand protein contact maps were created using BIOVIA Discovery Studio Visualizer® v20.1.[7] Each complex molecule produced in Section 2.7.1 was imported into this programme. Using the 'Receptor Ligand Interactions' function, then clicking 'show 2D diagrams', the 2D ligand protein maps were produced. These maps exhibited the critical points of contact and the interaction forged between the optimal conformer of

[7] Dassault Systèmes. BIOVIA Discovery Studio Visualizer. Version 20.1 [software]. Dassault Systèmes. 2020 [cited 2021 Jul 14; downloaded 2021 May 25]. Available from: https://www.3dsbiovia.com/products/collaborative-science/biovia-discovery-studio/visualization-download.php.

Maltanedienol and its respective protein receptor. The topology maps created in each case were saved and can be seen in Section 3.3.1.

2.8 *De novo* Drug Design

2.8.1 Creating 3D maps of the LBP

De novo drug design was carried out using LigBuilder® v1.2 (Wang et al., 2000). This programme allows the formation of LBP maps of the optimal conformer of Maltanedienol when bound to its respective receptor. The POCKET algorithm of this software permits the identification of pharmacophoric structural features and key site interaction of the *apo* receptor structure.

In this study, each of the *apo* receptors were used in *.pdb* file format according to the POCKET algorithm.

2.8.2 Creating Seed Structures

The 7 topology maps for each recruited receptor and its respective optimal Maltanedienol conformer were created as described in Section 2.7 and used to guide the seed creation process for *de novo* drug design.

Following the analysis of the 2D topology maps generated in BIOVIA Discovery Studio Visualizer® v20.1[7], between 1 and 2 seed structures were created for each of the 7 optimal conformers of Maltanedienol using Sybyl®-X (Ash et al., 2010). These seeds were created by following the following steps:

[7] Dassault Systèmes. BIOVIA Discovery Studio Visualizer. Version 20.1 [software]. Dassault Systèmes. 2020 [cited 2021 Jul 14; downloaded 2021 May 25]. Available from: https://www.3dsbiovia.com/products/collaborative-science/biovia-discovery-studio/visualization-download.php.

- Firstly looking at the areas on the 2D ligand protein contact maps which are presenting unfavourable bumps.
- The optimal conformer of Maltanedienol for its respective receptor (as determined by conformational analysis) was imported into SYBYL®-X as a *.mol2* file.
- The side-chains which produced unfavorable bumps in the contact map were removed by selecting the redundant atoms using the 'Selection' function and then deleted.
- The resulting molecule possessed an incomplete bond. This bond was altered into H.spc atom, to guide the GROW algorithm in LigBuilder® v1.2 (Wang et al., 2000) at the specified loci. By utilizing the 'Modify atom' function under 'Edit – Atom' and choosing 'only_type' and the H.spc option as atom type, the selected atom was altered into an H.spc atom.
- The seed structures were exported as *.mol2* files and named sequentially as 'PDB ID seed number', for example 2rbeseed1.
- This process was repeated to create up to two successful seeds of each optimal conformer of Maltanedienol for its respective receptor.

2.8.3 Sustained Growth of Seed Structures

LigBuilder® v1.2 (Wang et al., 2000) was utilised to generate novel structures built on the seed scaffolds generated. The GROW algorithm was used to produce all 11 seed structures, therefore the template followed was the *grow.index* file. The parameters implicated when utilising the GROW algorithm in LigBuilder® v1.2 (Wang et al., 2000) to produce novel structures and may be seen described in the Table 2.4.

Table 2.4 Parameters used in the GROW algorithm in LigBuilder® v1.2 (Wang et al., 2000) to generate *de novo* molecules.

Maximal Molecular Weight	600
Minimal Molecular Weight	300
Maximal LogP	6.00
Minimal LogP	3.00
Maximal Hb Donor Atom	6
Minimal Hb Donor Atom	2
Maximal Hb Acceptor Atom	6
Minimal Hb Acceptor Atom	2
Maximal pKd	10.00
Minimal pKd	5.00

When a seed sustained growth, the molecule could progress to the next step in the study. The next step involved the PROCESS module in Ligbuilder® v1.2 (Wang et al., 2000), to generate the *population.lig* and *ligands.lig* files to obtain the *de novo* molecules. Table 2.5 below outlines the parameters used for the PROCESS algorithm in LigBuilder® v1.2 (Wang et al., 2000). The PROCESS module was used to export the best novel structures from the total number of molecules generated from the GROW algorithm. The results and molecules were exported in a *results.mdb* folder.

Table 2.5 Parameters used for the PROCESS algorithm in LigBuilder® v1.2 (Wang et al., 2000).

Maximal Molecular Weight	500
Minimal Molecular Weight	200
Maximal LogP	5.00
Minimal LogP	2.00
Maximal pKd	10.00
Minimal pKd	1.00

The newly generated *de novo* molecules were filtered in Microsoft Excel (Excel, 2019) to ensure Lipinski Rule compliance (Lipinski et al., 2001). The molecules were first filtered by molecular weight (MW) and LogP from the data generated in LigBuilder® v1.2 (Wang et al., 2000). Molecules which had a MW of more than 500 and/or a LogP greater than 5 were filtered and removed from the results.

The results were then filtered by the number of H-bond donors and H-bond acceptors using BIOVIA Discovery Studio Visualizer® v20.1[7] and BIOVIA Draw® v17.1.[4] Using the filtered data, the resulting molecules were grouped according to family and affinity. Three results from each family with the highest affinity were chosen and each of their H-bond donors and H-bond acceptors were calculated. The chosen resultant molecule was

[4] Dassault Systèmes. BIOVIA Draw. Version 17.1 [software]. Dassault Systèmes. 2017 [cited 2021 Jul 14; downloaded 2021 May 25]. Available from: https://hts.c2b2.columbia.edu/draw/.
[7] Dassault Systèmes. BIOVIA Discovery Studio Visualizer. Version 20.1 [software]. Dassault Systèmes. 2020 [cited 2021 Jul 14; downloaded 2021 May 25]. Available from: https://www.3dsbiovia.com/products/collaborative-science/biovia-discovery-studio/visualization-download.php.

opened in BIOVIA Discovery Studio Visualizer® v20.1[7] and saved as an MDL MOL/SD file. This new created file was then opened in BIOVIA Draw® v17.1[4] and was saved as a *.mol2* file and the number of H-bond donors and H-bond acceptors was calculated from the 'Chemistry' tab using the 'Calculator' function. The number of H-bond donors and H-bond acceptors were inputted into the Microsoft Excel (Excel, 2019) sheet.

Table 2.6 Parameters set to filter the results from the molecules produced by LigBuilder® v1.2 (Wang et al., 2000) in Microsoft Excel (Excel, 2019), according to Lipinski's Rule of 5 (Lipinski et al., 2001).

Parameter	**Value**
Molecular Weight	< 500
LogP	< 5
Hydrogen Bond Acceptor (HBA)	≤ 10
Hydrogen Bond Donor (HBD)	≤ 5

[4] Dassault Systèmes. BIOVIA Draw. Version 17.1 [software]. Dassault Systèmes. 2017 [cited 2021 Jul 14; downloaded 2021 May 25]. Available from: https://hts.c2b2.columbia.edu/draw/.
[7] Dassault Systèmes. BIOVIA Discovery Studio Visualizer. Version 20.1 [software]. Dassault Systèmes. 2020 [cited 2021 Jul 14; downloaded 2021 May 25]. Available from: https://www.3dsbiovia.com/products/collaborative-science/biovia-discovery-studio/visualization-download.php.

Chapter 3

Results

3.1 Estimating the LBA and LBE of Maltanedienol conformers

Conformational analysis was carried out, which consisted of docking Maltanedienol into each of the 26 receptors' LBP and allowing single bond rotations within the confines of its perimeter. The twenty highest affinity conformers of Maltanedienol for its respective receptor were identified and their LBA expressed as pKd and LBE in kcal/mol was quantified in X-Score (Wang et al., 2002) and these values were utilised to produce line graphs. In each case, the conformer number was identified as optimal based on having the highest LBA (pKd) and the lowest LBE (kcal/mol), on the premise of a compromise between affinity and energetic stability.

The following graphs depict the data described above, as well as show the optimal conformer of Maltanedienol docked into each target receptor, proposed by the software of D'Emanuele (2019) which were found on the PDB (Bernstein et al., 1977) and which are involved in calcium fixation and/or bone remodelling.

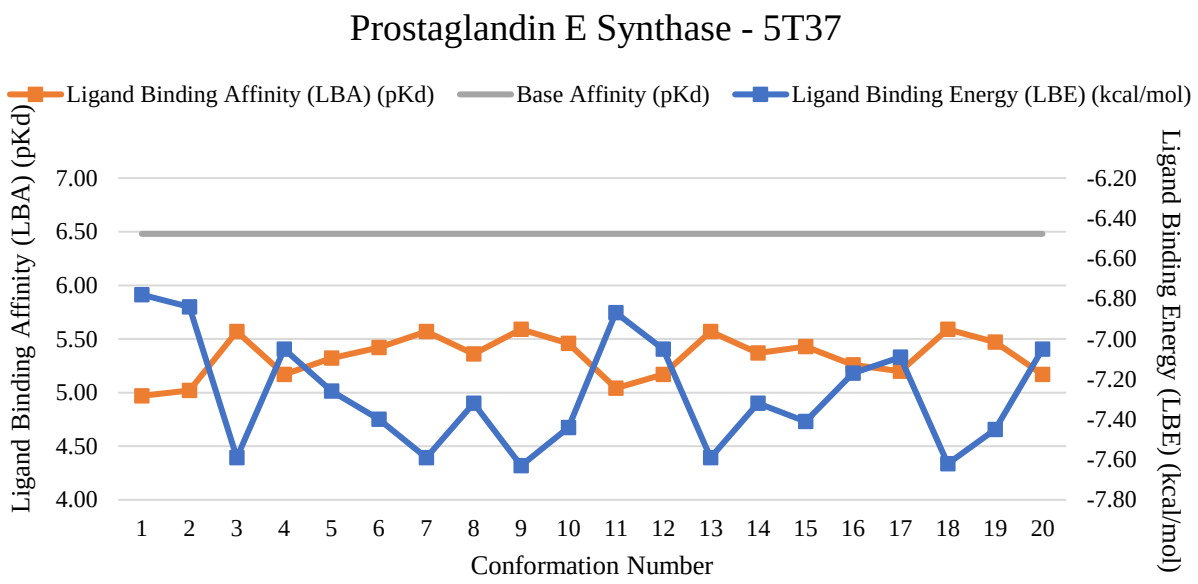

Figure 3.1 Graph of LBA (pKd) on the primary y-axis and LBA (kcal/mol) on the secondary y-axis vs Conformer Number on the x-axis for Maltanedienol docked into the LBP of Prostaglandin E Synthase as described in PDB ID: 5T37.

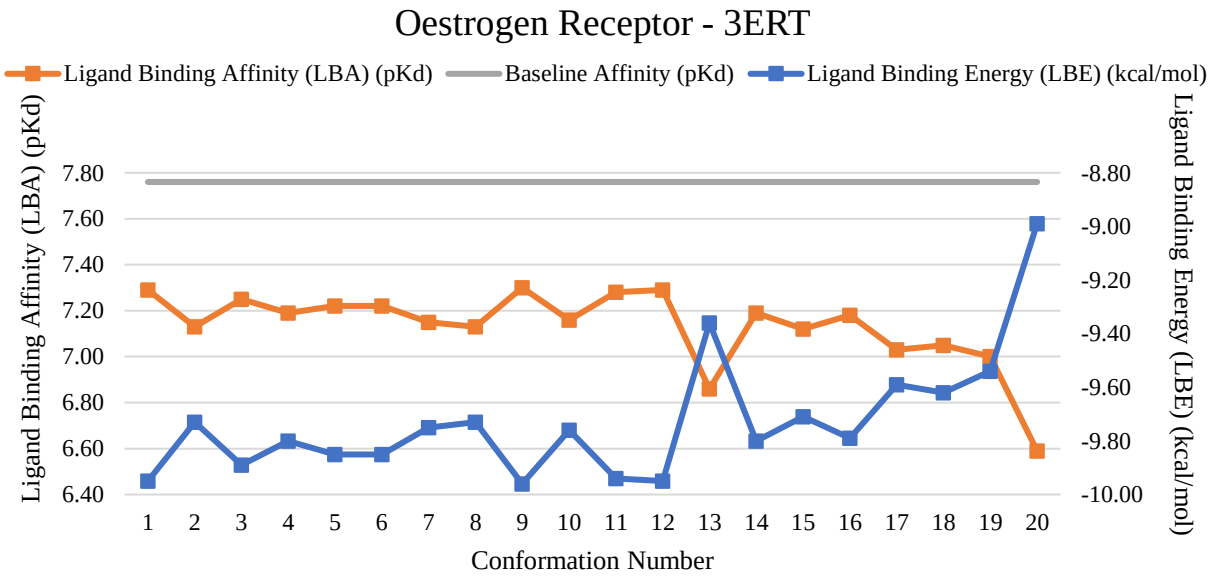

Figure 3.2 Graph of LBA (pKd) on the primary y-axis and LBA (kcal/mol) on the secondary y-axis vs Conformer Number on the x-axis for Maltanedienol docked into the LBP of the Oestrogen Receptor as described in PDB ID: 3ERT.

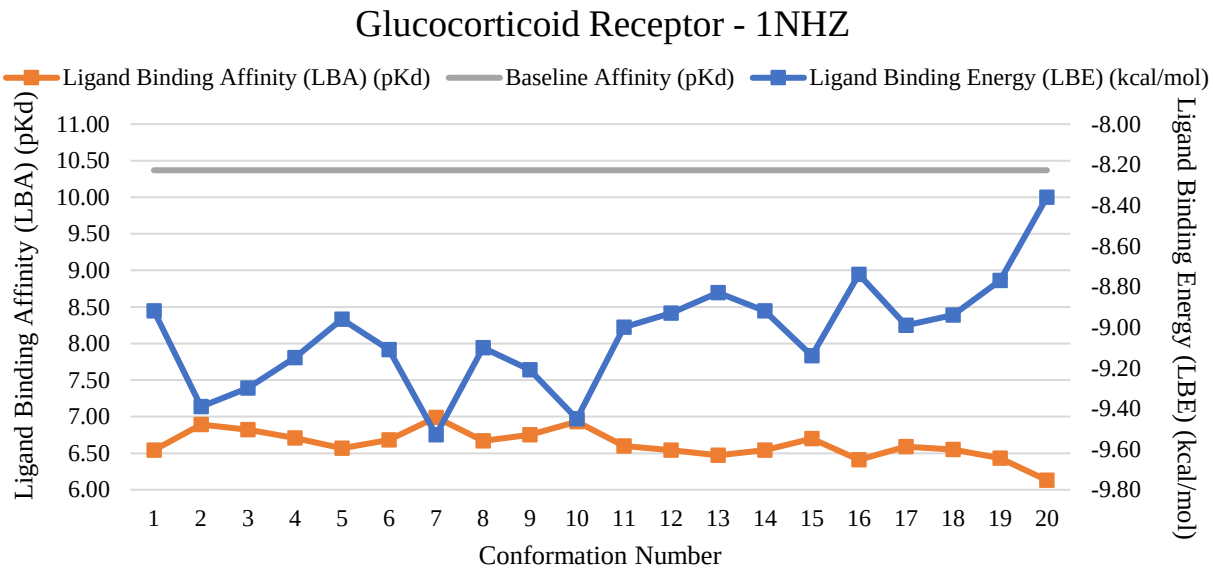

Figure 3.3 Graph of LBA (pKd) on the primary y-axis and LBA (kcal/mol) on the secondary y-axis vs Conformer Number on the x-axis for Maltanedienol docked into the LBP of the Glucocorticoid Receptor as described in PDB ID: 1NHZ.

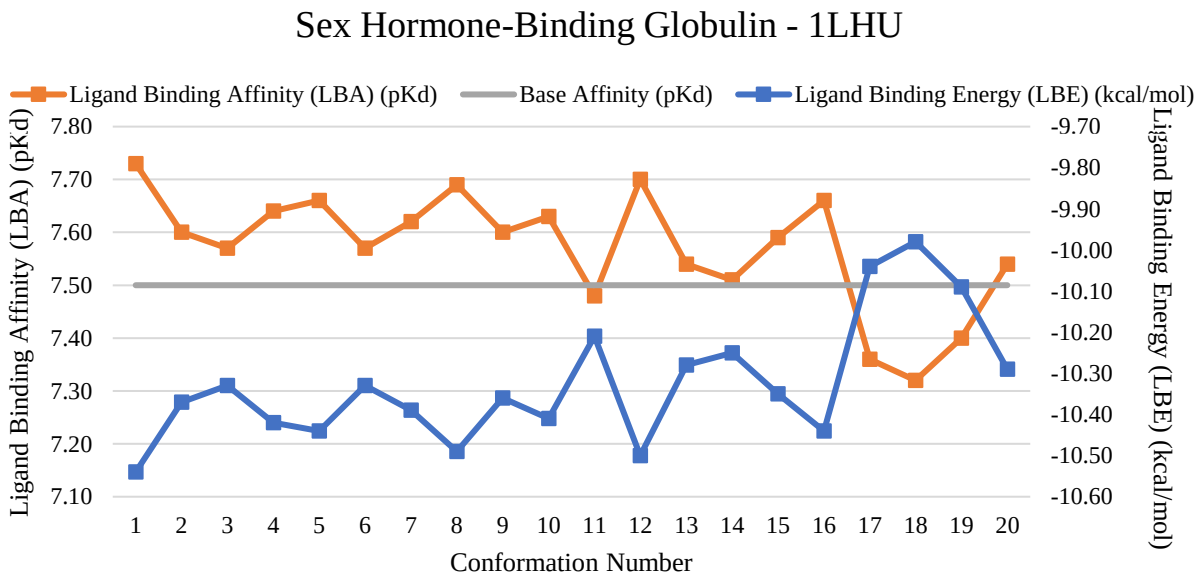

Figure 3.4 Graph of LBA (pKd) on the primary y-axis and LBA (kcal/mol) on the secondary y-axis vs Conformer Number on the x-axis for Maltanedienol docked into the LBP of the Sex Hormone-Binding Globulin as described in PDB ID: 1LHU.

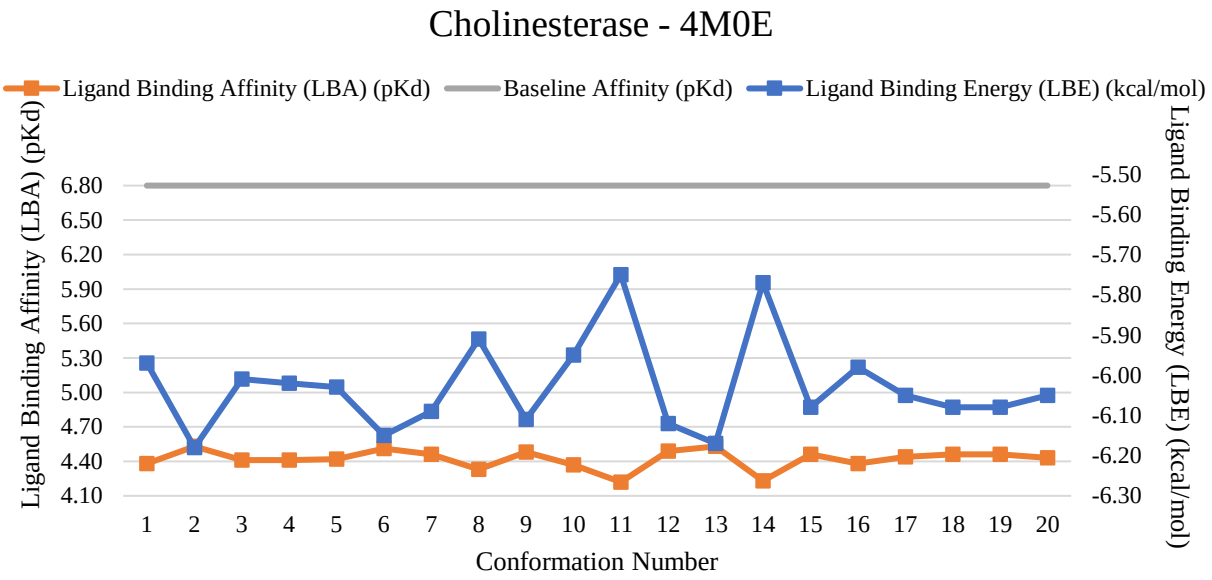

Figure 3.5 Graph of LBA (pKd) on the primary y-axis and LBA (kcal/mol) on the secondary y-axis vs Conformer Number on the x-axis for Maltanedienol docked into the LBP of Cholinesterase as described in PDB ID: 4M0E.

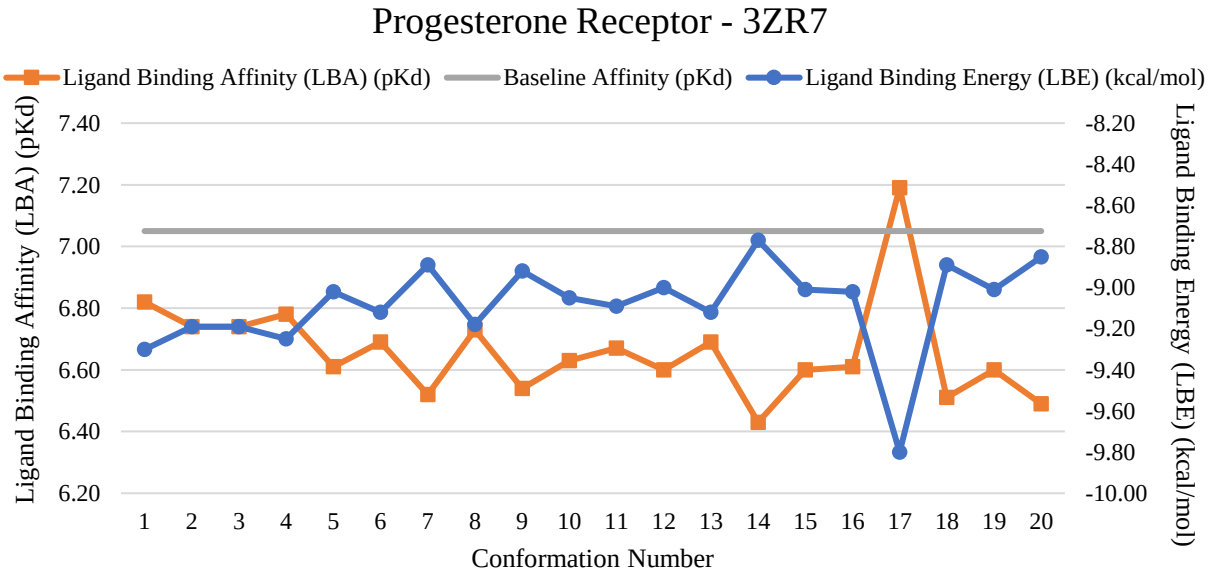

Figure 3.6 Graph of LBA (pKd) on the primary y-axis and LBA (kcal/mol) on the secondary y-axis vs Conformer Number on the x-axis for Maltanedienol docked into the LBP of the Progesterone Receptor as described in PDB ID: 3ZR7.

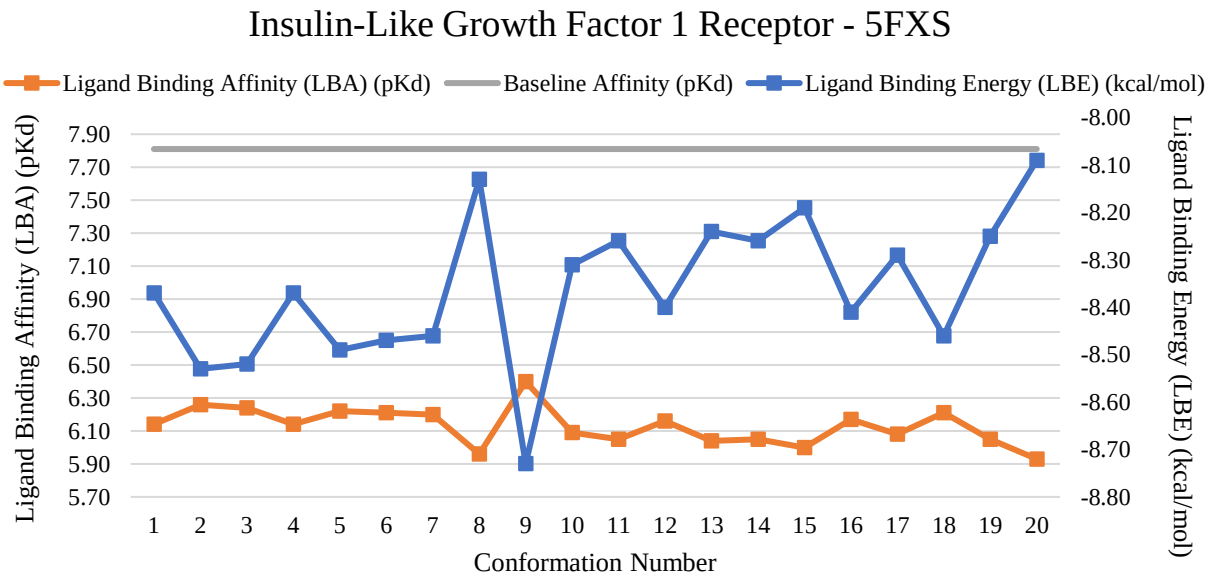

Figure 3.7 Graph of LBA (pKd) on the primary y-axis and LBA (kcal/mol) on the secondary y-axis vs Conformer Number on the x-axis for Maltanedienol docked into the LBP of the Insulin-Like Growth Factor 1 Receptor as described in PDB ID: 5FXS.

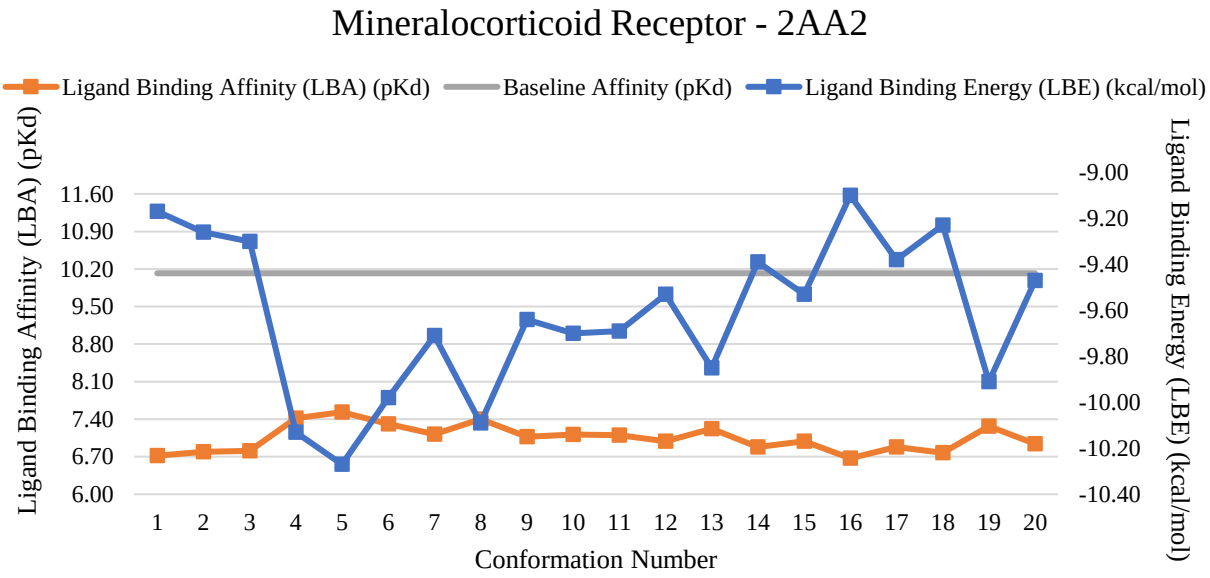

Figure 3.8 Graph of LBA (pKd) on the primary y-axis and LBA (kcal/mol) on the secondary y-axis vs Conformer Number on the x-axis for Maltanedienol docked into the LBP of the Mineralocorticoid Receptor as described in PDB ID: 2AA2.

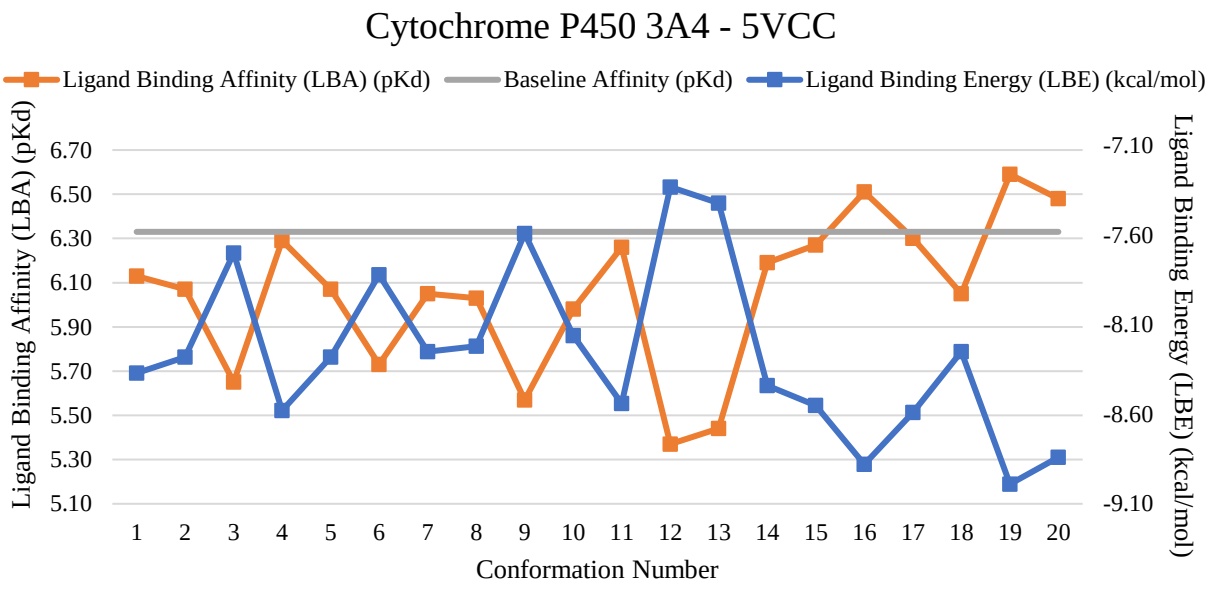

Figure 3.9 Graph of LBA (pKd) on the primary y-axis and LBA (kcal/mol) on the secondary y-axis vs Conformer Number on the x-axis for Maltanedienol docked into the LBP of the Cytochrome P450 3A4 as described in PDB ID: 5VCC.

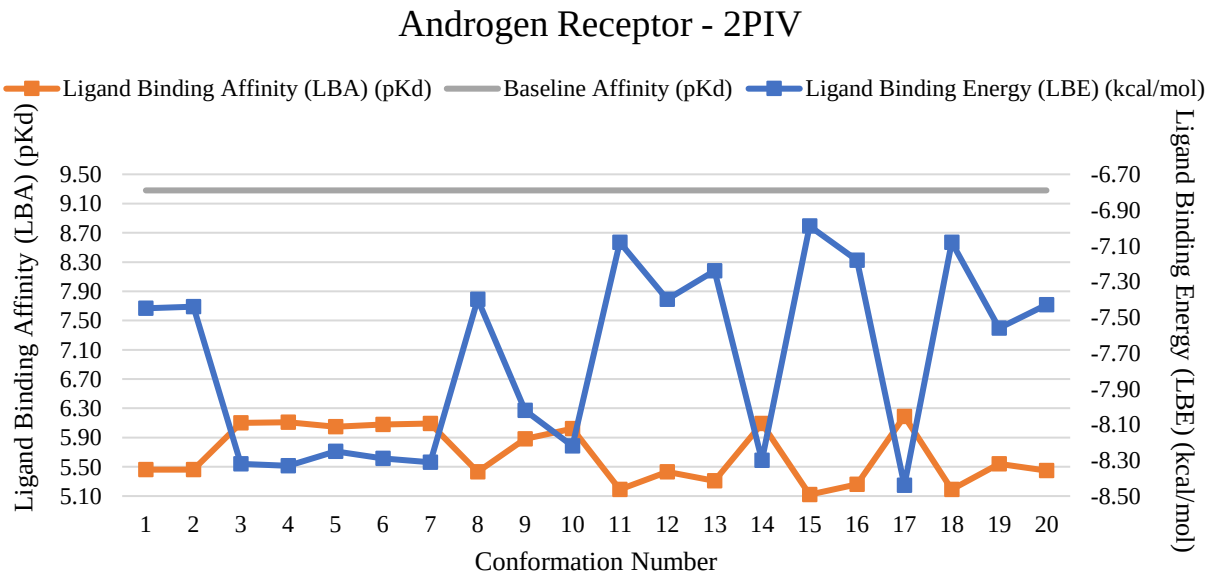

Figure 3.10 Graph of LBA (pKd) on the primary y-axis and LBA (kcal/mol) on the secondary y-axis vs Conformer Number on the x-axis for Maltanedienol docked into the LBP of the Androgen Receptor as described in PDB ID: 2PIV.

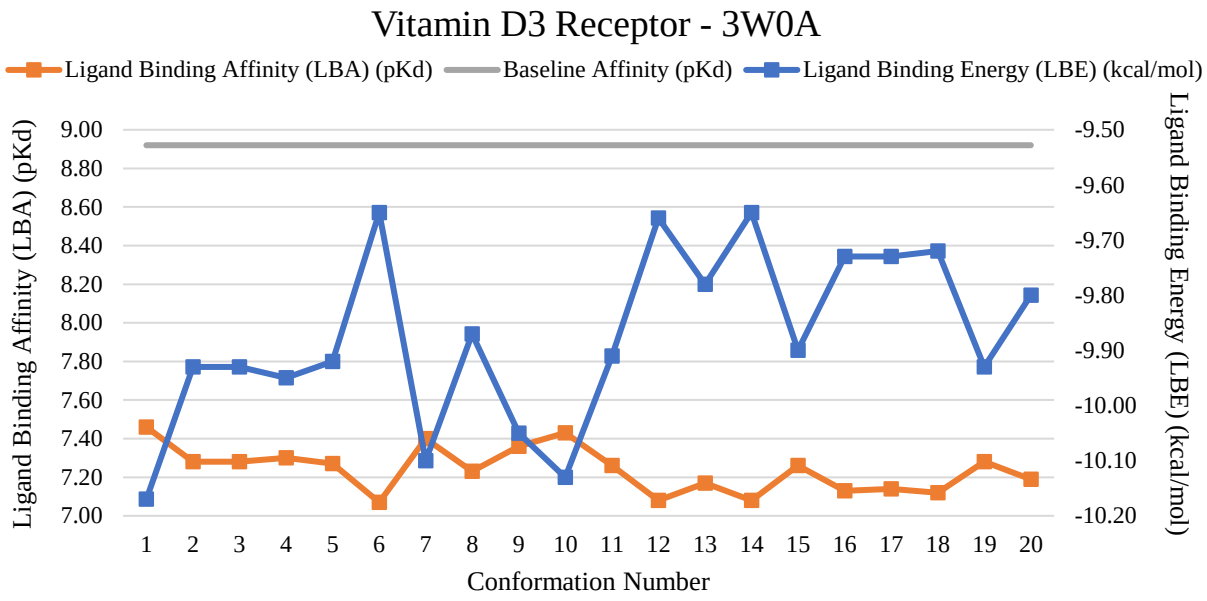

Figure 3.11 Graph of LBA (pKd) on the primary y-axis and LBA (kcal/mol) on the secondary y-axis vs Conformer Number on the x-axis for Maltanedienol docked into the LBP of the Vitamin D3 Receptor as described in PDB ID: 3W0A.

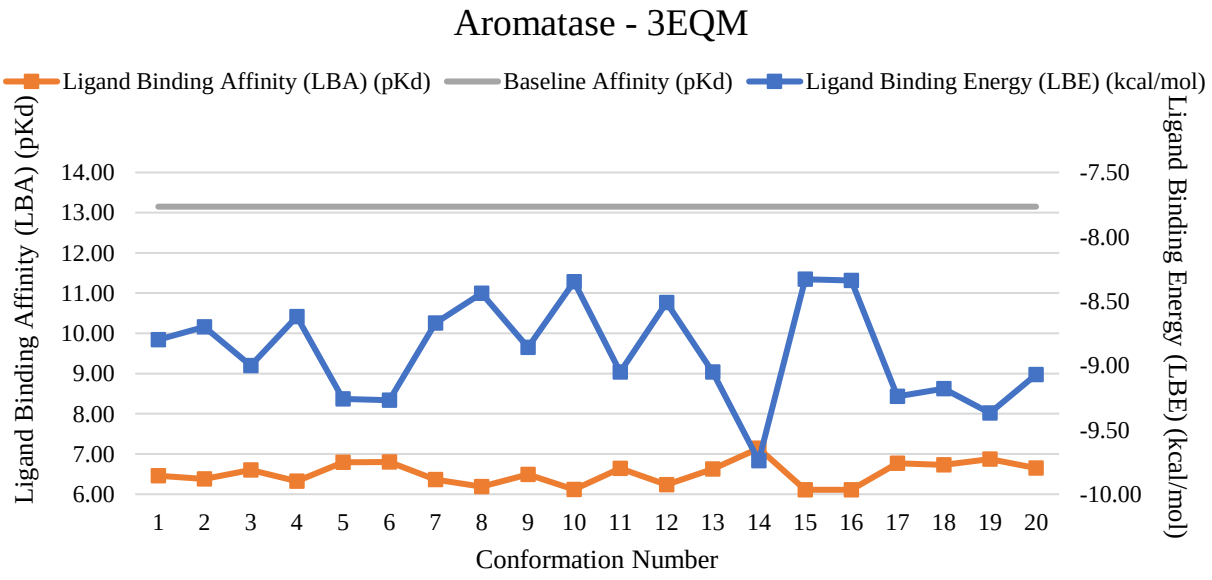

Figure 3.12 Graph of LBA (pKd) on the primary y-axis and LBA (kcal/mol) on the secondary y-axis vs Conformer Number on the x-axis for Maltanedienol docked into the LBP of Aromatase as described in PDB ID: 3EQM.

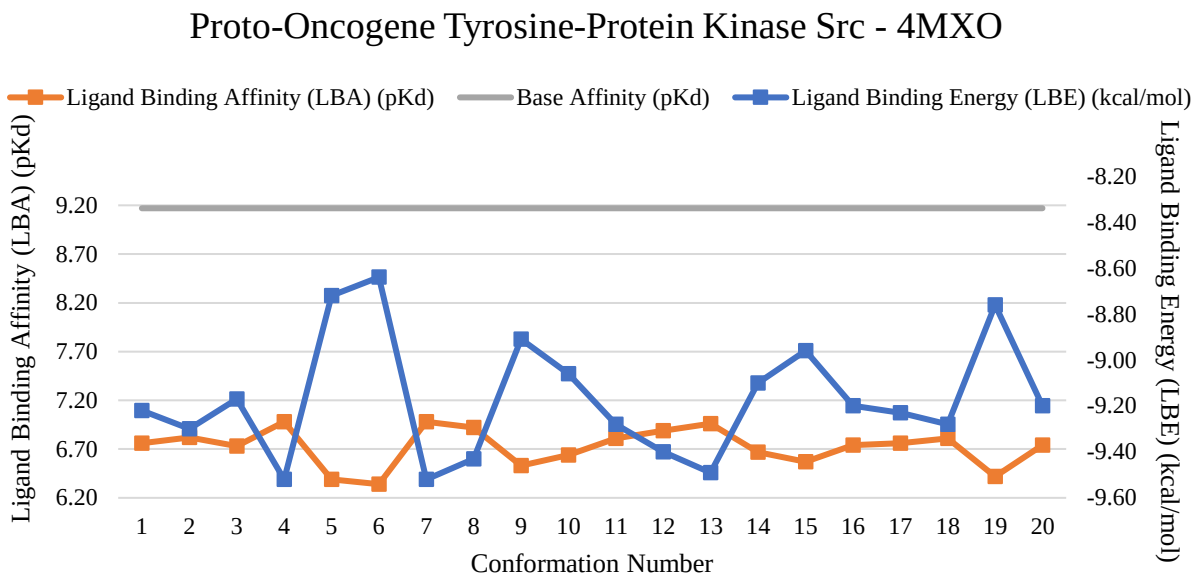

Figure 3.13 Graph of LBA (pKd) on the primary y-axis and LBA (kcal/mol) on the secondary y-axis vs Conformer Number on the x-axis for Maltanedienol docked into the LBP of the Proto-Oncogene Tyrosine-Protein Kinase Src as described in PDB ID: 4MXO.

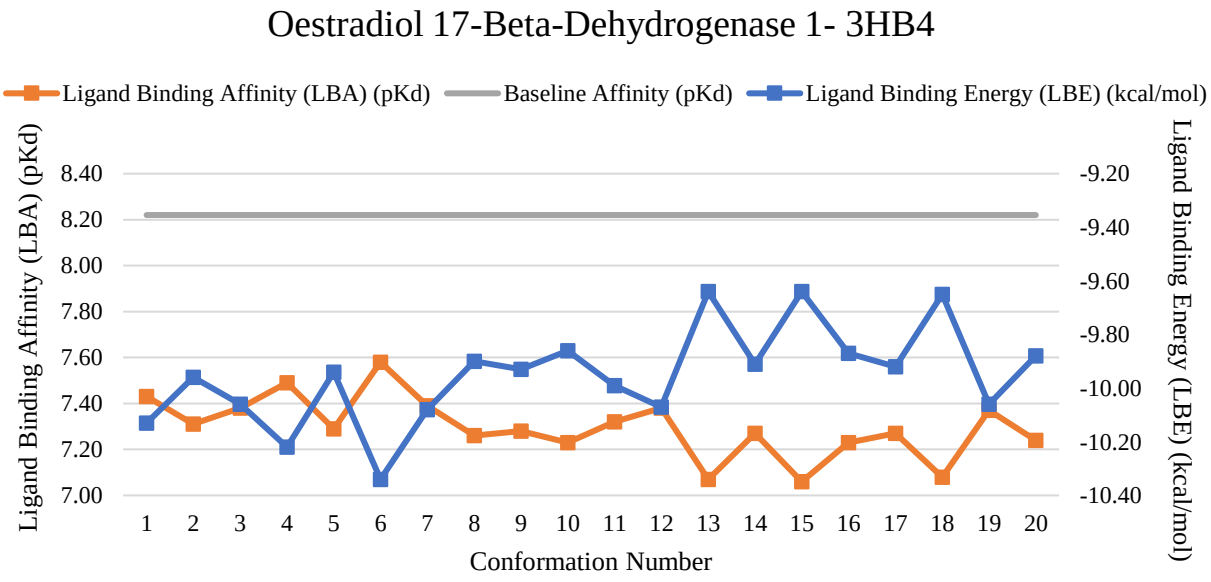

Figure 3.14 Graph of LBA (pKd) on the primary y-axis and LBA (kcal/mol) on the secondary y-axis vs Conformer Number on the x-axis for Maltanedienol docked into the LBP of Oestradiol 17-Beta-Dehydrogenase 1 as described in PDB ID: 3HB4.

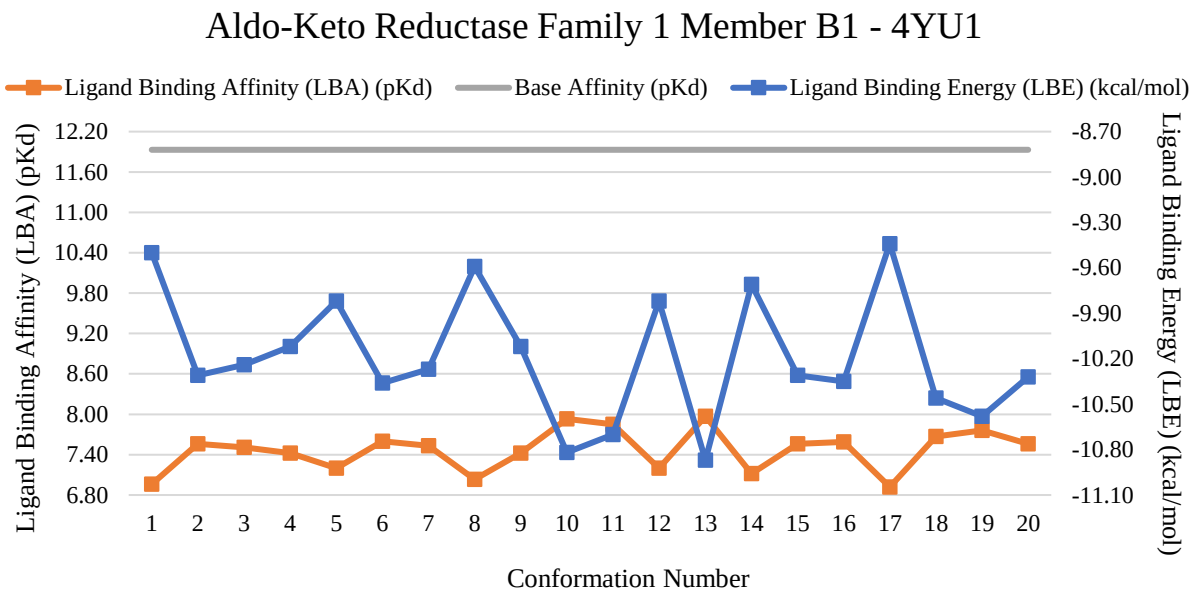

Figure 3.15 Graph of LBA (pKd) on the primary y-axis and LBA (kcal/mol) on the secondary y-axis vs Conformer Number on the x-axis for Maltanedienol docked into the LBP of the Aldo-Keto Reductase Family 1 Member B1 as described in PDB ID: 4YU1.

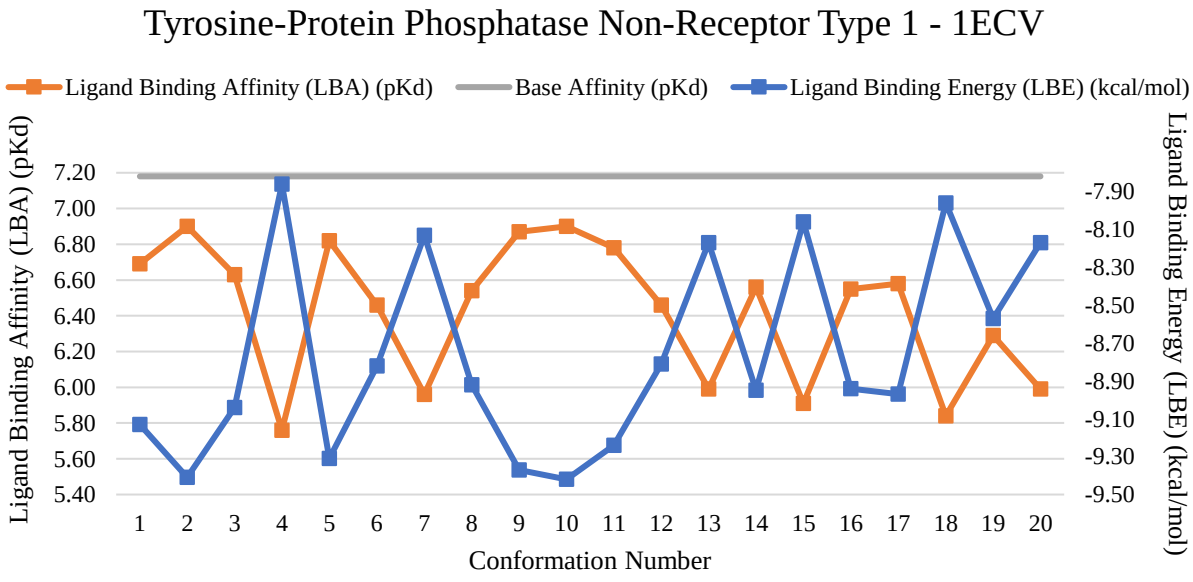

Figure 3.16 Graph of LBA (pKd) on the primary y-axis and LBA (kcal/mol) on the secondary y-axis vs Conformer Number on the x-axis for Maltanedienol docked into the LBP of the Tyrosine-Protein Phosphatase Non-Receptor Type 1 as described in PDB ID: 1ECV.

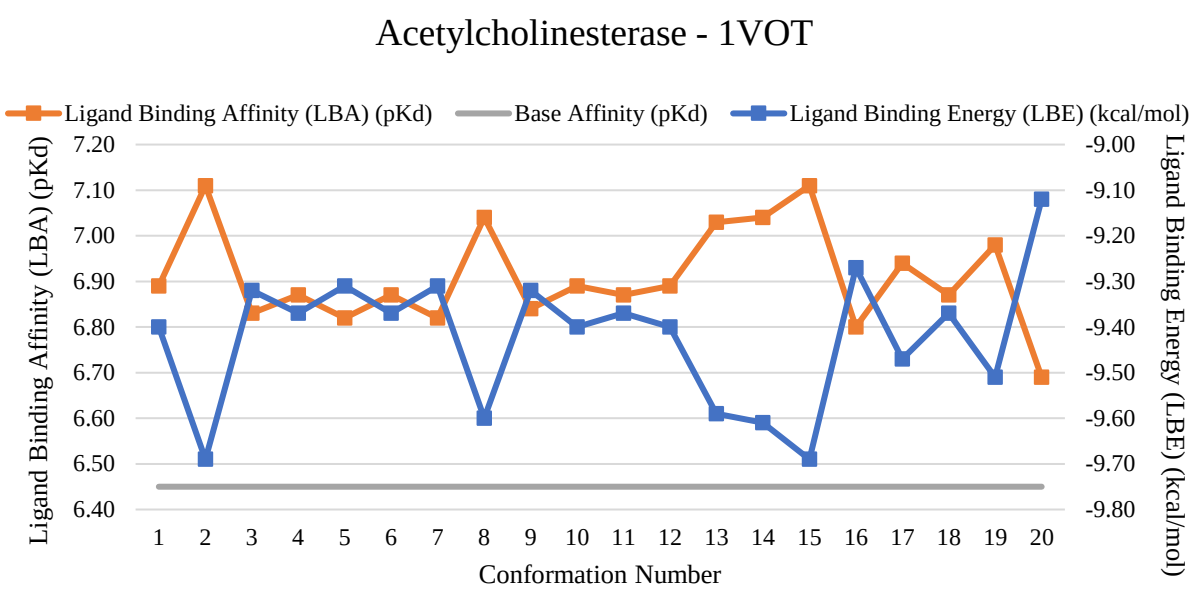

Figure 3.17 Graph of LBA (pKd) on the primary y-axis and LBA (kcal/mol) on the secondary y-axis vs Conformer Number on the x-axis for Maltanedienol docked into the LBP of Acetylcholinesterase as described in PDB ID: 1VOT.

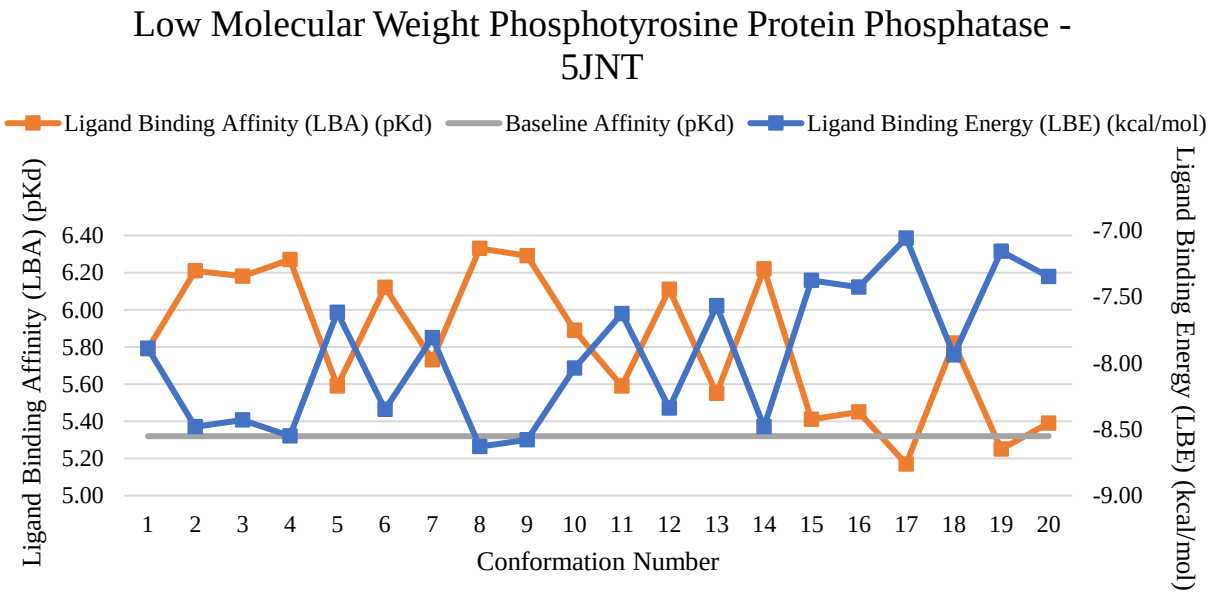

Figure 3.18 Graph of LBA (pKd) on the primary y-axis and LBA (kcal/mol) on the secondary y-axis vs Conformer Number on the x-axis for Maltanedienol docked into the LBP of the Low Molecular Weight Phosphotyrosine Protein Phosphatase as described in PDB ID: 5JNT.

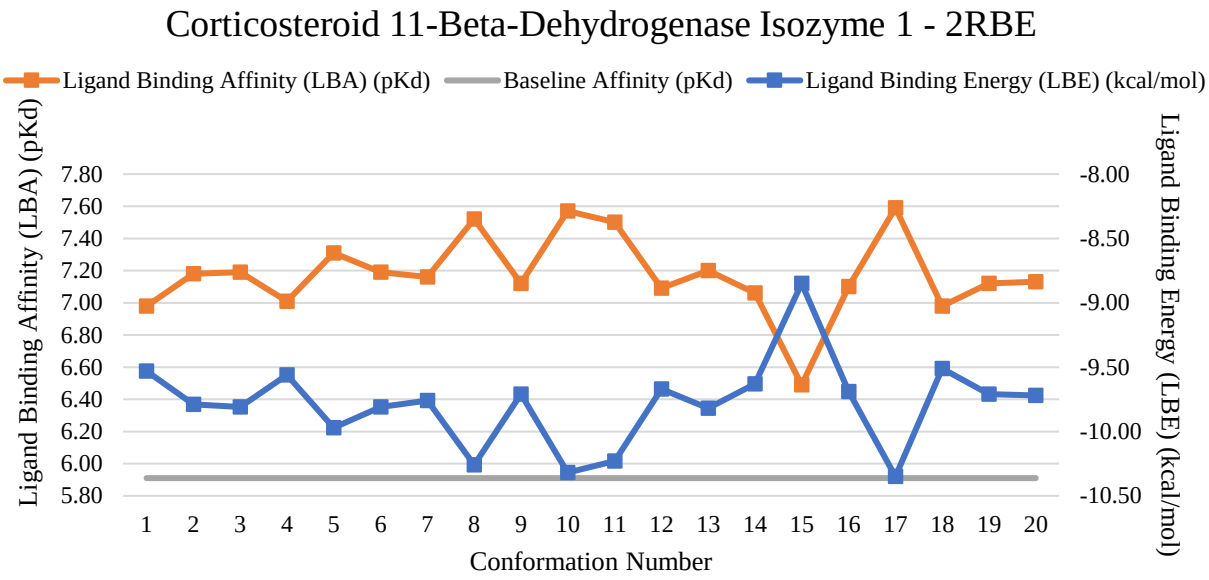

Figure 3.19 Graph of LBA (pKd) on the primary y-axis and LBA (kcal/mol) on the secondary y-axis vs Conformer Number on the x-axis for Maltanedienol docked into the LBP of the Corticosteroid 11-Beta-Dehydrogenase Isozyme 1 as described in PDB ID: 2RBE.

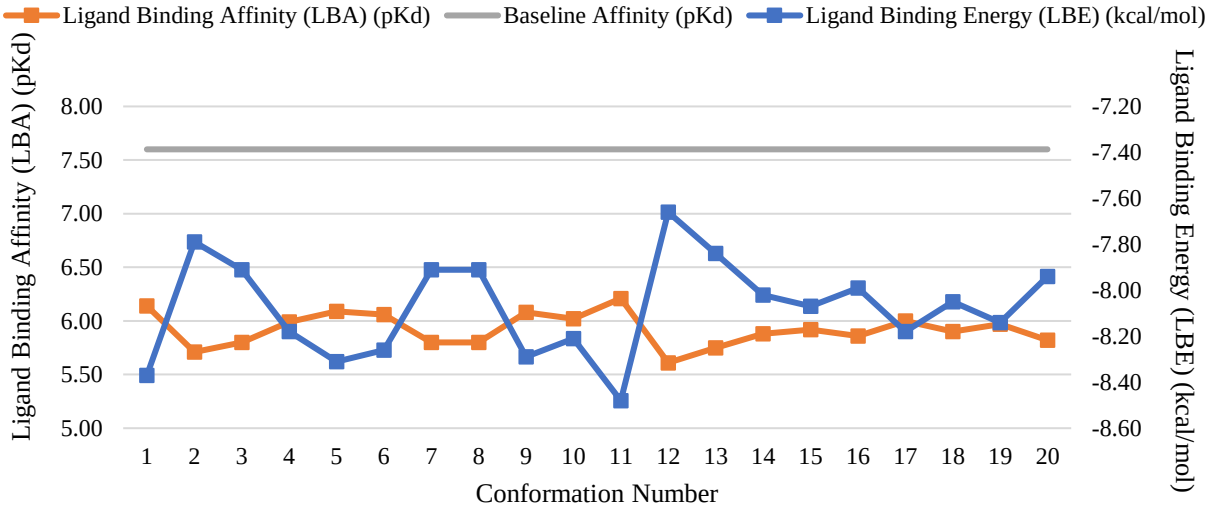

Figure 3.20 Graph of LBA (pKd) on the primary y-axis and LBA (kcal/mol) on the secondary y-axis vs Conformer Number on the x-axis for Maltanedienol docked into the LBP of the M-Phase Inducer Phosphatase 2 as described in PDB ID: 4WH9.

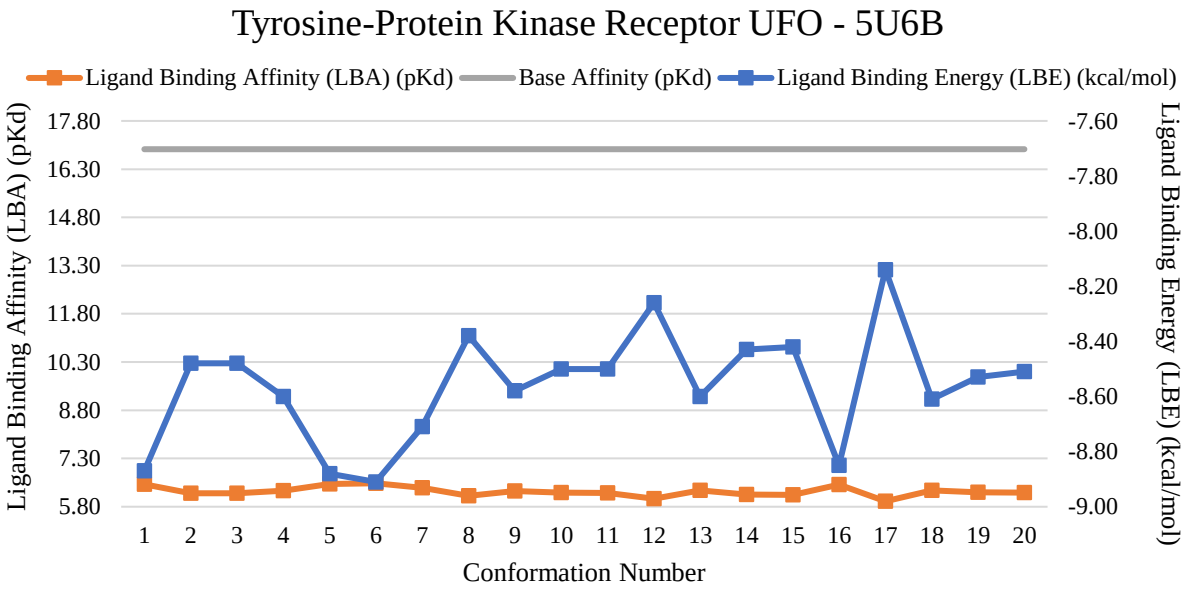

Figure 3.21 Graph of LBA (pKd) on the primary y-axis and LBA (kcal/mol) on the secondary y-axis vs Conformer Number on the x-axis for Maltanedienol docked into the LBP of the Tyrosine-Protein Kinase Receptor UFO as described in PDB ID: 5U6B.

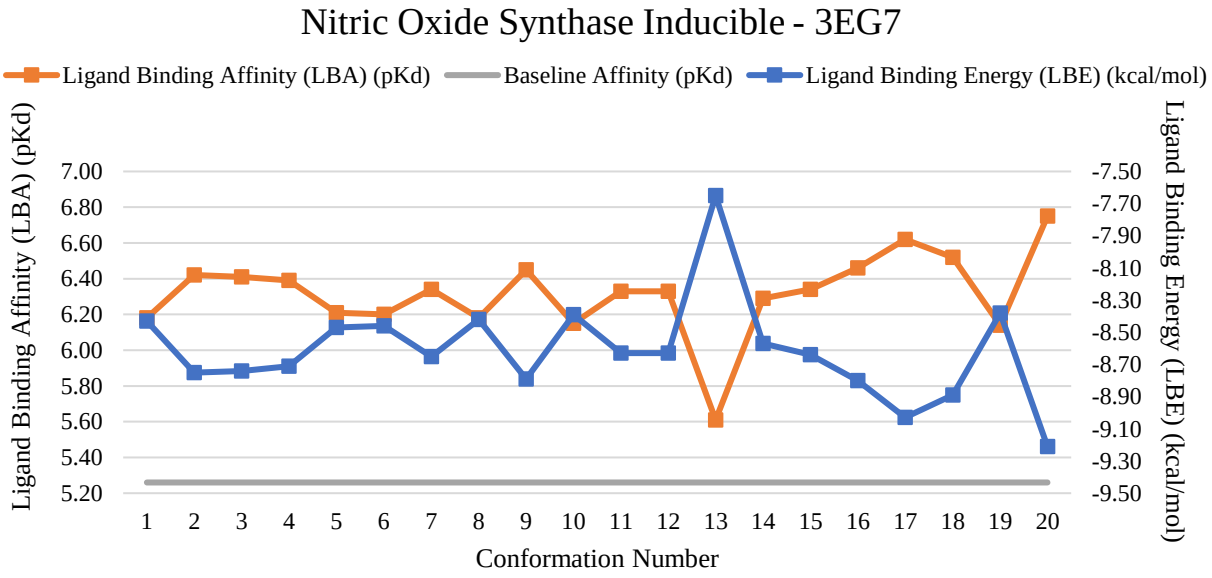

Figure 3.22 Graph of LBA (pKd) on the primary y-axis and LBA (kcal/mol) on the secondary y-axis vs Conformer Number on the x-axis for Maltanedienol docked into the LBP of Nitric Oxide Synthase Inducible as described in PDB ID: 3EG7.

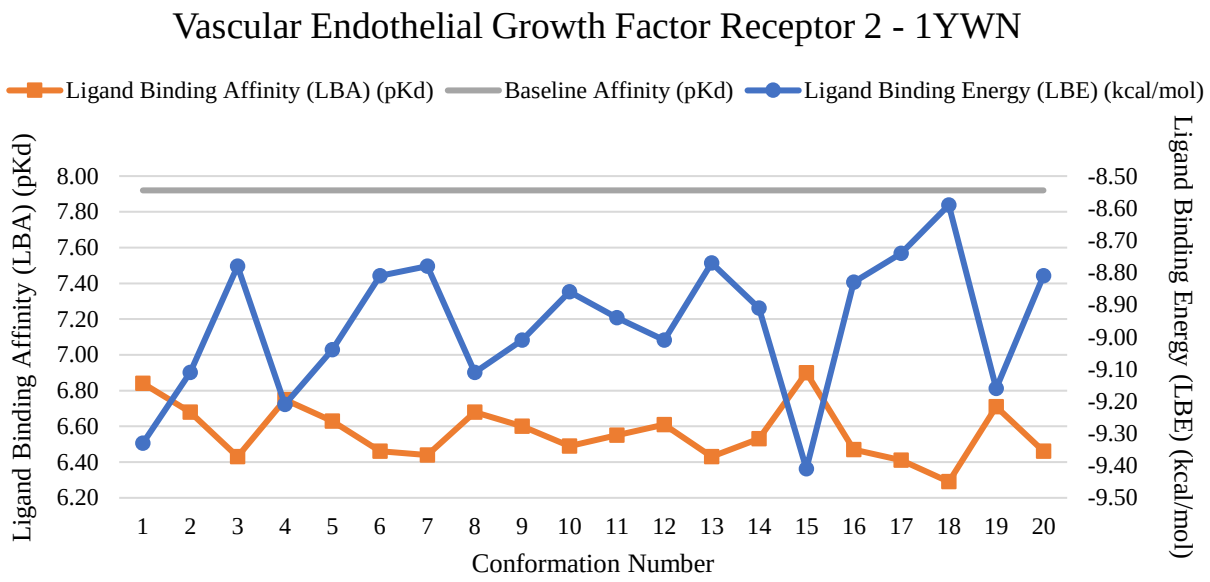

Figure 3.23 Graph of LBA (pKd) on the primary y-axis and LBA (kcal/mol) on the secondary y-axis vs Conformer Number on the x-axis for Maltanedienol docked into the LBP of the Vascular Endothelial Growth Factor Receptor 2 as described in PDB ID: 1YWN.

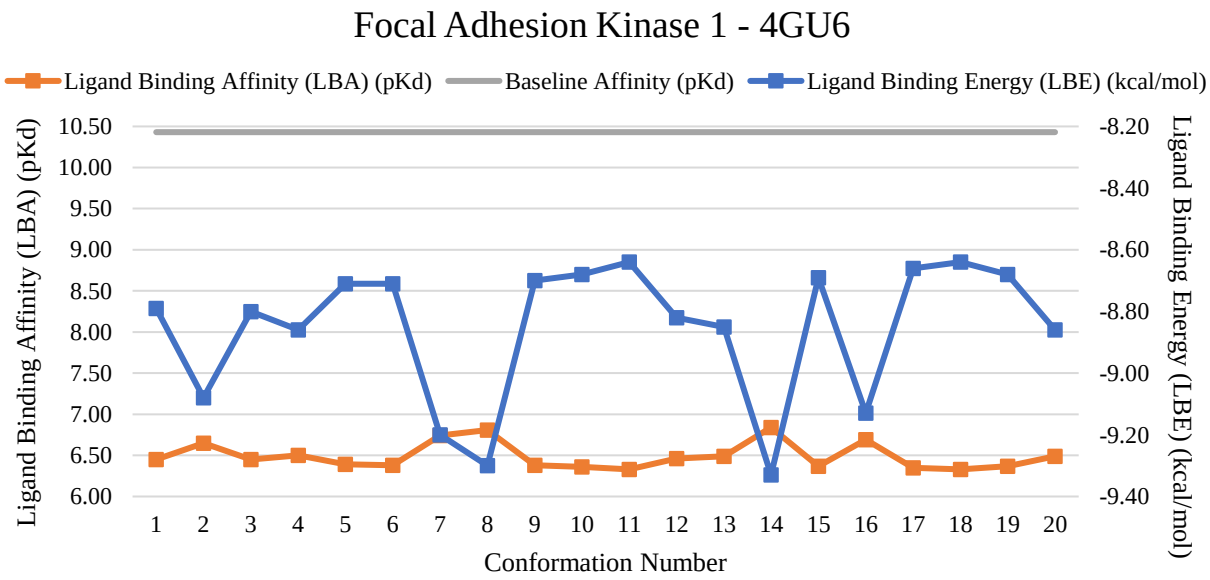

Figure 3.24 Graph of LBA (pKd) on the primary y-axis and LBA (kcal/mol) on the secondary y-axis vs Conformer Number on the x-axis for Maltanedienol docked into the LBP of the Focal Adhesion Kinase 1 as described in PDB ID: 4GU6.

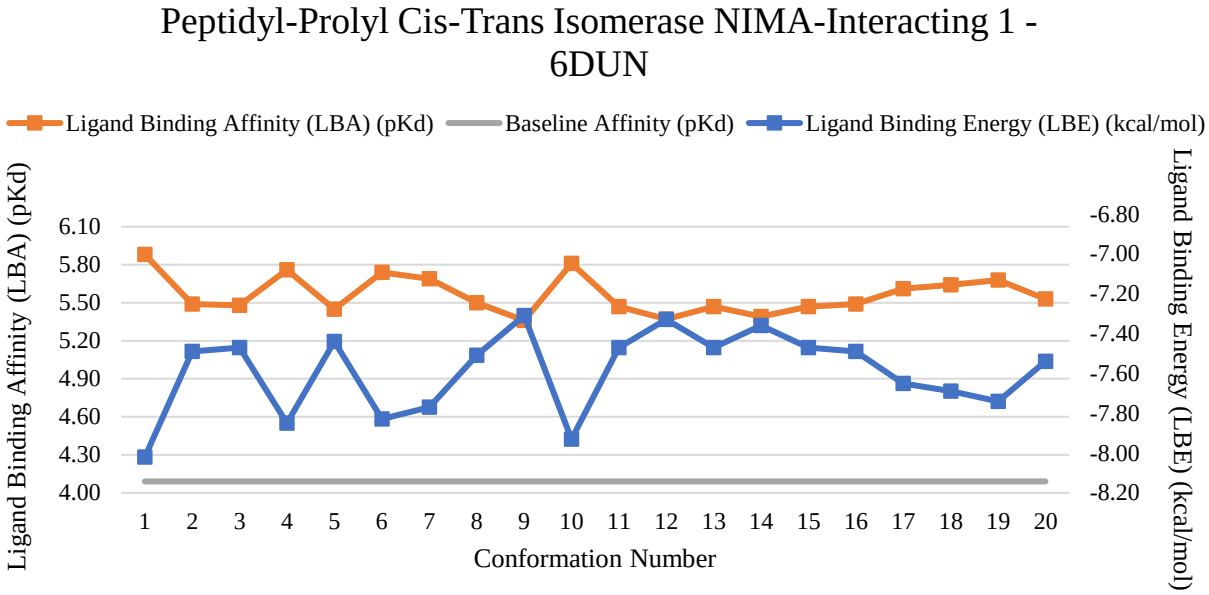

Figure 3.25 Graph of LBA (pKd) on the primary y-axis and LBA (kcal/mol) on the secondary y-axis vs Conformer Number on the x-axis for Maltanedienol docked into the LBP of Peptidyl-Prolyl Cis-Trans Isomerase NIMA-Interacting 1 as described in PDB ID: 6DUN.

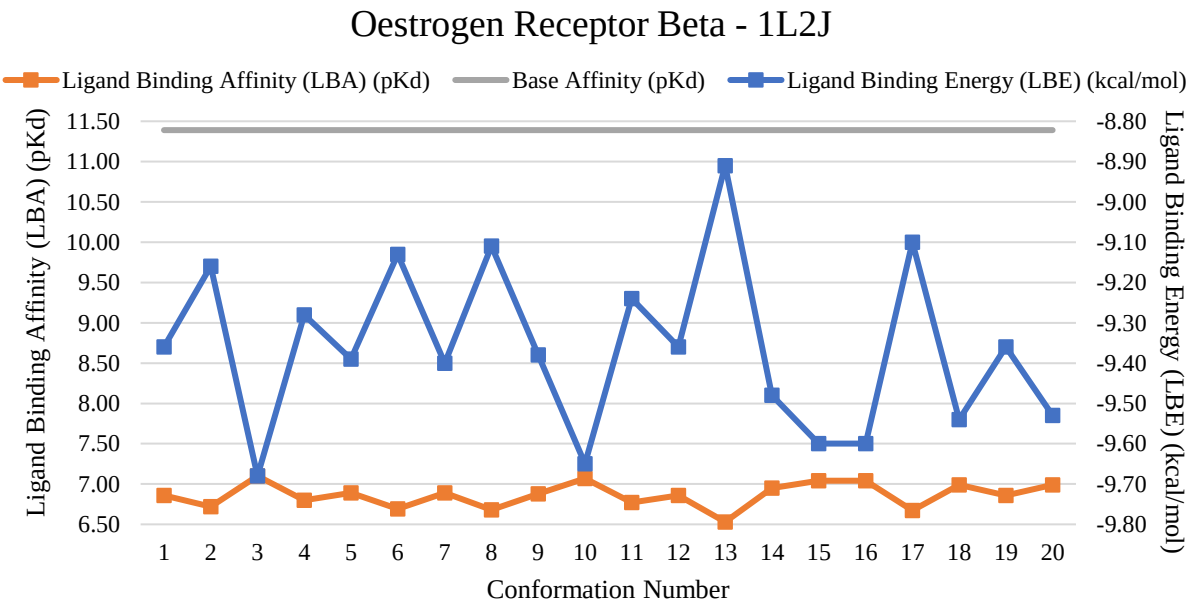

Figure 3.26 Graph of LBA (pKd) on the primary y-axis and LBA (kcal/mol) on the secondary y-axis vs Conformer Number on the x-axis for Maltanedienol docked into the LBP of the Oestrogen Receptor Beta as described in PDB ID: 1L2J.

3.2 Comparison of LBA

Table 3.1 LBA (pKd) of the optimal conformers of Maltanedienol for its potential *in vivo* targets (n=26) as identified by the datamining software of D'Emanuele (2019) whose function is related to calcium fixation or bone remodelling and which are crystallographically resolved on the PDB (Bernstein et al., 1977).

Number	**PDB ID**	**Target Name**	**LBA (pKd) of Maltanedienol for this target**	**LBA (pKd) of co-crystallised small molecule for this target**
1	5T37	Prostaglandin E Synthase (PGES)	5.59	6.48
2	3ERT	Oestrogen Receptor	7.30	7.76
3	1NHZ	Glucocorticoid Receptor	6.99	10.37
4	1LHU	Sex Hormone-Binding Globulin	7.73	7.50
5	4M0E	Cholinesterase	4.53	6.8
6	3ZR7	Progesterone Receptor	7.19	7.05
7	5FXS	Insulin-Like Growth Factor 1 Receptor	6.40	7.81
8	2AA2	Mineralocorticoid Receptor	7.53	10.12
9	5VCC	Cytochrome P450 3A4	6.59	6.33
10	2PIV	Androgen Receptor	6.19	9.28
11	3W0A	Vitamin D3 Receptor	7.46	8.92
12	3EQM	Aromatase	7.14	13.15

13	4MXO	Proto-Oncogene Tyrosine-Protein Kinase Src	6.98	9.17
14	3HB4	Oestradiol 17-Beta-Dehydrogenase 1	7.58	8.22
15	4YU1	Aldo-Keto Reductase Family 1 Member B1	7.97	11.93
16	1ECV	Tyrosine-Protein Phosphatase Non-Receptor Type 1	6.90	7.18
17	1VOT	Acetylcholinesterase	7.11	6.45
18	5JNT	Low Molecular Weight Phosphotyrosine Protein Phosphatase	6.33	5.32
19	2RBE	Corticosteroid 11-Beta-Dehydrogenase Isozyme 1	7.59	5.91
20	4WH9	M-Phase Inducer Phosphatase 2	6.21	7.60
21	5U6B	Tyrosine-Protein Kinase Receptor UFO	6.53	16.92
22	3E7G	Nitric Oxide Synthase, Inducible	6.75	7.26
23	1YWN	Vascular Endothelial Growth Factor Receptor 2	6.90	7.92
24	4GU6	Focal Adhesion Kinase 1	6.84	10.43

25	6DUN	Peptidyl-Prolyl Cis-Trans Isomerase NIMA-Interacting 1	5.88	4.09
26	1L2J	Oestrogen Receptor Beta	7.10	11.39

Table 3.2 LBA (pKd) of the optimal conformers of Maltanedienol for its potential *in vivo* targets (n=7), as identified by the data mining software of D'Emanuele (2019) which are crystallographically resolved on the PDB (Bernstein et al., 1977) and which had a LBA (pKd) of Maltanedienol for its specific target which is greater than that of the bound small molecule for its specific target.

PDB ID	**Target Name**	**LBA (pKd) of Maltanedienol for this target**	**LBA (pKd) of co-crystallised small molecule for this target**
1LHU	Sex Hormone-Binding Globulin	7.73	7.50
3ZR7	Progesterone Receptor	7.19	7.05
5VCC	Cytochrome P450 3A4	6.59	6.33
1VOT	Acetylcholinesterase	7.11	6.45
5JNT	Low Molecular Weight Phosphotyrosine Protein Phosphatase	6.33	5.32
2RBE	Corticosteroid 11-Beta-Dehydrogenase Isozyme 1	7.59	5.91

6DUN	Peptidyl-Prolyl Cis-Trans Isomerase NIMA-Interacting 1	5.88	4.09

Table 3.3 Potential *in vivo* targets (n=19) for Maltanedienol, as identified by the datamining software of D'Emanuele (2019) which are crystallographically resolved the PDB (Bernstein et al., 1977) and which have a LBA (pKd) of Maltanedienol for its specific target which is smaller than that of the bound small molecule for its specific target.

PDB ID	**Target Name**	**LBA (pKd) of Maltanedienol for this target**	**LBA (pKd) of co-crystallised small molecule for this target**
5T37	Prostaglandin E Synthase (PGES)	5.59	6.48
3ERT	Oestrogen Receptor	7.30	7.76
1NHZ	Glucocorticoid Receptor	6.99	10.37
4M0E	Cholinesterase	4.53	6.8
5FXS	Insulin-Like Growth Factor 1 Receptor	6.40	7.81
2AA2	Mineralocorticoid Receptor	7.53	10.12
2PIV	Androgen Receptor	6.19	9.28
3W0A	Vitamin D3 Receptor	7.46	8.92
3EQM	Aromatase	7.14	13.15
4MXO	Proto-Oncogene Tyrosine-Protein Kinase Src	6.98	9.17

3HB4	Oestradiol 17-Beta-Dehydrogenase 1	7.58	8.22
4YU1	Aldo-Keto Reductase Family 1 Member B1	7.97	11.93
1ECV	Tyrosine-Protein Phosphatase Non-Receptor Type 1	6.90	7.18
4WH9	M-Phase Inducer Phosphatase 2	6.21	7.60
5U6B	Tyrosine-Protein Kinase Receptor UFO	6.53	16.92
1YWN	Vascular Endothelial Growth Factor Receptor 2	6.90	7.92
4GU6	Focal Adhesion Kinase 1	6.84	10.43
1L2J	Oestrogen Receptor Beta	7.10	11.39
3E7G	Nitric Oxide Synthase, Inducible	6.75	7.26

3.3 *De novo* Growth

3.3.1 2D Ligand Protein Contact Maps

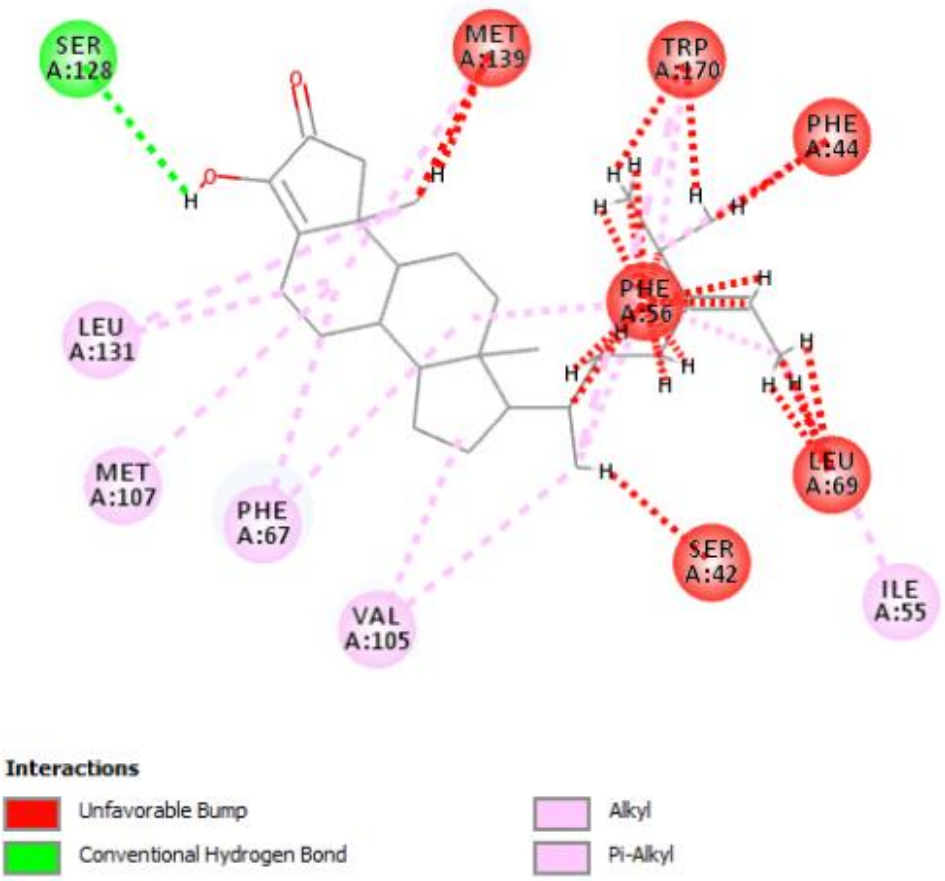

Figure 3.27 2D topology map describing the critical ligand binding interactions forged between Maltanedienol and the amino acids lining the LBP as described in PDB ID: 1LHU generated in BIOVIA Discovery Studio Visualizer® v20.1.[7]

[7] Dassault Systèmes. BIOVIA Discovery Studio Visualizer. Version 20.1 [software]. Dassault Systèmes. 2020 [cited 2021 Jul 14; downloaded 2021 May 25]. Available from: https://www.3dsbiovia.com/products/collaborative-science/biovia-discovery-studio/visualization-download.php.

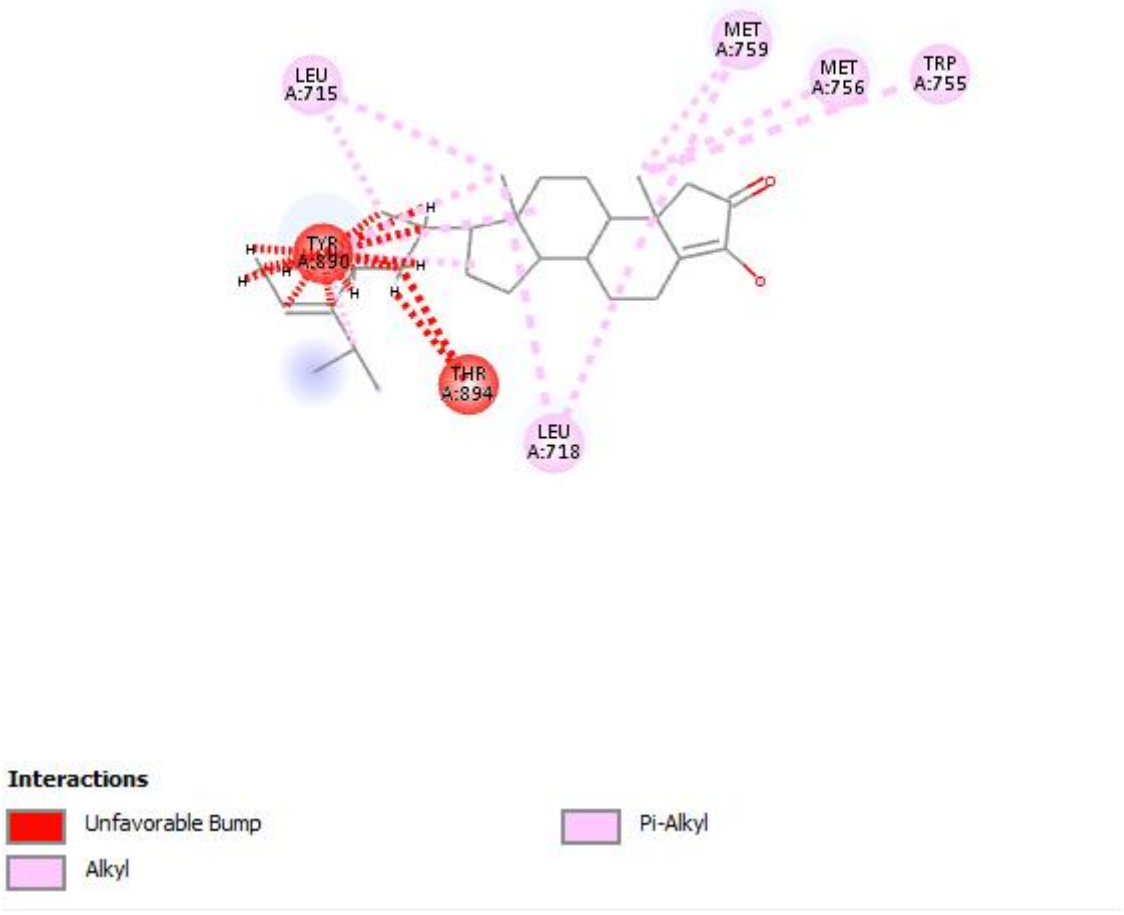

Figure 3.28 2D topology map describing the critical ligand binding interactions forged between Maltanedienol and the amino acids lining the LBP as described in PDB ID: 3ZR7 generated in BIOVIA Discovery Studio Visualizer® v20.1.[7]

[7] Dassault Systèmes. BIOVIA Discovery Studio Visualizer. Version 20.1 [software]. Dassault Systèmes. 2020 [cited 2021 Jul 14; downloaded 2021 May 25]. Available from: https://www.3dsbiovia.com/products/collaborative-science/biovia-discovery-studio/visualization-download.php.

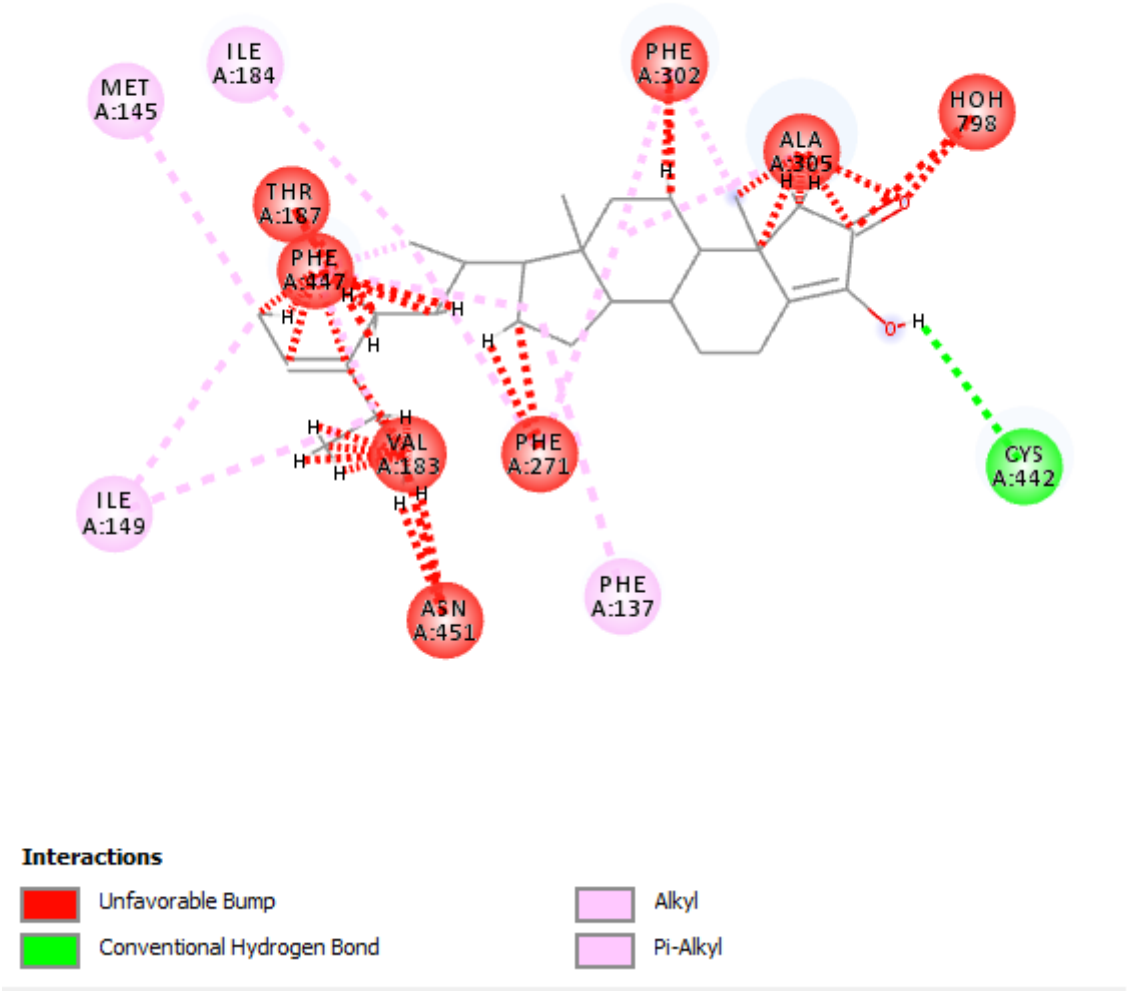

Figure 3.29 2D topology map describing the critical ligand binding interactions forged between Maltanedienol and the amino acids lining the LBP as described in PDB ID: 5VCC generated in BIOVIA Discovery Studio Visualizer® v20.1.[7]

[7] Dassault Systèmes. BIOVIA Discovery Studio Visualizer. Version 20.1 [software]. Dassault Systèmes. 2020 [cited 2021 Jul 14; downloaded 2021 May 25]. Available from: https://www.3dsbiovia.com/products/collaborative-science/biovia-discovery-studio/visualization-download.php.

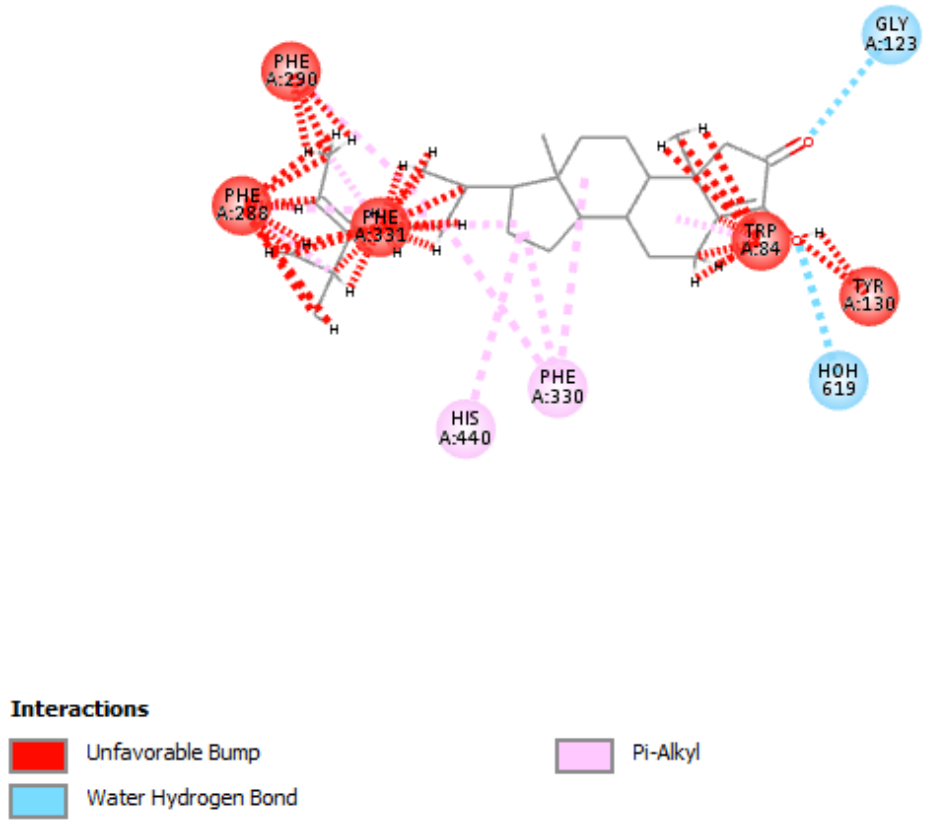

Figure 3.30 2D topology map describing the critical ligand binding interactions forged between Maltanedienol and the amino acids lining the LBP as described in PDB ID: 1VOT generated in BIOVIA Discovery Studio Visualizer® v20.1.[7]

[7] Dassault Systèmes. BIOVIA Discovery Studio Visualizer. Version 20.1 [software]. Dassault Systèmes. 2020 [cited 2021 Jul 14; downloaded 2021 May 25]. Available from: https://www.3dsbiovia.com/products/collaborative-science/biovia-discovery-studio/visualization-download.php.

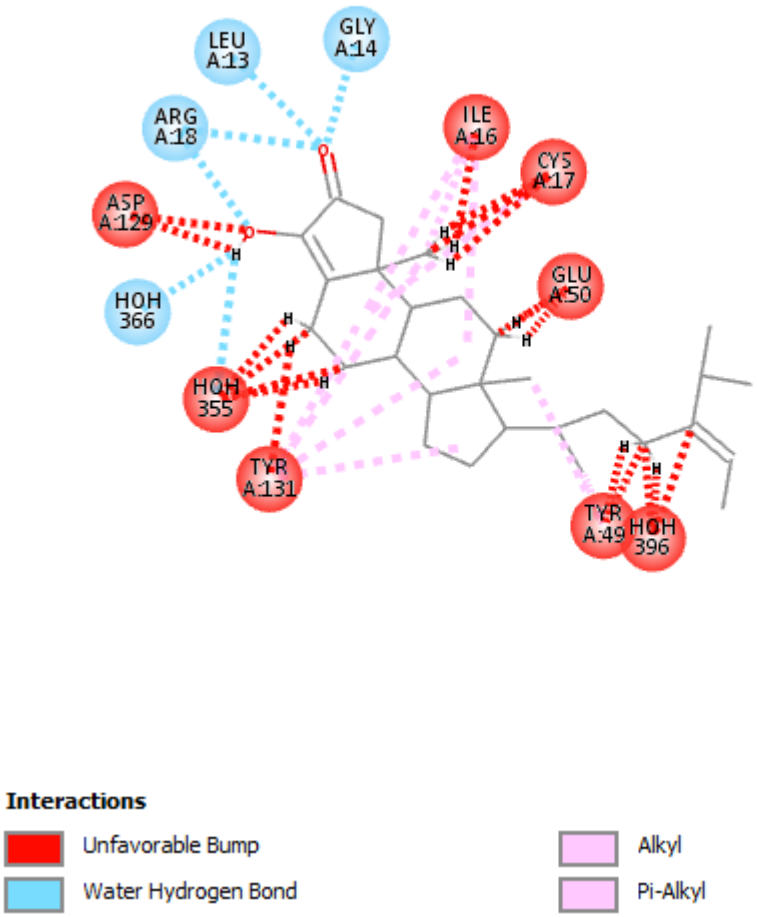

Figure 3.31 2D topology map describing the critical ligand binding interactions forged between Maltanedienol and the amino acids lining the LBP as described in PDB ID: 5JNT generated in BIOVIA Discovery Studio Visualizer® v20.1.[7]

[7] Dassault Systèmes. BIOVIA Discovery Studio Visualizer. Version 20.1 [software]. Dassault Systèmes. 2020 [cited 2021 Jul 14; downloaded 2021 May 25]. Available from: https://www.3dsbiovia.com/products/collaborative-science/biovia-discovery-studio/visualization-download.php.

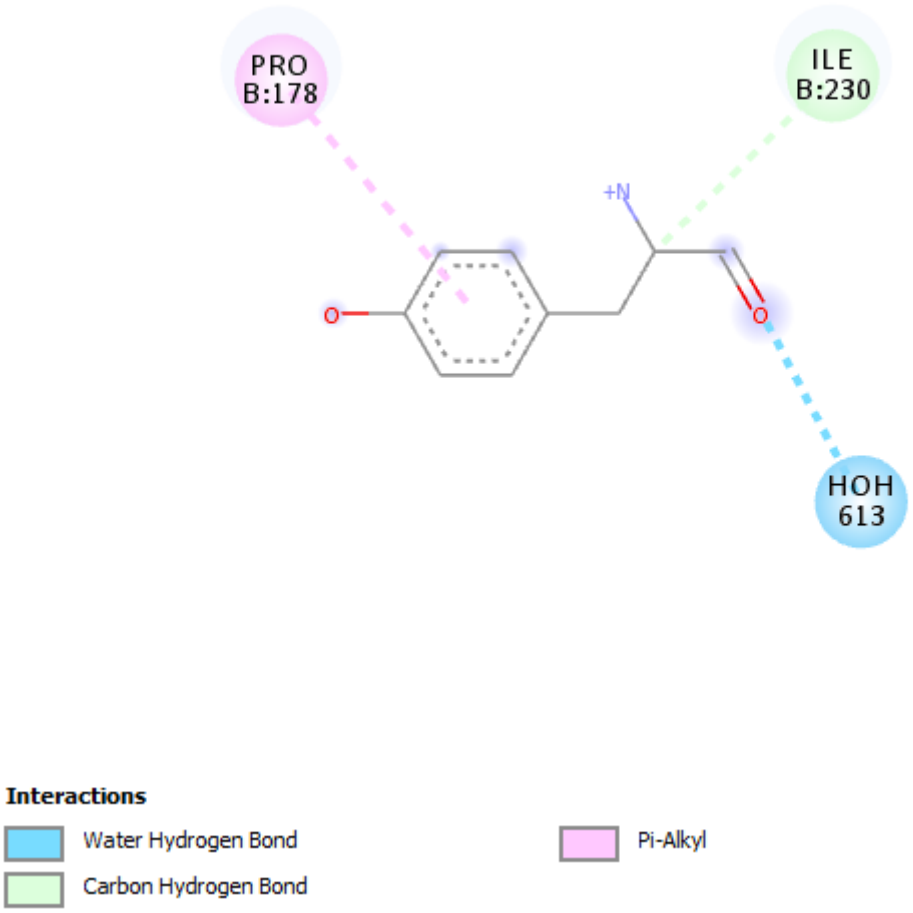

Figure 3.32 2D topology map describing the critical ligand binding interactions forged between Maltanedienol and the amino acids lining the LBP as described in PDB ID: 2RBE generated in BIOVIA Discovery Studio Visualizer® v20.1.[7]

[7] Dassault Systèmes. BIOVIA Discovery Studio Visualizer. Version 20.1 [software]. Dassault Systèmes. 2020 [cited 2021 Jul 14; downloaded 2021 May 25]. Available from: https://www.3dsbiovia.com/products/collaborative-science/biovia-discovery-studio/visualization-download.php.

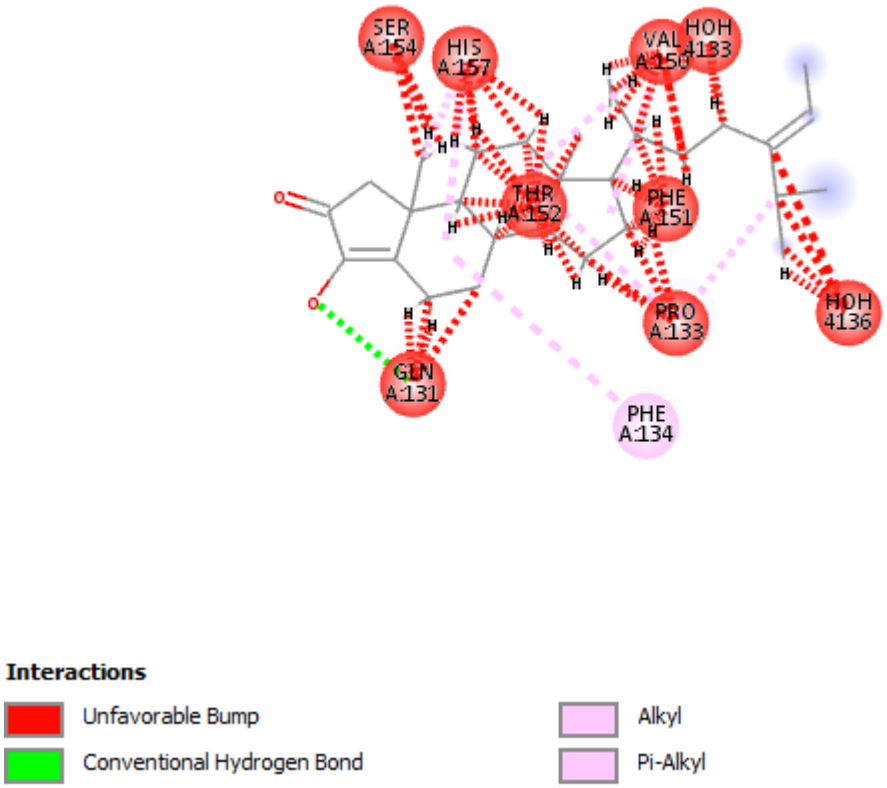

Figure 3.33 2D topology map describing the critical ligand binding interactions forged between Maltanedienol and the amino acids lining the LBP as described in PDB ID: 6DUN generated in BIOVIA Discovery Studio Visualizer® v20.1.[7]

[7] Dassault Systèmes. BIOVIA Discovery Studio Visualizer. Version 20.1 [software]. Dassault Systèmes. 2020 [cited 2021 Jul 14; downloaded 2021 May 25]. Available from: https://www.3dsbiovia.com/products/collaborative-science/biovia-discovery-studio/visualization-download.php.

3.3.2 Seed Structures

A range of 1-2 seeds were created for each optimal conformer of Maltanedienol for its respective receptor (n=7) in Sybyl®-X v1.1. The sticks seen in light blue represent the growing sites in each seed molecules, where directed user growth occurs.

Table 3.4 Seed molecules of Maltanedienol for the Acetylcholinesterase Receptor (PDB 1VOT) with selected H.spc atoms represented by a light blue stick, capable of sustaining molecular growth. Seeds were generated in Sybyl®-X v1.1 (Ash et al., 2010).

Seed Name	**Seed Structure**
1votseed10	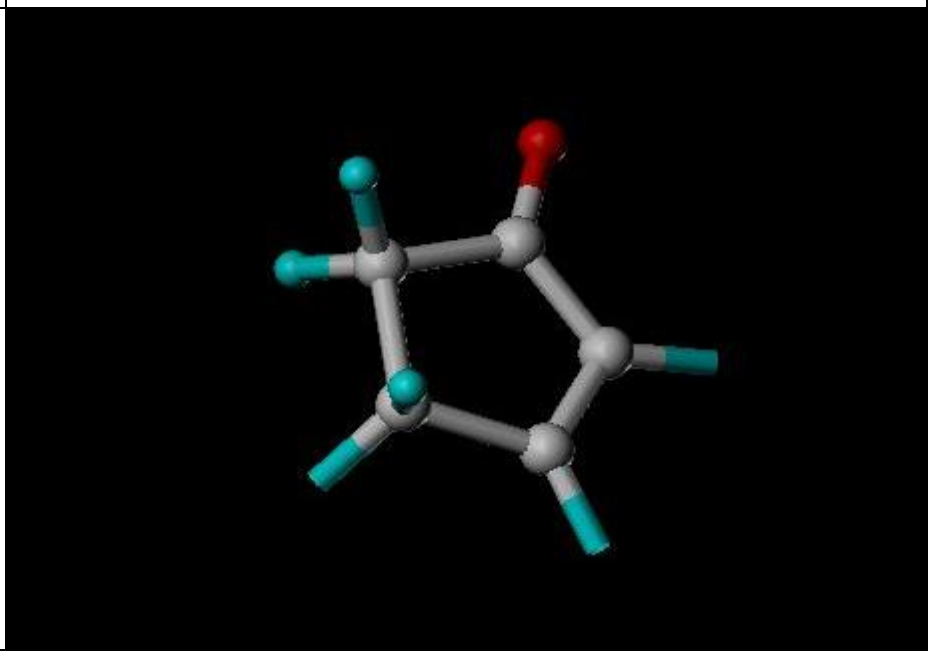

Table 3.5 Seed molecules of Maltanedienol for the Corticosteroid 11-Beta-Dehydrogenase Isozyme 1 (PDB 2RBE) with selected H.spc atoms represented by a light blue stick, capable of sustaining molecular growth. Seeds were generated in Sybyl®-X v1.1 (Ash et al., 2010).

Seed Name	**Seed Structure**
2rbeseed2	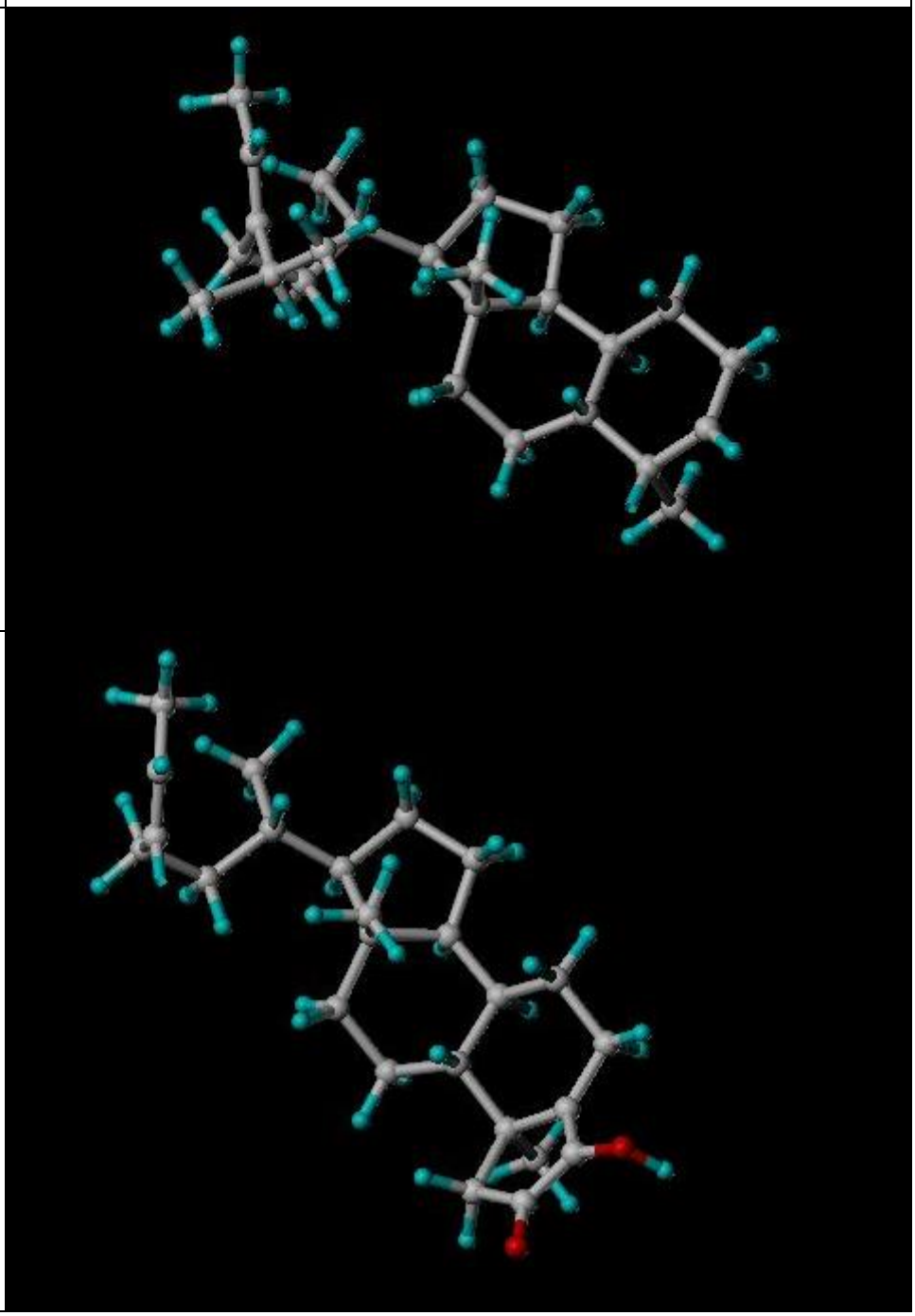
2rbeseed7	

Table 3.6 Seed molecules of Maltanedienol for the Low Molecular Weight Phosphotyrosine Protein Phosphatase (PDB 5JNT) with selected H.spc atoms represented by a light blue stick, capable of sustaining molecular growth. Seeds were generated in Sybyl®-X v1.1 (Ash et al., 2010).

Seed Name	**Seed Structure**
5jntseed5	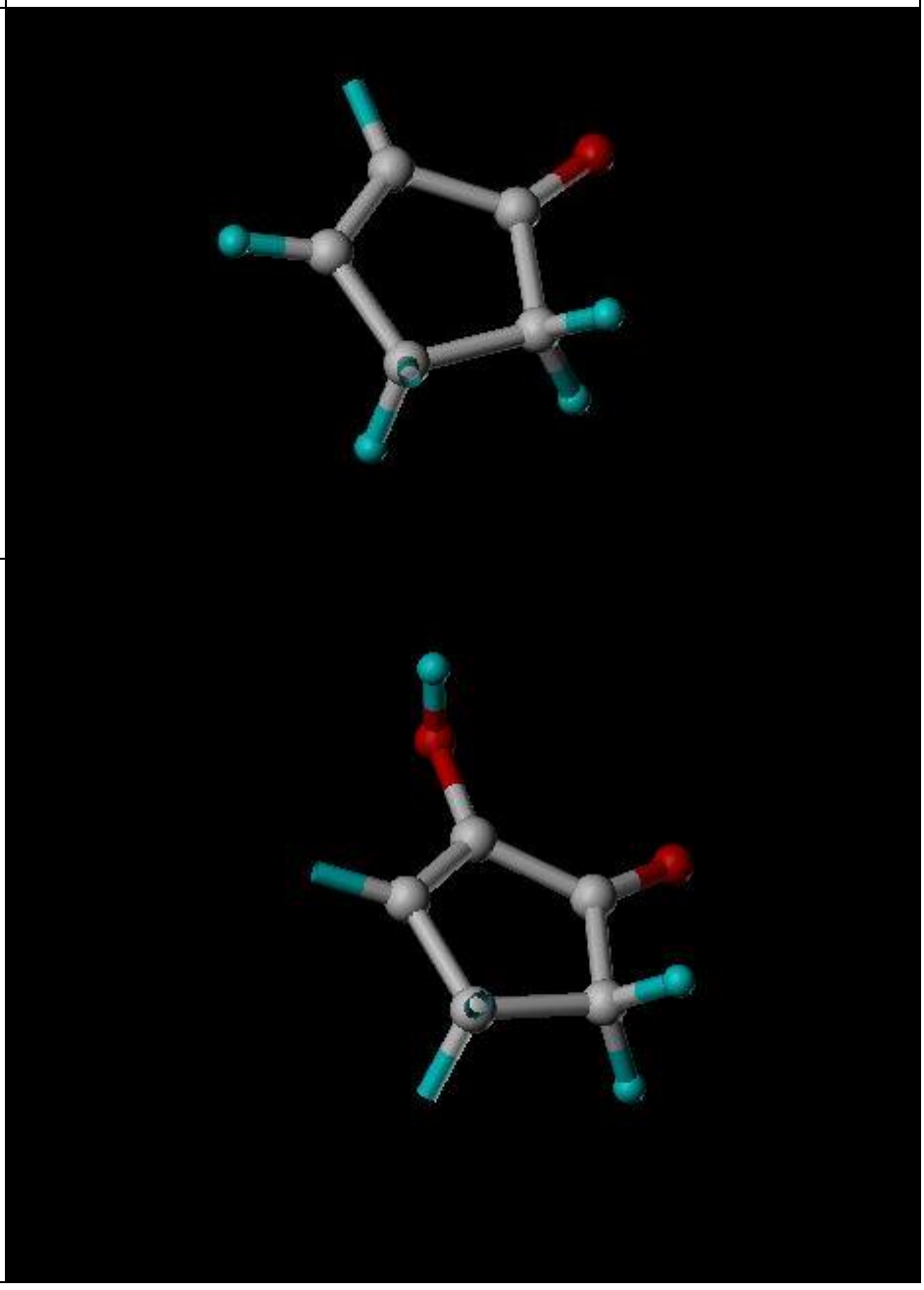
5jntseed6	

Table 3.7 Seed molecules of Maltanedienol for the Peptidyl-Prolyl Cis-Trans Isomerase NIMA-Interacting 1 (PDB 6DUN) with selected H.spc atoms represented by a light blue stick, capable of sustaining molecular growth. Seeds were generated in Sybyl®-X v1.1 (Ash et al., 2010).

Seed Name	**Seed Structure**
6dunseed7	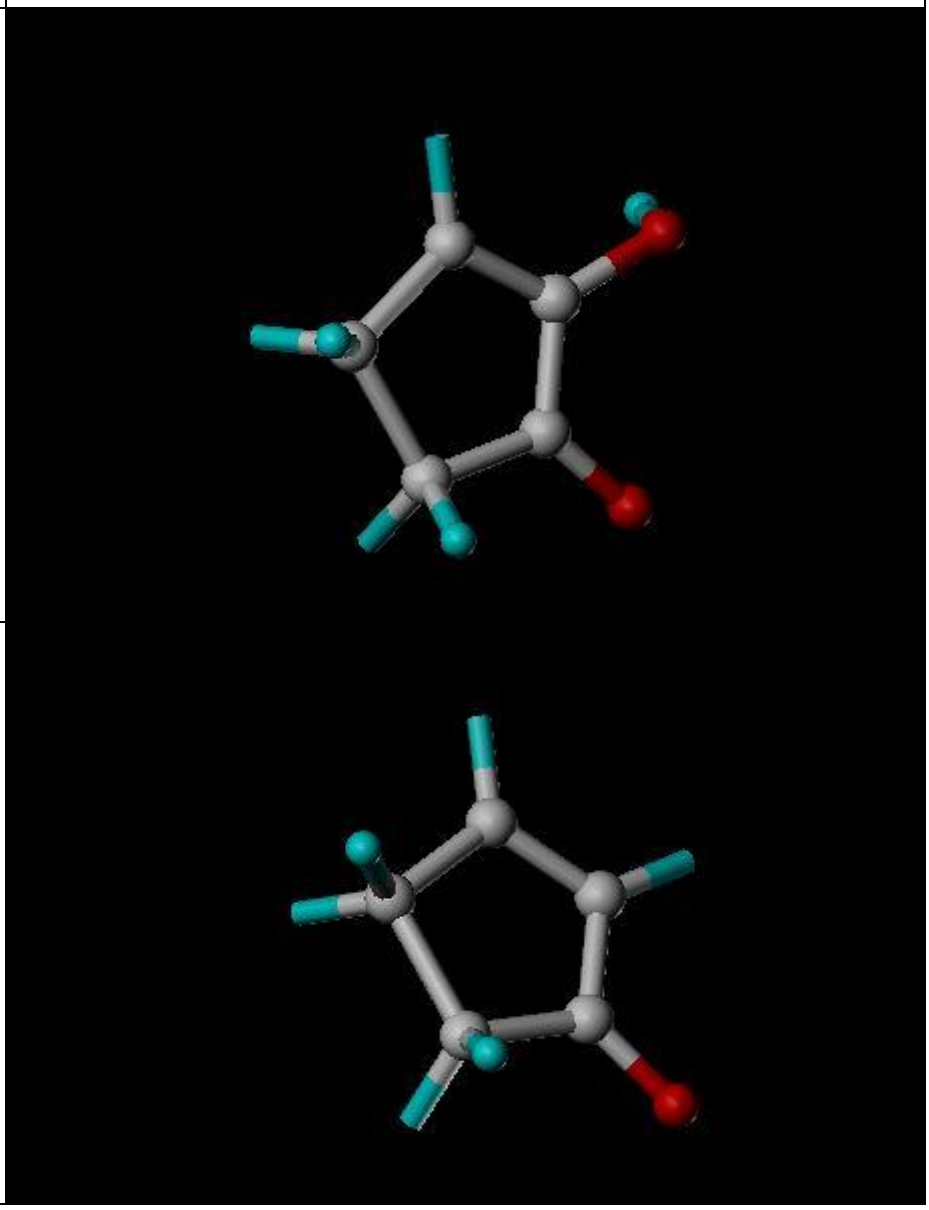
6dunseed8	

Table 3.8 Seed molecules of Maltanedienol for the Progesterone Receptor (PDB 3ZR7) with selected H.spc atoms represented by a light blue stick, capable of sustaining molecular growth. Seeds were generated in Sybyl®-X v1.1 (Ash et al., 2010).

Seed Name	**Seed Structure**
3zr7seed7	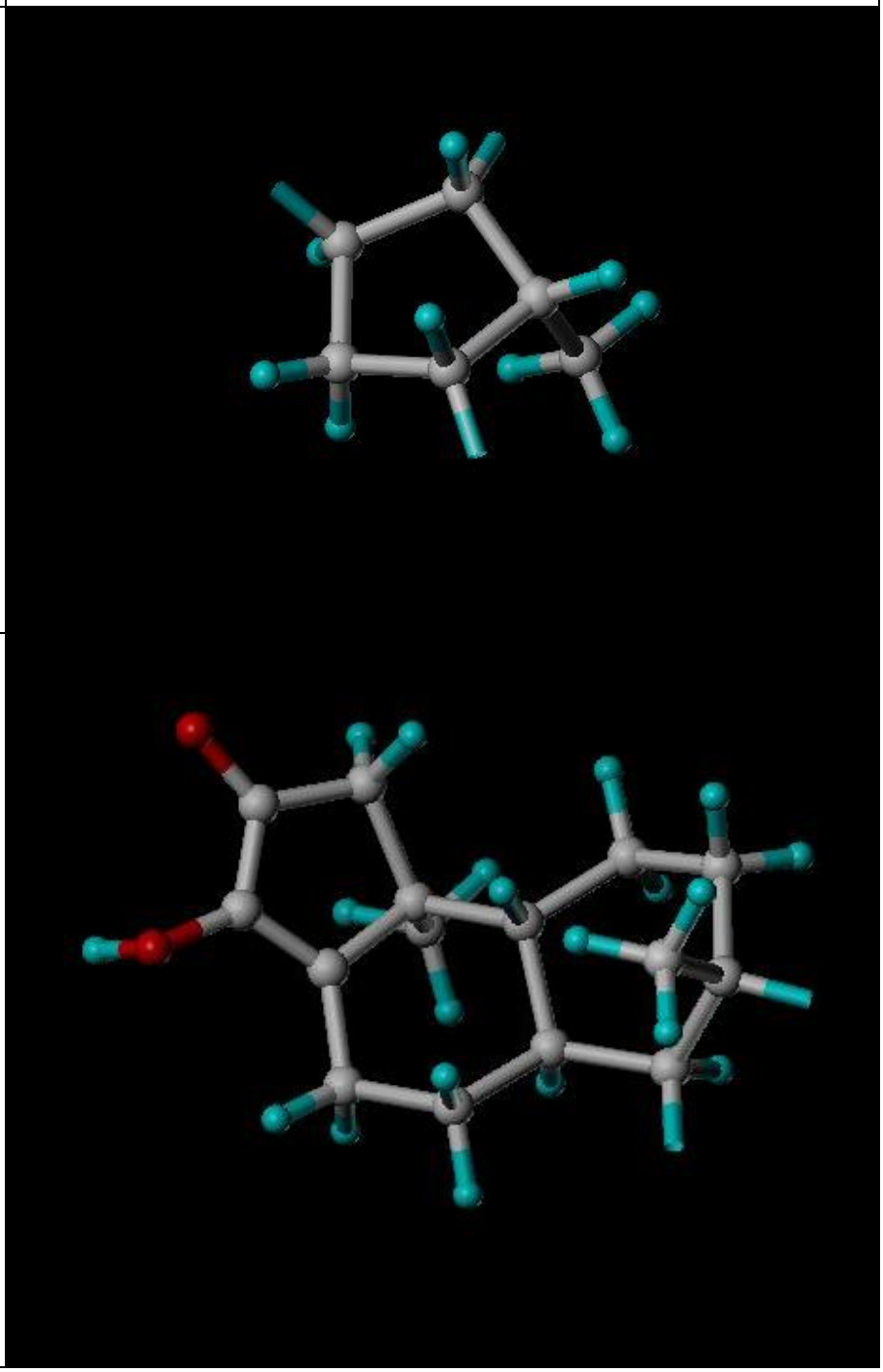
3zr7seed8	

Table 3.9 Seed molecules of Maltanedienol for the Sex Hormone-Binding Globulin (PDB 1LHU) with selected H.spc atoms represented by a light blue stick, capable of sustaining molecular growth. Seeds were generated in Sybyl®-X v1.1 (Ash et al., 2010).

Seed Name	**Seed Structure**
1lhuseed7	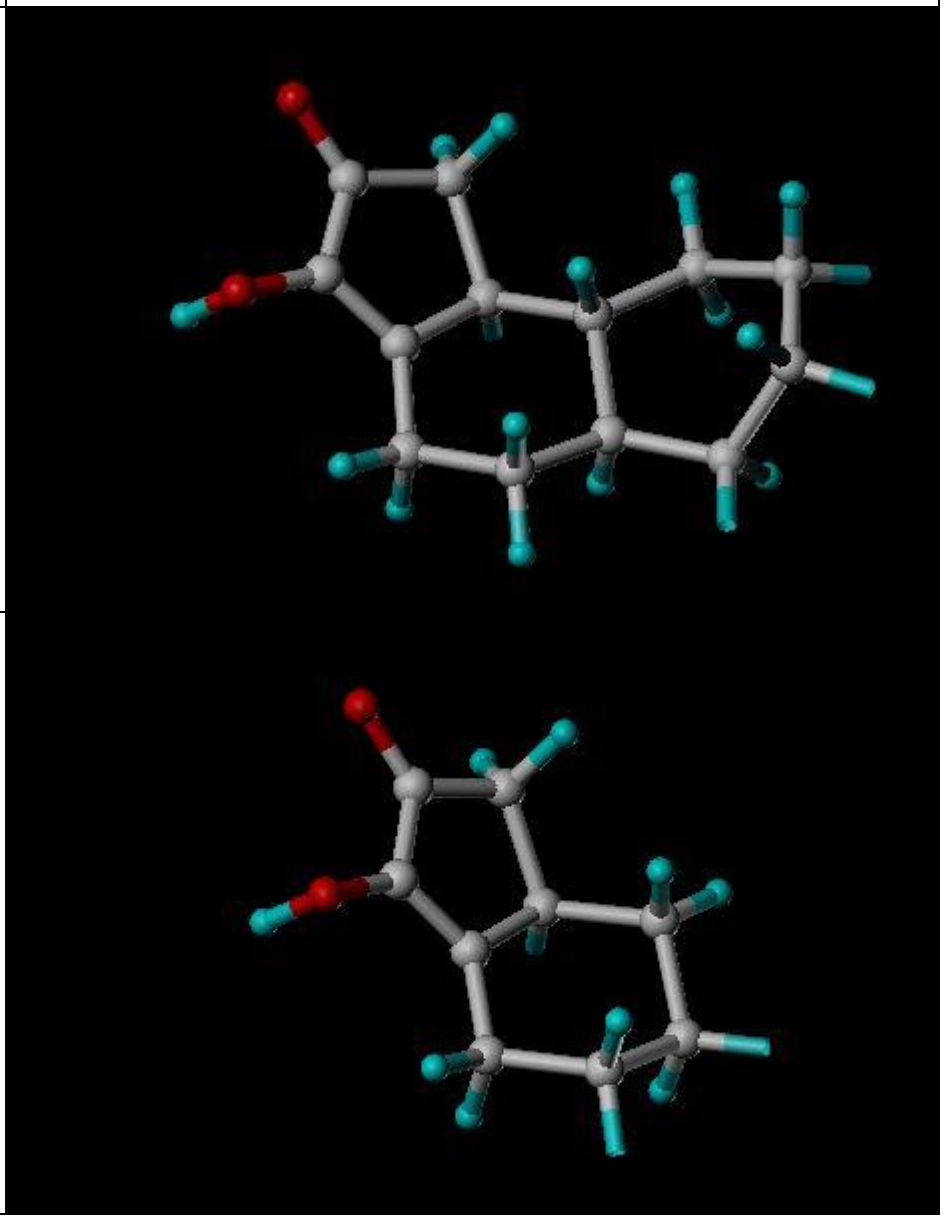
1lhuseed8	

The pharmacophoric space within the LBP of the Cytochrome P450 3A4 (PDB ID 5VCC) was not hospitable to molecular growth using the Maltanedienol based modelled seed structures. This was probably due to steric hindrance and amino acid non complementarity.

3.3.3 Ligands Generated by Structure-Based Drug Design

Below are tables for each seed structure created. The 3D structures are rendered in BIOVIA Discovery Studio Visualizer® v20.1[7] whilst the 2D structures are rendered in BIOVIA Draw® v17.1.[4] The characteristics of each molecule include family, molecular formula (MF), MW, LogP, affinity (pKd), chemical score (CS), hydrogen acceptor count (HAC) and hydrogen donor count (HDC).

Table 3.10 The highest affinity molecule generated from each family for the Acetylcholinesterase Receptor (PDB 1VOT) 1votseed10.

Res-ult	3D Structure	2D Structure	Characteristics
001	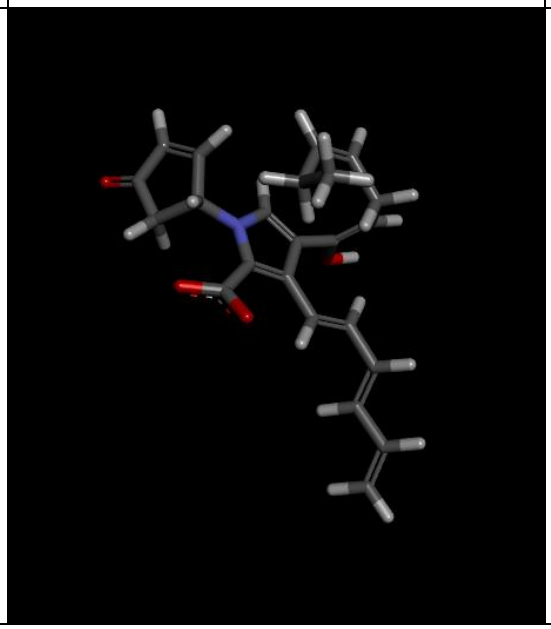	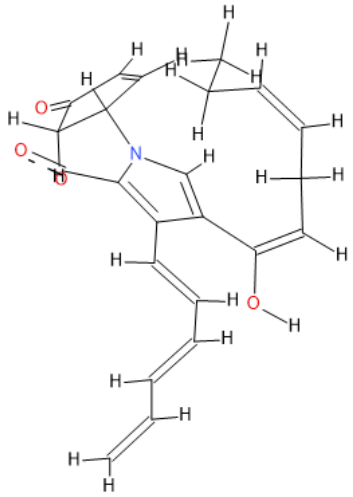	Family <1> MF: C23H24NO4 MW 378 LogP 4.79 Affinity (pKd): 7.6 CS -20 HAC 4 HDC 2

[7] Dassault Systèmes. BIOVIA Discovery Studio Visualizer. Version 20.1 [software]. Dassault Systèmes. 2020 [cited 2021 Jul 14; downloaded 2021 May 25]. Available from: https://www.3dsbiovia.com/products/collaborative-science/biovia-discovery-studio/visualization-download.php.

[4] Dassault Systèmes. BIOVIA Draw. Version 17.1 [software]. Dassault Systèmes. 2017 [cited 2021 Jul 14; downloaded 2021 May 25]. Available from: https://hts.c2b2.columbia.edu/draw/.

049	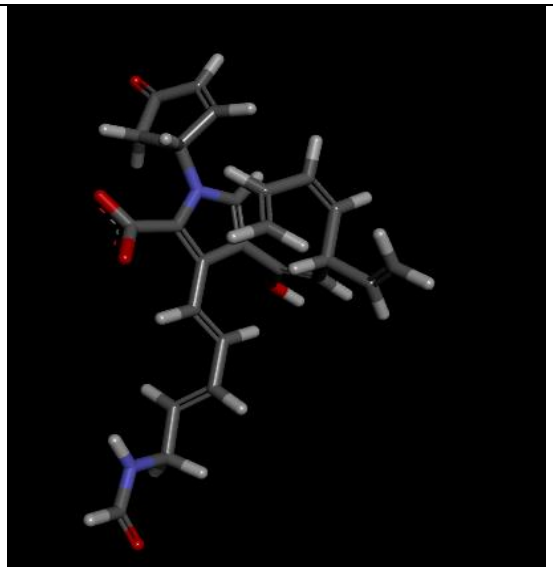	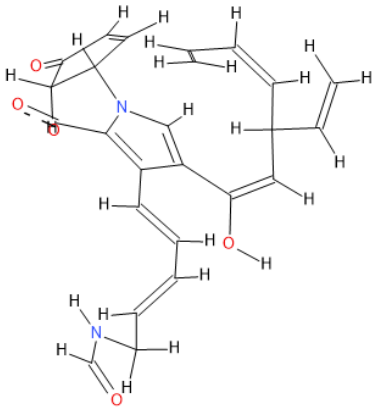	Family <2> MF C25H25N2O5 MW 433 LogP 3.62 Affinity (pKd) 6.58 CS -40 HAC 5 HDC 3
054	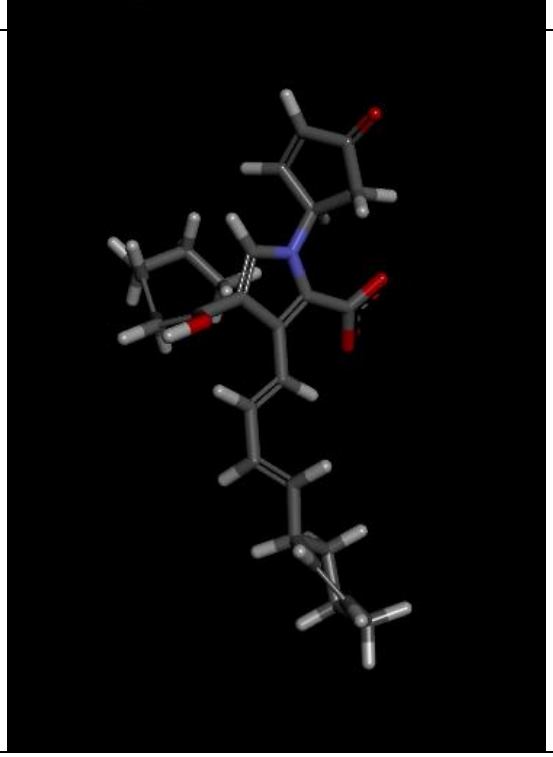	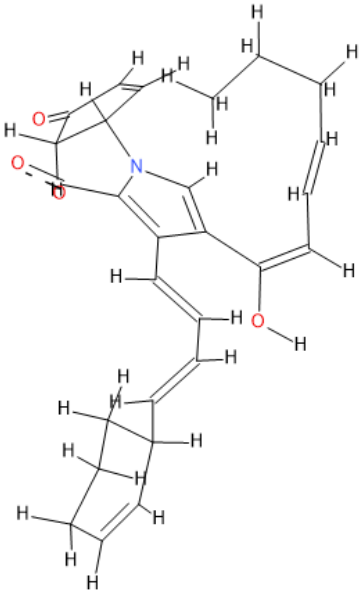	Family <3> MF C27H30NO4 MW 432 LogP 4.95 Affinity (pKd) 6.58 CS -40 HAC 4 HDC 2

057	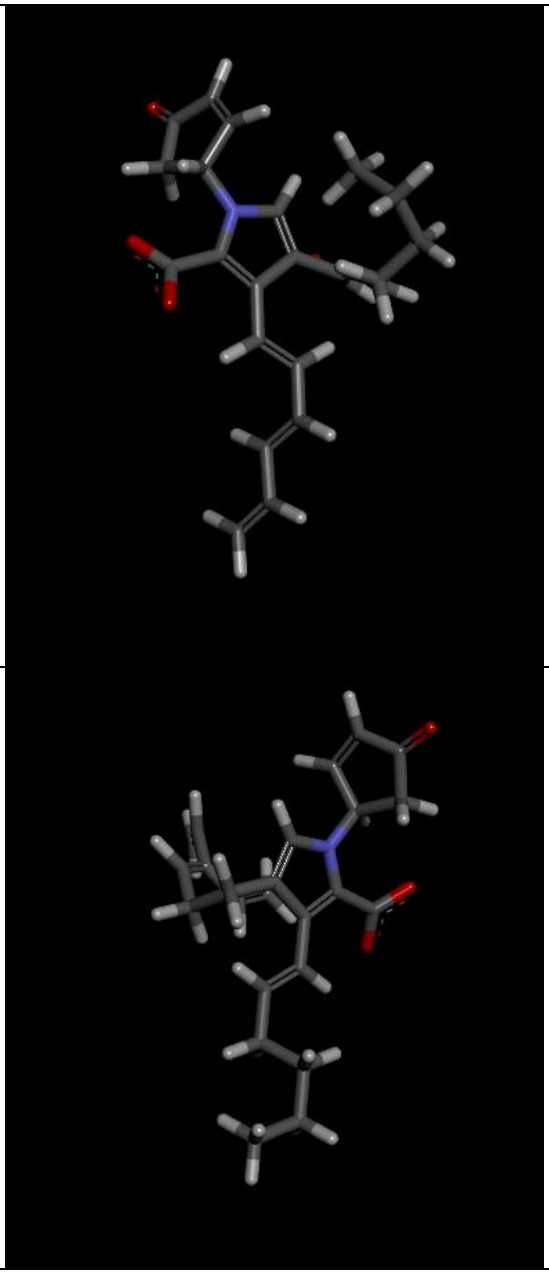	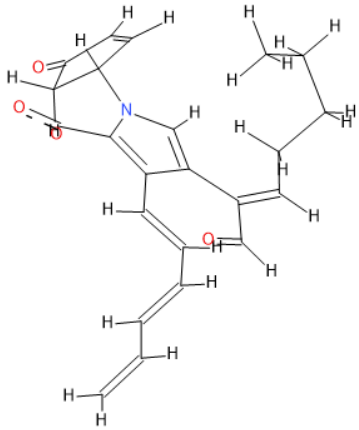	Family <4> MF C23H24NO4 MW 378 LogP 4.45 Affinity (pKd) 6.44 CS -20 HAC 4 HDC 1
065		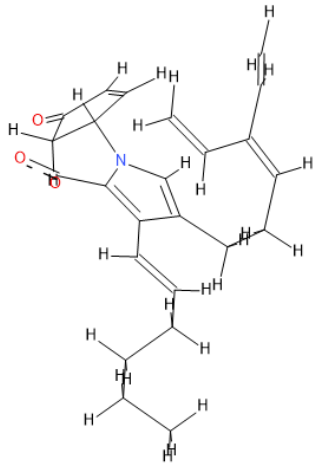	Family <5> MF C24H28NO3 MW 378 LogP 4.68 Affinity (pKd) 6.17 CS -20 HAC 3 HDC 1

073	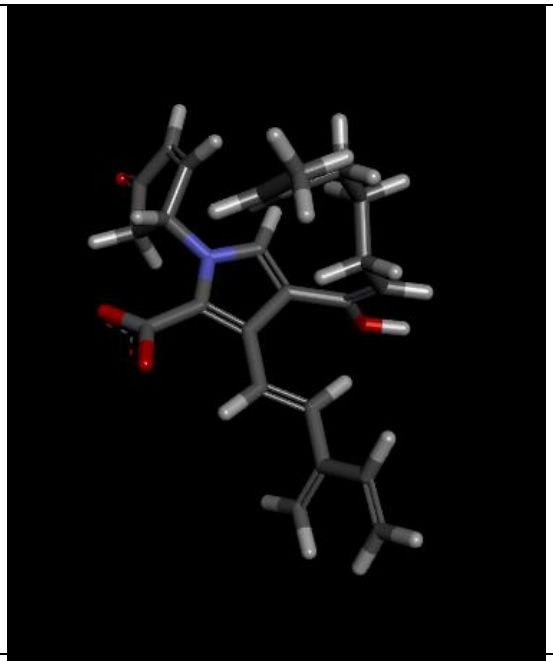	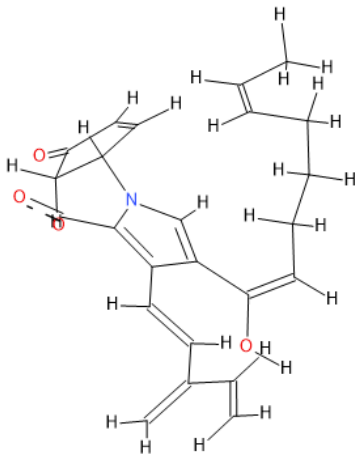	Family <6> MF C24H26NO4 MW 392 LogP 4.38 Affinity (pKd) 5.97 CS -20 HAC 4 HDC 2
089	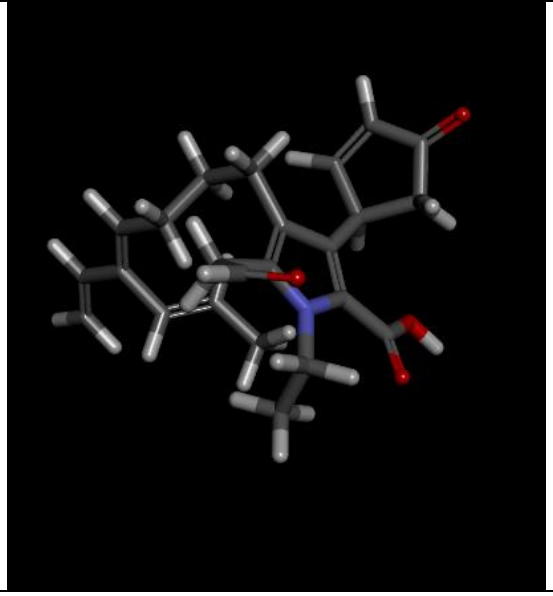	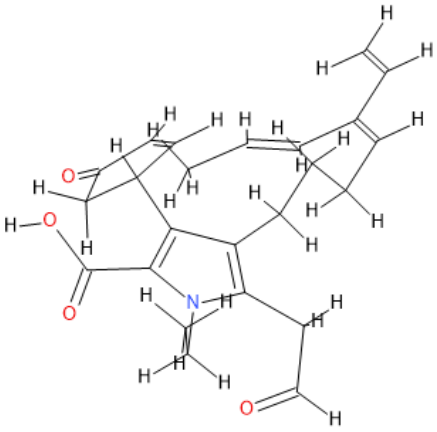	Family <7> MF C24H29NO4 MW 395 LogP 4.63 Affinity (pKd) 5.88 CS -20 HAC 4 HDC 1

091	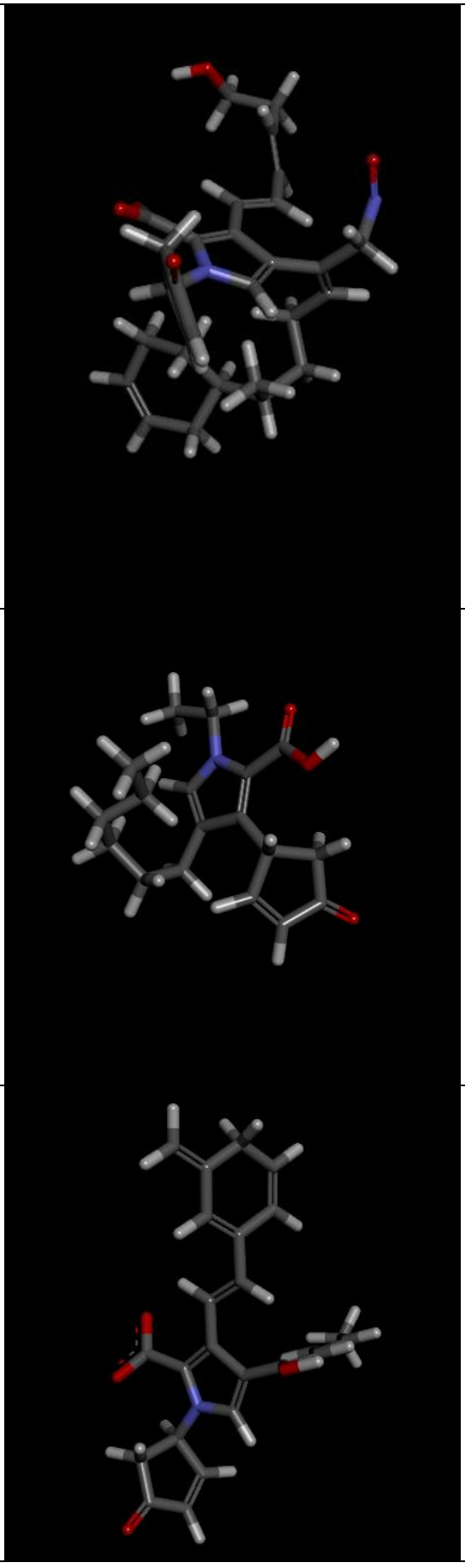	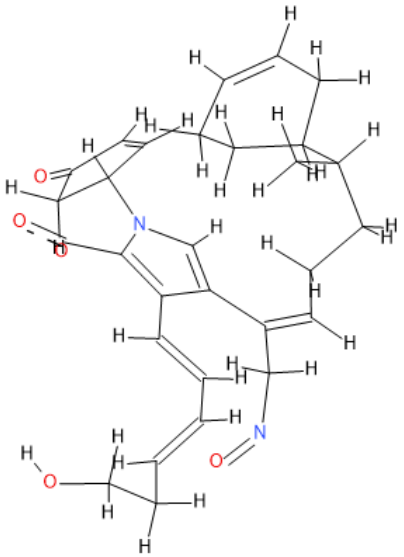	Family <8> MF C29H35N2O5 MW 491 LogP 3.63 Affinity (pKd) 5.84 CS -60 HAC 6 HDC 2
093		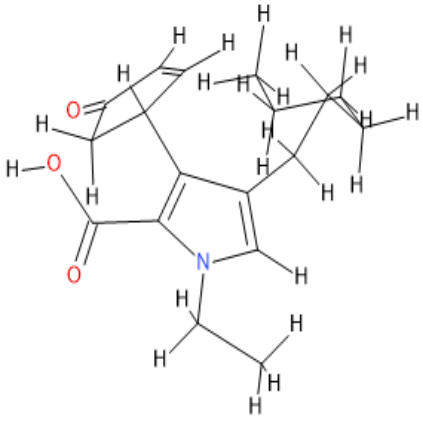	Family <9> MF C18H25NO3 MW 303 LogP 3.64 Affinity (pKd) 5.54 CS -20 HAC 3 HDC 1
096		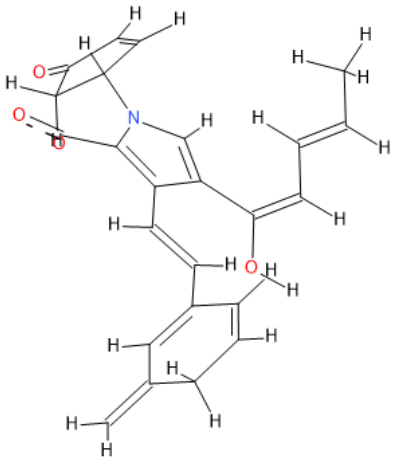	Family <10> MF C24H22NO4 MW 388 LogP 3.38 Affinity (pKd) 5.46 CS -20 HAC 4 HDC 2

098	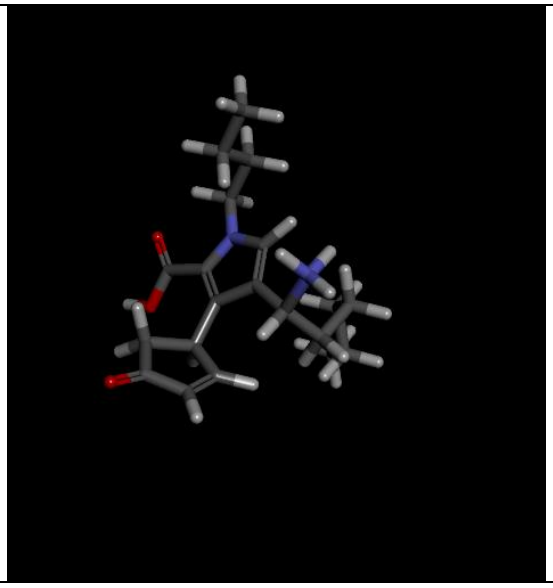	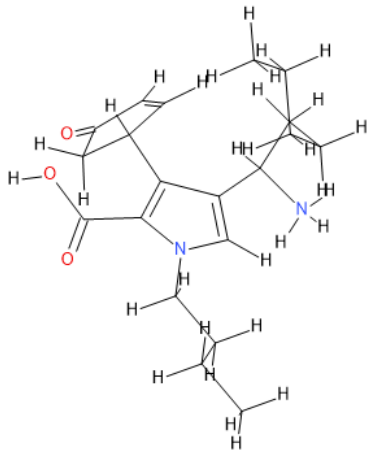	Family <11> MF C20H31N2O3 MW 347 LogP 3.32 Affinity (pKd) 5.44 CS -40 HAC 3 HDC 2

Table 3.11 The highest affinity molecule generated from each family for the Corticosteroid 11-Beta-Dehydrogenase Isozyme 1 (PDB 2RBE) 2rbeseed2.

Res-ult	3D Structure	2D Structure	Characteristics
014	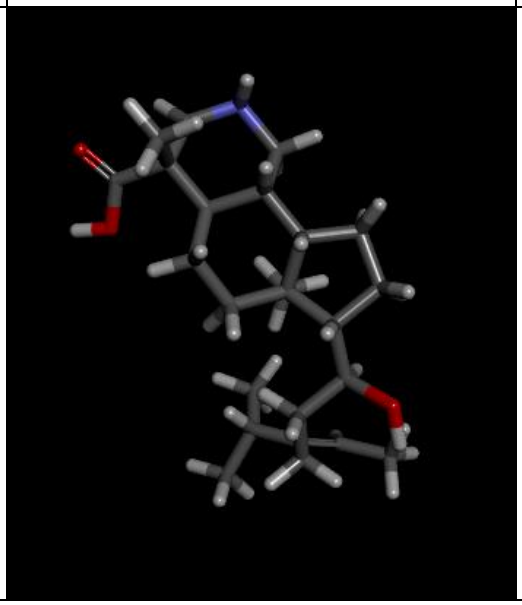	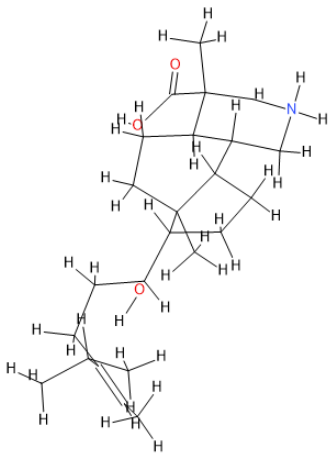	Family <2> MF C24H41NO3 MW 391 LogP 4.68 Affinity (pKd) 9.13 CS -170 HAC 3 HDC 3

053	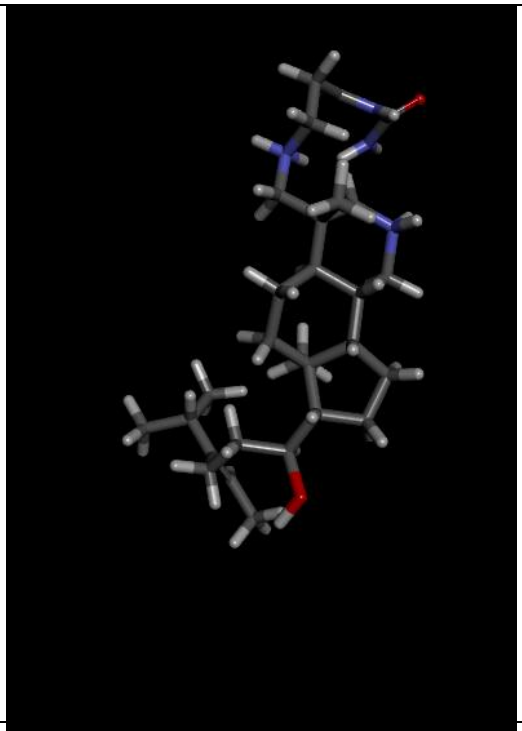	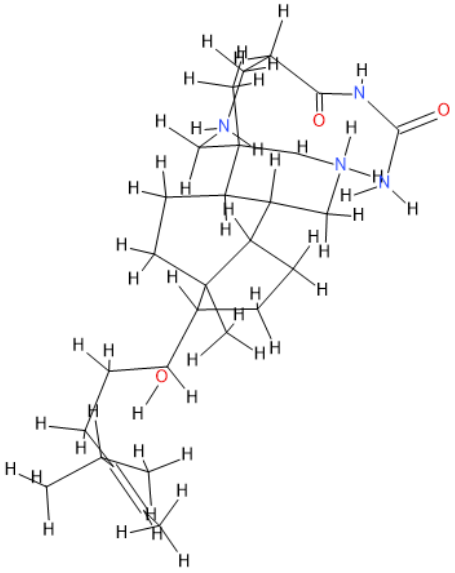	Family <3> MF C28H51N4O3 MW 491 LogP 3.4 Affinity (pKd) 8.95 CS -170 HAC 3 HDC 5
063	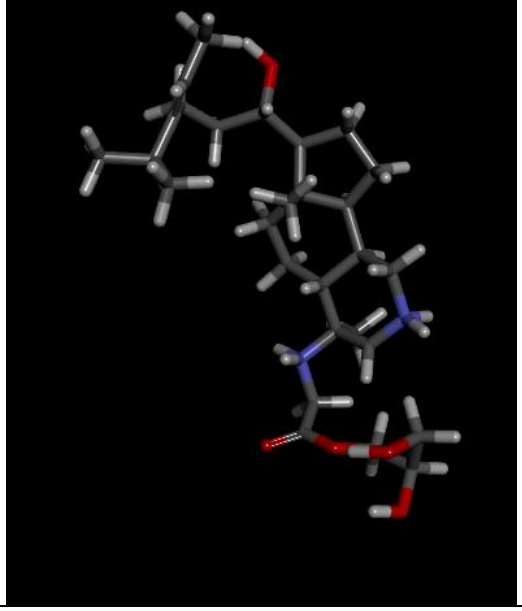	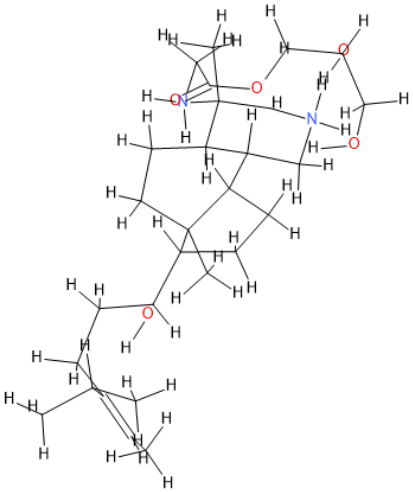	Family <4> MF C28H51N2O5 MW 495 LogP 3.65 Affinity (pKd) 9.38 CS -190 HAC 5 HDC 5

083	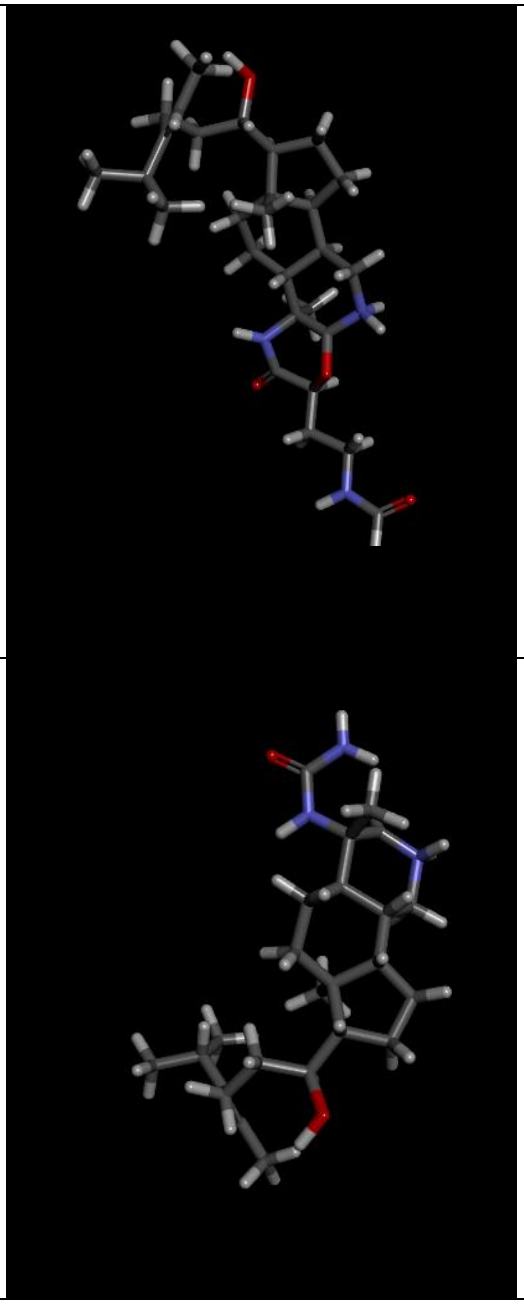	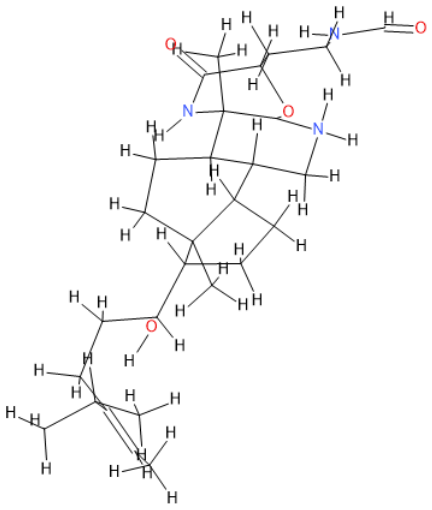	Family <5> MF C28H47N3O4 MW 489 LogP 4.81 Affinity (pKd) 8.5 CS -190 HAC 4 HDC 4
110		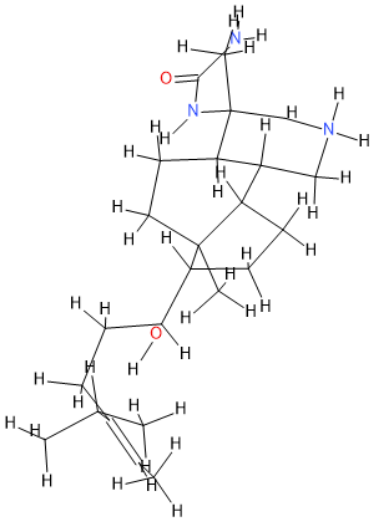	Family <6> MF C24H43N3O2 MW 405 LogP 4.33 Affinity (pKd) 8.93 CS -170 HAC 2 HDC 4

135	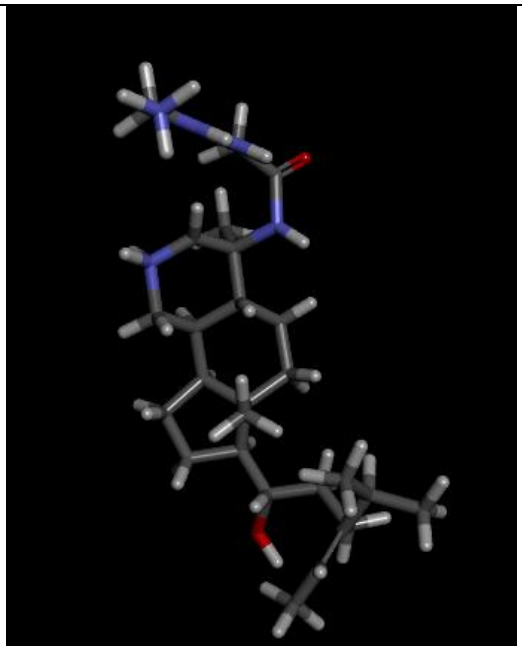	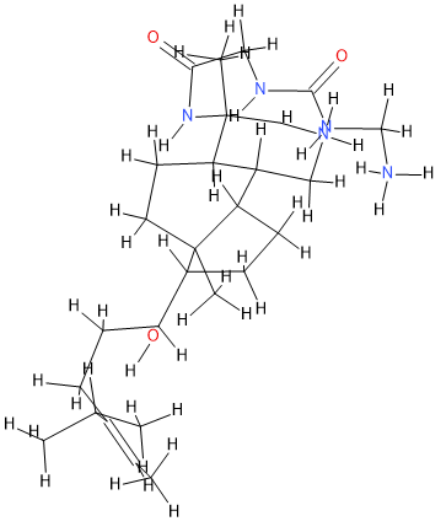	Family <8> MF C27H50N5O3 MW 492 LogP 3.39 Affinity (pKd) 8.75 CS -170 HAC 3 HDC 6
179	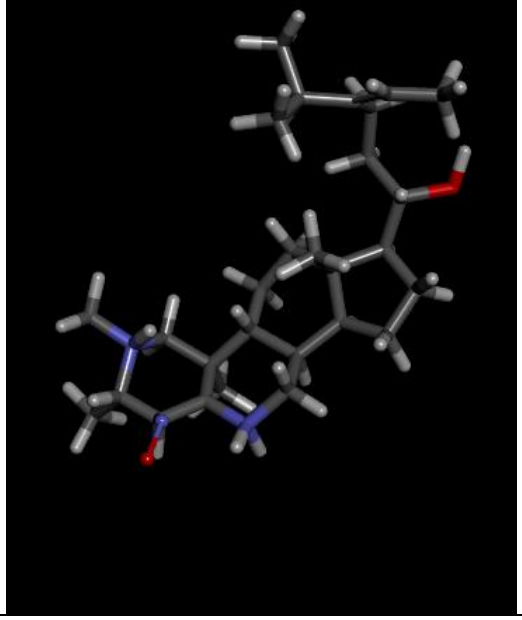	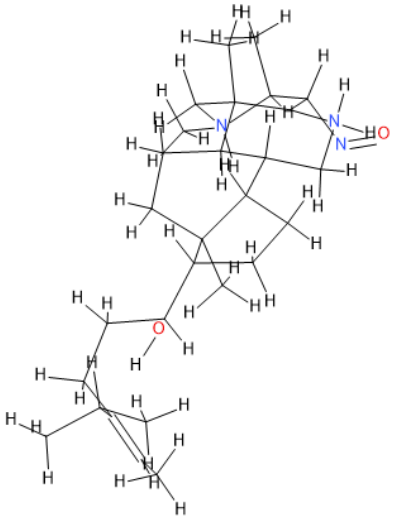	Family <12> MF C28H50N3O2 MW 460 LogP 4.38 Affinity (pKd) 6.79 CS -210 HAC 3 HDC 3

Table 3.12 The highest affinity molecule generated from each family for the Corticosteroid 11-Beta-Dehydrogenase Isozyme 1 (PDB 2RBE) 2rbeseed7.

Res-ult	3D Structure	2D Structure	Characteristics
012	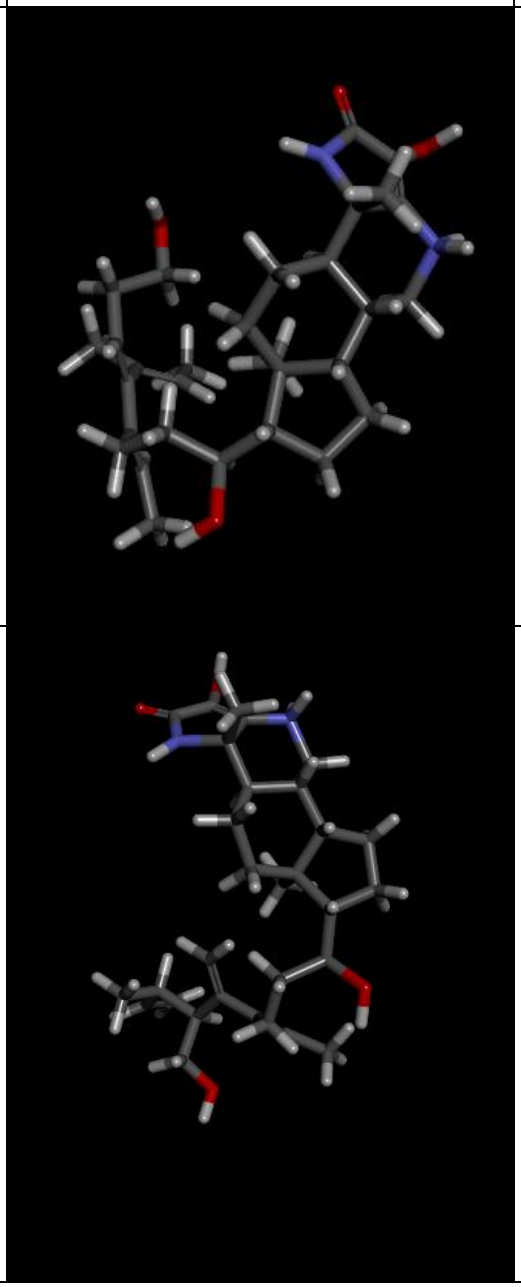	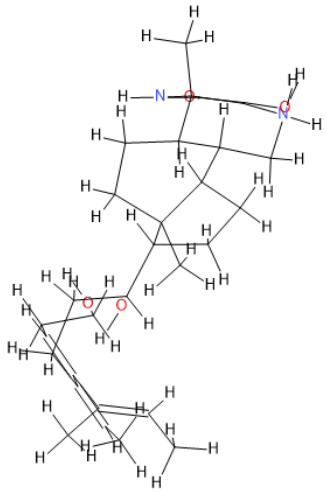	Family <2> MF C30H47N2O4 MW 499 LogP 4.59 Affinity (pKd) 9.49 CS -150 HAC 4 HDC 5
049		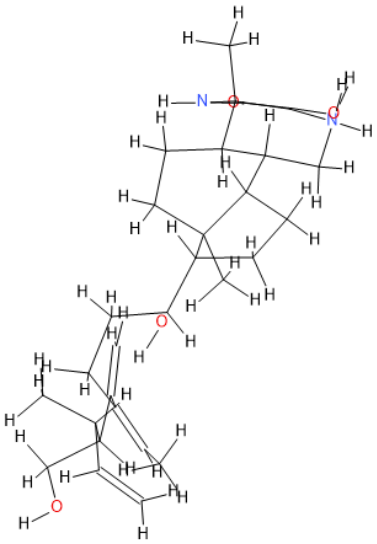	Family <3> MF C30H47N2O4 MW 499 LogP 4.46 Affinity (pKd) 8.04 CS -190 HAC 4 HDC 5

140	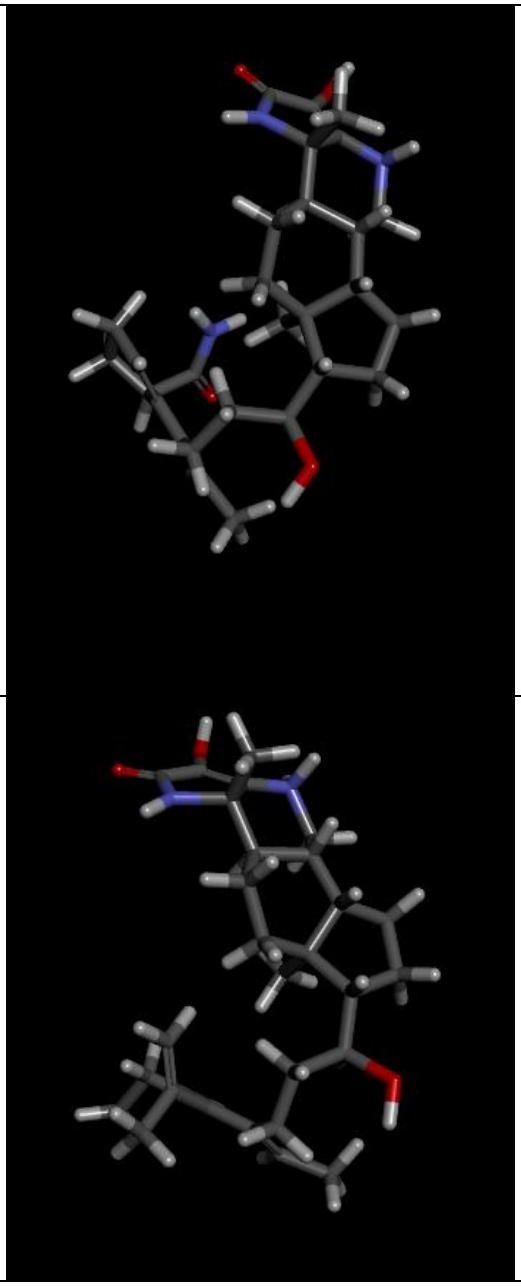	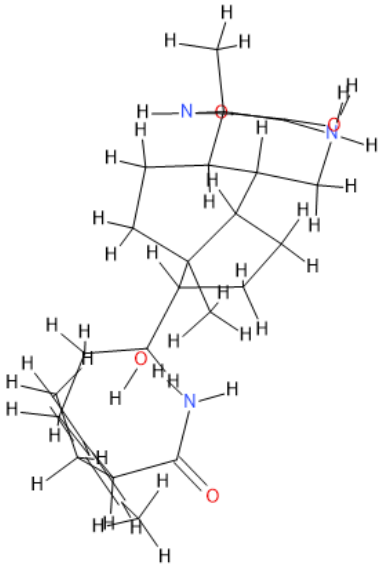	Family <7> MF C28H42N3O4 MW 484 LogP 3.6 Affinity (pKd) 8.22 CS -170 HAC 4 HDC 5
156		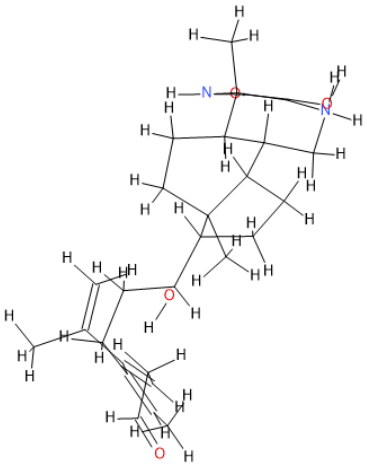	Family <8> MF C29H43N2O4 MW 483 LogP 4.77 Affinity (pKd) 9.21 CS -150 HAC 4 HDC 4

177	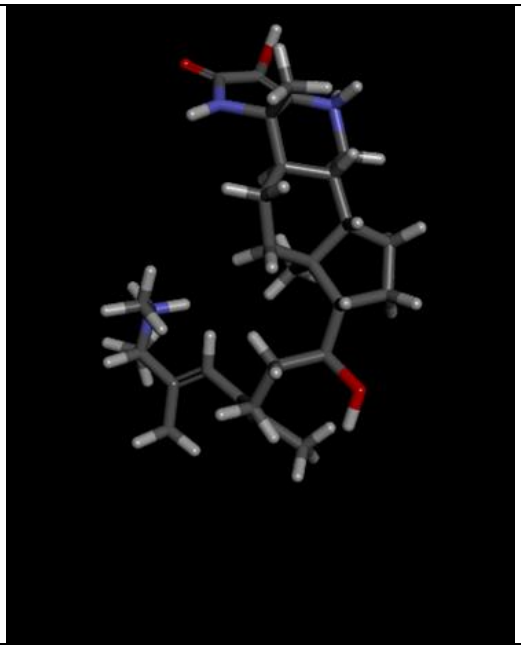	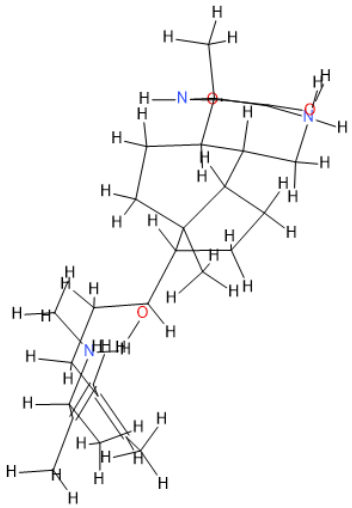	Family <9> MF C28H47N3O3 MW 473 LogP 4.45 Affinity (pKd) 7.64 CS -170 HAC 3 HDC 5

Table 3.13 The highest affinity molecule generated from each family for the Low Molecular Weight Phosphotyrosine Protein Phosphatase (PDB 5JNT) 5jntseed5.

Res-ult	3D Structure	2D Structure	Characteristics
001	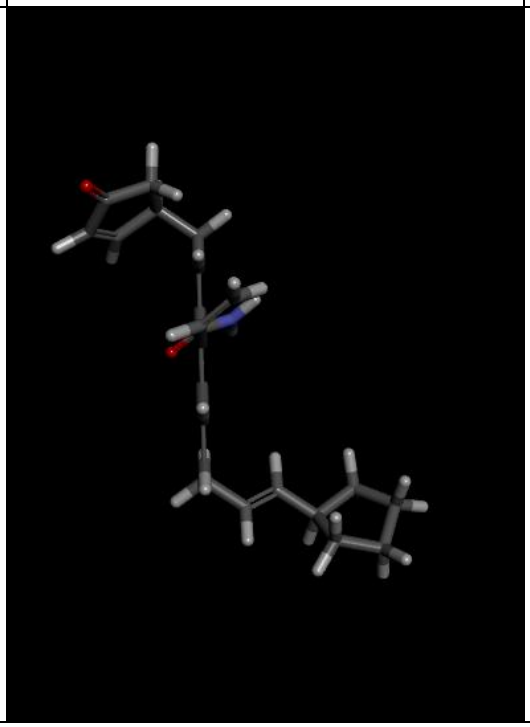	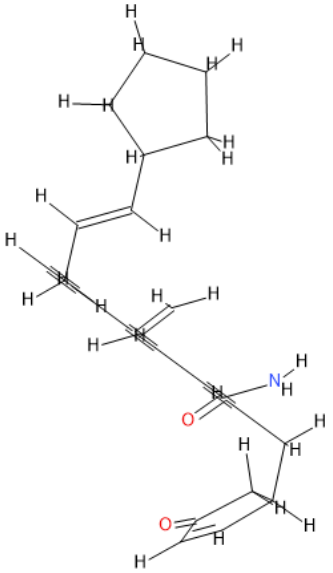	Family <1> MF C23H29NO2 MW 351 LogP 4.08 Affinity (pKd) 8.46 CS -70 HAC 2 HDC 1

073	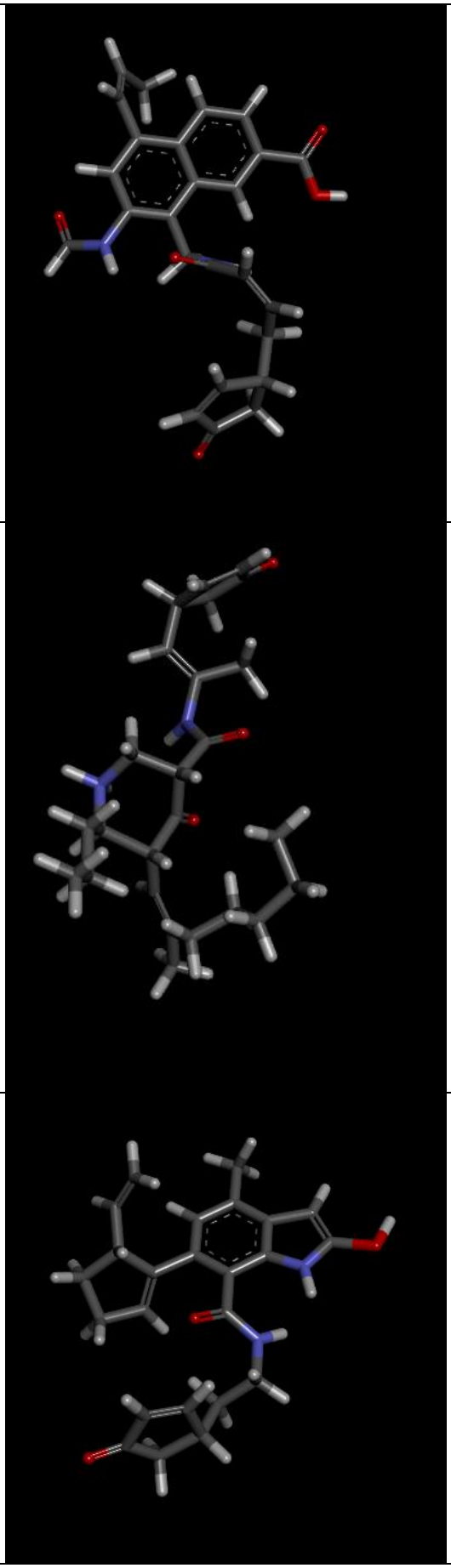	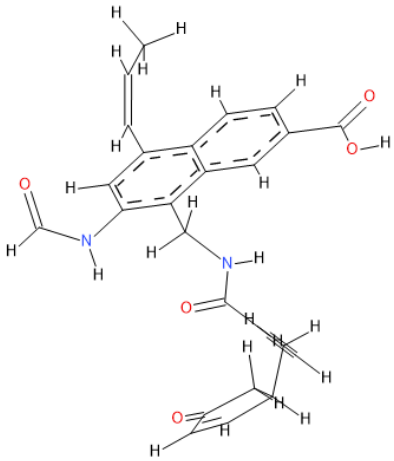	Family <2> MF C25H24N2O5 MW 432 LogP 3.29 Affinity (pKd) 6.77 CS -20 HAC 5 HDC 3
082		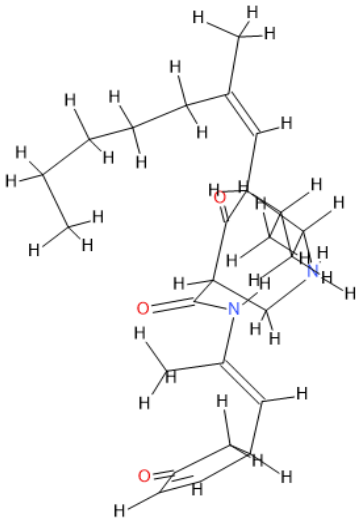	Family <3> MF C25H39N2O3 MW 415 LogP 3.39 Affinity (pKd) 7.73 CS -100 HAC 3 HDC 2
099		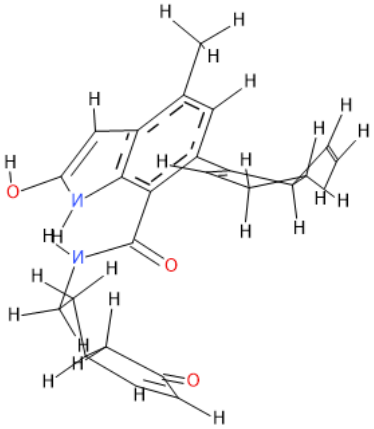	Family <4> MF C24H26N2O3 MW 390 LogP 4.97 Affinity(pKd) 7.15 CS -40 HAC 3 HDC 3

128	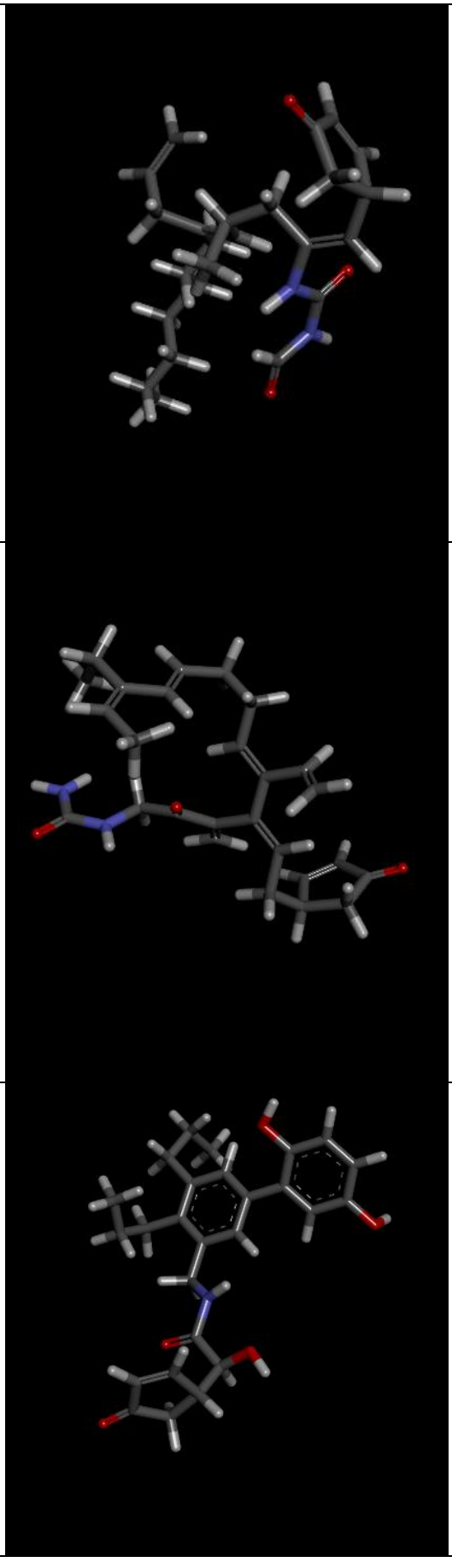	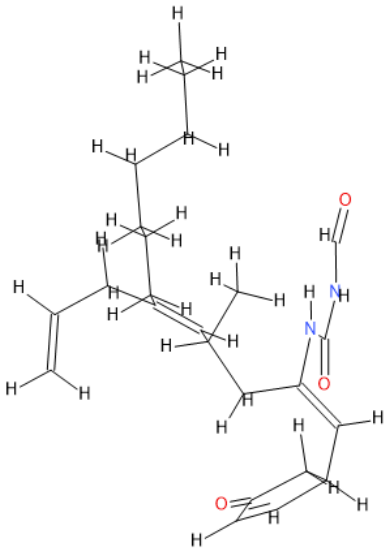	Family <5> MF C24H36N2O3 MW 400 LogP 4.81 Affinity (pKd) 7.53 CS -50 HAC 3 HDC 2
161		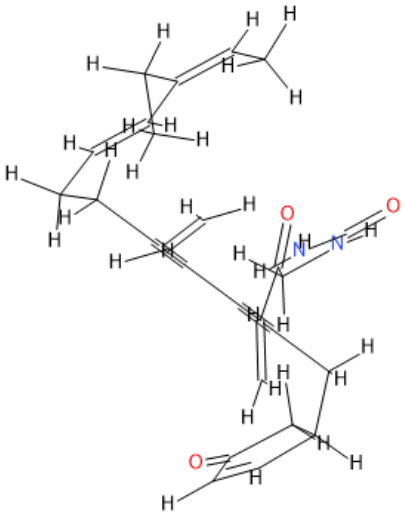	Family <6> MF C26H34N2O3 MW 422 LogP 3.41 Affinity (pKd) 7.46 CS -30 HAC 3 HDC 2
186		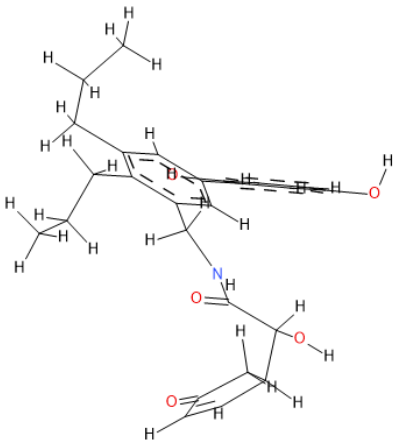	Family <7> MF C26H31NO5 MW 437 LogP 4.41 Affinity(pKd) 7.34 CS -40 HAC 5 HDC 4

191	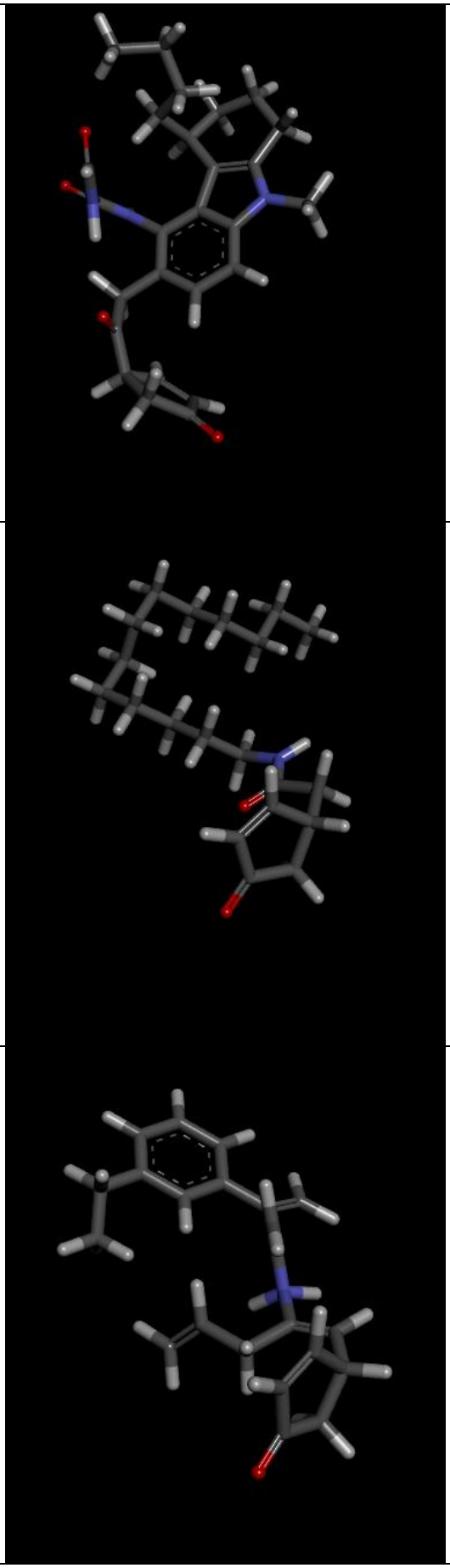	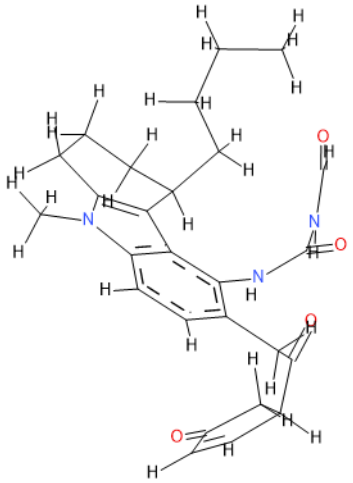	Family <8> MF C26H31N3O4 MW 449 LogP 4.12 Affinity (pKd) 6.96 CS -80 HAC 4 HDC 2
193		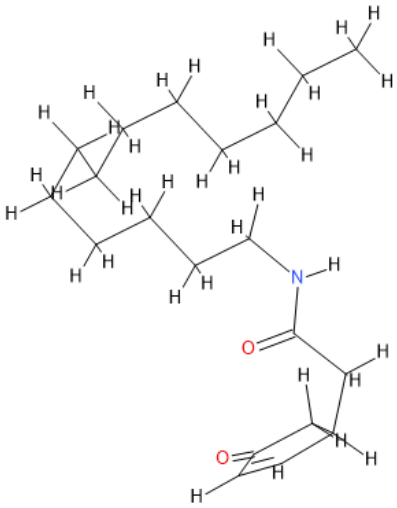	Family <9> MF C20H35NO2 MW 321 LogP 4.82 Affinity (pKd) 6.79 CS -20 HAC 2 HDC 1
200		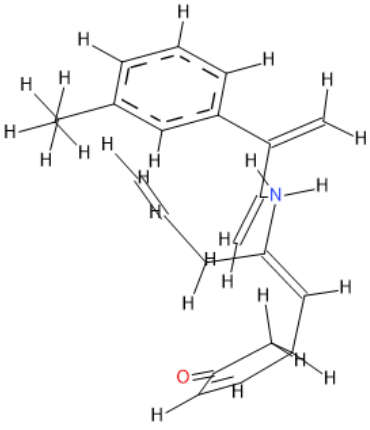	Family <11> MF C22H26NO MW 320 LogP 4.93 Affinity (pKd) 6.08 CS -20 HAC 1 HDC 1

Table 3.14 The highest affinity molecule generated from each family for the Low Molecular Weight Phosphotyrosine Protein Phosphatase (PDB 5JNT) 5jntseed6.

Res-ult	3D Structure	2D Structure	Characteristics
011	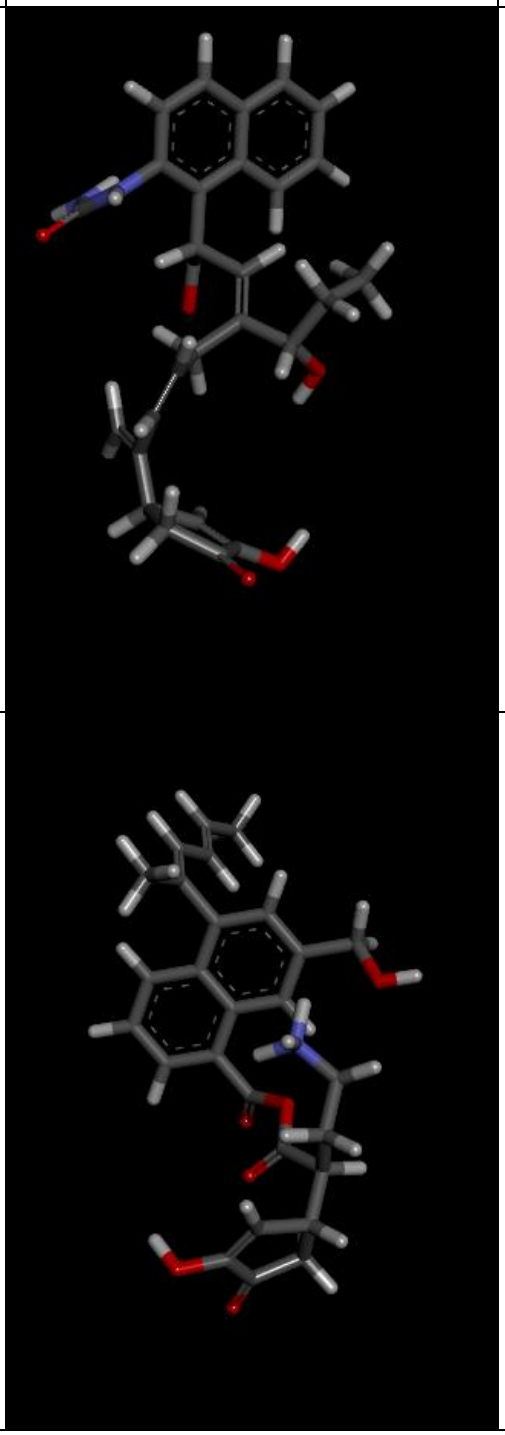	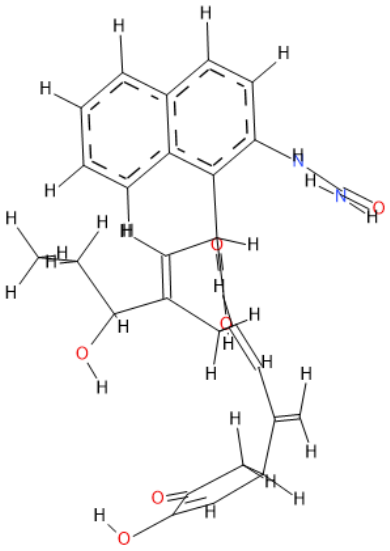	Family <1> MF C28H30N2O6 MW 490 LogP 3.16 Affinity (pKd) 8.11 CS -60 HAC 6 HDC 5
045		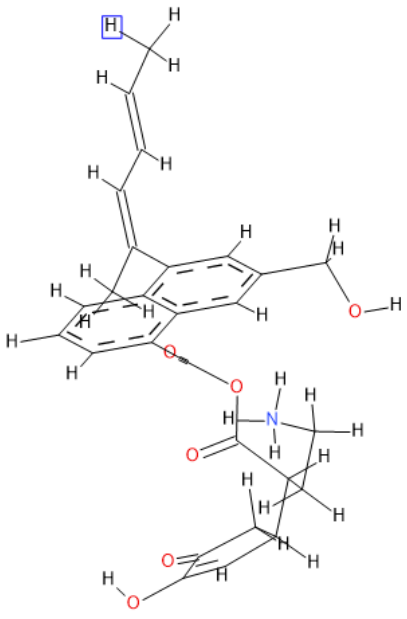	Family <2> MF C27H30NO6 MW 464 LogP 4.86 Affinity (pKd) 8.19 CS -50 HAC 6 HDC 3

114	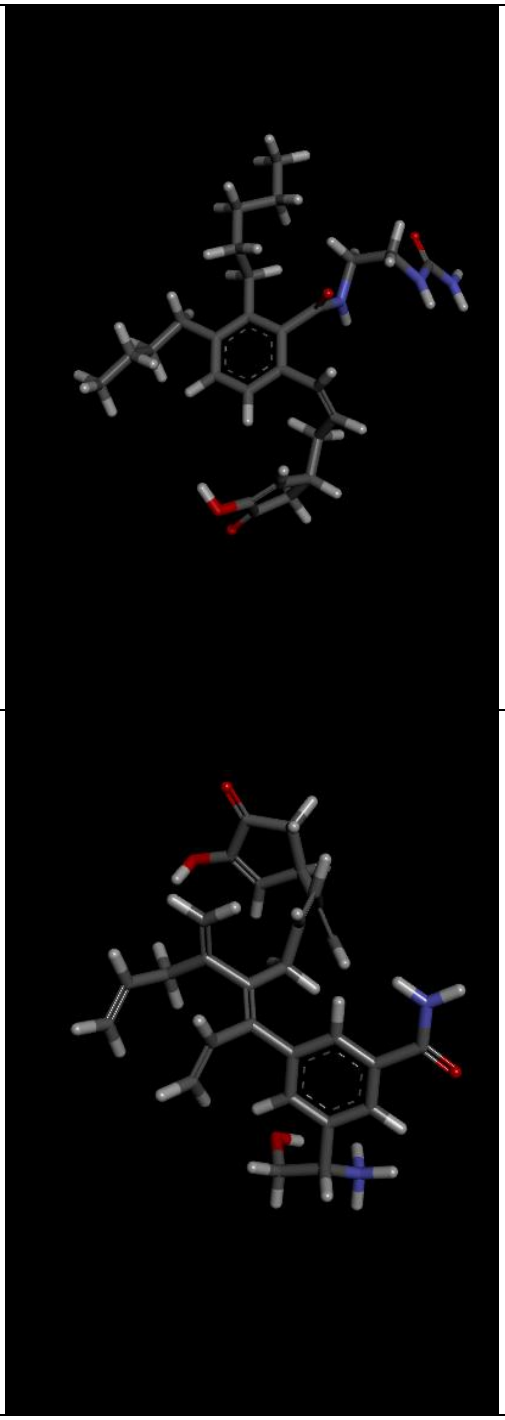	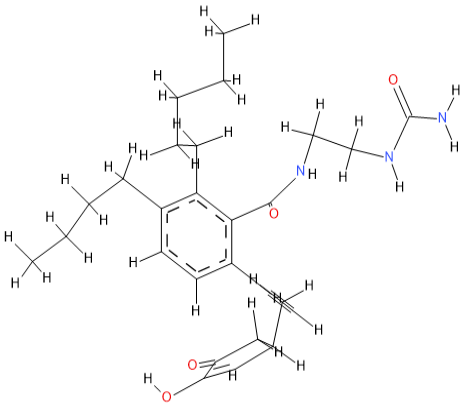	Family <3> MF C27H39N3O4 MW 469 LogP 4.93 Affinity (pKd) 8.03 CS -30 HAC 4 HDC 4
153		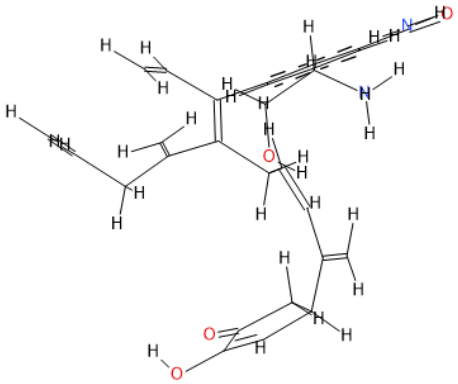	Family <5> MF C28H33N2O4 MW 461 LogP 3.48 Affinity (pKd) 8.5 CS -40 HAC 4 HDC 4

198	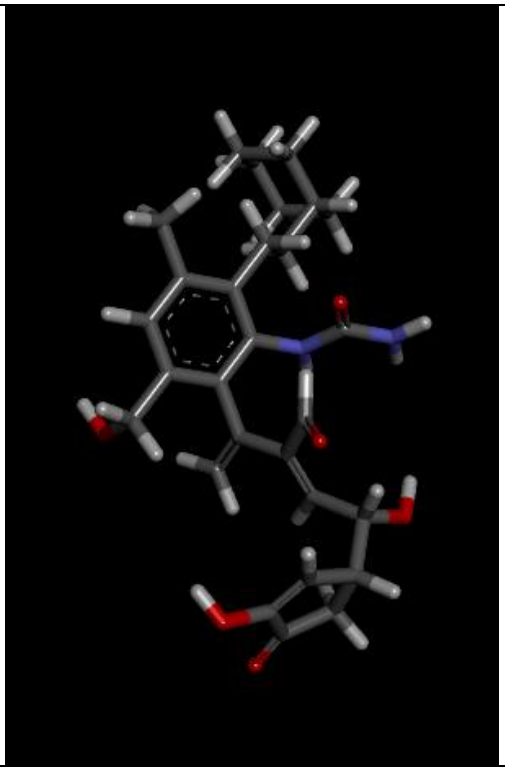	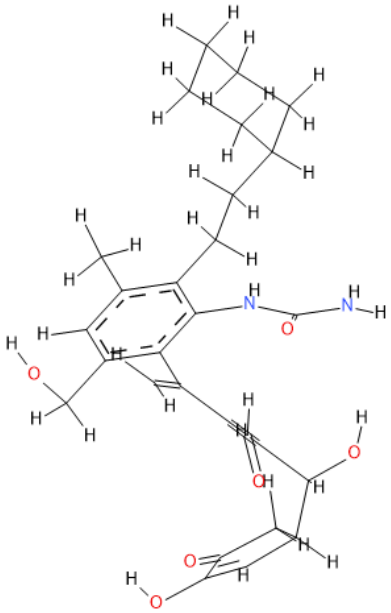	Family <6> MF C28H36N2O6 MW 496 LogP 4.09 Affinity (pKd) 8 CS -60 HAC 6 HDC 5

Table 3.15 The highest affinity molecule generated from each family for the Peptidyl-Prolyl Cis-Trans Isomerase NIMA-Interacting 1 (PDB 6DUN) 6dunseed7.

Res-ult	3D Structure	2D Structure	Characteristics
001	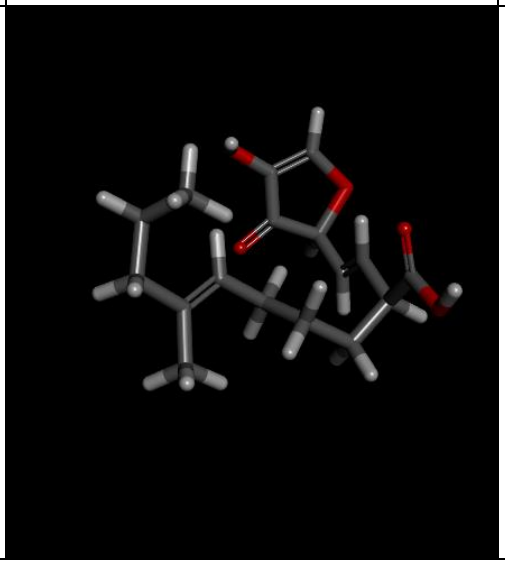	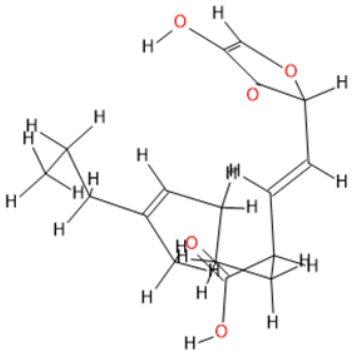	Family <1> MF C17H24O5 MW 308 LogP 3.97 Affinity (pKd) 7.89 CS -50 HAC 5 HDC 2

054	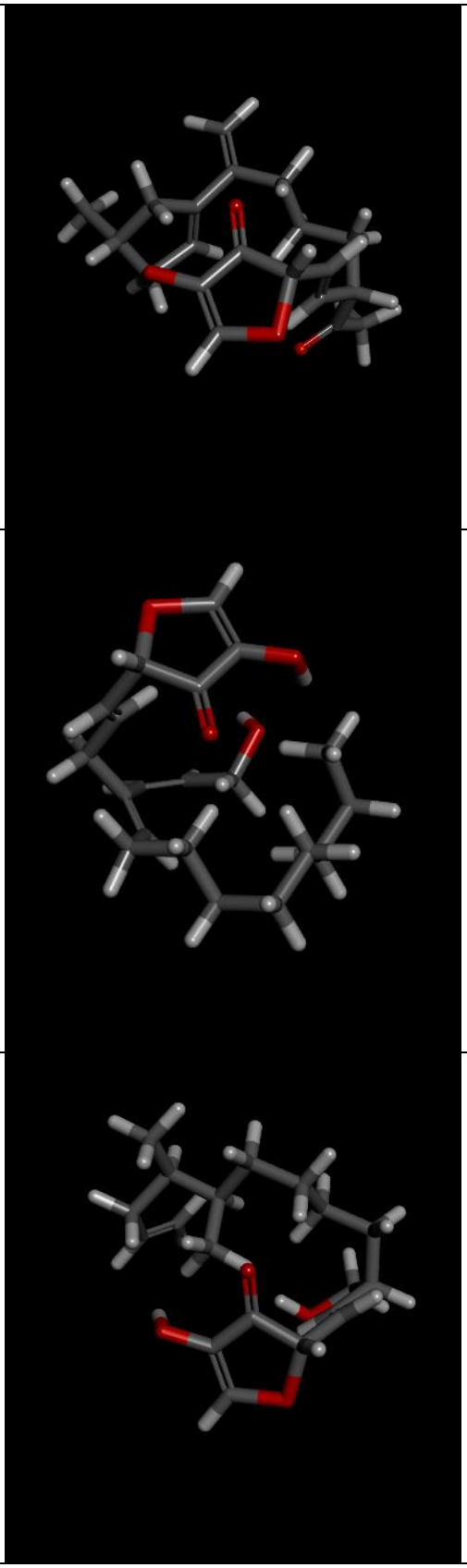	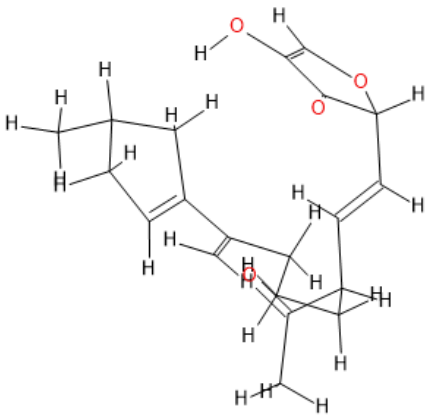	Family <2> MF C20H26O4 MW 330 LogP 3.49 Affinity (pKd) 7.68 CS -70 HAC 4 HDC 1
081		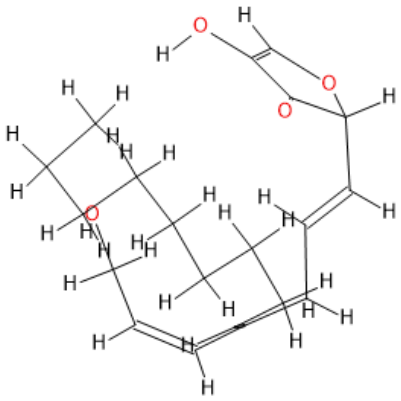	Family <3> MF C20H30O4 MW 334 LogP 4.61 Affinity (pKd) 7.58 CS -20 HAC 4 HDC 2
113		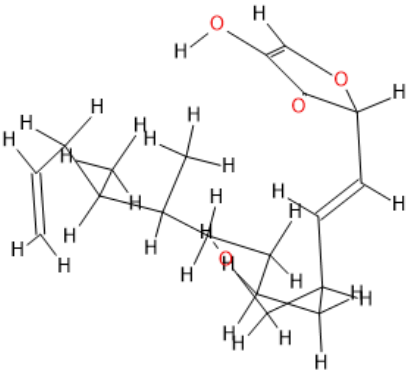	Family <4> MF C19H30O4 MW 322 LogP 4.59 Affinity (pKd) 7.31 CS -100 HAC 4 HDC 2

142	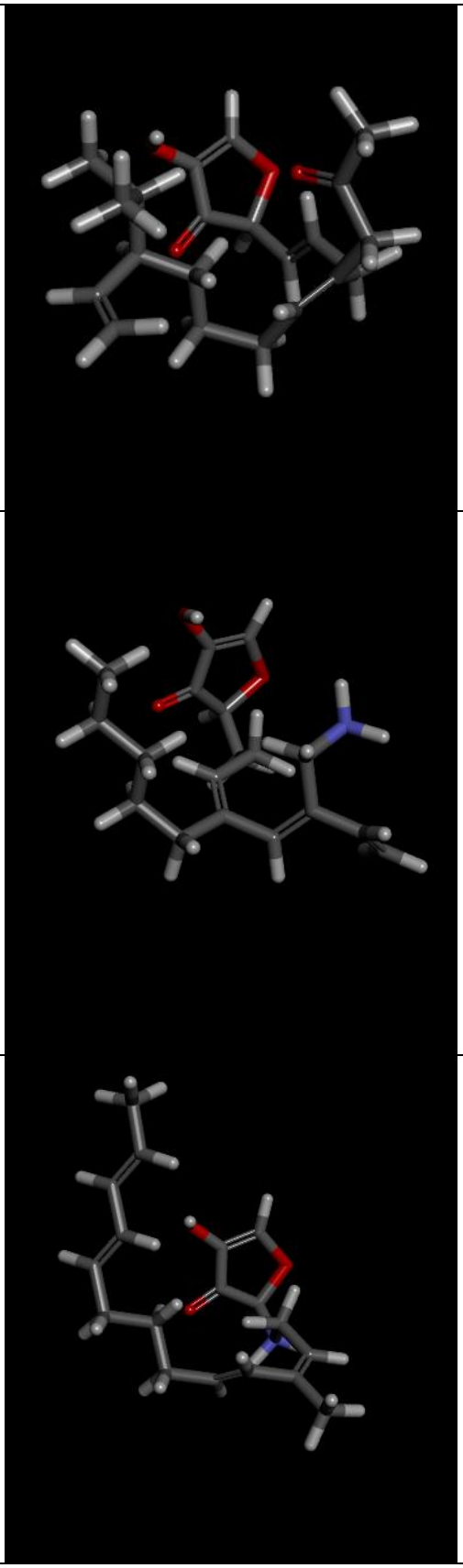	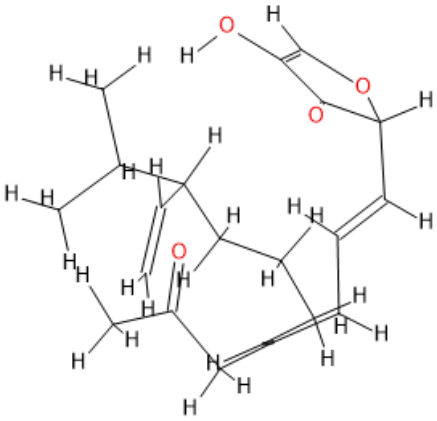	Family <5> MF C21H30O4 MW 346 LogP 4.41 Affinity (pKd) 7.39 CS -60 HAC 4 HDC 1
177		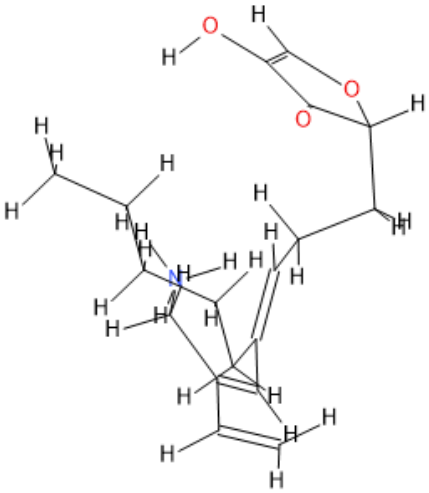	Family <6> MF C18H28NO3 MW 306 LogP 4.21 Affinity (pKd) 6.82 CS -20 HAC 3 HDC 2
187		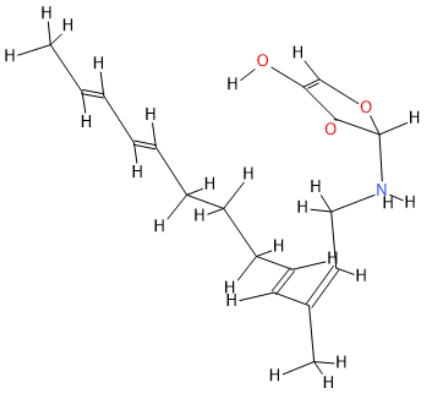	Family <7> MF C18H26NO3 MW 304 LogP 4.03 Affinity (pKd) 6.17 CS -30 HAC 3 HDC 2

Table 3.16 The highest affinity molecule generated from each family for the Peptidyl-Prolyl Cis-Trans Isomerase NIMA-Interacting 1 (PDB 6DUN) 6dunseed8.

Res-ult	3D Structure	2D Structure	Characteristics
001	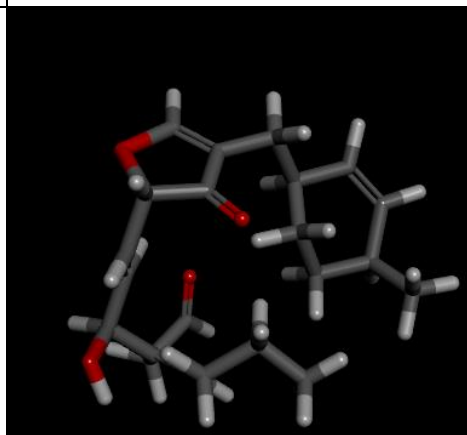	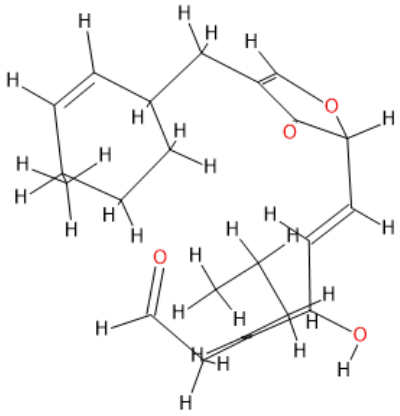	Family <1> MF C22H30O4 MW 358 LogP 3.12 Affinity (pKd) 6.86 CS -110 HAC 4 HDC 1
027	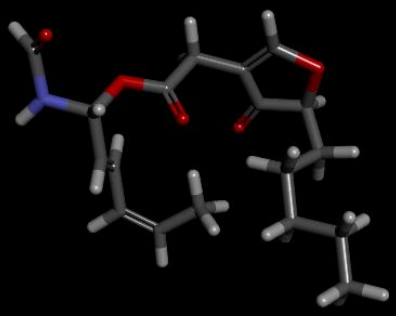	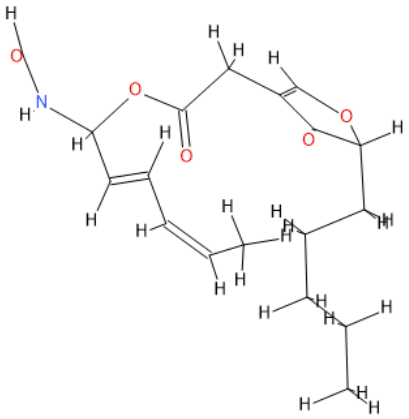	Family <2> MF C18H25NO5 MW 335 LogP 4.06 Affinity (pKd) 6.75 CS -40 HAC 5 HDC 1
075	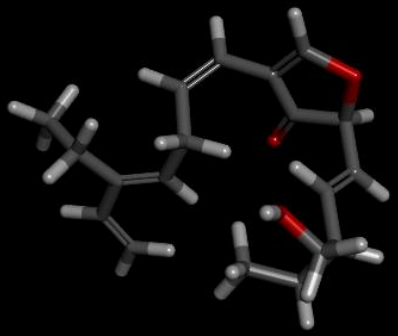	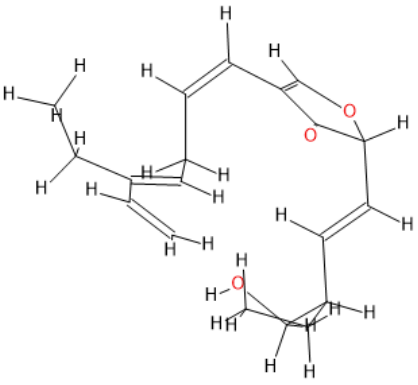	Family <3> MF C19H26O3 MW 302 LogP 4.2 Affinity (pKd) 6.34 CS -40 HAC 3

			HDC 1
092	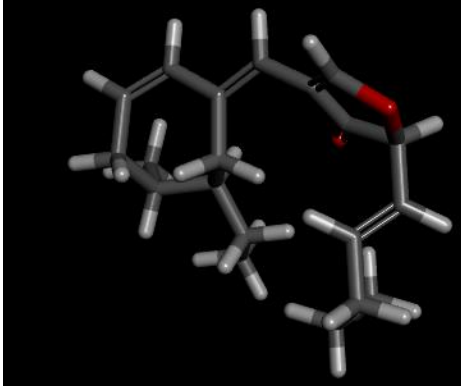	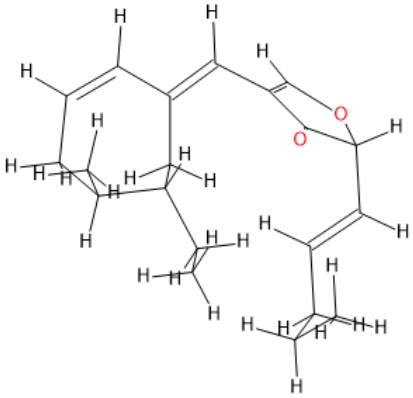	Family <4> MF C20H28O2 MW 300 LogP 4.83 Affinity (pKd) 6.56 CS -90 HAC 2 HDC 0
139	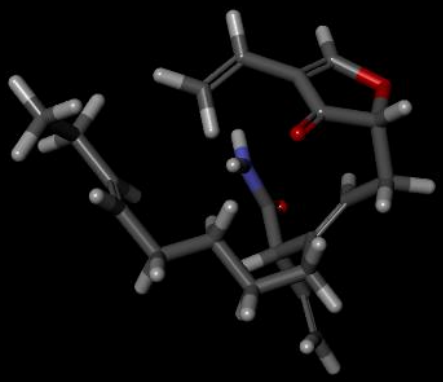	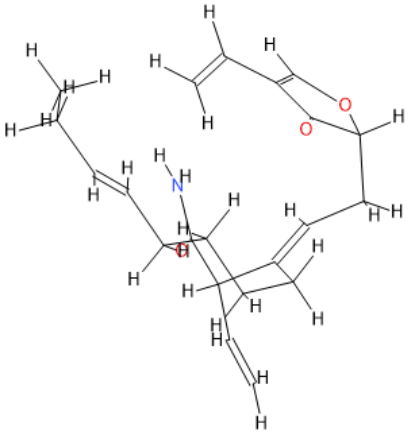	Family <5> MF C21H29NO3 MW 343 LogP 3.34 Affinity (pKd) 6.27 CS -50 HAC 3 HDC 1
142	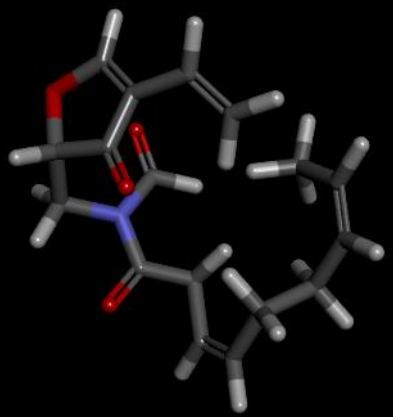	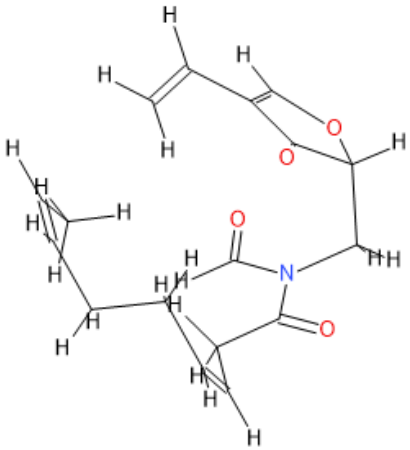	Family <6> MF C17H21NO4 MW 303 LogP 3.41 Affinity (pKd) 6.21 CS -20 HAC 4 HDC 0

143	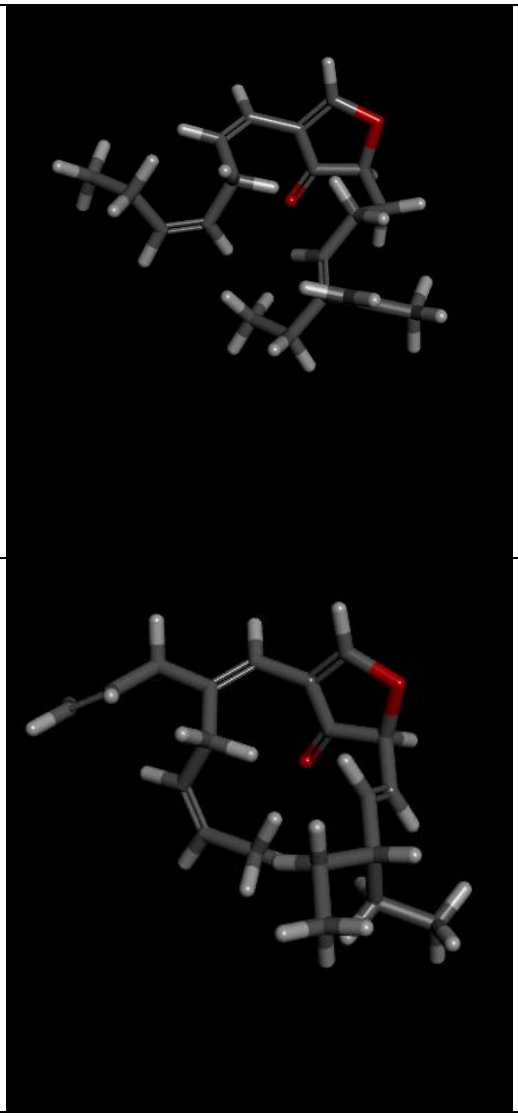	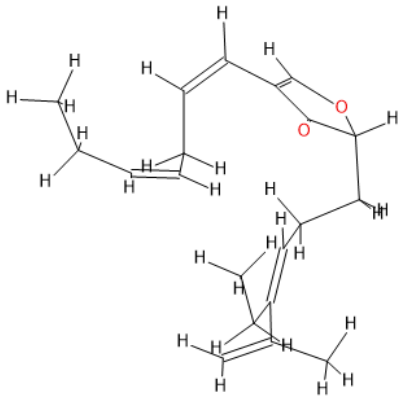	Family <7> MF C20H28O2 MW 300 LogP 4.94 Affinity (pKd) 6.16 CS -30 HAC 2 HDC 0
149		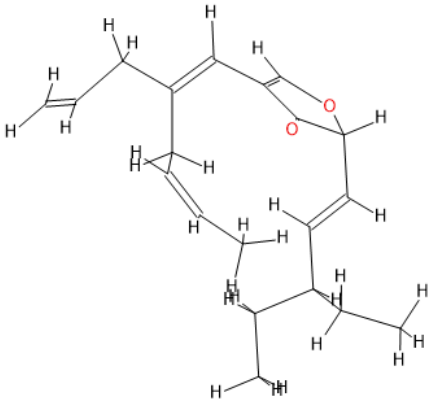	Family <8> MF C20H28O2 MW 300 LogP 4.98 Affinity (pKd) 5.9 CS -40 HAC 2 HDC 0

Table 3.17 The highest affinity molecule generated from each family for the Progesterone Receptor (PDB 3ZR7) 3zr7seed7.

Res-ult	3D Structure	2D Structure	Characteristics
007	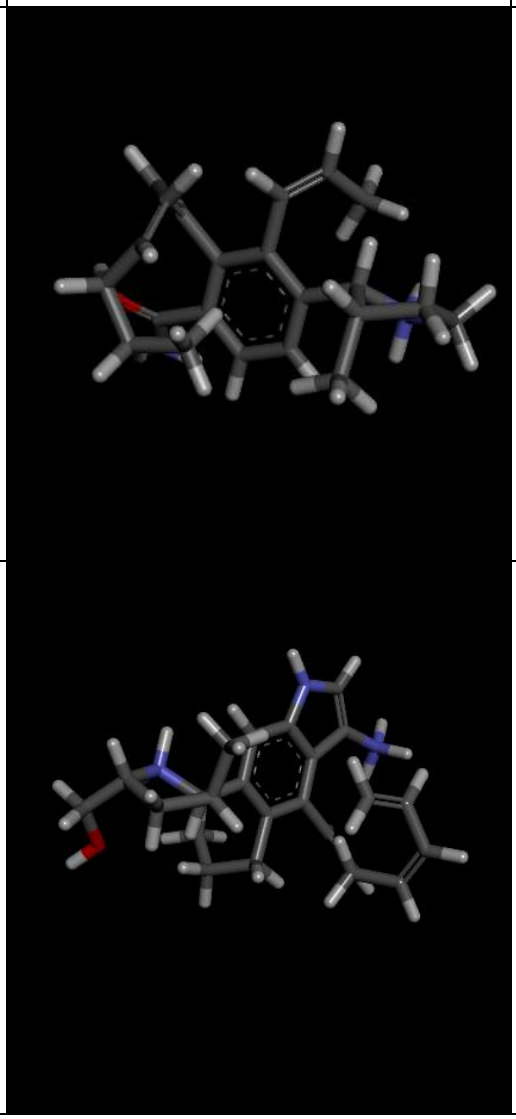	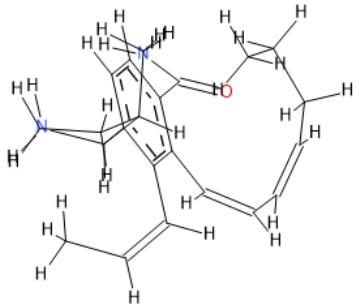	Family <1> MF C22H31N2O MW 339 LogP 4.92 Affinity (pKd) 9.23 CS -40 HAC 1 HDC 2
099		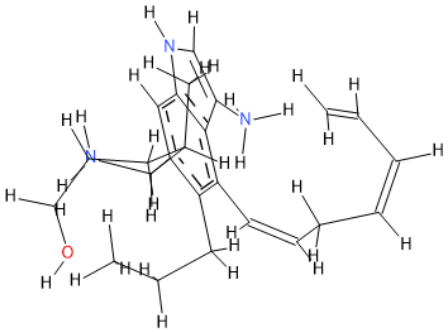	Family <2> MF C24H35N3O MW 381 LogP 4.86 Affinity (pKd) 8.45 CS -60 HAC 1 HDC 4

117	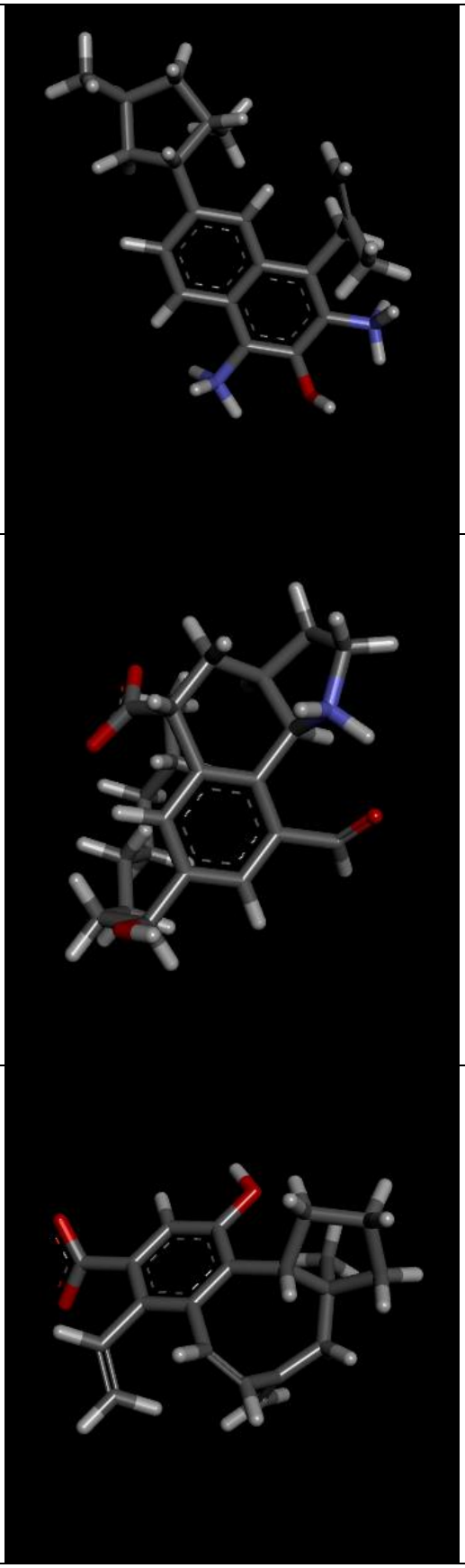	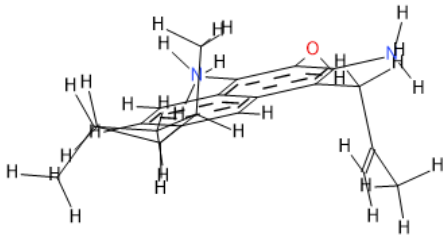	Family <3> MF C21H30N2O MW 326 LogP 4.98 Affinity (pKd) 8.77 CS -60 HAC 1 HDC 3
171		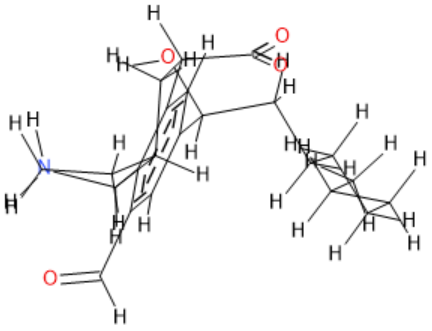	Family <4> MF C22H31NO4 MW 373 LogP 3.6 Affinity (pKd) 8.01 CS -80 HAC 4 HDC 3
189		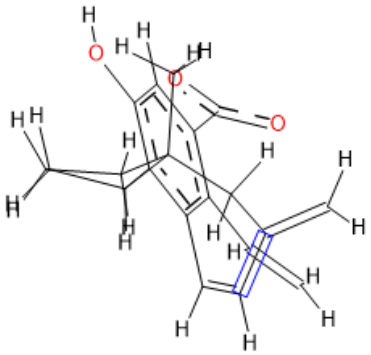	Family <5> MF C20H21O3 MW 309 LogP 4.54 Affinity (pKd) 8.19 CS -40 HAC 3 HDC 2

Table 3.18 The highest affinity molecule generated from each family for the Progesterone Receptor (PDB 3ZR7) 3zr7seed8.

Res-ult	3D Structure	2D Structure	Characteristics
001	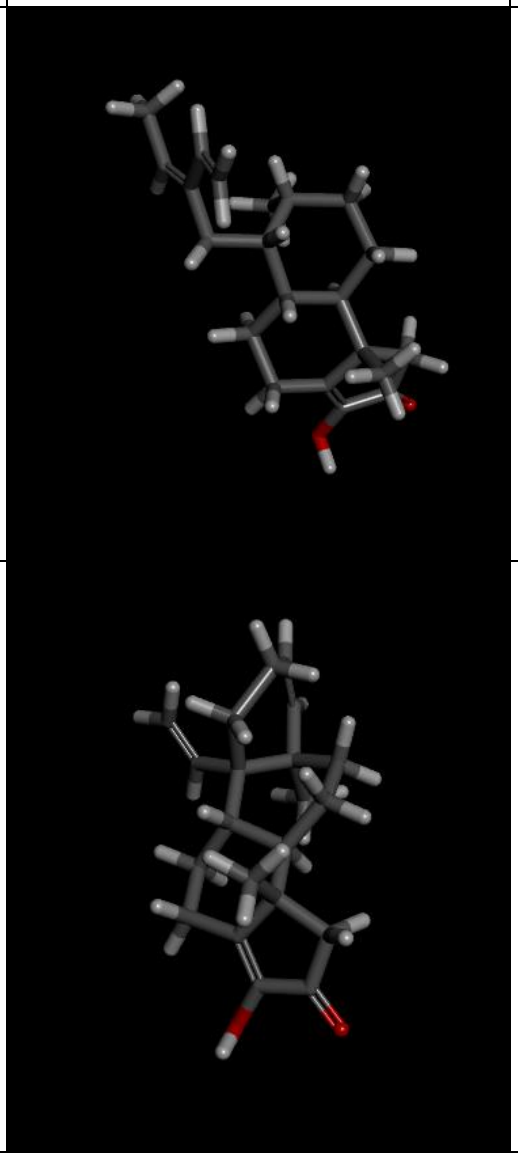	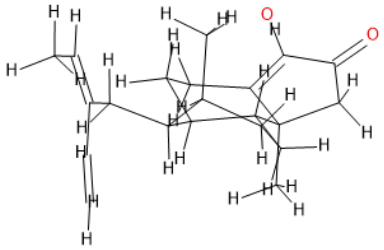	Family <1> MF C21H30O2 MW 314 LogP 4.97 Affinity (pKd) 9.39 CS -120 HAC 2 HDC 1
014		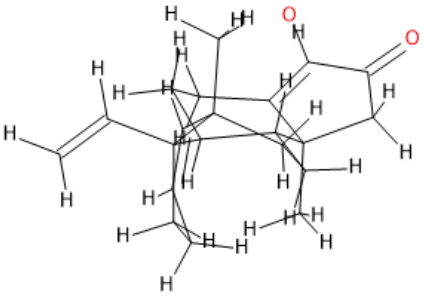	Family <2> MF C21H28O2 MW 312 LogP 4.45 Affinity (pKd) 7.98 CS -120 HAC 2 HDC 1

028	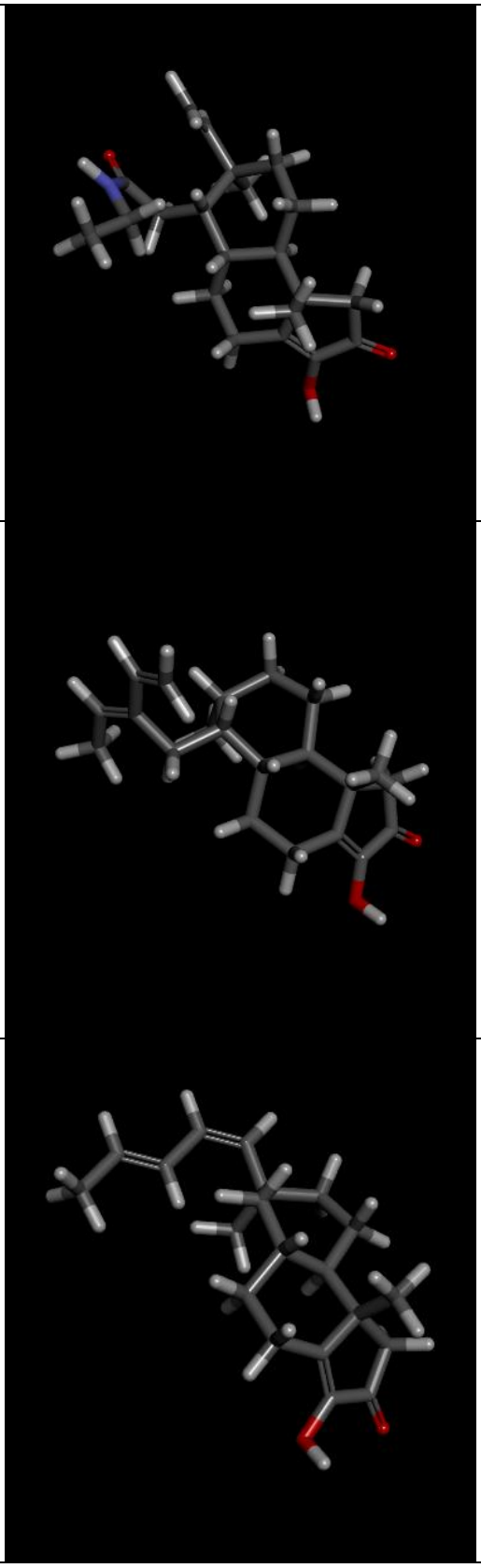	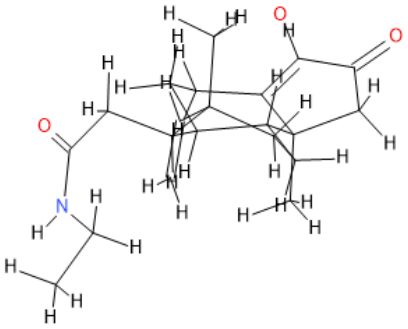	Family <3> MF C21H31NO3 MW 345 LogP 3.3 Affinity (pKd) 6.06 CS -120 HAC 3 HDC 2
030		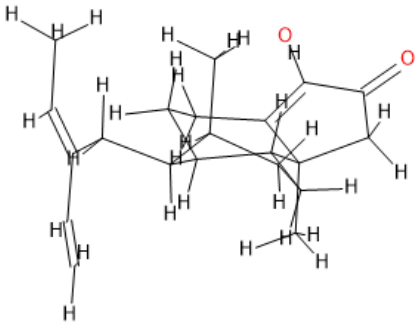	Family <4> MF C21H30O2 MW 314 LogP 4.97 Affinity (pKd) 8.72 CS -120 HAC 2 HDC 1
041		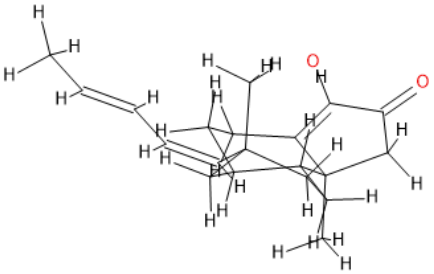	Family <5> MF C20H28O2 MW 300 LogP 4.68 Affinity (pKd) 8.05 CS -100 HAC 2 HDC 1

046	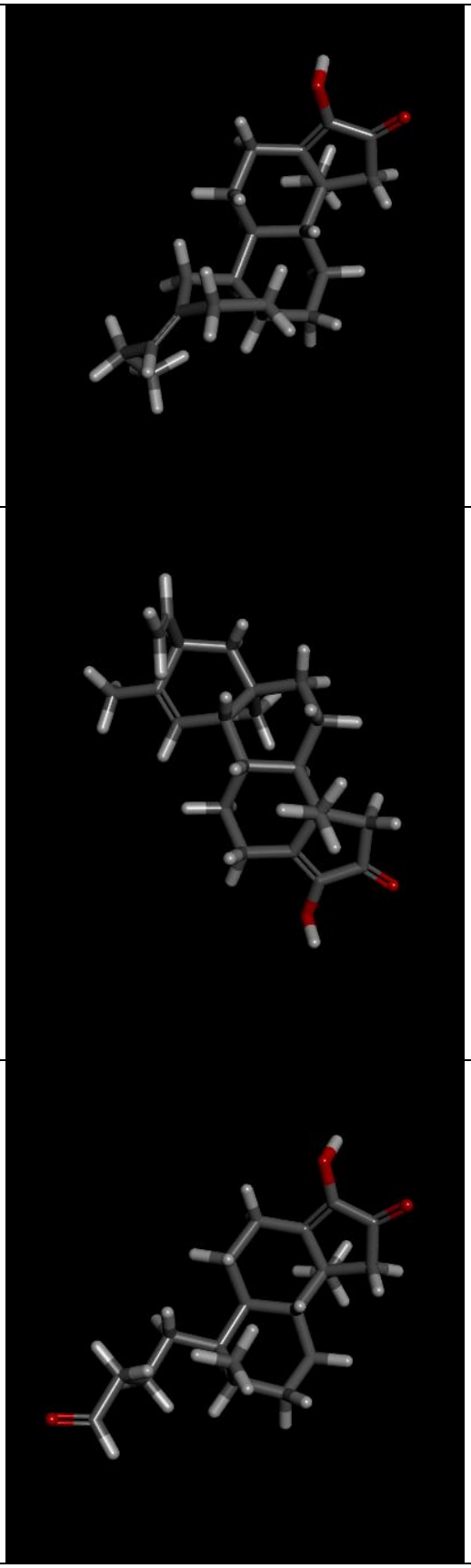	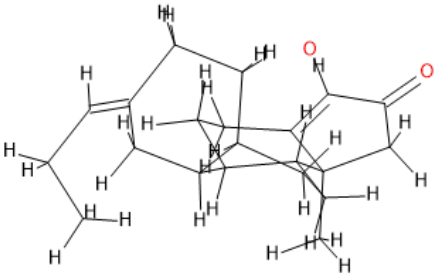	Family <6> MF C21H30O2 MW 314 LogP 4.53 Affinity (pKd) 8.53 CS -120 HAC 2 HDC 1
055		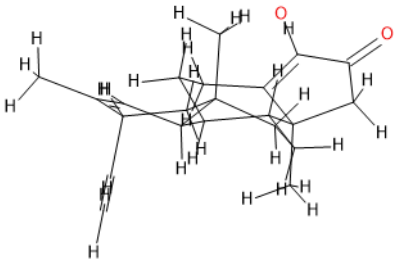	Family <7> MF C22H30O2 MW 326 LogP 4.91 Affinity (pKd) 7.89 CS -140 HAC 2 HDC 1
071		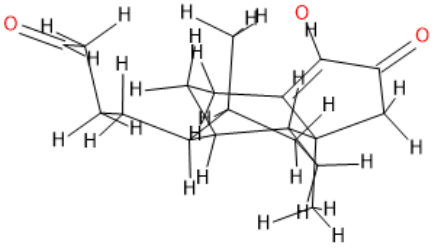	Family <8> MF C19H28O3 MW 304 LogP 4.03 Affinity (pKd) 7.34 CS -120 HAC 3 HDC 1

079	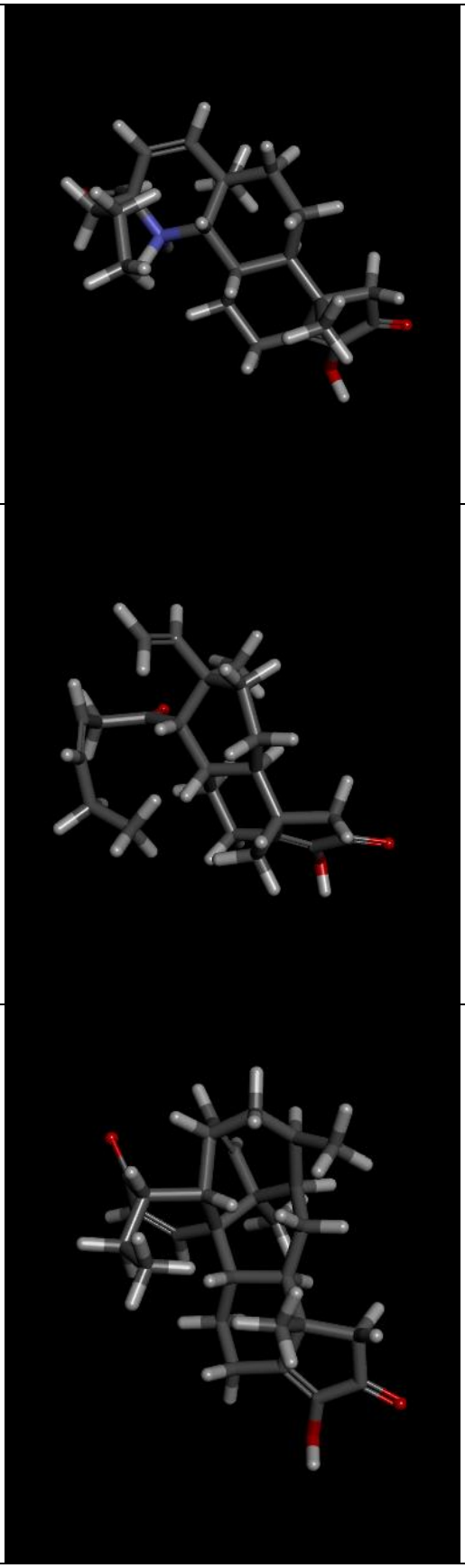	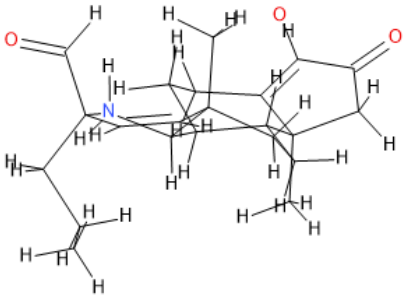	Family <9> MF C22H32NO3 MW 358 LogP 3.21 Affinity (pKd) 7.3 CS -140 HAC 3 HDC 2
083		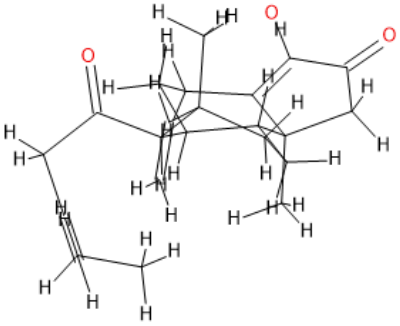	Family <10> MF C23H32O3 MW 356 LogP 3.99 Affinity (pKd) 6.96 CS -120 HAC 3 HDC 1
099		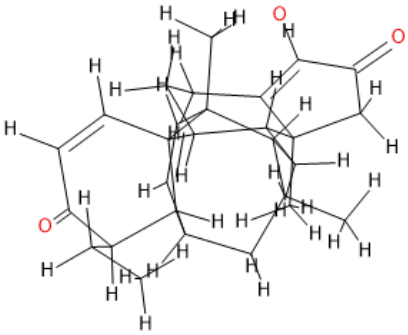	Family <11> MF C28H36O3 MW 420 LogP 4.95 Affinity (pKd) 6.6 CS -220 HAC 3 HDC 1

103		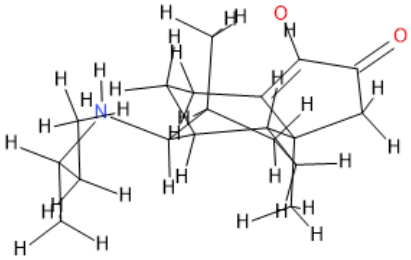	Family <13> MF C19H32NO2 MW 306 LogP 3.39 Affinity (pKd) 6.02 CS -140 HAC 2 HDC 2
105	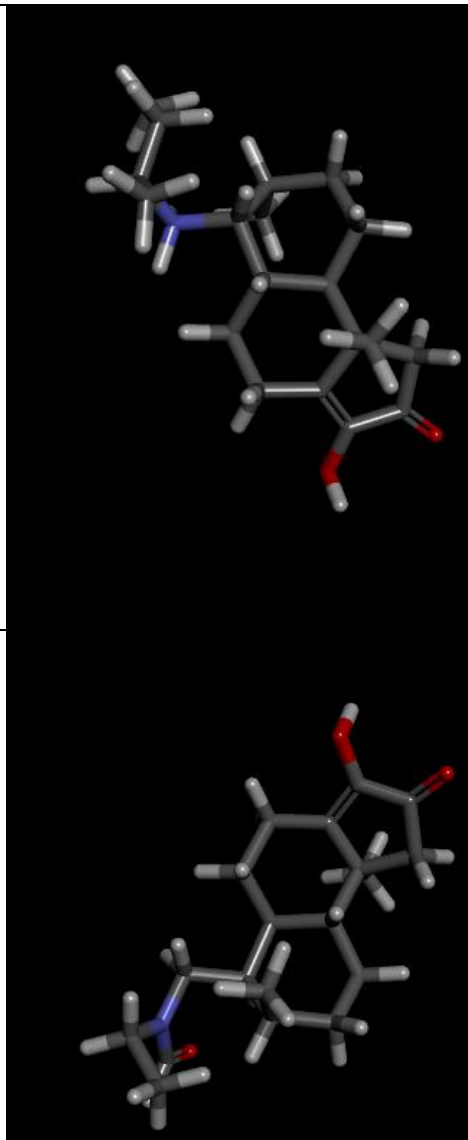	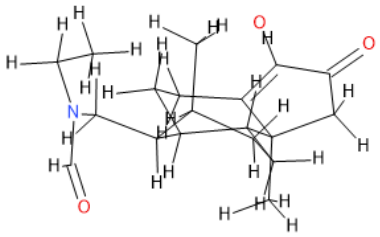	Family <14> MF C19H29NO3 MW 319 LogP 3.4 Affinity (pKd) 5.97 CS -120 HAC 3 HDC 1
106		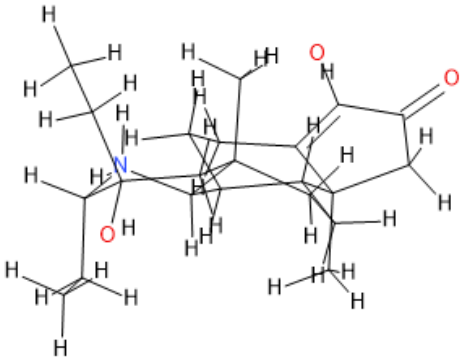	Family <15> MF C22H36NO3 MW 362 LogP 3.19 Affinity (pKd) 5.83 CS -160 HAC 3 HDC 3

Table 3.19 The highest affinity molecule generated from each family for the Sex Hormone-Binding Globulin (PDB 1LHU) 1lhuseed7.

Res-ult	3D Structure	2D Structure	Characteristics
006	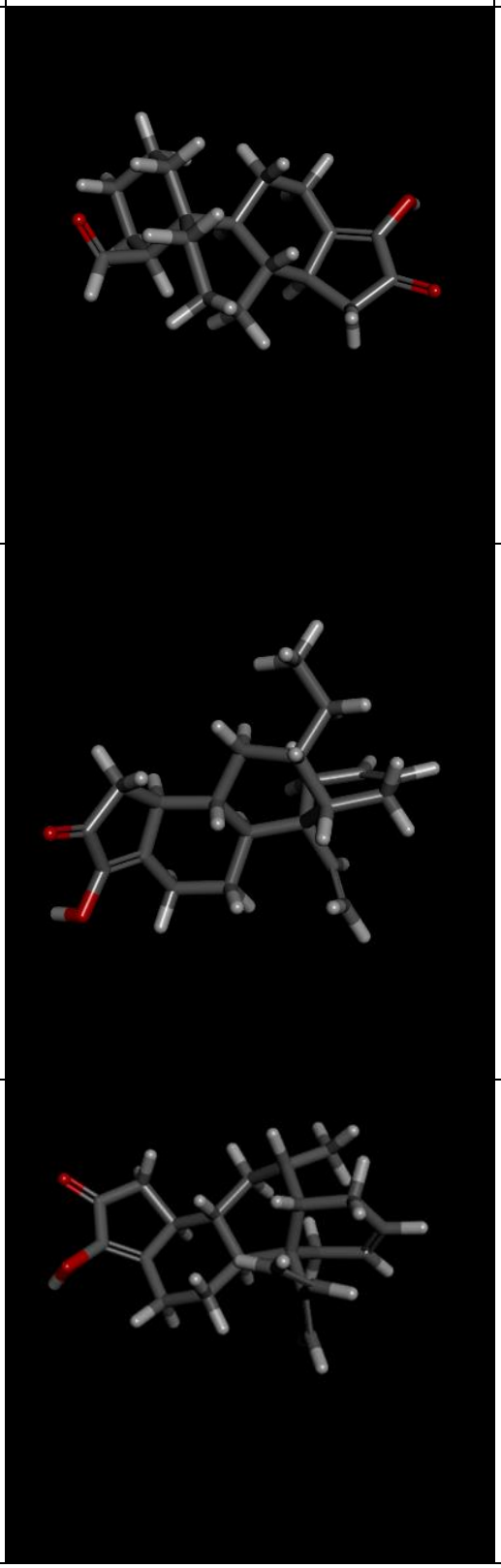	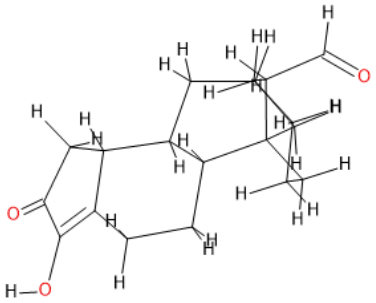	Family <1> MF C19H26O3 MW 302 LogP 4.72 Affinity (pKd) 8.41 CS -100 HAC 3 HDC 1
017		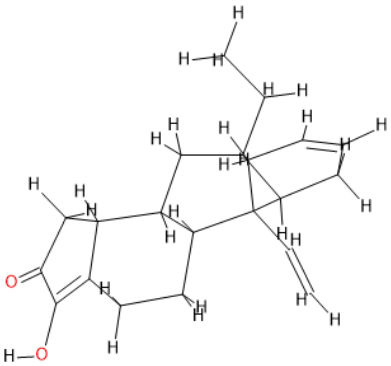	Family <2> MF C21H28O2 MW 312 LogP 4.71 Affinity (pKd) 9.11 CS -120 HAC 2 HDC 1
029		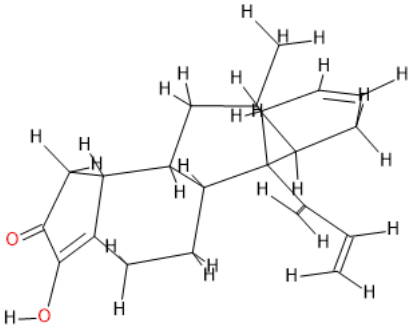	Family <3> MF C22H28O2 MW 324 LogP 4.66 Affinity (pKd) 8.82 CS -120 HAC 2

			HDC 1
055	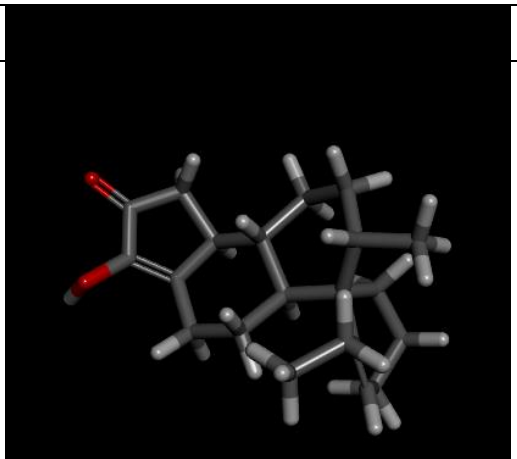	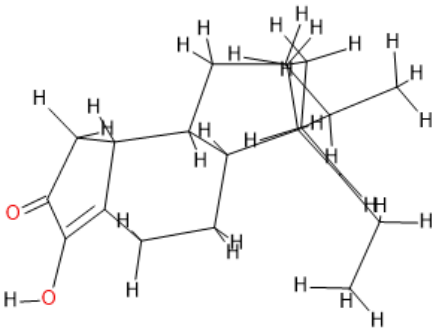	Family <4> MF C21H30O2 MW 314 LogP 4.52 Affinity (pKd) 8.39 CS -100 HAC 2 HDC 1
077		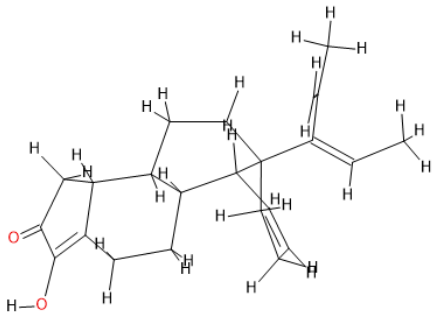	Family <5> MF C23H30O2 MW 338 LogP 4.82 Affinity (pKd) 8.18 CS -130 HAC 2 HDC 1
083		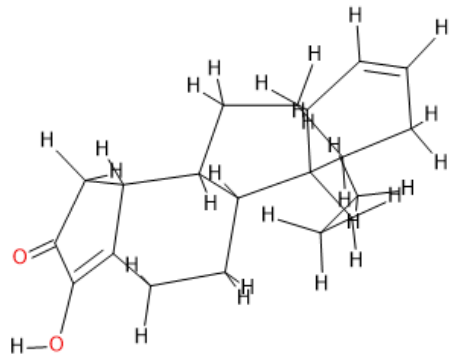	Family <6> MF C20H28O2 MW 300 LogP 4.98 Affinity (pKd) 8.75 CS -100 HAC 2 HDC 1

093	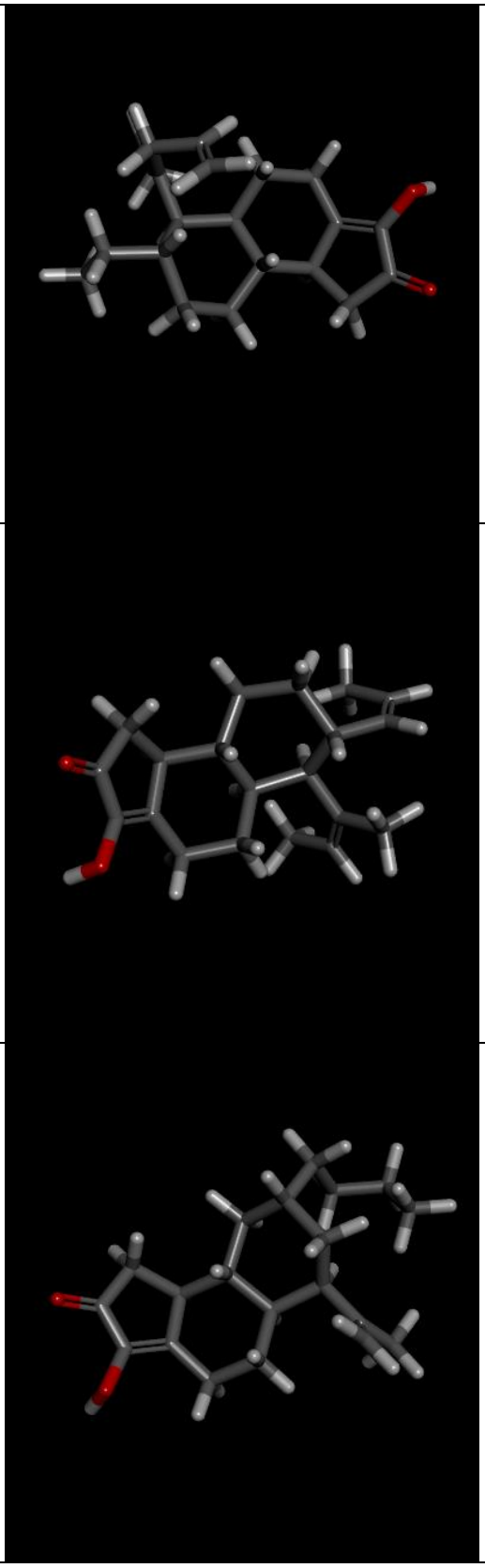	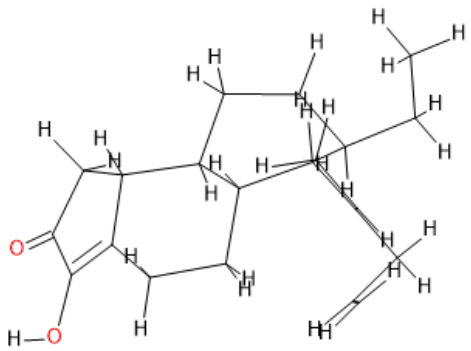	Family <7> MF C21H30O2 MW 314 LogP 4.95 Affinity (pKd) 8.3 CS -100 HAC 2 HDC 1
105		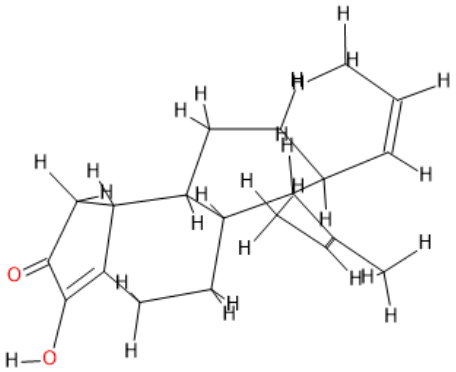	Family <8> MF C20H28O2 MW 300 LogP 4.46 Affinity (pKd) 7.66 CS -100 HAC 2 HDC 1
117		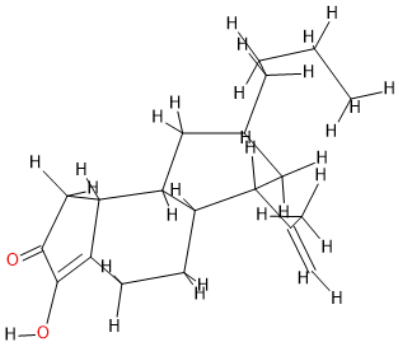	Family <9> MF C20H30O2 MW 302 LogP 4.92 Affinity (pKd) 7.65 CS -100 HAC 2 HDC 1

122	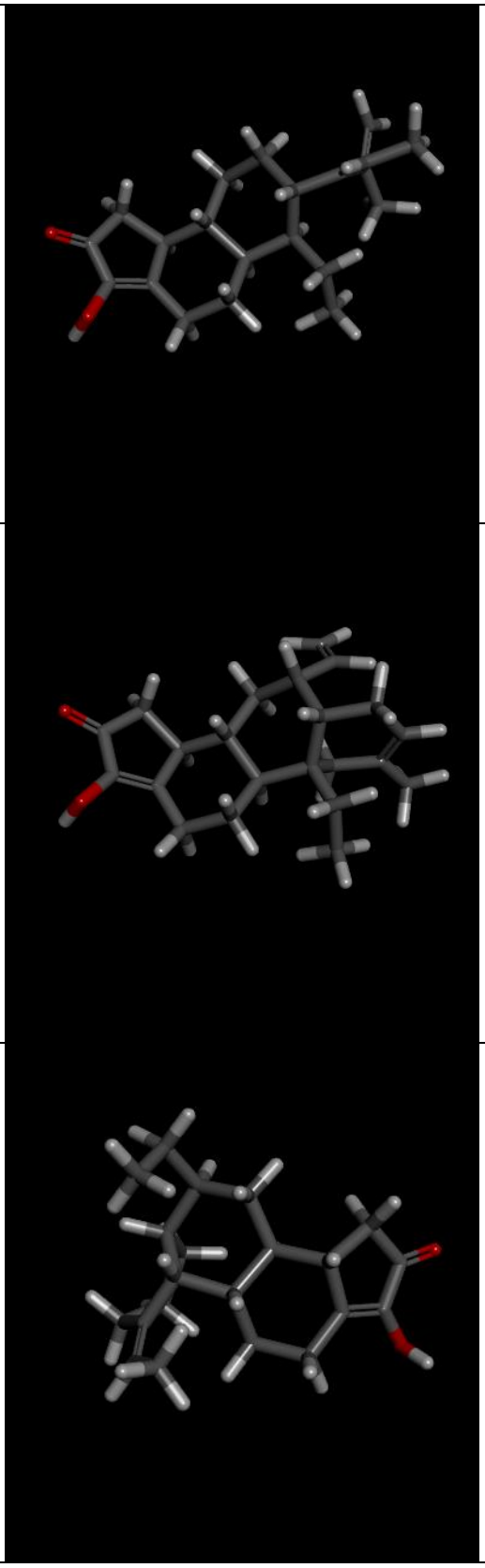	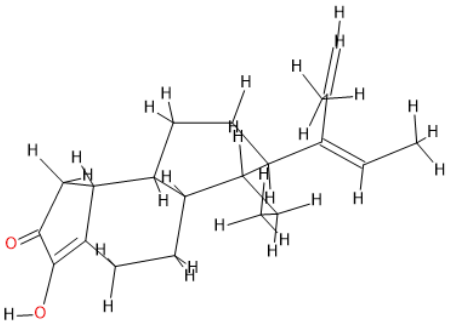	Family <10> MF C21H30O2 MW 314 LogP 4.91 Affinity (pKd) 8.12 CS -100 HAC 2 HDC 1
130		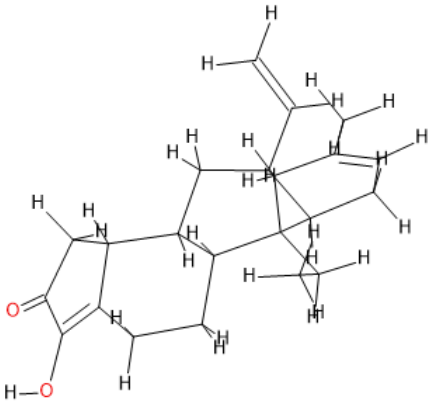	Family <11> MF C22H30O2 MW 326 LogP 4.96 Affinity (pKd) 8.52 CS -120 HAC 2 HDC 1
135		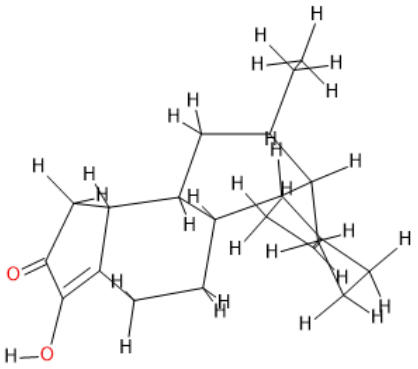	Family <12> MF C21H30O2 MW 314 LogP 4.72 Affinity (pKd) 8.17 CS -150 HAC 2 HDC 1

159	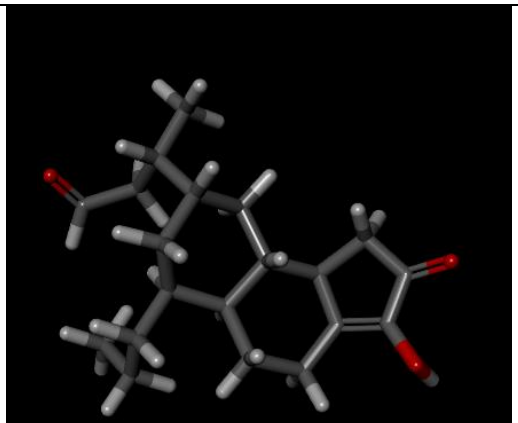	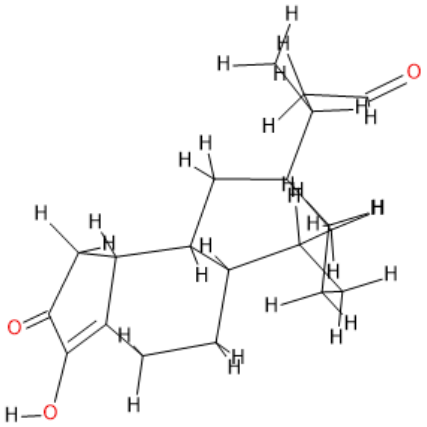	Family <13> MF C20H30O3 MW 318 LogP 4.48 Affinity (pKd) 7.33 CS -120 HAC 3 HDC 1
170	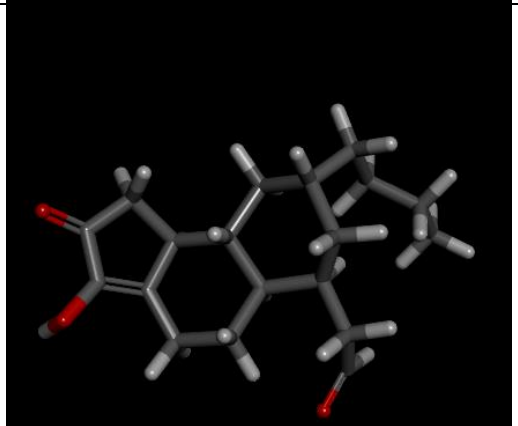	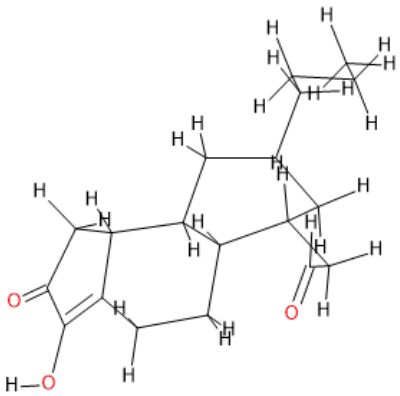	Family <14> MF C19H28O3 MW 304 LogP 4.19 Affinity (pKd) 6.62 CS -100 HAC 3 HDC 1
173	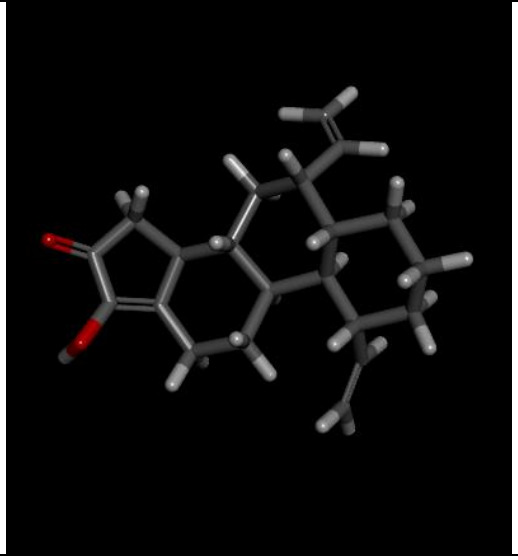	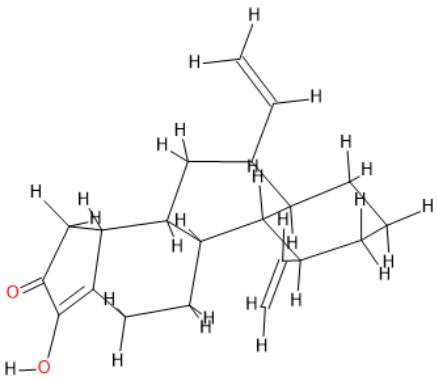	Family <15> MF C21H28O2 MW 312 LogP 4.95 Affinity (pKd) 7.2 CS -170 HAC 2 HDC 1

181	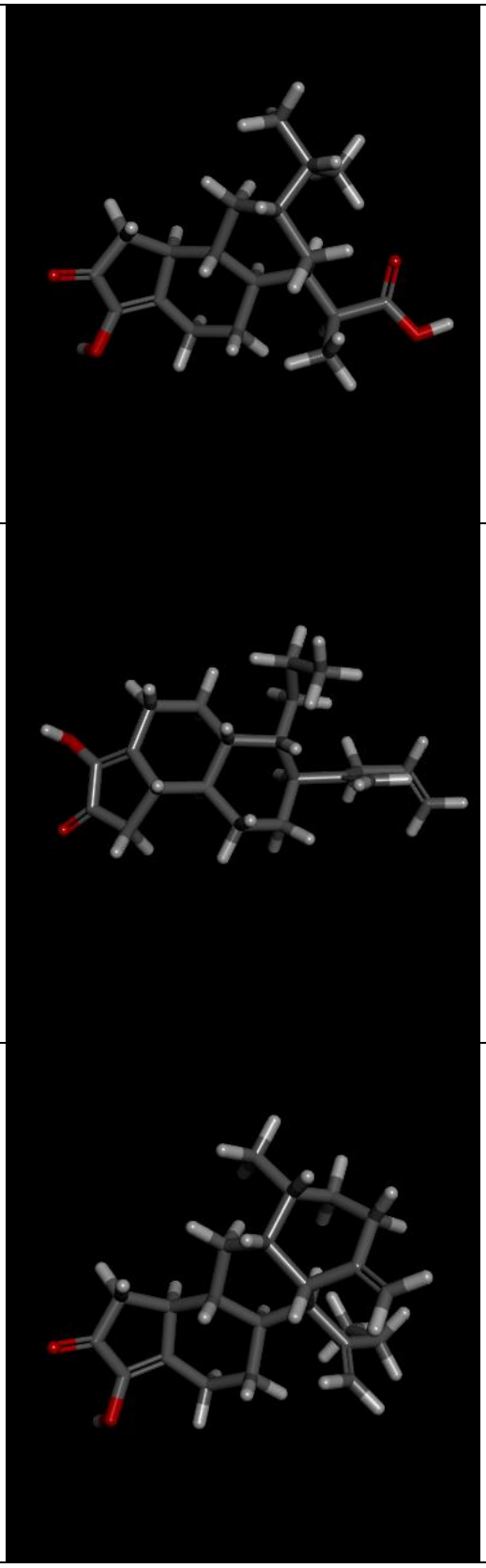	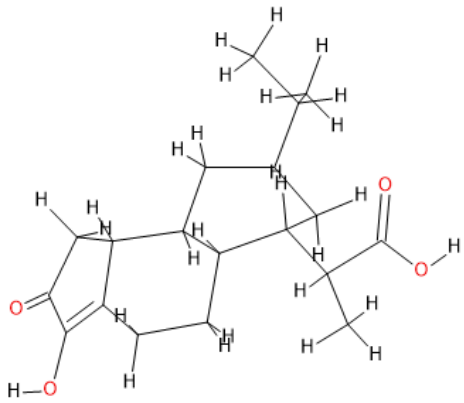	Family <16> MF C19H28O4 MW 320 LogP 4.49 Affinity (pKd) 7.77 CS -140 HAC 4 HDC 2
187		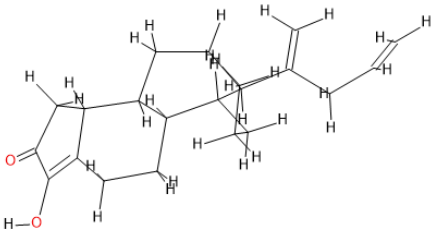	Family <17> MF C21H30O2 MW 314 LogP 4.99 Affinity (pKd) 7.52 CS -100 HAC 2 HDC 1
193		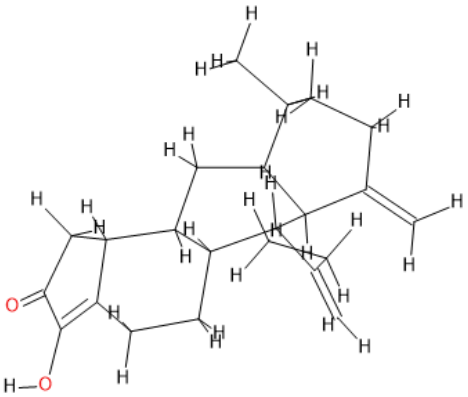	Family <18> MF C23H32O2 MW 340 LogP 4.65 Affinity (pKd) 7.53 CS -170 HAC 2 HDC 1

198	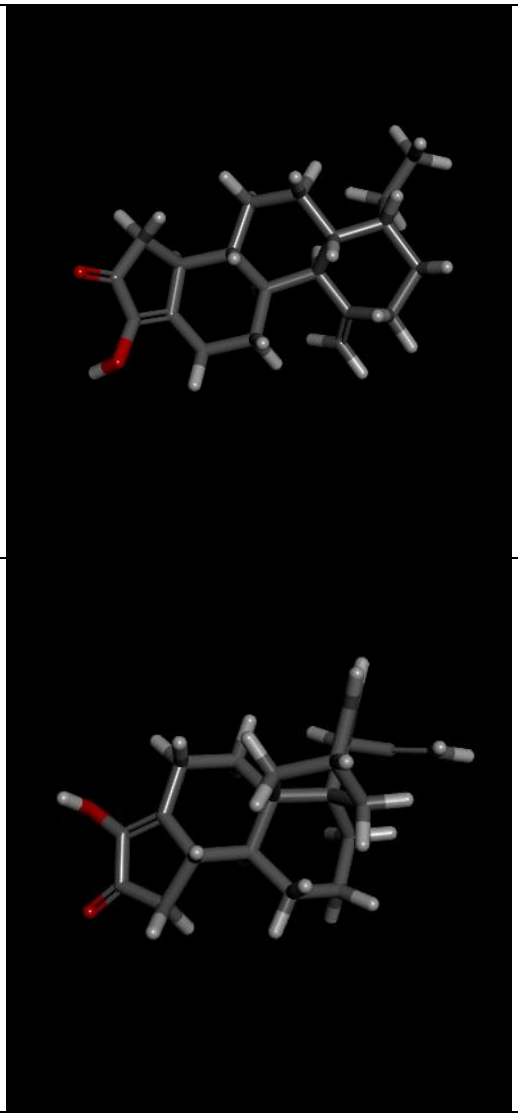	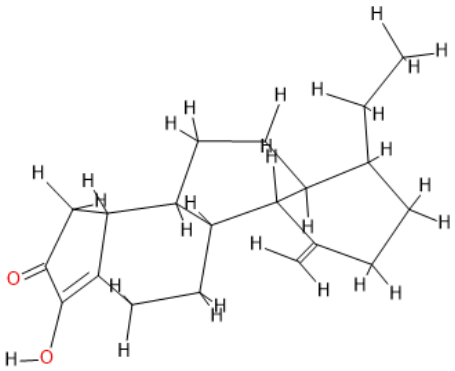	Family <19> MF C20H28O2 MW 300 LogP 4.41 Affinity (pKd) 6.88 CS -150 HAC 2 HDC 1
200		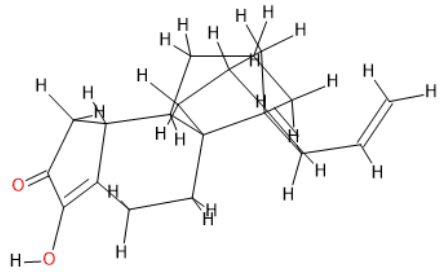	Family <21> MF C21H26O2 MW 310 LogP 4.7 Affinity (pKd) 6.34 CS -180 HAC 2 HDC 1

Table 3.20 The highest affinity molecule generated from each family for the Sex Hormone-Binding Globulin (PDB 1LHU) 1lhuseed8.

Res-ult	3D Structure	2D Structure	Characteristics
007	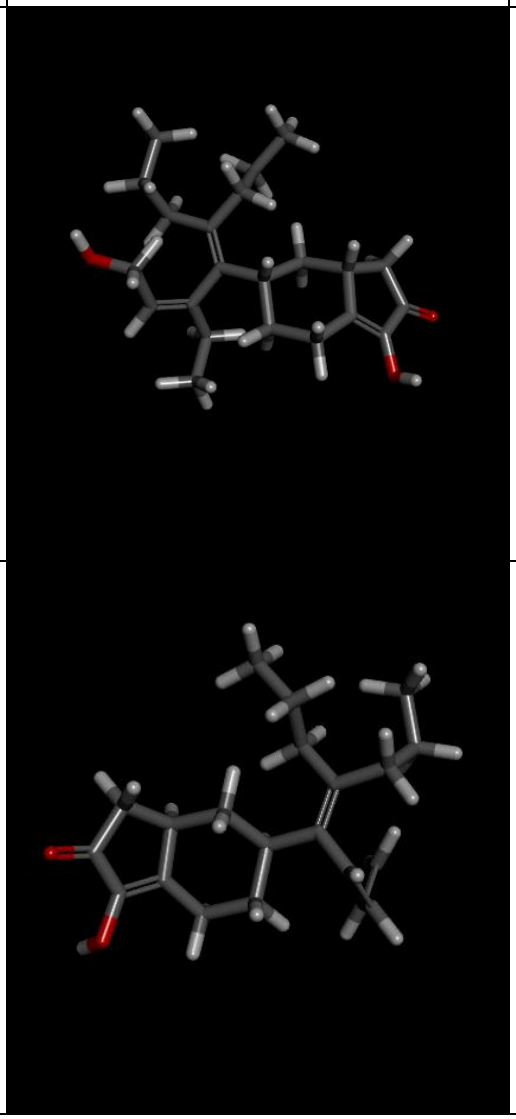	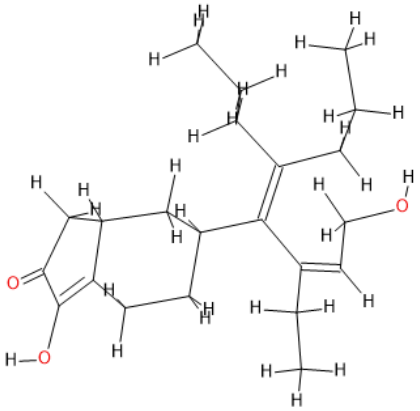	Family <1> MF C22H34O3 MW 346 LogP 3.68 Affinity (pKd) 7.19 CS -40 HAC 3 HDC 2
012		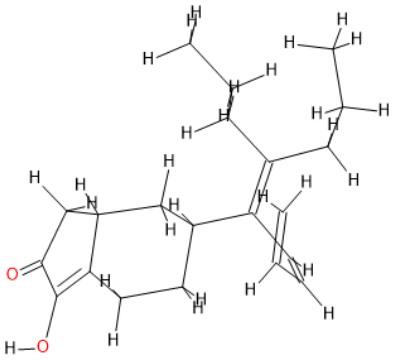	Family <2> MF C21H30O2 MW 314 LogP 4.49 Affinity (pKd) 7.62 CS -40 HAC 2 HDC 1

036		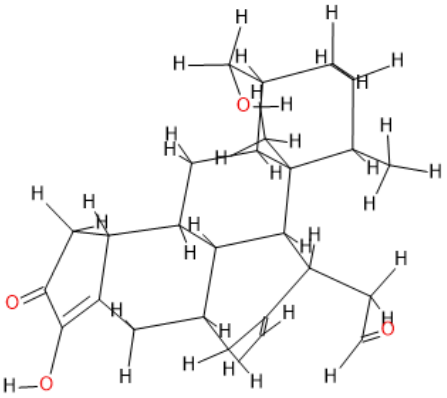	Family <3> MF C26H36O4 MW 412 LogP 3.84 Affinity (pKd) 5.59 CS -200 HAC 4 HDC 2
038	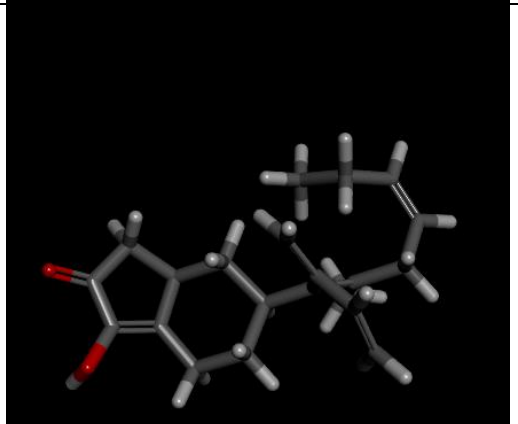	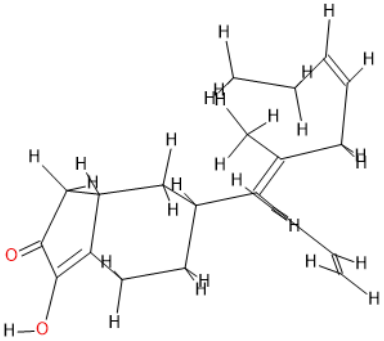	Family <4> MF C21H28O2 MW 312 LogP 4.42 Affinity (pKd) 7.52 CS -40 HAC 2 HDC 1
046	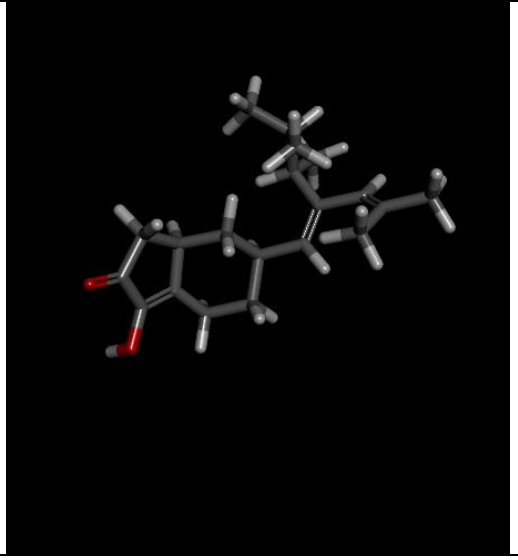	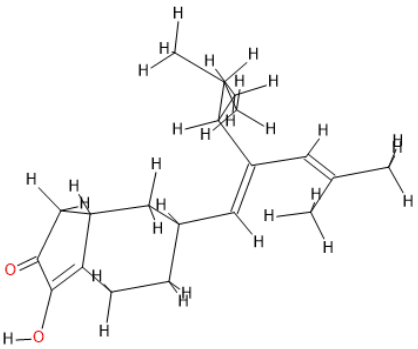	Family <5> MF C20H30O2 MW 302 LogP 4.51 Affinity (pKd) 6.26 CS -80 HAC 2 HDC 1

048	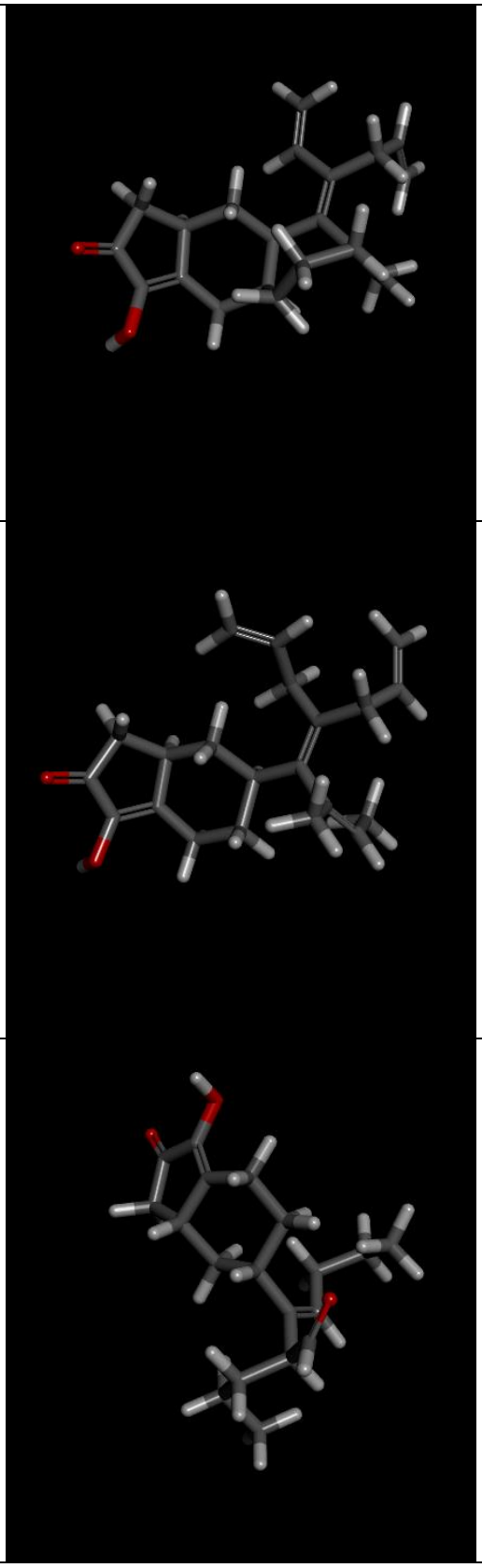	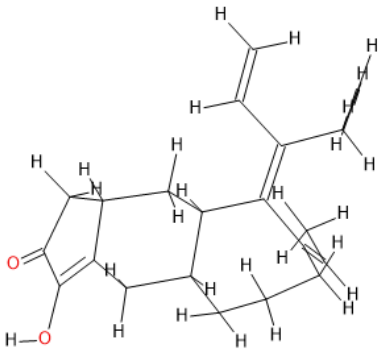	Family <6> MF C22H28O2 MW 324 LogP 4.56 Affinity (pKd) 6.94 CS -60 HAC 2 HDC 1
050		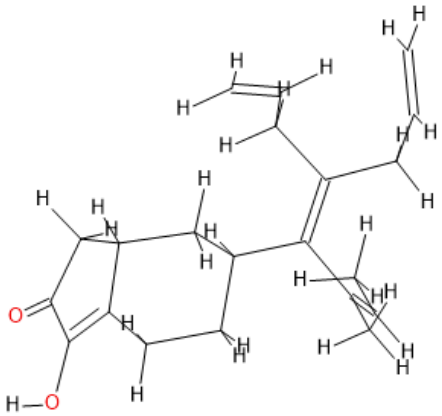	Family <7> MF C21H28O2 MW 312 LogP 4.32 Affinity (pKd) 6.8 CS -40 HAC 2 HDC 1
056		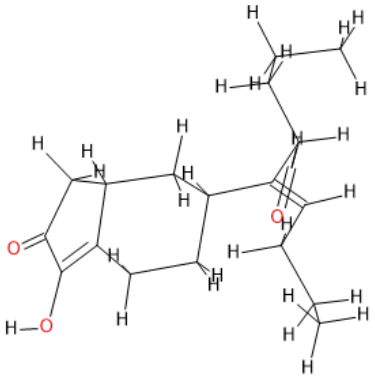	Family <8> MF C19H28O3 MW 304 LogP 4.47 Affinity (pKd) 6.44 CS -60 HAC 3 HDC 1

Chapter 4

Discussion

This is both an exploratory and a validation study. It seeks, on one hand, to identify the receptors for which Maltanedienol has the highest LBA (pKd) and to investigate these as the possible *in vivo* targets for this molecule, from a calcium deposition perspective. It seeks furthermore, once *in vitro* studies are carried out, to assess the utility of the software proposed by D'Emanuele (2019) as a predictive tool for the identification of hitherto unidentified *in vivo* targets using a ligand-based approach.

This study is an extrapolation of the findings of D'Emanuele (2019) which, based on the structure of Maltanedienol identified structurally, morphologically and electronically similar molecules from the ChEMBL® (Bento et al., 2014) database. The 59 receptor targets, identified by the data mining software of D'Emanuele (2019), were filtered based on whether their function was related to calcium fixation or bone remodelling. This resulted in 36 potential targets. This step was carried out since Maltanedienol has been identified from the alga *Padina pavonica* and *in vivo* studies have shown that this species is capable of synthesising and releasing a substance that has a positive effect on calcium fixation, through its fronds.

Only 26 of the 36 endogenous recruited targets were crystallographically described on the PDB (Bernstein et al., 1977) and thus represented the target cohort considered in this study. For each recruited target complex, the small cognate molecule was extracted from its LBP using Sybyl®-X v1.1 (Ash et al., 2010) and the mutual affinity calculated utilising X-Score v1.3 (Wang et al., 2002). Since no information regarding the possible bioactive conformation of Maltanedienol within the 26 *apo* targets was available, conformational analysis was performed in each case using Sybyl®-X v1.1 (Ash et al., 2010), to identify the optimal conformer of Maltanedienol within the LBP. The LBA (pKd) and LBE

(kcal/mol) were calculated for each conformer of each target receptor using X-Score v1.3 (Wang et al., 2002). LBA (pKd) and LBE (kcal/mol) were plotted on the y-axis of a line graph against conformer number, on the x-axis. The conformer with the greatest peak height difference between LBA (pKd) and LBE (kcal/mol) was the optimal conformer and identified as the most likely bioactive scaffold based on high affinity and greatest stability.

The LBA (pKd) of the optimal conformer of Maltanedienol for each receptor was compared to that of the endogenous small molecule for the same receptor. For those cases where the affinity of the optimal conformer of Maltanedienol was greater than that of the endogenous small molecule, a predicted case could be made for the optimal conformer of Maltanedienol binding to the target preferentially in a competitive scenario. This step filtered the study down to the following 7 receptors:

- 1LHU: Sex Hormone-Binding Globulin
- 3ZR7: Progesterone Receptor
- 5VCC: Cytochrome P450 3A4
- 1VOT: Acetylcholinesterase
- 5JNT: Low Molecular Weight Phosphotyrosine Protein Phosphatase
- 2RBE: Corticosteroid 11-Beta-Dehydrogenase Isozyme 1
- 6DUN: Peptidyl-Prolyl Cis-Trans Isomerase NIMA-Interacting 1

Sybyl®-X v1.1 (Ash et al., 2010) was used to dock the optimal conformer of Maltanedienol to its respective *apo* receptor. 2D topology maps were created to describe ligand binding contacts between each optimal conformer of Maltanedienol and its respective receptor. These maps were produced in BIOVIA Discovery Studio

Visualizer® v20.1[7] for each of the seven receptors which were recruited for this study and were used to guide the seed creation process for *de novo* drug design.

The *de novo* approach allowed for the design of seed structures. Seed structures were created for each of the 7 optimal conformers of Maltanedienol using Sybyl®-X v1.1 (Ash et al., 2010). LigBuilder® v1.2 (Wang et al., 2000) was used to generate novel structures built on the seed scaffolds generated using the GROW algorithm. The pharmacophoric space within the LBP of the Cytochrome P450 3A4 (PDB 5VCC) was not hospitable to molecular growth using the Maltanedienol based modelled seed structures. This was probably due to steric hindrance and amino acid non-complementarity. This meant that a total of 6 receptors was ultimately used in this *de novo* study. As previously outlined in Section 2.8 of the methodology, the *de novo* designed Lipinski Rule compliant molecules were grouped according to pharmacophoric similarity and ranked in order of affinity.

This discussion will give special attention to the results obtained when the PR was the target receptor. This is because there is a substantial body of literature that supports the notion that the PR is involved in bone remodelling and calcium fixation. Various studies have indicated, furthermore, that the significant role that the PR potentially plays in bone remodelling must be further studied in the context of it being a novel target for the management of osteoporosis (Kot et al., 2017; Prior, 2018; Yao et al., 2010).

[7] Dassault Systèmes. BIOVIA Discovery Studio Visualizer. Version 20.1 [software]. Dassault Systèmes. 2020 [cited 2021 Jul 14; downloaded 2021 May 25]. Available from: https://www.3dsbiovia.com/products/collaborative-science/biovia-discovery-studio/visualization-download.php.

2D topology maps describing the binding modality of the optimal conformer of Maltanedienol and that of the optimal *de novo* designed molecule within PR_LBP were generated. These were compared to each other and to another 2D topology maps that showed the critical interactions forged between the PR and its co-crystallised small molecule agonist 2-Chloro-N-[[4-(3,5-Dimethylisoxazol-4-Yl) Phenyl]Methyl]-1,4-Dimethyl-1h-Pyrazole-4-Sulfonamide as described in PDB (Bernstein et al., 1977) crystallographic deposition 3ZR7. This process allowed for a comparison of the amino acids critical to the binding of all 3 small molecules to the PR and for the identification of commonalities and differences between all 3 small molecules. This information is vital in understanding the diverse interactions that Maltanedienol and its derivatives make within the PR_LBP and in the elucidation of which interactions could potentially drive PR mediated calcium deposition in bone.

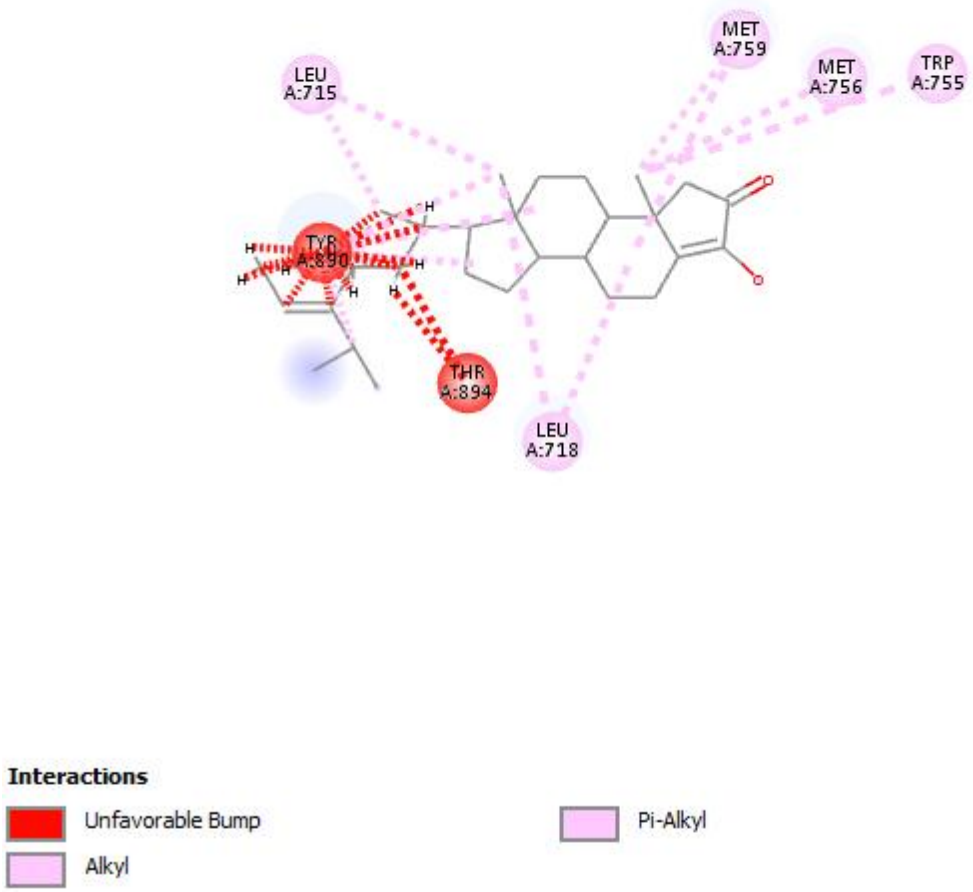

Figure 4.1 2D topology map describing the critical ligand binding interactions forged between the optimal conformer of Maltanedienol for the PR and the amino acids lining the LPB as described in PDB ID: 3ZR7 generated in BIOVIA Discovery Studio Visualizer® v20.1. [7]

[7] Dassault Systèmes. BIOVIA Discovery Studio Visualizer. Version 20.1 [software]. Dassault Systèmes. 2020 [cited 2021 Jul 14; downloaded 2021 May 25]. Available from: https://www.3dsbiovia.com/products/collaborative-science/biovia-discovery-studio/visualization-download.php.

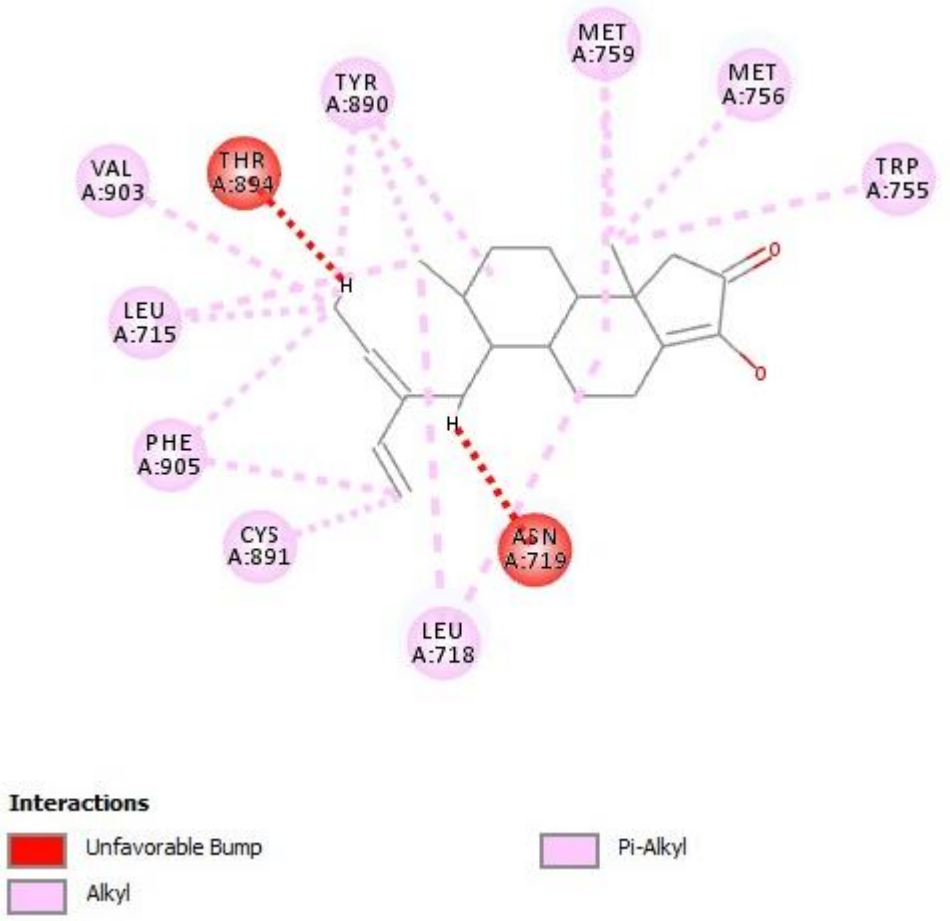

Figure 4.2 2D topology map describing the critical ligand binding interactions forged between the highest affinity *de novo* design molecule and the amino acids lining the LPB as described in PDB ID: 3ZR7 generated in BIOVIA Discovery Studio Visualizer® v20.1.[7]

7 Dassault Systèmes. BIOVIA Discovery Studio Visualizer. Version 20.1 [software]. Dassault Systèmes. 2020 [cited 2021 Jul 14; downloaded 2021 May 25]. Available from: https://www.3dsbiovia.com/products/collaborative-science/biovia-discovery-studio/visualization-download.php.

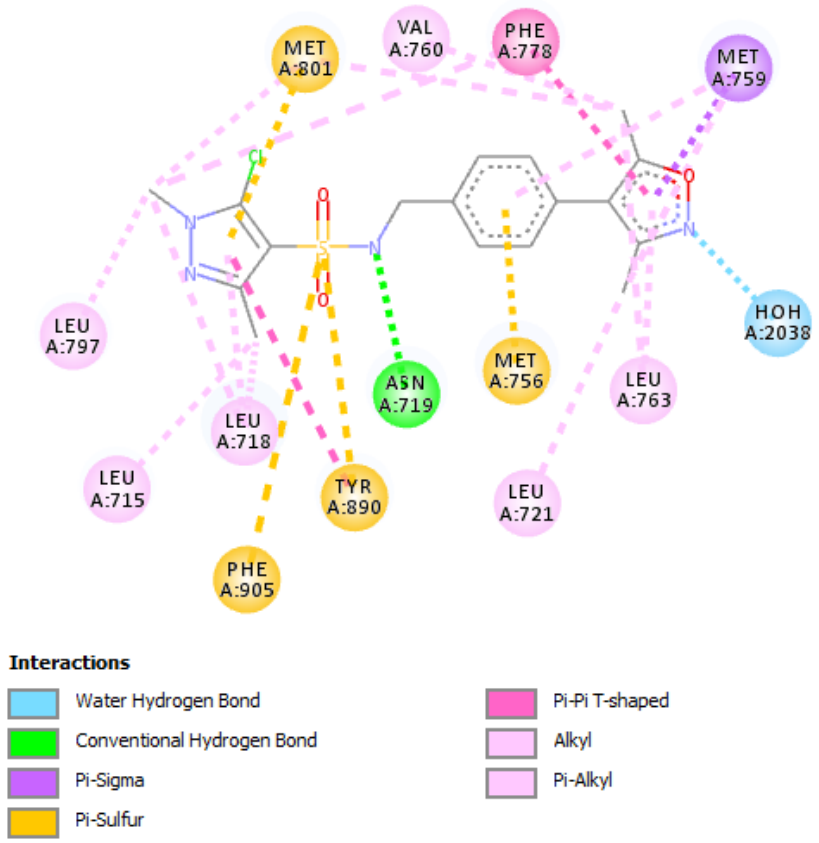

Figure 4.3 2D topology map describing the critical ligand binding interactions forged between the co-crystallised molecule of the PR and the amino acids lining the LBP as described in PDB ID: 3ZR7 generated in BIOVIA Discovery Studio Visualizer® v20.1.[7]

7 Dassault Systèmes. BIOVIA Discovery Studio Visualizer. Version 20.1 [software]. Dassault Systèmes. 2020 [cited 2021 Jul 14; downloaded 2021 May 25]. Available from: https://www.3dsbiovia.com/products/collaborative-science/biovia-discovery-studio/visualization-download.php.

Table 4.1 Shows the critical bonding interactions between the optimal conformer of Maltanedienol for the PR, the highest affinity *de novo* design molecule and the endogenous molecule of the PDB ID 3ZR7 as small ligands and the amino acids lining the LBP perimeter. Amino acid interactions common to all three can be see above the dark line.

Optimal Conformer of Maltanedienol	**Highest affinity *de novo* design molecule**	**Endogenous Molecule**
LEU715	LEU715	LEU715
LEU718	LEU718	LEU718
MET756	MET756	MET756
MET759	MET759	MET759
TRP755	TRP755	X
X	PHE905	PHE905
X	TYR890	TYR890
X	VAL903	PHE778
X	CYS891	VAL760
X	X	MET801
X	X	LEU797
X	X	ASN719
X	X	LEU721
X	X	LEU763
X	X	HDH2038

Table 4.2 Table showing the unfavourable bumps forged between the optimal conformer of Maltanedienol and the highest affinity *de novo* design molecule with the amino acids lining the LBP perimeter.

Optimal Conformer of Maltanedienol	**Highest affinity *de novo* design molecule**
THR894	THR894
TYR890	ASN719

Table 4.3 Comparing the affinities (pKd) of the optimal conformer of Maltanedienol, the highest affinity *de novo* design molecule and the endogenous molecule.

	Affinity (pKd)
Optimal Conformer of Maltanedienol	7.19
Highest affinity *de novo* design molecule	9.39
Endogenous Molecule	7.05

Table 4.1 portrays the optimal conformer of Maltanedienol, highest affinity *de novo* design molecule and endogenous molecule which all forged identical stabilising interactions within LBP. This table aids in understanding why Maltanedienol fits into the LBP since all three ligands forged similar interactions and this a satisfactory result.

In the case of the co-crystallised ligand 2-Chloro-N-[[4-(3,5-Dimethylisoxazol-4-Yl) Phenyl]Methyl]-1,4-Dimethyl-1h-Pyrazole-4-Sulfonamide, there is more extensive binding to the PR when compared to the optimal conformer of Maltanedienol and to the

highest affinity *de novo* designed molecule. This co-crystallised ligand interacts with the PR receptor through a series of alkyl and pi-alkyl bonds, hydrogen bonds with water, conventional hydrogen bonds, pi-sigma, pi-sulfur, pi-pi T-shaped interactions. Both the optimal Maltanedienol conformer, and the optimal *de novo* designed molecule interact with the PR through a dense network of alkyl and pi-alkyl interactions which accounts for their higher affinity relative to the endogenous ligand. It is interesting to note how there are two unfavourable bumps that have been forged by the optimal conformer of Maltanedienol and highest affinity *de novo* design molecule with two amino acids (refer to Table 4.2). The THR894 is the mutual amino acid which forged an unfavourable bump for both optimal conformer of Maltanedienol and highest affinity *de novo* design molecule and therefore this should be addressed in further rounds of optimisation.

When comparing the highest affinity *de novo* design molecule to the endogenous ligand, the favourable interaction forged by the ASN719 amino acid in the endogenous ligand, has changed into an unfavourable one in the comparing the highest affinity *de novo* design molecule and consequently, this should be further investigated computationally.

The increased affinity of the highest affinity *de novo* design molecule is due to the more extensive interactions within the LBP when compared to the optimal conformer of Maltanedienol and thus an improvement has been achieved after performing the *de novo* drug design. While on paper, the highest affinity *de novo* design molecule is proving to be a more confident ligand, studies and literature have also proved that Maltanedienol produces a biological effect. As a result, Maltanedienol should not be discounted in future rounds of drug development however, the first step has been carried out in this study, by optimising Maltanedienol and the interactions that it forges.

Advantageously, the *de novo* process forged 2 new contacts within LBP; namely the TYR890 and PHE905. Maltanedienol had not forged these interactions, however they had been forged by the endogenous ligand. Thus, this process has allowed us to tap even more into the LBP from the point of view of stabilising interactions.

In conclusion, the choice of the PR as a point of discussion is valid, as the literature indicates this. One anticipates that on looking at the atomic interactions that both Maltanedienol and the highest affinity *de novo* design molecule produces interactions that are appropriate, as they are borne out as a result of what is already functioning within the PR_ LBP.

For these reasons, the next steps of this project would be to organise a molecular dynamic simulation study that compares the motions of the endogenous ligand, Progesterone, Maltanedienol and of the highest affinity *de novo* design molecule and compare their motions and observe how the PR will behave when the various ligands are bound to it. Bearing in mind that one is on the right track, one would anticipate similar motions between Progesterone and what is bound endogenously. Contrastingly, Maltanedienol and the highest affinity *de novo* design molecule should behave similarly between them since the aim is to produce the same biological response.

A substantial assumption was made upon focusing on the PR since there were still 5 remaining receptors which could have been investigated and this is a process that should have been carried out. Yet, this was not done due to time constraints and this should be tackled in future studies. Additionally, this study also omitted the other receptors that

were not involved in calcium fixation or bone metabolism, nonetheless this study is already being tackled.

There are several limitations to this study; firstly, not all the targets were described on the PDB (Bernstein et al., 1977) so a potential receptor may have been overlooked. The second limitation being that this study was selective during the in-depth analysis phase. Thirdly, this study was static, as opposed to dynamic. Henceforth, I propose this being considered as a future study as at present attempts of *in vitro* assays are intangible.

References

Al-Enazi NM, Awaad AS, Zain ME, Alqasoumi SI. Antimicrobial, antioxidant and anticancer activities of *Laurencia catarinensis*, *Laurencia majuscula* and *Padina pavonica* extracts. Saudi Pharmaceutical Journal: SPJ: The Official Publication of the Saudi Pharmaceutical Society. 2018; 26(1):44-52.

Ash S, Cline MA, Homer RW, Hurst T, Smith GB. ChemInform Abstract: SYBYL® Line Notation (SLN): A Versatile Language for Chemical Structure Representation. ChemInform. 2010; 28(18): 66-78.

Bado I, Gugala Z, Fuqua SA, Zhang XH. Oestrogen Receptors in Breast and Bone: From Virtue of Remodeling To Vileness of Metastasis. Oncogene. 2017; 36(32):4527-37.

Beavan S, Horner A, Bord S, Ireland D, Compston J. Colocalization of Glucocorticoid and Mineralocorticoid Receptors in Human Bone. Journal of Bone and Mineral Research: The Official Journal of the American Society for Bone and Mineral Research: The Official Journal of The American Society for Bone and Mineral Research. 2001; 16(8):1496-504.

Bento AP, Gaulton A, Hersey A, Bellis LJ, Chambers J, Davies M, et al. The ChEMBL Bioactivity Database: An Update. Nucleic Acids Research. 2014; 42(Database Issue):D1083-90.

Berman HM, Westbrook J, Feng Z, Gailliland G, Bhat TN, Weissig H, et al. The Protein Data Bank. Nucleic Acids Research. 2000; 28(1): 235–42.

Bernstein FC, Koetzle TF, Williams GJ, Meyer EF Jr, Brice MD, Rodgers JR, et al. The Protein Data Bank: A Computer-Based Archival File for Macromolecular Structures. Journal of Molecular Biology. 1977; 112(3):535-42.

Bland R, Worker CA, Noble BS, Eyre LJ, Bujalska IJ, Sheppard MC, et al. Characterization of 11beta-Hydroxysteroid Dehydrogenase Activity and Corticosteroid Receptor Expression in Human Osteosarcoma Cell Lines. The Journal of Endocrinology. 1999; 161(3):455-64.

Blunden G. Biologically Active Compounds from Marine Organisms. Phytotherapy Research: PTR. 2001; 15(2):89-94.

Cassar M, Shoemake C, Azzopardi LM, Saliba C, Gutierrez G. *de novo* Design of Non-Steroidal Oestrogen Receptor Modulating Molecules using Maltanedienol as a Lead Molecule. International Journal of Drug Design and Discovery. 2013; 4(1):965-77.

Castillo AB, Blundo JT, Chen JC, Lee KL, Yereddi NR, Jang E, Kumar S, Tang WJ et al. Focal Adhesion Kinase Plays a Role in Osteoblast Mechanotransduction *In Vitro* But Does Not Affect Load-Induced Bone Formation *In Vivo*. Public Library of Science One [Internet]. 2012; 7(9):1-11 [cited 2021 Jul 14]. Available from: https://journals.plos.org/plosone/article?id=10.1371/journal.pone.0043291.

Castillo AB, Triplett JW, Pavalko FM, Turner CH. Oestrogen Receptor-Beta Regulates Mechanical Signaling in Primary Osteoblasts. American Journal of Physiology,

Endocrinology and Metabolism [Internet]. 2014; 306(8):E937-44 [cited 2021 Jul 14]. Available from: https://www.ncbi.nlm.nih.gov/pmc/articles/PMC3989741/.

Cho YA, Jue SS, Bae WJ, Heo SH, Shin SI, Kwon IK, et al. PIN1 Inhibition Suppresses Osteoclast Differentiation and Inflammatory Responses. Journal of Dental Research. 2015; 94(2):371-80.

Cooper MS, Walker EA, Bland R, Fraser WD, Hewison M, Stewart PM. Expression and Functional Consequences of 11β-Hydroxysteroid Dehydrogenase Activity in Human Bone. Bone. 2000; 27(3):375-81.

Cooper MS, Bujalska I, Rabbitt E, Walker EA, Bland R, Sheppard MC, et al. Modulation Of 11beta-Hydroxysteroid Dehydrogenase Isozymes by Proinflammatory Cytokines in Osteoblasts: An Autocrine Switch from Glucocorticoid Inactivation to Activation. Journal of Bone and Mineral Research: The Official Journal of the American Society for Bone and Mineral Research. 2001; 16(6):1037-44.

Cremers S, Papapoulos S. Pharmacology of Bisphosphonates. Bone. 2011; 49(1):42-9.

D'Emanuele J. Discovery of Medicinal Molecules Based on Similarity Networks [dissertation]. Msida (Malta): University of Malta; 2019.

DeSelm CJ, Miller BC, Zou W, Beatty WL, van Meel E, Takahata, et al. Autophagy Proteins Regulate the Secretory Component of Osteoclastic Bone Resorption. Developmental cell. 2011; 21(5):966-74.

Doody KM, Bussières-Marmen S, Li A, Paquet M, Henderson JE, Tremblay ML. T Cell Protein Tyrosine Phosphatase Deficiency Results in Spontaneous Synovitis and Subchondral Bone Resorption in Mice. Arthritis and Rheumatism. 2012; 64(3):752-61.

El Gamal AA. Biological Importance of Marine Algae. Saudi Pharmaceutical Journal: SPJ: The Official Publication of the Saudi Pharmaceutical Society. 2010; 18(1):1-25.

Falzon AV. Evaluation of The Affinity of the Small Molecule Maltanedienol for Farnesyl Pyrophosphate Synthase [dissertation]. Msida (Malta): University of Malta; 2017.

Ferron M, Wei J, Yoshizawa T, Del Fattore A, DePinho RA, Teti A, et al. Insulin Signaling in Osteoblasts Integrates Bone Remodeling and Energy Metabolism. Cell. 2010; 142(2):296-308.

Frey J, Stonko D, Faugere M, Riddle RC. Hypoxia-Inducible Factor-1α Restricts the Anabolic Actions of Parathyroid Hormone. Bone Research. 2014; 2:1-10.

Fumoto T, Ishii KA, Ito M, Berger S, Schütz G, Ikeda K. Mineralocorticoid Receptor Function in Bone Metabolism and its Role in Glucocorticoid-Induced Osteopenia. Biochemical and Biophysical Research Communications. 2014; 447(3):407-12.

Galea RP. The Effect of a Marine Alga, *Padina pavonica*, on Maltese Menopausal Women [project]. Msida (Malta): University of Malta; 2009.

Gay CM, Balaji K, Byers LA. Giving AXL the Axe: Targeting AXL in Human Malignancy. British Journal of Cancer. 2017; 116(4):415–23.

George MM, New MI, Ten S, Sultan C, Bhangoo A. The Clinical and Molecular Heterogeneity Of 17βhsd-3 Enzyme Deficiency. Hormone Research in Paediatrics. 2010; 74(4):229-40.

Gil-Díaz T, Haroun R, Tuya F, Betancor S, Viera-Rodríguez MA. Effects of Ocean Acidification on the Brown Alga *Padina pavonica*: Decalcification Due to Acute and Chronic Events. Public Library of Science One [Internet]. 2014; 9(9):1-9 [cited 2021 Jul 14]. Available from: https://journals.plos.org/plosone/article?id=10.1371/journal.pone.0108630.

Goodsell DS, Dutta S, Zardecki C, Voigt M, Berman HM, Burley SK. The RCSB PDB "Molecule of the Month": Inspiring a Molecular View of Biology. PLoS Biology [Internet]. 2015; 13(5):1-12 [cited 2021 Jul 14]. Available from: https://journals.plos.org/plosbiology/article?id=10.1371/journal.pbio.1002140.

Grisaru D, Lev-Lehman E, Shapira M, Chaikin E, Lessing JB, Eldor A, et al. Human Osteogenesis Involves Differentiation-Dependent Increases in The Morphogenically Active 3' Alternative Splicing Variant of Acetylcholinesterase. Molecular and Cellular Biology [Internet]. 1999; 19(1):788-95 [cited 2021 Jul 14]. Available from: https://mcb.asm.org/content/19/1/788.long.

Guriec N, Colin M, Delarue J, Jiménez Alba C, Camino Callarisa A, Varella Negre E, *et al*. Effects of a Maltanediol and Fucosterol High Content Alga Extract on the Zootechnical Performance and Nutritional Characteristics of the Meat of Rabbits Receiving an Alpha-Linolenic Rich Feed. Journal of the World Rabbit Science. 2014; 22(4):323-4.

Haupt M, Kauschke V, Sender J, Kampschulte M, Kovtun A, Dürselen L et al. Bone Status of Adult Female Butyrylcholinesterase Gene-Deficient Mice. International Immunopharmacology. 2015; 29(1):208-14.

Herbert RJ, Ma L, Marston A, Farnham WF, Tittley I, Cornes RC. The Calcareous Brown Alga *Padina pavonica* in Southern Britain: Population Change and Tenacity Over 300 Years. Marine Biology. 2016; 163:46.

Hilborn E, Stål O, Jansson A. Oestrogen and Androgen-Converting Enzymes 17β-Hydroxysteroid Dehydrogenase and Their Involvement in Cancer: with a special focus on 17β-Hydroxysteroid Dehydrogenase Type 1, 2, and Breast Cancer. Oncotarget [Internet]. 2017; 8(18):30552-62 [cited 2021 Jul 14]. Available from: http://www.oncotarget.com/index.php?journal=oncotarget&page=article&op=view&path[]=15547&pubmed-linkout=1.

Hoppé E, Bouvard B, Royer M, Audran M, Legrand E. Sex Hormone-Binding Globulin in Osteoporosis. Joint Bone Spine [Internet]. 2010; 77(4):306-12 [cited 2021 Jul 14]. Available from: https://www.sciencedirect.com/science/article/pii/S1297319X10000692?via%3Dihub.

Hu K, Olsen BR. The Roles of Vascular Endothelial Growth Factor in Bone Repair and Regeneration. Bone. 2016; 91:30–8.

Hu K, Olsen BR. Vascular Endothelial Growth Factor Control Mechanisms in Skeletal Growth and Repair. Developmental Dynamics: An Official Publication of the American Association of Anatomists [Internet]. 2017; 246(4):227-34 [cited 2021 Jul 14]. Available from: https://anatomypubs.onlinelibrary.wiley.com/doi/full/10.1002/dvdy.24463

Hulley PA, Bishop T, Vernet A, Schneider JE, Edwards JR, Athanasou NA et al. Hypoxia-Inducible Factor 1-alpha Does Not Regulate Osteoclastogenesis but Enhances Bone Resorption Activity Via Prolyl-4-Hydroxylase 2. The Journal of Pathology. 2017; 242(3):322-33.

Inaba M, Terada M, Nishizawa Y, Shioi A, Ishimura E, Otani S, Morii H. Protective Effect of An Aldose Reductase Inhibitor Against Bone Loss in Galactose-Fed Rats: Possible Involvement of the Polyol Pathway in Bone Metabolism. Metabolism: Clinical and Experimental. 1999; 48(7):904-9.

Inada M, Matsumoto C, Uematsu S, Akira S, Miyaura C. Membrane-Bound Prostaglandin E Synthase-1-Mediated Prostaglandin E2 Production by Osteoblast Plays a Critical Role in Lipopolysaccharide-Induced Bone Loss Associated with Inflammation. Journal of Immunology: Official Journal of the American Association of Immunologists. 2006; 177(3):1879-85.

Inkson CA, Brabbs AC, Grewal TS, Skerry TM, Genever PG. Characterization of Acetylcholinesterase Expression and Secretion During Osteoblast Differentiation. Bone. 2004; 35(4):819-27.

Ismail A, Ktari L, Ahmed M, Bolhuis H, Boudabbous A, Stal LJ, *et al*. Antimicrobial Activities of Bacteria Associated with the Brown Alga *Padina pavonica*. Frontiers in Microbiology [Internet]. 2016; 7:1-13 [cited 2021 Jul 14]. Available from: https://www.frontiersin.org/articles/10.3389/fmicb.2016.01072/full

Issa S, Schnabel D, Feix M, Wolf L, Schaefer HE, Russell DW, et al. Human Osteoblast-Like Cells Express Predominantly Steroid 5alpha-Reductase Type 1. The Journal of Clinical Endocrinology and Metabolism. 2002; 87(12):5401-7.

Johnson VR, Russell BD, Fabricius KE, Brownlee C, Hall-Spencer JM. Temperate and Tropical Brown Macroalgae Thrive, Despite Decalcification, Along Natural CO2gradients. Global Change Biology. 2012; 18(9):2792-803.

Jones G, Prosser DE, Kaufmann M. Cytochrome P450-Mediated Metabolism of Vitamin D. Journal of Lipid Research. 2014; 55(1):13-31.

Kang H, Yang K, Xiao L, Guo L, Guo C, Yan Y, et al. Osteoblast Hypoxia-Inducible Factor-1α Pathway Activation Restrains Osteoclastogenesis via the Interleukin-33-MicroRNA-34a-Notch1 Pathway. Frontiers in Immunololgy [Internet]. 2017; 8:1-15 [cited 2021 Jul 14]. Available from: https://www.frontiersin.org/articles/10.3389/fimmu.2017.01312/full.

Kang YS, Park SY, Yim CH, Kwak HS, Gajendrarao P, Krishnamoorthy N, et al. The CYP3A4*18 Genotype in the Cytochrome P450 3A4 Gene, a Rapid Metabolizer of Sex Steroids, is Associated with Low Bone Mineral Density. Clinical Pharmacology and Therapeutics. 2009; 85(3):312-8.

Khaled N, Hiba M, Asma C. Antioxidant and Antifungal activities of *Padina pavonica* and *Sargassum Vulgare* from the Lebanese Mediterranean Coast. Advances in Environmental Biology. 2012; 6(1):42-8.

Khalid AB, Krum SA. Oestrogen Receptors Alpha and Beta in Bone. Bone. 2016; 87:130-5.

Kim JH, Kim K, Kim I, Seong S, Kim N. c-Src-Dependent and -Independent Functions of Matk in Osteoclasts and Osteoblasts. The Journal of Immunology: Official Journal of The American Association of Immunologists. 2018; 200(7):2455-63.

Kolanjinathan K, Ganesh P, Saranraj P. Pharmacological Importance of Seaweeds: A Review. World Journal of Fish and Marine Sciences. 2014; 6(1):1-15.

Kot A, Zhong ZA, Zhang H, Lay YE, Lane NE, Yao W. Sex Dimorphic Regulation of Osteoprogenitor Progesterone in Bone Stromal Cells. Journal of Molecular Endocrinology. 2017;59(4):351-363.

Krassas GE, Papadopoulou P. Oestrogen Action on Bone Cells. Journal of Musculoskeletal and Neuronal Interactions. 2001; 2(2):143-51.

Lee JS, Lee HJ, Lee JW, Lee SC, Heo JS. Osteogenic Effect of Inducible Nitric Oxide Synthase (iNOS)-Loaded Mineralized Nanoparticles on Embryonic Stem Cells. Cellular Physiology and Biochemistry: International Journal of Experimental Cellular Physiology, Biochemistry, and Pharmacology [Internet]. 2018; 51(2):746-62 [cited 2021 Jul 14]. Available from: https://www.karger.com/Article/Fulltext/495330

Lee KC, Jessop H, Suswillo R, Zaman G, Lanyon LE. The Adaptive Response of Bone to Mechanical Loading in Female Transgenic Mice is Deficient in the Absence of Oestrogen Receptor-Alpha And -Beta. The Journal of Endocrinology. 2004; 182(2):193-201.

Legrand E, Gibert C, Gallois Y, Mathieu E, Boux de casson F, Basle MF. The Sex Hormone Binding Globulin in Male Osteoporosis. Annals of the Rheumatic Diseases. 2001; 60(Suppl 1):254.

Li F, Wang W, Gu M, Gyoneva S, Zhang J, Huang S, et al. L-Type Calcium Channel Activity in Osteoblast Cells is Regulated by the Actin Cytoskeleton Independent of Protein Trafficking. Journal of Bone and Mineral Metabolism. 2011; 29(5):515-25.

Lipinski CA, Lombardo F, Dominy BW, Feeney PJ. Experimental and Computational Approaches to Estimate Solubility and Permeability in Drug Discovery and Development Settings. Advanced Drug Delivery Reviews 2001; 46(1-3):3-26.

Locatelli V, Bianchi VE. Effect of GH/IGF-1 on Bone Metabolism and Osteoporosis. International Journal of Endocrinology. 2014; 2014:1-25.

Manolagas SC, O'Brien CA, Almeida M. The Role of Oestrogen and Androgen Receptors in Bone Health and Disease. Nature Reviews Endocrinology. 2013; 9(12):699-712.

Marzia M, Sims NA, Voit S, Migliaccio S, Taranta A, Bernardini S, et al. Decreased c-Src Expression Enhances Osteoblast Differentiation and Bone Formation. The Journal of Cell Biology. 2000; 151(2):311-20.

Merlotti D, Gennari L, Stolakis K, Nuti R. Aromatase Activity and Bone Loss in Men. Journal of Osteoporosis. 2011; 2011:1-11.

Moutsatsou P, Kassi E, Papavassiliou AG. Glucocorticoid Receptor Signaling in Bone Cells. Trends in Molecular Medicine. 2012; 18(6):348-59.

Murakami M, Nakatani Y, Tanioka T, Kudo I. Prostaglandin E synthase. Prostaglandins & Other Lipid Mediators. 2002; 68-69:383-99.

Okazaki M, Pentecost A, Tanaka Y, Miyata M. A Study of Calcium Carbonate Deposition in the Genus *Padina* (Phaephyceae, Dictyotales). British Phycological Journal. 1986; 21(2):217-24.

Pace Debono M. Evaluating the Use of the Seaweed *Padina pavonica* (L.) as a Diet for the Mass Production of the Rotifer *Brachionus plicatilis* [project]. Msida (Malta): University of Malta; 1998.

Prior JC. Progesterone for the prevention and treatment of osteoporosis in women. Climacteric:the journal of the International Menopause Society.2018;21(4):366-374.

Sasano H, Uzuki M, Sawai T, Nagura H, Matsunaga G, Kashimoto O, et al. Aromatase in Human Bone Tissue. Journal of Bone and Mineral Research: The Official Journal of The American Society for Bone and Mineral Research. 1997; 12(9):1416-23.

Shen ZJ, Hu J, Ali A, Pastor J, Shiizaki K, Blank RD, et al. Pin1 Null Mice Exhibit Low Bone Mass and Attenuation of BMP Signaling. Public Library of Science One [Internet]. 2013; 8(5):1-13 [cited 2021 Jul 14]. Available from: https://europepmc.org/article/pmc/pmc3651169.

Silberfeld T, Bittner L, Fernández-García C, Cruaud C, Rousseau F, de Reviers B, et al. Species Diversity, Phylogeny and Large Scale Biogeographic Patterns of the Genus *Padina* (Phaeophyceae, Dictyotales). Journal of Phycology. 2013; 49(1):130-42.

Smit AJ. Medicinal and Pharmaceutical Uses of Seaweed Natural Products: A Review. Journal of Applied Phycology. 2004; 16(4):245-62.

Sobel V, Schwartz B, Zhu YS, Cordero JJ, Imperato-McGinley J. Bone Mineral Density in the Complete Androgen Insensitivity and 5alpha-Reductase-2 Deficiency Syndromes. The Journal of Clinical Endocrinology and Metabolism. 2006; 91(8):3017-23.

Spieker J, Ackermann A, Salfelder A, Vogel-Höpker A, Layer PG. Acetylcholinesterase Regulates Skeletal *In Ovo* Development of Chicken Limbs by ACh-Dependent and -Independent Mechanisms. Public Library of Science One [Internet]. 2016; 11(8):1-19 [cited 2021 Jul 14]. Available from: http://dx.plos.org/10.1371/journal.pone.0161675

Spieker J, Mudersbach T, Vogel-Höpker A, Layer PG. Endochondral Ossification Is Accelerated in Cholinesterase-Deficient Mice and in Avian Mesenchymal Micromass Cultures. Public Library of Science One [Internet]. 2017; 12(1):1-23 [cited 2021 Jul 14]. Available from: http://dx.plos.org/10.1371/journal.pone.0170252

Stewart PM. Tissue-Specific Cushing's Syndrome, 11b-Hydroxysteroid Dehydrogenases and the Redefinition of Corticosteroid Hormone Action. European Journal of Endocrinology. 2003; 149:163–8.

Takahashi A, Mulati M, Saito M, Numata H, Kobayashi Y, Ochi H, et al. Loss of Cyclin-Dependent Kinase 1 Impairs Bone Formation but Does Not Affect the Bone-Anabolic Effects of Parathyroid Hormone. Journal of Biological Chemistry [Internet]. 2018; 293(50):19387-99 [cited 2021 Jul 14]. Available from: http://www.jbc.org/cgi/pmidlookup?view=long&pmid=30366983

Tamimi I, Madathil SA, Kezouh A, Nicolau B, Karp I, Tamimi F. Effect of Acetylcholinesterase Inhibitors on Post-Surgical Complications and Mortality Following A Hip Fracture: A Cohort Study. Journal of Musculoskeletal and Neuronal Interactions [Internet]. 2017; 17(2):69-77 [cited 2021 Jul 14]. Available from: https://www.ncbi.nlm.nih.gov/pmc/articles/PMC5492321/

Tamura Y, Takeuchi Y, Suzawa M, Fukumoto S, Kato M, Miyazono K et al. Focal Adhesion Kinase Activity Is Required for Bone Morphogenetic Protein--Smad1 Signaling and Osteoblastic Differentiation in Murine MC3T3-E1 Cells. Journal of Bone and Mineral Research: The Official Journal of The American Society for Bone and Mineral Research. 2001; 16(10):1772-9.

The UniProt Consortium. UniProt: The Universal Protein Knowledgebase. Nucleic Acids Research. 2017;45(Database issue): D158-69.

Vogel-Hopker A, Sperling LE, Layer PG. Co-Opting Functions of Cholinesterases in Neural, Limb and Stem Cell Development. Protein and Peptide Letters. 2012; 19(2):155-64.

Wang Q, Wang G, Wang B, Yang H. Activation of TGR5 Promotes Osteoblastic Cell Differentiation and Mineralization. Biomedicine & Pharmacotherapy [Internet]. 2018; 108:1797-803 [cited 2021 Jul 14]. Available from: https://www.sciencedirect.com/science/article/pii/S0753332218325319?via%3Dihub

Wang R, Gao Y, Lai L. LigBuilder: A Multi Purpose Progam for Structure-Based Drug Design. Journal of Molecular Modeling. 2000; 6:498-516.

Wang R, Lai L, Wang S. Further Development and Validation of Empirical Scoring Functions for Structure-Based Binding Affinity Prediction. Journal of Computer-aided Molecular Design. 2002; 16:11-26.

Wang Y, Zhu J, DeLuca HF. Identification of the Vitamin D Receptor in Osteoblasts and Chondrocytes but Not Osteoclasts in Mouse Bone. Journal of Bone and Mineral Research: The Official Journal of the American Society for Bone and Mineral Research. 2014; 29(3):685–92.

Wheeler MA, Townsend MK, Yunker LA, Mauro LJ. Transcriptional Activation of The Tyrosine Phosphatase Gene, OST-PTP, During Osteoblast Differentiation. Journal of Cellular Biochemistry [Internet]. 2002; 87(4):363-76 [cited 2021 Jul 14]. Available from: https://onlinelibrary.wiley.com/doi/abs/10.1002/jcb.10297

Wimalawansa SJ. Nitric oxide and Bone. Annals of the New York Academy of Sciences. 2010; 1192:391-403.

Windahl SH, Andersson N, Börjesson AE, Swanson C, Svensson J, Movérare-Skrtic S, et al. Reduced Bone Mass and Muscle Strength in Male 5a-Reductase Type 1 Inactivated Mice. Public Library of Science One [Internet]. 2011; 6(6):1-8 [cited 2021 Jul 14]. Available from: https://journals.plos.org/plosone/article?id=10.1371/journal.pone.0021402

Wu J, Henning P, Sjögren K, Koskela A, Tuukkanen J, Movérare-Skrtic S, et al. The Androgen Receptor is Required for Maintenance of Bone Mass in Adult Male Mice. Molecular and Cellular Endocrinology. 2019; 479:159–69.

Xu ML, Bi CWC, Liu EYL, Dong TTX, Tsim KWK. Wnt3a Induces the Expression of Acetylcholinesterase During Osteoblast Differentiation Via the Runx2 Transcription

Factor. The Journal of Biological Chemistry [Internet]. 2017; 292(30):12667-78 [cited 2021 Jul 14]. Available from: https://pubmed.ncbi.nlm.nih.gov/28607150/

Yamamoto Y, Yoshizawa T, Fukuda T, Shirode-Fukuda Y, Yu T, Sekine K, et al. Vitamin D Receptor in Osteoblasts Is A Negative Regulator of Bone Mass Control. Endocrinology [Internet]. 2013; 154(3):1008-20 [cited 2021 Jul 14]. Available from: https://pubmed.ncbi.nlm.nih.gov/23389957/

Yao W, Dai W, Shahnazari M, Pham A, Chen Z, Chen H, et al. Inhibition of the Progesterone Nuclear Receptor During the Bone Linear Growth Phase Increases Peak Bone Mass in Female Mice. Public Library of Science One [Internet]. 2010; 5(7):1-13 [cited 2021 Jul 14]. Available from: https://pubmed.ncbi.nlm.nih.gov/20625385/.

Zaidi SK, Sullivan AJ, Medina R, Ito Y, van Wijnen AJ, Stein JL, et al. Tyrosine Phosphorylation Controls Runx2-Mediated Subnuclear Targeting of YAP to Repress Transcription. The EMBO Journal [Internet]. 2004; 23(4):790-9 [cited 2021 Jul 14]. Available from: https://pubmed.ncbi.nlm.nih.gov/14765127/

Zambuzzi WF, Granjeiro JM, Parikh K, Yuvaraj S, Peppelenbosch MP, Ferreira, CV. Modulation of Src Activity by Low Molecular Weight Protein Tyrosine Phosphatase During Osteoblast Differentiation. Cellular Physiology and Biochemistry: International Journal of Experimental Cellular Physiology, Biochemistry, and Pharmacology [Internet]. 2008; 22(5-6):497-506 [cited 2021 Jul 14]. Available from: https://www.karger.com/Article/Pdf/185506

Zee T, Settembre C, Levine RL, Karsenty G. T-Cell Protein Tyrosine Phosphatase Regulates Bone Resorption and Whole-Body Insulin Sensitivity Through Its Expression in Osteoblasts. Molecular and Cell Biology [Internet]. 2012; 32(6):1080-8 [cited 2021 Jul 14]. Available from: https://pubmed.ncbi.nlm.nih.gov/22252315/

Zhang D, Jiang Y, Song D, Zhu Z, Zhou C, Dai L, et al. Tyrosine-Protein Phosphatase Non-Receptor Type 2 Inhibits Alveolar Bone Resorption in Diabetic Periodontitis Via Dephosphorylating CSF1 Receptor. Journal of Cellular and Molecular Medicine [Internet] 2019; 23(10):6690-9 [cited 2021 Jul 14]. Available from: https://onlinelibrary.wiley.com/doi/full/10.1111/jcmm.14545

Zhang X, Li X, Wang R. Interpretation of the Binding Affinities of PTP1B Inhibitors with the MM-GB/SA Method and the X-Score Scoring Function. Journal of Chemical Information and Modeling. 2009; 49(4): 1033-48.

Zhang X, Li F, Guo L, Hei H, Tian L, Peng W et al. Forskolin Regulates L-Type Calcium Channel through Interaction between Actinin 4 and β3 Subunit in Osteoblasts. Public Library of Science One [Internet]. 2015;10(4):1-17 [cited 2021 Jul 14]. Available from: https://journals.plos.org/plosone/article?id=10.1371/journal.pone.0124274

List of Publications and Abstracts

Abstract Submission (BMS-LDDD-2021-316)

Admin <admin@bentham.manuscriptpoint.com>
17/08/2021 15:14

To: ellacoppini@hotmail.com Cc: lddd@benthamscience.net; fatimasiddiqui@benthamscience.net

Dear Dr. Coppini,

Thankyou for submitting Abstract 'Identification and Preliminary Validation of Potential Endogenous Targets for Maltanedienol' in journal 'LDDD'

Regards

Editorial Office
Letters in Drug Design & Discovery
Bentham Science Publishers

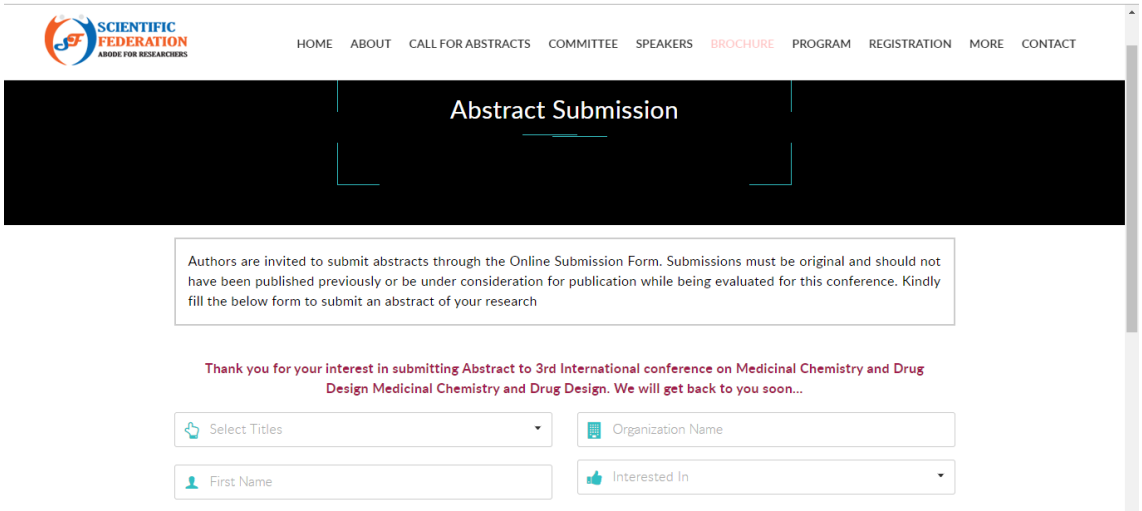

Appendices

L-Università ta' Malta

Ella Coppini <ella.coppini.16@um.edu.mt>

FRECMDS_2021_182 - ID:- 9560_24082021_Ella Coppini

FACULTY RESEARCH ETHICS COMMITTEE <research-ethics.ms@um.edu.mt> 30 August 2021 at 13:05
To: Ella Coppini <ella.coppini.16@um.edu.mt>
Cc: Claire Shoemake <claire.zerafa@um.edu.mt>

Dear Ms Coppini,

Since your self-assessment resulted in no issues being identified, FREC will file your application for record and audit purposes but will not review it.

Any ethical and legal issues including data protection issues are your responsibility and that of the supervisor.

Good luck with your project!

Regards,
Annalise

L-Università ta' Malta

Annalise Mallia Duca | Secretary

Faculty Research Ethics Committee
Faculty of Medicine and Surgery
Medical School, Mater Dei Hospital
+356 2340 1803

https://www.um.edu.mt/ms/students/researchethics